Physiological studies on the production and defense mechanisms of reactive oxygen species and reactive carbonyl species during photosynthesis in higher plants

Takagi, Daisuke

(Degree)
博士（農学）

(Date of Degree)
2016-03-25

(Date of Publication)
2017-03-01

(Resource Type)
doctoral thesis

(Report Number)
甲第6661号

(URL)
https://hdl.handle.net/20.500.14094/D1006661

Doctoral Dissertation

Physiological studies on the production and defense mechanisms of reactive oxygen species and reactive carbonyl species during photosynthesis in higher plants

高等植物光合成の駆動が引き起こす活性酸素および活性カルボニル化合物の
生成メカニズムとその防御メカニズムに関する生理学的研究

February 2016

Graduate School of Agricultural Science

Kobe University

Daisuke Takagi

CONTENTS

SUMMARY

Under aerobic conditions, all organisms are threatened by oxidative stress, and it is a fate for them to struggle to oxidative stress. The main cause of oxidative stress under aerobic condition is referred to reactive oxygen species (ROS) like O_2^-, H_2O_2 and OH·. In higher plants, the major ROS production sites are mitochondria, peroxisomes, and chloroplasts. Among these ROS production sites, photosystem I is a major production site of reactive oxygen species (ROS) in photosynthetic electron transport reaction in higher plants, and it is well-known that environmental stresses like drought stimulate the ROS production at PSI. Besides ROS produced at PSI stimulate the oxidative stress in cell by their diffusion, ROS cause damage to PSI itself. When PSI suffers ROS-dependent oxidative damage, which is termed as PSI photoinhibition, photosynthetic electron transport reaction is considerably impaired. Because the decrease in photosynthetic electron transport reaction suppresses the energy supply for CO_2-fixaton in the Calvin-cycle, PSI photoinhibition causes the decrease in CO_2-fixation, and growth retardation in higher plants. Based on these observations, improving the PSI photoinhibition and reducing ROS production in photosynthetic electron transport reaction would contribute to protecting plants fitness. However, the production mechanism and production site of ROS at PSI have not been determined. Therefore, the protection mechanisms for PSI photoinhibition is also less discussed because of the ambiguity of ROS production mechanism at PSI.

Reducing sugars, which are essential for living things including animals and plants to produce ATP and NADH in mitochondria also have potential to cause oxidative stress in the cell by producing ROS or sugar-derived reactive carbonyl species (RCS) which enable to modify proteins, lipids or DNAs. These facts suggest that higher plants faec in two potential dangers of the oxidative stress induced by sugar-accumulation by CO_2-fixation and photosynthesis electron transport reaction in chloroplasts. Besides oxidative stress damages cell components directly, oxidative stress stimulates the production of secondary toxic compounds. Among the targets of ROS, lipids, especially poly unsaturated fatty acids (PUFAs) are susceptible to ROS-dependent oxidative stress.

When PUFAs have suffered oxidative stress, their fluidities and physiological functions are impaired, furthermore, lipid-derived RCS are produced by their break-down. In higher plants, chloroplasts are consisted with highly unsaturated fatty acids, therefore, lipids in chloroplast would be vulnerable to oxidative stress. That is, the chance to produce lipid-derived RCS and to suffer their toxicity also would be high. However, direct evidence whether the sugar-production by photosynthesis poses a threat to produce sugar-derived RCS has not been mentioned in higher plants. In addition, the production of lipid-derived RCS in chloroplast and its toxicity for plant physiological reaction have not been clarified.

In this study, I aimed to elucidate the mechanisms of ROS production at PSI, and PSI photoinhibition in higher plants; furthermore, I also aimed to find the protection mechanisms for PSI photoinhibition based on the mechanisms of PSI photoinhibition. In addition, I studied the production mechanism of sugar-derived RCS in chloroplast, and the physiological toxicity of lipid-derived RCS in higher plants. These studies are expected to show the physiological targets to suppress the oxidative stress in higher plants, and these studies also contribute to exhibiting the valuable phenotype for improving the tolerance to oxidative stress.

In chapter 2, I studied the molecular mechanisms of ROS production at PSI by using chloroplasts isolated from spinach leaves. In this chapter, I found that ROS are produced within the thylakoid membrane when electron carriers in PSI become highly reduced. Moreover, I found that tromal ROS-detoxification enzymes cannot protect PSI from its photoinhibition. On the other hand, I found that wheat plants can develop the protection mechanism against PSI photoinhibition depending on their growth light environment and wheat cultivars.

In chapter 3, I considered that the accumulation of reduced electron carriers in PSI should avoid for preventing from PSI photoinhibition. Based on this consideration, I studied the regulation mechanisms to oxidize PSI during photosynthesis. In this chapter, I found that photorespiration, instead of Alternative electron flows like water-water cycle or cyclic electron flow around PSI, functions to oxidize PSI electron carriers through the formation of H^+ gradient (ΔpH) across the

thylakoid membranes under the conditions where the Calvin-cycle activity is limited.

In chapter 4, to identify the central component to regulate ΔpH in photosynthetic electron transport reaction, I tried to isolate the *Arabidopsis thaliana* mutant mutagenized by ethyl methane sulfonate (EMS), which is impaired the ΔpH-dependent regulatory system in photosynthetic electron transport reaction. In this chapter, I isolated new allelic mutant of γ-subunit in chloroplast localized CF_0CF_1-ATPsynthase, and I found that the physiological importance of H^+-efflux regulation by chloroplastic ATPsynthase for regulating the redox-state in PSI.

In Chapter 5, to elucidate whether photosynthesis itself stimulates the production of sugar-derived RCS in chloroplasts, I analyzed the relationship between the production of sugar-derived RCS and photosynthesis rate in chloroplast isolated from spinach leaves, and leaves in wheat plant. When 3-phosphoglyceric acid (3-PGA) was added to drive the Calvin cycle in isolate chloroplasts under illumination, I found that sugar-derived RCS, methylglyoxal (MG) and glyoxal (GLO) were synthesized in chloroplasts. Similar to isolated chloroplasts, the content of MG and GLO in leaves increased under high CO_2 conditions where photosynthesis is stimulated compared to ambient conditions in leaves of wheat plants. From these results, I proposed that driving photosynthesis accompanies with the production of sugar-derived RCS in chloroplasts.

In Chapter 6, I analyzed the effects of lipid-derived RCS on plant physiological reactions by using *Arabidopsis thaliana* knock-out and knock-down mutants of chloroplast-localized alkenal-one oxidoreductase (AOR) which serves the detoxification of lipid-derived RCS in chloroplasts. In this chapter, I found that AOR mutants in *Arabidopsis thaliana* (*aor*) showed growth retardation under normal growth conditions, compared to wild-type plants (WT). To elucidate the cause of growth retardation in *aor*, I conducted detail analysis about photosynthesis and respiration. Then, I found that photosynthesis activity was similar between WT and *aor* under growth light conditions, however, *aor* showed lower respiration rate in the dark conditions, compared to WT. Furthermore, I found that the activity of phosphoenolpyruvate carboxylase (PEPC), which functions in glycolysis, was suppressed, and starch degradation in the dark was also suppressed in *aor*. These results indicated

that growth retardation in *aor* caused by the suppression of carbon-utilization during night. Indeed, *aor* and WT showed similar growth when they were grown under continuous illumination. From these results, I proposed that the detoxification of lipid-derived RCS within chloroplast is important for protecting cell component and maintaining plant growth. From these results, I discussed the physiological targets for improving the oxidative stress induced by ROS and RCS in higher plants.

Chapter1

GENERAL INTRODUCTION

The effect of environmental stress for plant productivity

~the importance of the study about photosynthetic electron transport regulation in higher plants~

On earth, world population is now increasing, and this increase accompanies with the increase in the demand for food. In Wheeler and Braum (2013), it has been estimated that agricultural products are required to increase by 50 % by 2030 for satisfying food demands. Therefore, the increase in crop plant productivity is urgent problem which have to be achieved.

Cultivation environment for crop plants changes moment by moment. For example, atmospheric carbon dioxide (CO_2) concentration, and atmospheric temperature continue to increase after the Industrial Revolution (Wheeler and Braum, 2013). On the other hand, chronic salt damage and drought are spreading in cropland in the world (Munns and Tester, 2008; Wheeler and Braum, 2013). Under such environmental stress conditions, stomatal closure is stimulated in leaves and this phenomenon limits the CO_2 supply for CO_2-fixation in chloroplasts. Because the limitation of CO_2-fixation in chloroplasts reduces starch synthesis, plants suffer from the impairment of the carbon-utilization and the growth defect (Gibon et al., 2009). In fact, these environmental stresses directly connect with the decrease in crop productivity. Moreover, the cause of the decrease in crop yield is occupied about 85 % by environmental stress in agriculture (Kramer and Boyer, 1985).

At same time, under these environmental conditions, the energy production by photosynthetic electron transport reaction exceeds to the energy consumption in the Calvin-cycle (Kramer and Evans, 2011; Schöttler et al., 2015). Excess energy in photosynthetic electron transport reaction easily leaks to oxygen (O_2) and stimulates the production of reactive oxygen species (ROS) (Kotchoni et al., 2006; Kramer and Evans, 2011). Oxidative stress is inevitable for all organisms that live in aerobic conditions. The main cause of oxidative stress is reactive oxygen species (ROS) such

as superoxide anion radical (O_2^-), hydrogen peroxide (H_2O_2), singlet oxygen ($^1O_2$) and hydroxyl radical (HO·). O_2^- is regarded as a primary ROS, so various kinds of ROS are generated from O_2^- (Buonocore et al., 2010). O_2^- disproportionates to H_2O_2 and O_2 by superoxide dismutase localized in cytosol, mitochondria and chloroplasts (Alscher et al., 2002). The half-life of H_2O_2 is about 1 ms, that is 1,000 times longer than of O_2^- (Møller et al., 2007). For this longer half-life, H_2O_2 can diffuse to wide range in the cell and give an oxidative attack on biochemical molecules. H_2O_2 is generally scavenged by ascorbate-peroxidase (APX), catalase, glutathione peroxidase (GPX) or peroxiredpxin (Prx), and converted into H_2O (Miyake and Asada, 1992; Vandenabeele et al., 2004; Navrot et al., 2006; Bhatt and Tripathi, 2011; Gaber et al., 2012). However, if H_2O_2 escapes from these antioxidant system, HO·, that is the most reactive ROS, is formed by the reaction of H_2O_2 with free metal ion (Fe^{2+}, Cu^{2+}) via Fenton reaction (Lloyd et al., 1997). Furthermore, HO· is also formed from O_2^- and H_2O_2 via Haber-Weiss reaction (Kehrer, 2000). ROS are highly reactive against cell components, and cause the decrease in photosynthesis and impairment of plant growth (Apel and Hirt, 2004; Mittler, 2006).

These negative effects of environmental stresses are not limited to chronic stress, but transient environmental stresses also impair plant fitness. For example, transient drought stress within a week is enough to modify the structure of chloroplasts, and impairs photosynthesis even after re-watering (Miyashita et al., 2005). In addition, fluctuating light also impairs the photosynthesis activity *in vivo* within an hour (Kono et al., 2014). These observations indicate that high-energetic photosynthetic electron transport reaction needs to be well-adjusted, and to be regulated immediately when plants have been exposed to environmental stresses. From these above observations, the elucidation of the ROS production mechanism in photosynthetic electron transport reaction, and the identification of gene resources which regulate the photosynthetic electron transport reaction and prevent the production of ROS would contribute to discover the target trait for improving plant productivity under various environmental conditions.

Photosynthetic electron transport reaction on the thylakoid membranes in higher plants

Light energy is essential for driving photosynthesis, and initially the special pairs of chlorophylls in Photosystem (PS) II (P680) and in PSI (P700) are excited by light absorption. The excitation of P680 chlorophyll produces of electrons by H_2O oxidation, and these electrons transfer to PSI through, plastoquinone (PQ), cytochrome (Cyt) b_6f, and plastocyanine (PC) (Fig. I-1). The excitation of P700 chlorophyll further transfers electrons to $NADP^+$ and produces NADPH through ferredoxin (Fd), and Fd/NAD(P)H oxidoreductase (FNR). This photosynthetic electron flow [termed as linear electron flow (LEF)] coupled with proton (H^+)-influx into the luminal side of the thylakoid membranes. In addition to the release of H^+ by H_2O oxidation at PSII, Q-cycle between Cyt b_6f and plastoquinol (PQH_2) contributes to translocate H^+ into the luminal side of the thylakoid membranes, and these reactions make H^+ gradient (ΔpH) across the thylakoid membranes (Cramer et al., 2006). During the formation of ΔpH, counter ions (K^+, Mg^{2+}, and Cl^-) move to dissolve electrochemical gradient (ΔΨ) through specific ion transporters like TPK3 (Carraretto et al. 2013). This enables to make large ΔpH across the thylakoid membranes (Kramer et al., 2003). ΔpH is major *proton motive force* (*pmf*) for ATP synthesis in chloroplasts, and ΔpH drives CF_0CF_1-ATPsynthase (ATPase) to phosphorylate ADP (Fig. I-1) (Groth and Strotmann, 1999; Kramer et al., 2003). NADPH and ATP are utilized in the metabolic reaction like the Calvin-cycle and photorespiration under the illumination.

Excess energy caused photoinhibition in PSII and PSI

Light is required for higher plants to drive photosynthesis. However, excess light energy causes photoinhibition in chloroplasts (Melis, 1999). Photosystem (PS) II is very sensitive to environmental stresses, such as high-light intensity or drought, and the decrease in D1 protein is stimulated under such stress conditions (Aro et al., 1993). This phenomenon is called photoinhibition of PSII.

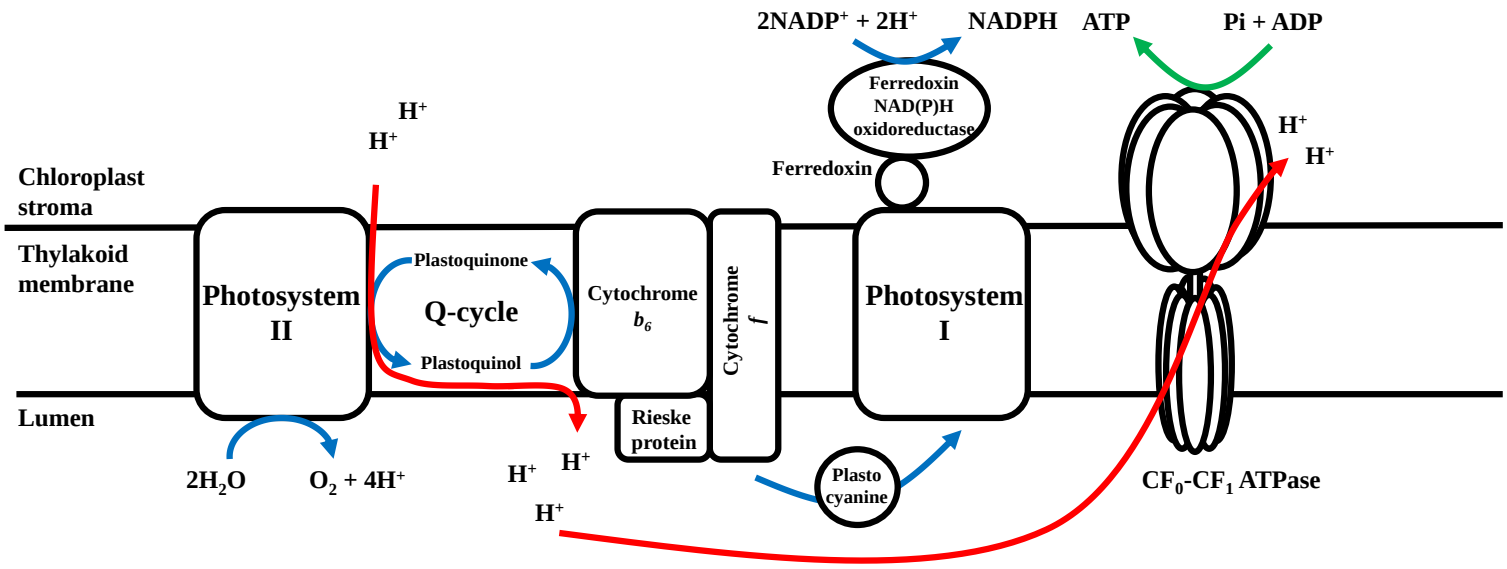

Figure I-1

The over-view of photosynthetic electron transport chain in higher plants.

Blue arrows indicate the pathway of electrons, red arrows indicate the pathway of protons, and green arrows indicate the production of ATP at CF_0CF_1-ATP synthase.

The occurrence of photoinhibition greatly reduces plant productivity (Melis, 1999; Külheim et al., 2002). In previous studies, the cause of photoinhibition in PSII has been shown to be caused by singlet oxygen ($^1O_2$), which is produced through a charge recombination reaction between $P680^+$ and the reduced secondary electron acceptor (Q_A^-) in PSII, and $^1O_2$ is thought to stimulate the degradation of D1 protein (Asada and Takahashi, 1987; Krieger-Liszkay, 2005; Hideg et al., 2007; Gill and Tuteja, 2010; Vass, 2011). In addition to $^1O_2$, recent studies have revealed that superoxide (O_2^-) is also produced by PSII and this also causes photoinhibition (Bondarava et al., 2010; Zulfugarov et al., 2014). In contrast to the theory that the cause of photoinhibition in PSII is oxidative degradation of D1 protein, several studies now suggest that ROS suppress *de novo* D1 protein synthesis through the oxidative inactivation of thioredoxin-regulated elongation factor G, which would function in protein translation for D1 protein (Kojima et al., 2007; Nishiyama et al., 2011).

PSI suffers from photoinhibition as well as PSII. Photoinhibition in PSI is also caused by ROS (Sonoike and Terashima, 1994; Terashima et al., 1994; Sonoike et al., 1995; Sonoike, 1995, 1996; Sejima et al., 2014). In PSI, the risk of ROS production increases when the photosynthetic electron transport chain is in a highly reduced state (Sonoike and Terashima, 1994; Allahverdiyeva et al., 2005; Oelze et al., 2011; Grieco et al., 2012). In fact, PSI photoinhibition is observed when PSI electron carriers become reduced, and this impairs plant growth (Allahverdiyeva et al., 2005; Munekage et al., 2008; DalCorso et al., 2008; Soursa et al., 2012; Grieco et al., 2012; Kono et al., 2014). Importantly, the recovery of photoinhibited PSI is very slow, unlike photoinhibited PSII, which recovers rapidly ($t_{1/2}$ about 60 min) (Melis, 1999; Sonoike, 2011). Furthermore, PSI photoinhibition reduces CO_2 assimilation rate in leaves (Zivcak et al., 2015a). Therefore, PSI photoinhibition is more serious than PSII photoinhibition in higher plants. However, the molecular mechanisms of PSI photoinhibition is less clarified, compared to that of PSII photoinhibition (Sonoike, 2011; Vass, 2012). For improving the tolerance toward the oxidative damage by ROS in PSI, it is essential to elucidate the molecular mechanism of PSI photoinhibition in higher plants.

Protecting mechanisms toward photoinhibition in PSII and PSI

~the importance of the regulation of ΔpH across the thylakoid membranes~

ΔpH has important functions to regulate the redox-state in the photosynthetic electron transport chain besides the formation of ATP at ATPase. Non-photochemical quenching (NPQ) is a major ΔpH-dependent regulatory system in photosynthesis (Niyogi et al., 1998; Müller et al., 2001; Nilkens et al., 2010). The energy-dependent NPQ (qE) is regulated by PsbS in PSII, and PsbS requires the protonation to stimulate the energy dissipation at PSII-light harvesting complex (LHC) II antenna complex (Li et al., 2000; Niyogi et al., 2004). ΔpH is also required for activating violaxanthin (Vio) de-epoxidase to convert Vio to zeaxanthin (Zea) in xanthophyll cycle, and Zea dissipates excess energy as a heat in PSII by quenching excited chlorophylls directly or arranging LHCII composition (termed as qZ quenching) (Demmig-Adams and Adams, 1996; Niyogi et al., 1998; Holzwarth et al., 2009; Nilkens et al., 2010). These ΔpH-dependent regulatory systems prevent PSII from its photinhibition. Furthermore, ΔpH contributes to adjust the redox-state of PSI (Soursa et al., 2012; Tikhonov, 2013). PQH_2 oxidation at Cyt b_6f is a limiting step in photosynthetic electron transport, and ΔpH further slows down this reaction (Tikhonov, 2013). In addition, ΔpH induces reversible Ca^{2+} release at oxygen evolving complex (OEC) in PSII, and slows down H_2O oxidation (Krieger and Weis, 1993). These ΔpH-dependent regulations limit the electron transport from PSII to PSI, and prevent the over-reduction of electron carriers in PSI. Indeed, the formation of ΔpH induces the accumulation of oxidized state of P700 chlorophylls, and alleviates PSI photoinhibition induced by over-reduction in PSI (Soursa et al., 2012; Kono et al., 2014; Sejima et al., 2014).

To induce the protection mechanism for protecting PSII and PSI from photoinhibition, ΔpH is required. Many reports have believed that Alternative electron flow (AEF) is required for regulating ΔpH during photosynthesis (Fig. I-2) (e.g. Miayke, 2010). As major AEFs, water-water cycle (WWC) and cyclic electron flow around PSI (CEF) are well focused (Miyake, 2010). WWC has been proposed in Asada (1999), and this reaction is initiated by O_2 reduction at PSI to produce

superoxide (O_2^-) (Mehler, 1951). Subsequently, O_2^- is disproportionated to H_2O_2 and O_2 by thylakoid bound- and stromal-Cu/Zn superoxide dismutase (SOD). (Hayakawa et al., 1984; Ogawa et al., 1995). H_2O_2 is detoxified into H_2O by thylakoid bound- and stromal ascorbate peroxidase (APX) (Miyake and Asada, 1992). In this detoxification reaction catalyzed by APX, ascorbate (Acs) is required as a substrate of APX, and Asc is oxidized to monodehydroascorbate (MDA) (Miyake and Asada, 1992, 1994). MDA act as an electron acceptor at PSI, and Asc is regenerated through MDA reduction at PSI (Forti and Ehrenheim, 1993). Forti and Elli (1996) reported that the addition of Asc in isolated thylakoid membranes increases ATP synthesis activity. This observation means that the regeneration of Acs stimulates the photosynthetic electron transport reaction and H^+-influx in to the luminal side of the thylakoid membranes. Based on these reports, WWC stimulates photosynthetic electron transport activity through O_2 and MDA reduction in chloroplasts.

CEF is first proposed in Arnon (1955), and developed in Arnon (1959) and Tagawa et al. (1963). They observed that H^+-influx into the luminal side of the thylakoid membranes occurs by PSI without PSII in thylakoid membranes. Today, as a major electron transport pathway in CEF, two pathways are proposed, one is NAD(P)H dehydrogenase like complex (NDH) dependent pathway, and other is proton gradient regulation 5 (PGR5)/PGR5 like 1 (PGRL1) dependent pathway (Shikanai, 2007). Recent studies show that Fd functions as an electron carrier in these CEF pathway (Yamamoto et al., 2011; Yamamoto and Shikanai, 2013).

By the remarkable progress of the techniques in molecular genetics and molecular biology, various components involving AEF and the regulation of ΔpH are proposed these days. The isolation of the mutant is a strong tool for considering the molecular function through their phenotypes. However, it has been less discussed whether these AEFs are truly capable to support the photosynthetic electron transport reaction. That is, recent reports have focused on the existence of the component or phenomenon; however the quality like enzyme activity and the quantity of the AEFs are less focused. For example, the quantity of NDH-complex on the thylakoid membranes is considerably low (one NDH-complex per 100 PSI), and the quality of electron transport reaction is

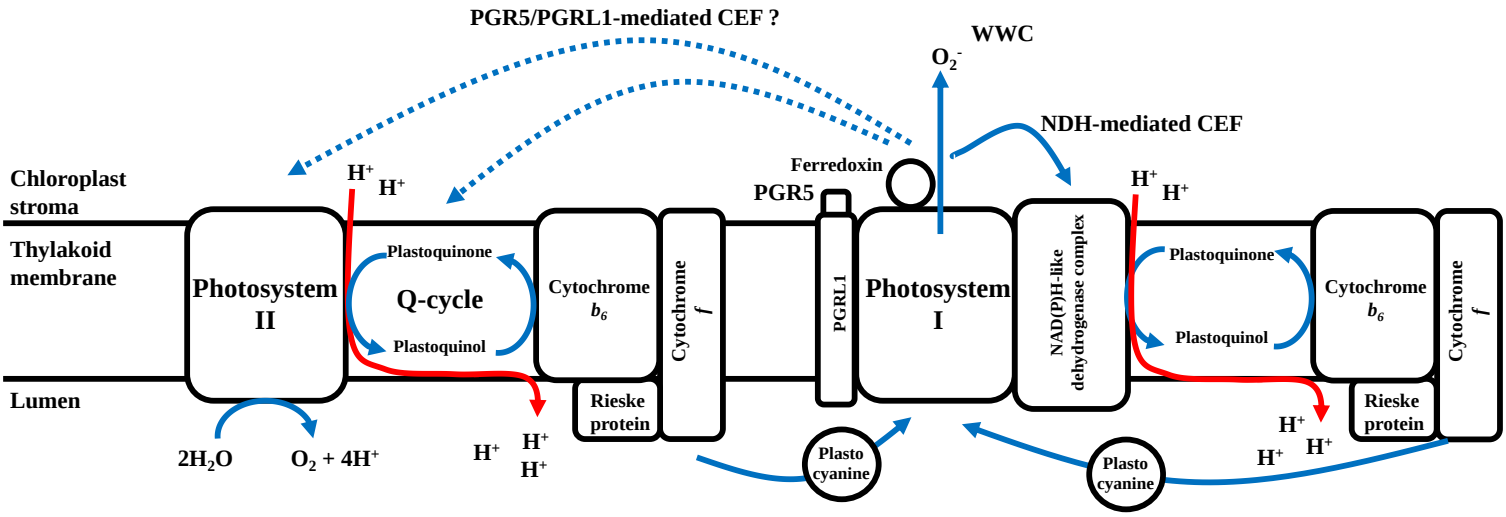

Figure I-2

The over-view of AEF in higher plants.

Blue arrows indicate the pathway of electrons, and red arrows indicate the pathway of protons.

far from the rate of LEF (Sazanov et al., 1998; Trouillard et al., 2012). Therefore, molecular mechanisms involving the regulation of AEF and ΔpH have been unclear when these mechanisms are considered quantitatively and qualitatively (Takagi and Miyake, 2014).

Sugars and sugar-derived RCS also stimulates oxidative stress in the cell

In addition to the above biochemical reactions, sugars also stimulate oxidative stress. Reducing sugars such as glucose or fructose undergo autoxidation to directly produce ROS (Wolff and Dean, 1987; Zhao et al., 1998). Sugars also induce oxidative stress by producing sugar-derived reactive carbonyl species (RCS) via Maillard reaction (Vistoli et al., 2013; Suh et al., 2014). In heterotrophs, including humans, glycolysis is the most important metabolic pathway in the formation of cellular energy sources (i.e., NADPH and ATP) from sugars. However, this pathway inevitably generates RCS such as including methylglyoxal (MG), glyoxal (GLO), and 3-deoxyglucosone (3-DG) as by-products. The production mechanisms of sugar-derived RCS are shown as follows. First, triose phosphate isomerase (TPI) catalyzes the equilibration reaction between dihydroxyacetone phosphate (DHAP) and glyceraldehyde 3-phosphate (GAP), producing MG and GLO as a by-product (Phillips and Thornalley 1993). Second, DHAP non-enzymatically reacts with GAP to produce MG and GLO (Phillips and Thornalley 1993). Third, the aldehyde group of sugars reacts with free amino acids or amino acid groups in proteins to produce Schiff base, which is converted to a RCS by Amadori rearrangement (Vistoli et al. 2013). Fourth, sugars containing an aldehyde group undergo auto-oxidation and degradation to produce MG, GLO, and 3-DG (Vistoli et al. 2013). Fifth, sugar auto-oxidation produces O_2^- (Medina-Navarro et al. 2003), which are rapidly converted into H_2O_2 and O_2 by superoxide dismutase. The Fenton reaction catalyzes the conversion of these products into the most reactive ROS, OH·, using transition metals (Stadtman and Levine 2003). The degradation of sugars by OH· produces RCS as by-products. Therefore, RCS are inevitably generated by sugar metabolism in the glycolytic pathway essential for cellular energy production in heterotrophs.

Sugar-derived RCS react with all major cell components including DNA, proteins, and lipids,

resulting in reduced or aberrant physiological functions. For example, the interaction between MG, GLO, or 3-DG and amino acids (Arg, Lys, or His) produces glycated amino acids in proteins: carboxylmethyl-Lys (CML), carboxylethyl-Lys (CEL), GLO-Arg, GLO-His, and 3DG-His (Thornalley et al. 1999; Vistoli et al., 2013). They crosslink to form dimers (GOLD, GLO-derived lysine dimer; MOLD, MG-derived lysine dimer; and DOLD, 3DG-derived lysine dimer) (Aldini et al. 2013, Vistoli et al. 2013). Because these modifications involve the conformational change of protein or the formation of cross linkage between proteins, the modified proteins lose their physiological functions and cause metabolic disorder (Yan and Harding, 1997; Niwa and Tsukushi, 2001; Morgan et al., 2002; Lee et al., 2005; Hamelin et al., 2007; Bakala et al., 2012). These RCS-modified proteins, which are termed as advanced glycation endo-products (AGEs). These AGEs are found in excess in patients with diabetes mellitus, and they are associated with major complications including retinopathy, nephropathy, neuropathy, arteriosclerosis, and cardiac insufficiency (Jaganjac et al. 2013).

In contrast to heterotrophs, how do photosynthetic autotrophs which produce sugars by themselves cause the threat of RCS attacks? Do higher plants suffer from sugar-derived RCS dependent oxidative damage? Saito et al. (2011) reported that MG acts as a Hill oxidant in chloroplast, and stimulates the ROS production in photosynthesis. MG accumulates in higher plants under various abiotic stress conditions (cold, drought, salt etc.) (Hossain et al., 2009). Yadav et al. (2005) reported that the content of MG in plant tissue increased by 73% under salinity stress conditions, compared to normal conditions. Moreover, the accumulated MG disturbs the redox state of glutathione, which is non-enzymatic antioxidant, in the plant cell and suppresses the detoxification of ROS (Yadav et al., 2005). Based on these reports, the production and accumulation of sugar-derived RCS would stimulate oxidative stress in plant cell. Importantly, although the accumulation of sugar-derived RCS in plant cell is observed, the mechanisms how sugar-derived RCS are produced and the production site of sugar-derived RCS in plant cell have remained to be clarified.

The vulnerability of lipid in chloroplast against ROS, and the effect of lipid-derived RCS in chloroplasts

Amongst biomolecules, lipids, especially polyunsaturated fatty acids (PUFAs), are easily oxidized by ROS. When PUFAs react with ROS, sequential lipid peroxidation reactions start to occur. An allylic/bis-allylic hydrogen atom in PUFAs is highly reactive against ROS, especially OH· (Møller et al., 2007; Poon, 2009). The allylic hydrogen atom in PUFAs is extracted by these radical species, and then lipid radical (L·) is formed (Vistoli et al., 2013). Subsequently, the L· reacts with O_2 and forms lipid peroxyl (LOO·) and lipid alkoxyl radical (LO·) (Vistoli et al., 2013). LOO· and LO· cause radical chain oxidation to lipid peroxidation by reacting with neighboring lipid molecules, as a result of which lipid peroxide (LOOH) and L· accumulate (Catala, 2010). This sequential lipid peroxidation cycle disturbs membrane structures and its fluidity; thus, the physiological functions of membranes are inactivated (Pamplona, 2011). Furthermore, LOOH produces lipid-derived RCS such as α, β-unsaturated carbonyls, di-carbonyls, and keto-aldehydes as intermediate products through their break-down (Vistoli et al., 2013). The electrophilic moieties in lipid-derived RCS are capable of reacting with DNA and proteins that contain nucleophilic amino acids (such as Cys, His, Lys, and Arg), and form advanced lipoxidation end products (ALEs) through the formation of Michael adducts and Schiff bases (Esterbauer et al., 1991; Miyata et al., 2000; Aldini et al., 2006). The formation of ALEs from DNA and proteins is accompanied by their structural changes or cross-linkages, and DNA and proteins lose their intrinsic physiological functions (Pamplona, 2011).

Chloroplasts in higher plants are PUFA-rich organelles. Monogalactosyldiacylglycerol (MGDG) and digalactosyldiacylglycerol (DGDG) are major constituents of chloroplasts, and fatty-acid moieties, which constitute these lipid molecules, are highly unsaturated (MGDG, 18:3 approximately 60%, 16:3 approximately 30%; DGDG, 18:3 approximately 70%, 16:3 approximately 2%) (Douce et al., 1974; Kelly et al., 2003; Block et al., 2007). Chloroplasts are major ROS-producing organelles, and O_2^-, OH· and $^1O_2$ are inevitably produced by photosynthetic electron transport reactions (Asada and Takahashi, 1987). These facts suggest that chloroplasts are exposed to

a high risk of lipid peroxidation. Indeed, Mano et al. (2014a) reported that the *Arabidopsis fad7fad8* double mutant contained less lipid-derived RCS [acrolein, crotonaldehyde, and malondialdehyde (MDA)] in leaves, compared to wild-type plant (WT) leaves. Both *Arabidopsis FAD7* and *FAD8* encode chloroplastic ω-3 fatty acid desaturases that convert 16:2 and 18:2 fatty acids into 16:3 and 18:3 fatty acids (Iba et al., 1993; McConn et al., 1994). Hence, the double *fad7fad8* mutant suppressed the production of 16:3 and 18:3 fatty acids, and these lipid molecules that constitute chloroplasts are less unsaturated (McConn et al., 1994). These reports indicate that chloroplasts are an important source of lipid-derived RCS in plants.

As well as sugar-derived RCS, lipid-derived RCS also modify various enzymes in plant cells and inhibit their catalytic activities. The additions of acrolein, crotonaldehyde, or 4-hydroxyl-2-nonenal (HNE) to isolated chloroplasts inhibit the activities of the Calvin cycle enzymes, especially thiol-regulated phosphoribulokinase (PRK) and glyceraldehyde-3-phosphate dehydrogenase (GAPDH) (Mano et al., 2009). The inhibition of enzyme activities reduces the CO_2 assimilation rate in chloroplasts (Mano et al., 2009). In addition, Rubisco, 33 kDa oxygen evolving complex (OEC), and light harvesting complex (LHC) are modified by MDA under heat stress conditions *in vivo* (Yamauchi et al., 2008; Yamauchi and Sugimoto, 2010). Furthermore, recent studies revealed that lipid-derived RCS modify not only chloroplastic enzymes but also cytosolic and mitochondrial enzymes in plant leaves (Fujita and Hossain, 2003; Hoque et al., 2012a; Mano et al., 2014b). These facts indicate that the production and accumulation of lipid-derived RCS should be dangerous for plants. However, in spite of these studies on the effect of lipid-derived RCS in plants, the mechanism of how lipid-derived RCS affect plant physiological reactions such as photosynthesis or respiration is less clear *in vivo*. Does lipid-derived RCS threaten of plant fitness in plant life cycle? Because of these problems, the danger of the accumulation of lipid-derived RCS in plants is still elusive.

Objectives of this study

In the above section, I reviewed the phenomenon of photoihibition and protecting mechanism toward the photoinhibition. However, their detail molecular mechanisms have remained to be clarified. Furthermore, although RCS stimulates the oxidative stress in chloroplasts, the production mechanisms of the RCS in plant cells are not identified. In addition, it has not been clarified how the accumulation of RCS modifies physiological reaction in plant cells.

In this study, I aimed to clarify two things as follows; first, the molecular mechanisms of PSI photoinhibition in higher plants, and the regulatory mechanisms of photosynthetic electron transport reaction for preventing ROS production and PSI photoinhibition. Second, the production mechanisms and the physiological effects of sugar- and lipid-derived RCS in plant cells. These knowledges obtained in this study are important to improve plant fitness against ROS and RCS produced in plant cells, especially under environmental stress conditions, and this is also expected to help the generation of high-yield crop plants by applying the feature of the tolerance toward ROS and RCS, which involves in the oxidative stress.

Chapter 2

Elucidation of the mechanisms of oxygen-dependent photoinhibition in photosystem I

~ High-light acclimation gives wheat plants tolerance to O_2-dependent PSI photoinhibition induced by reactive oxygen species produced within thylakoid membranes ~

ABSTRACT

Photosystem I (PSI) photoinhibition suppresses plant photosynthesis and growth. However, the mechanism underlying PSI photoinhibition has not been fully clarified. To study the PSI photoinhibition mechanism, I applied repetitive short-pulse (rSP) illumination, which causes photoinhibition specific to PSI in isolated chloroplasts and wheat leaves. I found rSP treatment caused PSI photoinhibition in isolated chloroplasts in the presence of O_2, however chloroplastic superoxide dismutase and ascorbate peroxidase activities did not affect PSI photoinhibition. Importantly, PSI photoinhibition was largely alleviated in the presence of methyl viologen, which stimulates the production of reactive oxygen species (ROS) at stromal region by accepting electrons from PSI. These results suggest that PSI photoinhibition is caused by ROS produced within thylakoid membranes when PSI becomes highly reduced, but ROS produced in the stromal region in chloroplasts are not major causes of PSI photoinhibition. Furthermore, I found that singlet oxygen partially involved in PSI photoinhibition induced by rSP treatment. In addition to above *in vitro* analysis, I showed that the extent of PSI photoinhibition is alleviated in wheat plants grown under high-light conditions, compared to those grown under low-light conditions. I observed that the acclimatory response toward the PSI photoinhibition is different between wheat cultivars, although photosynthetic electron transport activity before rSP treatment is similar. On the basis of these results, I suggest that high-light acclimation induces protection mechanisms against PSI photoinhibition, which are independent of photosynthetic electron transport activity in wheat plants.

INTRODUCTION

The occurrence of PSI photoinhibition has been confirmed in many studies. However, the molecular mechanisms underlying PSI photoinhibition have not been clarified. For example, the production site of ROS, which induce PSI photoinhibition, has not been discovered. Furthermore, it is difficult to analyze PSI photoinhibition because PSI is highly resistant to photoinhibition (Terashima et al., 1994). In previous studies, specific materials and experimental conditions (such as chilling sensitive plants and cold temperatures) are often used to induce PSI photoinhibition *in vivo* (Terashima et al., 1994; Sonoike et al., 1995). These experimental limitations complicate the elucidation of the molecular mechanisms underlying PSI photoinhibition, and the mechanisms that protect PSI from photoinhibition.

Recently, our research group have succeeded in establishing a method to specifically induce PSI photoinhibition in higher plant leaves by repetitively illuminating leaves with short-pulse light under dark conditions at room temperature [named repetitive short-pulse (rSP) treatment] (Sejima et al., 2014; Zivcak et al., 2015a, b). PSI photoinhibition induced by rSP treatment requires O_2, and rSP treatment decreases the total content of P700 chlorophyll. Based on these results, I proposed that rSP treatment stimulates the production of ROS in PSI, and that ROS decreases P700 chlorophyll levels. Furthermore, I also observed that there was a decrease in P700 chlorophyll when I used a light intensity similar to the sun (2,000 μE m^{-2} s^{-1}) in rSP treatment (Sejima et al., 2014). This result indicated that sunflecks stimulate PSI photoinhibition under natural field conditions. The elucidation of the PSI photoinhibition induced by rSP treatment would improve our understanding of the mechanism underlying photoinhibition in PSI under natural field conditions.

In this study, I investigated two aspects of the process. First, the mechanism underlying O_2-dependent PSI photoinhibition induced by rSP treatment; and second, I clarified whether the susceptibility to PSI photoinhibition changes in higher plants depending on their growth light environment or plant species. I found that ROS produced within the thylakoid membranes promoted the degradation of P700 chlorophyll during rSP treatment and induced PSI photoinhibition.

Furthermore, I found that PSI photoinhibition induced by rSP treatment is alleviated in wheat plants grown under high-light conditions, compared to those grown under low-light conditions. The extent to which PSI photoinhibition is alleviated depended on the type of wheat cultivar. From these results, I discussed the relationship between ROS production mechanism, PSI photoinhibition, and protection mechanisms against PSI photoinhibition.

MATERIALS AND METHODS

Isolation of intact chloroplasts from spinach leaves

Intact chloroplasts were isolated from spinach (*Spinacia oleracea* L.) leaves purchased from a local market and purified by Percoll density gradient centrifugation, as described previously (Takagi et al., 2012). The isolated chloroplasts were suspended in a reaction mixture [50 mM 4-(2-hydroxyethyl) piperazine-1-ethansulfonic acid-potassium hydrate (HEPES-KOH), pH 7.6; 0.33 M sorbitol; 10 mM sodium chloride (NaCl); 1 mM magnesium chloride ($MgCl_2$); 2 mM 2-({2-[bis(carboxymethyl)amino]ethyl-(carbonymethyl)}amino)acetic acid (EDTA); and 0.5 mM monopotassium phosphate (KH_2PO_4)]. The intactness of the purified chloroplasts was determined by the ferricyanide method (Heber and Santarius, 1970), and 85–95% of the intact chloroplasts were used in our experiment. The chlorophyll content was determined as described previously (Arnon, 1949).

Oxygen exchange analysis in isolated chloroplasts

A chloroplast suspension that had either been incubated in a dark for 1 h or subjected to rSP treatment for 1 h was placed in an oxygen electrode cuvette (DW 2/2; Hansatech Ltd, King's Lyn, UK) equipped with actinic red light (AL) (> 640 nm). Temperature was maintained at 25^{o}C and controlled by circulating temperature controlled water through the water jacket. The PSII, PSI, and whole chain activities were measured as described in Miyake and Okamura (2003). PSII activity in the chloroplasts was determined by the O_2 evolution rate. 2,6-dimethyl benzoquinone (500 μM) and nigericin (0.5 μM) were added to the chloroplast suspension, and illuminated with AL. PSI activity was determined by the O_2 absorption rate. Dichlorophenolindophenol (70 μM), nigericin (0.5 μM), KCN (0.1 mM), ascorbate (1 mM), MV (100 μM), and 3-(3,4‐dichlorophenyl)‐1,1‐

dimethylurea (10 μM) were added to the chloroplast suspension, and illuminated with AL. Whole-chain activity of the photosynthetic electron transport reaction was determined by the O_2 absorption rate. Nigericin (0.5 μM), KCN (0.1 mM), and MV (100 μM) were also added to chloroplast suspension, and illuminated with AL.

Enzyme assay of chloroplastic SOD and APX

Chloroplastic APX activities were determined in a reaction mixture containing isolated chloroplasts (60 μg Chl), 50 mM potassium phosphate (pH 7.0), 0.5 mM ascorbate, and 5 mM H_2O_2 (Miyake and Asada, 1992). APX activities were measured by H_2O_2-dependent oxidation of ascorbate. The oxidation of ascorbate was monitored by the decrease in absorbance at 290 nm (The absorption coefficient was 2.8 mM^{-1} cm^{-1}). Chloroplastic SOD activities were determined using the xanthine oxidase/cytochrome c method (McCord and Fridovich, 1969). Chloroplastic SOD activities were measured in a reaction mixture containing isolated chloroplasts (60 μg Chl), 300 mM potassium phosphate (pH 8.0), 60 μM cytochrome c, 0.3 mM xanthine, and 120 mU xanthine oxidase. The reduction of cytochrome *c* was measured at 550 nm.

Plant materials

In this study, I used three spring wheat cultivars [*Triticum aestivum* L. cv. Chinese Spring (CS), Bob White (Bob), and Haruyokoi (Haru)] and three winter wheat cultivars [*Triticum aestivum* L. cv. Mironovskaya 808 (M808), Norin 61 (N61), and Akadaruma (Aka)]. Seeds were imbibed using wet cotton at 4°C for 3 days to promote synchronized germination. The imbibed seeds were grown in a mixture of soil (Metro-Mix 350; Sun Gro Horticulture, Bellevue, WA, USA) and vermiculite (Konan, Osaka, Japan) in pots (7.5 cm × 7.5 cm in width and 6 cm in depth). The plants were placed in an

environmentally controlled chamber with 14 h of light (25°C) and 10 h of darkness (20°C). The light intensity was 700–800 μE m^{-2} s^{-1} (HL conditions) or 50–60μE m^{-2} s^{-1} (LL conditions). The seedlings were watered every second day with 0.1% Hyponex solution (N:P:K = 5:10:5, Hyponex, Osaka, Japan). Analyses were carried out on fully expanded mature leaves of plants grown for at least 6 weeks.

Measurements of chlorophyll, and total carotenoid content in leaves.

The chlorophyll and total carotenoids content was measured by the method of Porra et al., (1989), and the method of Wellburn, (1994). Leaf segments were incubated in N, N-dimethylformamide at 4^{o}C overnight. Absorbance at 750, 663.8, 646.8 nm, and 480 nm were measured to calculate chlorophyll, and total carotenoids content. Chlorophyll and total carotenoids content in leaves was represented by leaf area base.

Measurement of chlorophyll fluorescence and $P700^{+}$

Chlorophyll fluorescence and $P700^{+}$ were simultaneously measured with a Dual-PAM-100 (Heintz Walz GmbH, Effeltrich, Germany). Atmospheric gas (40 Pa CO_2/21 kPa O_2) and gas with the indicated mixture of pure O_2 and CO_2 were prepared by mixing 20.1% (v/v) O_2 in 79.9% (v/v) N_2, 1% (v/v) CO_2 in 99% N_2, and pure N_2 gas using a mass-flow controller (Kofloc model 1203; Kojima Instrument Co., Kyoto, Japan) was used in this study. The gases were saturated with water vapor at 13.5 ± 0.1°C and the leaf temperature was maintained at 25°C. The chlorophyll fluorescence parameters were calculated as follows (Baker 2008): maximum quantum efficiency of PSII photochemistry, Fv/Fm = (Fm − Fo) / Fm; quantum yield of photochemical energy conversion in PSII, Y(II) = (Fm' − Fs) / Fm'; Fo, minimum fluorescence yield; Fm, maximum fluorescence yield; and Fs, steady state fluorescence yield. Measuring light (0.1 μE m^{-2} s^{-1}) and saturated pulse (20,000 μE m^{-2} s^{-1}, 300 ms) were applied to determine Fo and Fm. The oxidation-reduction state of $P700^{+}$

was determined according to the methods of Klughammer and Schreiber (1994) as follows: quantum yield of photochemical energy in PSI, Y(I) = (Pm' − P) / Pm; quantum yield of non-photochemical quenching due to the acceptor side limitation, Y(NA) = (Pm − Pm') / Pm; and quantum yield of non-photochemical quenching due to the donor side limitation, Y(ND) = P / Pm. The maximum oxidation level of P700 chlorophyll (Pm) was obtained by a saturated pulse under far-red light and reflected the maximum amount of photooxidized P700 chlorophyll. The parameter P reflects the steady state oxidation level of $P700^{+}$, and Pm' was obtained by a saturated pulse at a steady state. Actinic light (AL), a mixture of red light and blue light, was used to measure the photosynthetic parameters.

rSP treatment

The rSP treatment was applied to chloroplasts that had been isolated from spinach leaves or wheat leaves that had been dark-adapted for at least 1 h, as described previously (Sejima et al., 2014). Isolated chloroplasts or wheat plants were illuminated with short-pulses (20,000 μE m^{-2} s^{-1}, 300 ms) every 10 s in the absence of AL for 1 h under the experimental conditions indicated in the figure legends. After rSP treatment, the photosynthetic parameters of PSII and PSI activity were determined as described in the figure legends.

SDS-PAGE

For protein analysis, an amount of leaf tissue (1.3 cm^2) was homogenized with a pestle in 300 μl extraction buffer (80 mM Tris-HCl, pH 6.8, 1 mM EDTA, 5 % (w/v) glycerol, 2% (w/v) n-Octyl-β-D-glucopyranoside). The homogenate was centrifuged at 15,000 × *g* for 15 min at 4°C, and the supernatant was collected. The proteins were electrophoresed on 12.5 % (w/v) SDS-polyacrylamide gels, as described in Laemmli et al. (1970).

Western blotting

The Proteins were separated by SDS-PAGE, transferred onto polyvinylidene difluoride (PVDF) membrane (Merk Millipore, Massachusetts , USA), and then blocked with blocking one reagent (Nakalai Tesque, Kyoto, Japan) for 30 min at room temperature (25 ^{o}C). The PVDF membrane was subsequently incubated with specific peptide antibody for 1 h at room temperature (25 ^{o}C). The PVDF membrane was washed 3 times with TBS tween buffer (10 mM Tris-HCl (pH 7.4), 0.14 M NaCl, 0.1 % (v/v) Tween-20) and incubated with ECL^{TM} peroxidase labeled anti-rabbit antibody (GE Healthcare, Buckinghamshire, UK) for 1 h at room temperature (25 ^{o}C). The PVDF membrane was washed three times with TBS tween buffer. Proteins were detected with an alkaline phosphatase labeling.

Statistical analysis

All measurement data were expressed as mean value ± SEM of at least three independent analyses. I used ANOVA, Student's t-test, and Tukey-Kramer HSD test to detect differences between the wheat cultivars. All statistical analyses were performed using Microsoft Excel 2010 (Microsoft, Washington, USA) and JMP8 (SAS Institute Inc., Tokyo, Japan).

RESULTS

rSP treatment specifically induces PSI photoinhibition in isolated chloroplasts

First, I applied repetitive short-pulse (rSP) treatment to isolated chloroplasts to elucidate the PSI photoinhibition mechanism induced by rSP treatment, using the method of Sejima et al. (2014) (Fig. II-1). In the rSP treatment, the light intensity of the short-pulse was set to 20,000 μE m^{-2} s^{-1}, the pulse duration was set at 300 ms, and the illumination frequency was every 10 s under dark conditions. Figure II-1a shows the time-course for the change in quantum yield in PSII [Y(II)] and PSI [Y(I)] during rSP treatment. Y(I) considerably decreased during rSP treatment in the absence of electron acceptors in the reaction mixture. Y(ND) and Y(NA) indicate the extent of photosynthetic electron transport limitation at donor-side and the acceptor-side in PSI (Klughammer and Schreiber, 1994). Y(NA) increased during rSP treatment (Fig. II-1b). In contrast, Y(ND) was not induced during the rSP treatment (Fig. II-1c). These results indicate that rSP treatment suppresses the photosynthetic electron transport reaction at the acceptor side of PSI in isolated chloroplasts. On the other hand, Y(II) was less affected during rSP treatment compared to Y(I) (Fig. II-1a). These results are consistent with previous results obtained from intact leaves (Sejima et al., 2014; Zivcak et al., 2015a, b).

I estimated the residual activity of PSII and PSI after rSP treatment, based on the change in the maximum quantum yield of PSII (Fv/Fm) and total amount of P700 chlorophyll (Pm) before and after rSP treatment (Fig. II-1d). The rSP treatment decreased PSII activity to 80%, and PSI activity to 18%. I also analyzed the effect of rSP treatment on PSII, PSI, and whole-chain photosynthetic electron transport activities. PSII activity was estimated from DMBQ-dependent O_2 evolution rate, but there was no difference between the control and rSP treatment samples (Fig. II-2a). In contrast, PSI and the whole-chain photosynthetic electron activities, estimated from the MV-dependent O_2 absorption rate, decreased considerably in the rSP treatment sample, compared to the control (Fig.II-2b and c).

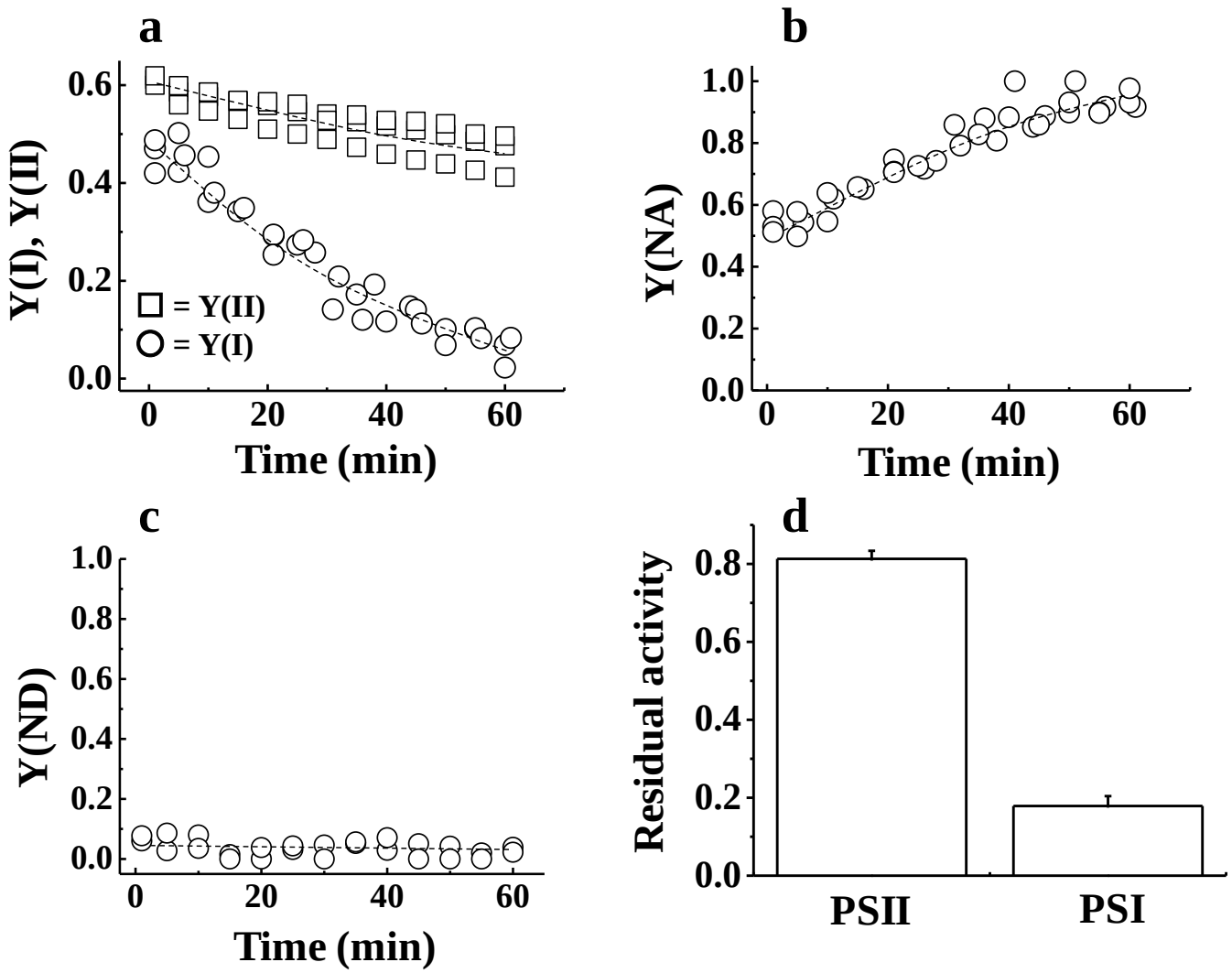

Figure II-1

Time-course analysis of photosynthetic parameters [(a) Y(I) and Y(II), (b) Y(NA), (c) Y(ND)] in isolated chloroplasts. The reaction mixture contained 30 μg ml^{-1} isolated chloroplasts. Isolated chloroplasts were illuminated every 10 s with a short-pulse (300 ms, 20,000 μE m^{-2} s^{-1}) and for 1 h without AL illumination. Experiments were repeated three times. After rSP treatment, the reaction mixture was kept in the dark for 30 min, and Fv/Fm and Pm were measured. Data were normalized to Fv/Fm and Pm before rSP treatment, and data are represented as the residual activity of PSII and PSI after rSP treatment (d). Data are expressed as mean ± SEM of three independent experiments.

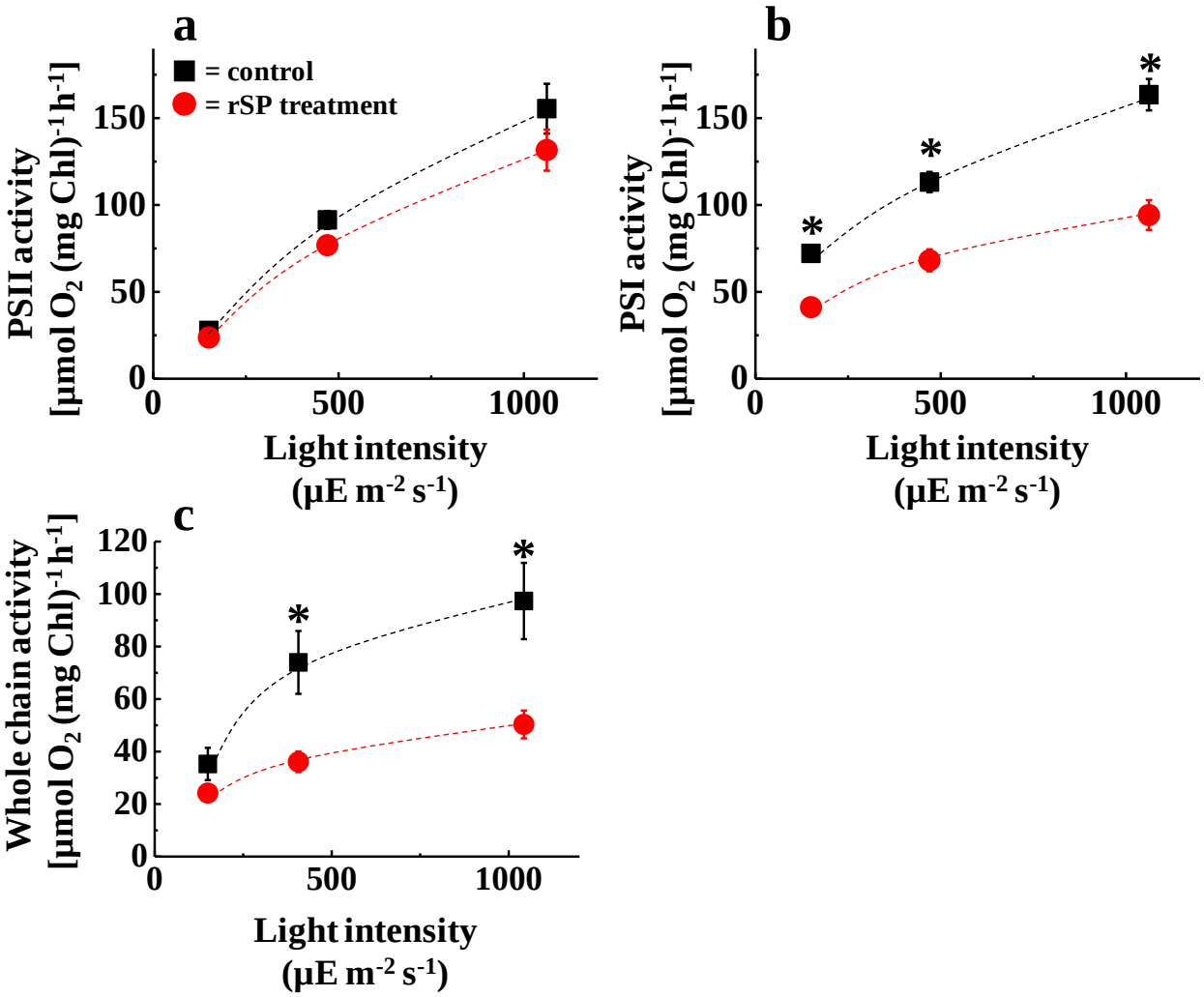

Figure II-2

The light response of PSII (a), PSI (b), and whole-chain photosynthetic electron transport activity (c) in isolated chloroplasts. The reaction mixture contained 30 µg ml^{-1} isolated chloroplasts. Photosynthetic electron activities were measured using an O_2 electrode (see Materials and Methods). Black square indicates photosynthetic electron activities of the control sample that was kept in the dark for 1 h. Red circle indicates photosynthetic electron activities of samples that were processed by SP treatment for 1 h. Data are expressed as the mean ± SEM of three independent experiments. Asterisks indicate a significant difference between the control sample and the rSP treatment sample (Student's *t*-test, $p < 0.05$).

These results indicate that rSP treatment induces photoinhibition that is specific to PSI in isolated chloroplasts, which is similar to leaves (Sejima et al., 2014; Zivcak et al., 2015a, b).

I performed western blot analysis to confirm whether PSI photoinhibition induced by rSP treatment accompanied with protein degradation in PSI. I found that PSI core protein, PsaA, did not decrease after rSP treatment even though P700 chlorophyll content was largely decreased (Fig. II-3). This result indicated that rSP treatment does not stimulate the protein degradation in PSI. As well as PsaA, PSII core protein, PsbB, did not decreased after rSP treatment (Fig. II-3). That is, PSII photoinhibition does not occur at protein level.

Effects of O_2 and methyl viologen on PSI photoinhibition in isolated chloroplasts

I analyzed the effect of rSP treatment under anaerobic conditions to reveal whether PSI photoinhibition requires O_2 in isolated chloroplasts in a similar manner to leaves. Nitrogen gas was bubbled into the reaction mixture to create anaerobic conditions. The decrease in Y(I) during rSP treatment was alleviated under anaerobic conditions compared to aerobic conditions (Fig. II-4a). Furthermore, the residual activity of PSI after rSP treatment was also significantly alleviated under anaerobic conditions compared to aerobic conditions (Fig. II-4b). These results indicate that O_2 stimulates PSI photoinhibition.

Next, I analyzed the effects of methyl viologen (MV) on the rSP treatment (Fig. II-4a). MV accepts electrons from PSI and the reduced MV donates electrons to O_2 to produce the superoxide radical (O_2^-) under aerobic conditions (Babbs et al., 1989). In the presence of MV, there was hardly any decrease in Y(I) during rSP treatment (Fig. II-4a). The residual activity of PSI was significantly higher compared to when MV was not added (Fig. II-4b). In previous reports, PSI photoinhibition was suppressed by limiting photosynthetic electron flow from PSII (Sonoike, 1996a; Sejima et al., 2014). Because MV is able to efficiently accept electrons from PSI, this means that limiting step of the linear electron transport reaction moves from the acceptor side of PSI to plastoquinone (PQ),

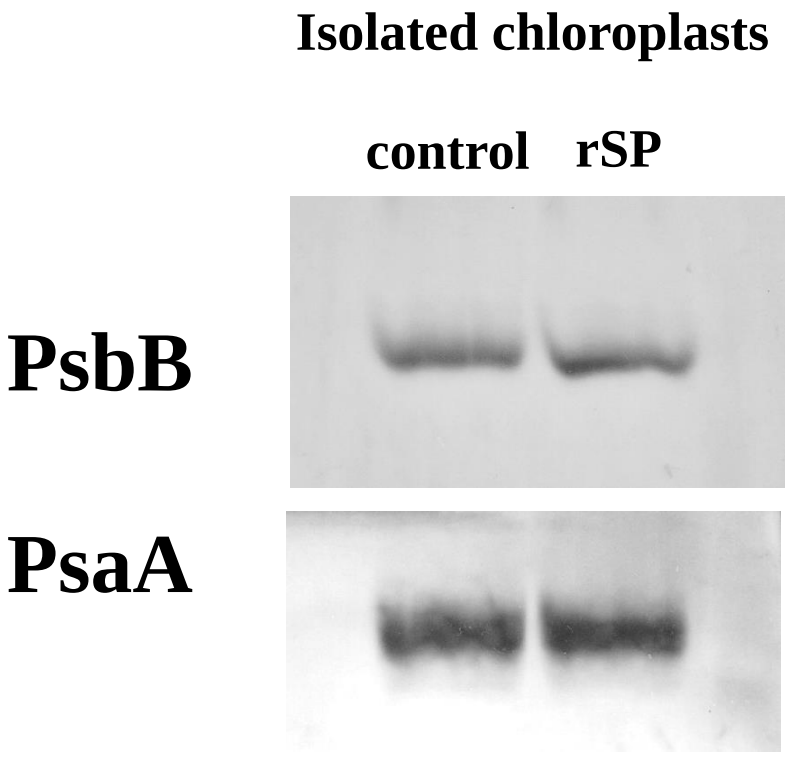

Figure II-3

The comparison of PSII and PSI core protein content in isolated chloroplast between before and after SP treatment. Isolated chloroplasts before rSP treatment were used as a control, and isolated chloroplasts treated rSP treatment for 1h were used as an rSP treated sample. I used antiserum specific to PsbB and PsaA for quantifying PSII and PSI core protein content. The protein corresponding to 0.6 μg chlorophyll was loaded in each lane.

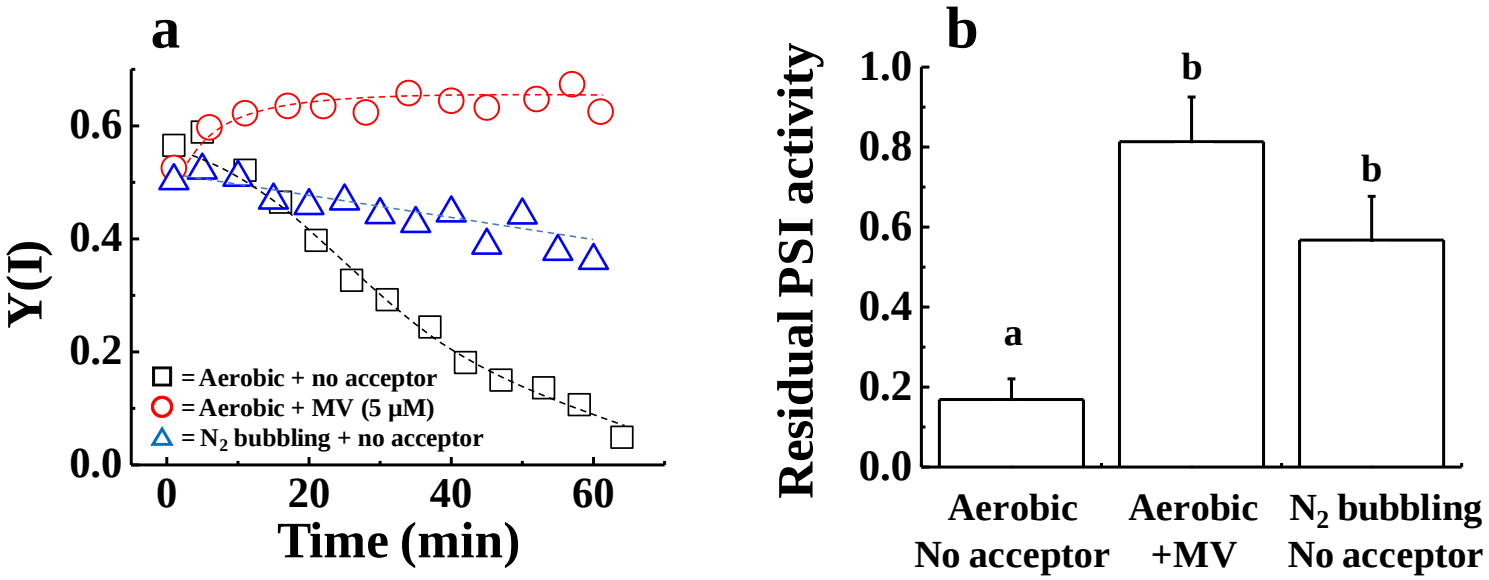

Figure II-4

The time-course analysis of Y(I) in isolated chloroplasts under different experimental conditions (a). The reaction mixture contained 30 µg ml^{-1} isolated chloroplasts. Black square indicates Y(I) in the absence of electron acceptors under aerobic conditions. Red circle indicates Y(I) in the presence of MV (5 µM) under aerobic conditions. Blue triangle indicates Y(I) in the absence of electron acceptors under anaerobic conditions. Experiments were repeated at least three times and representative data are shown. After rSP treatment, the reaction mixture was kept in the dark for 30 min, and the Pm was measured. Data were normalized to the Pm before rSP treatment, and data are the residual activity of PSI after rSP treatment (b). Data are expressed as mean ± SEM of three independent experiments. Different letters above the columns indicate a significant difference between the treatments (Tukey-Kramer HSD test, $p < 0.05$).

which is oxidized by Cytb_6f turnover in the presence of MV (Tikhonov, 2013). Therefore, I cannot dismiss the possibility that the MV-dependent photosynthetic electron transport reaction forms a proton gradient (ΔpH) across the thylakoid membranes during rSP treatment, and that ΔpH suppresses PSI photoinhibition (Sejima et al., 2014).

Effects of the protonophore, nigericin, on PSI photoinhibition

To examine whether MV forms a ΔpH and suppresses PSI photoinhibition during rSP treatment, I applied a protonophore, nigericin, to isolated chloroplasts during rSP treatment. In the absence of MV, the addition of nigericin partially accelerated a decline in Y(I) during rSP treatment, compared to in the absence of nigericin (Fig. II-5). This indicated that a ΔpH was produced during rSP treatment and that electron flow from the donor-side of PSI to the acceptor-side would be limited. This suppresses the reduction of O_2 and the production ROS in PSI. Indeed, the kinetics of oxidized P700 chlorophyll during short-pulse illumination differed considerably in the absence and presence of nigericin (Fig. II-6). In the presence of nigericin, oxidized P700 chlorophyll was rapidly reduced during short-pulse illumination compared to when nigericin was not added. This result indicates that a ΔpH was induced during rSP treatment and this contributed to the suppression of photosynthetic electron flow from PSII to oxidized P700 chlorophyll. On the other hand, in the presence of MV, the addition of nigericin to the reaction mixture did not lead to a decrease in Y(I) (Fig. II-5). This result showed that the reduction in PSI photoinhibition by MV could be due to the leakage of electrons from the acceptor side of PSI, rather than the stimulation of ΔpH formation. The kinetics of oxidized P700 chlorophyll during shot-pulse in the presence of MV showed that oxidized state in P700 chlorophyll was maintained during short-pulse, regardless of the addition of nigericin (Fig. II-6). This result indicated that MV effectively accepts electrons from PSI, and oxidizes P700 chlorophyll during short-pulse illumination.

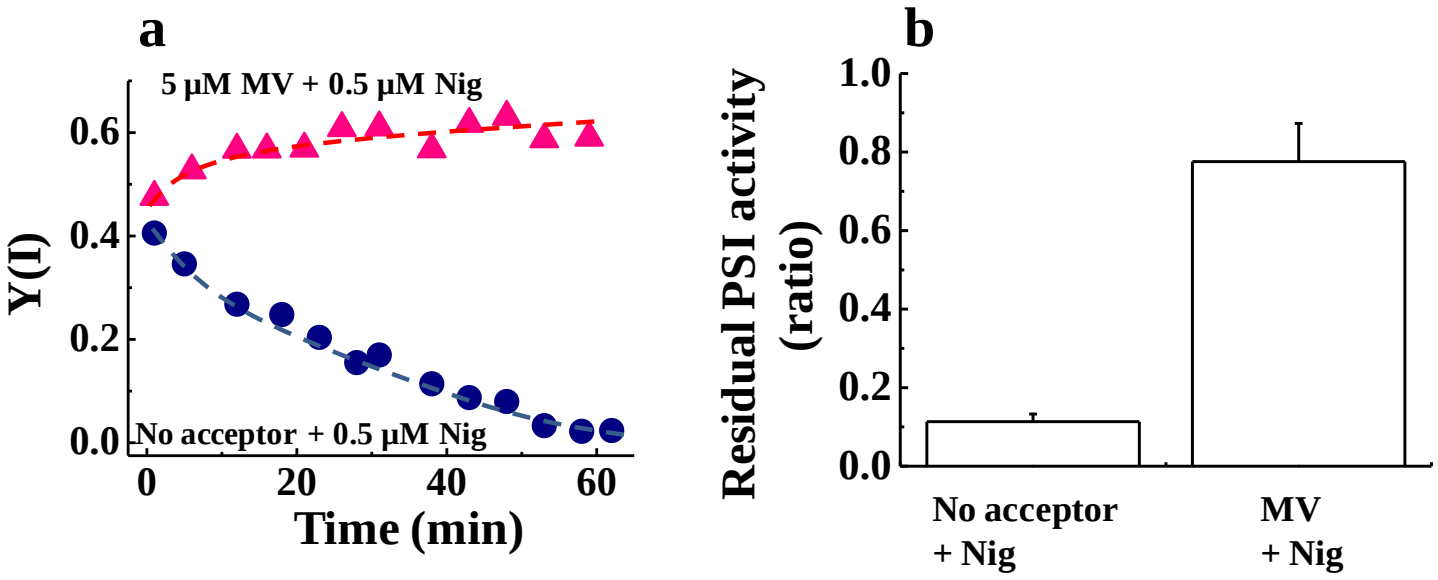

Figure II-5

The effect of nigericin on rSP treatment in the absence and presence of MV. The reaction mixture contains 30 µg ml^{-1} isolated chloroplasts and 0.5 µM nigericin. (a) The time-course analysis of Y(I) in isolated chloroplasts in the absence and presence of MV (5 µM). Experiments were repeated at least three times and representative data are shown. (b) The residual activity of PSI after rSP treatment in the absence and presence of MV. After rSP treatment, the reaction mixture was kept in the dark for 30 min and the Pm was measured. Data were normalized to the Pm before rSP treatment, and the data represents the residual activity of PSI after rSP treatment. Data are expressed as mean ± SEM of three independent experiments.

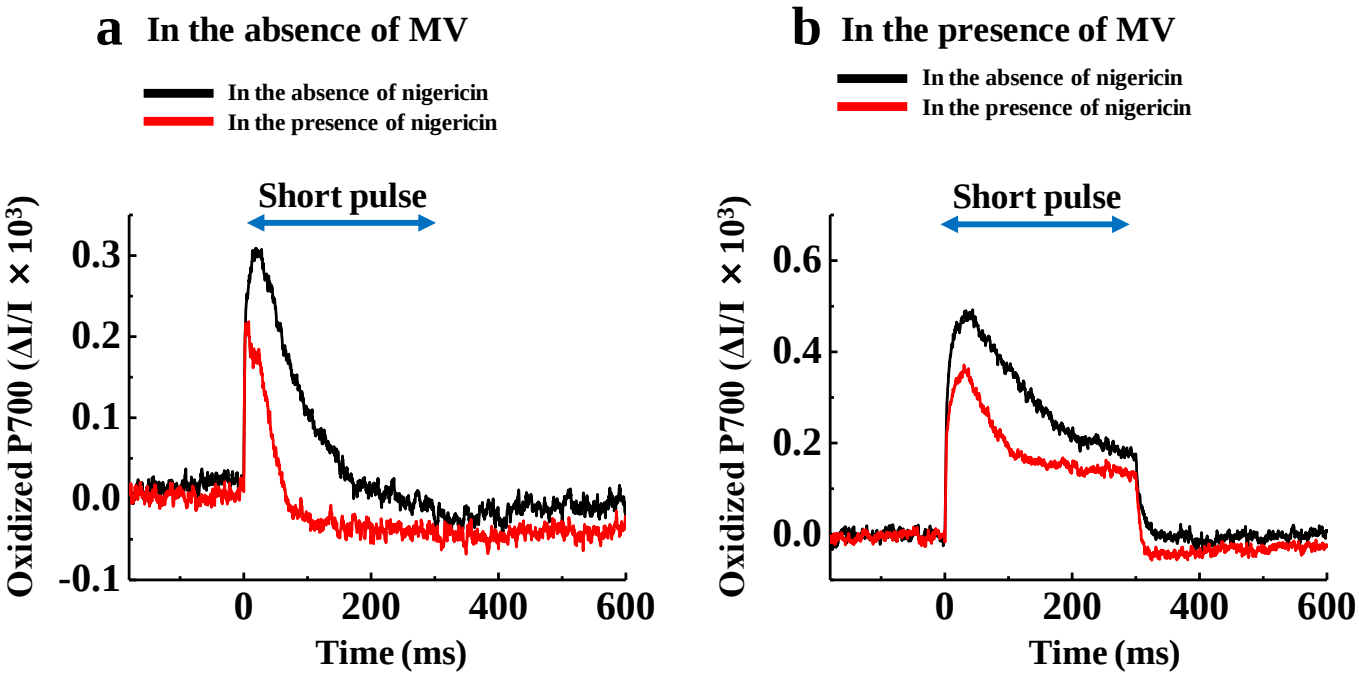

Figure II-6

The kinetics of oxidized P700 induced by a short-pulse in the absence of MV (a) and in the presence of MV (b). The data were obtained after rSP treatment was applied for 5 min. Black line shows the condition in the absence of nigericin. Red line shows the condition in the presence of nigericin. Experiments were at least three times. Short-pulse was illuminated every 10 s, and averaged data during three short-pulse illuminations were shown. The reaction mixture contains 30 μg ml^{-1} isolated chloroplasts.

Chloroplastic superoxide dismutase and ascorbate peroxidase cannot protect PSI from photoinhibition induced by rSP treatment

Higher plants have superoxide dismutase (SOD) and ascorbate peroxidase (APX) in their chloroplasts, and they help detoxify ROS (Miyake et al., 1992; Asada, 2000). First, I analyzed the effects of rSP treatment on chloroplastic SOD and APX to examine whether chloroplastic SOD and APX activities are maintained in isolated chloroplasts during rSP treatment. Comparing chloroplastic SOD and APX activities before and after rSP treatment showed that their activities did not change (Fig. II-7). This result indicated that ROS detoxification activities in isolated chloroplasts were maintained during rSP treatment. Thus, PSI photoinhibition induced by rSP treatment is probably independent of chloroplastic SOD and APX activities. To confirm this possibility, I added KCN to the reaction mixture to inhibit chloroplastic SOD and APX activities and applied the rSP treatment. The addition of KCN did not affect the decrease in Y(I) during rSP treatment (Fig. II-8a). Furthermore, the residual activity of PSI after rSP treatment did not change in the absence or the presence of KCN (Fig. II-8b). These results indicated that chloroplastic SOD and APX do not protect PSI from photoinhibition induced by rSP treatment.

Both O_2^- and $^1O_2$ contribute to PSI photoinhibition induced by rSP treatment

PSI is major ROS production site, and O_2^- was generally recognized to be produced at PSI (Takahashi and Asada, 1988). However, recent reports provide the evidence that PSI also produces $^1O_2$, and $^1O_2$ relates to PSI photoinhibition (Cazzaniga et al., 2012; Rutherford et al., 2012). Furthermore, I revealed that inactivation of APX and SOD does not affect PSI photoinhibition (Fig. II-8). This might indicate that PSI photoinhibition was induced by $^1O_2$ but not O_2^- during rSP treatment. To examine this possibility whether $^1O_2$ related to PSI photoinhibition induced by rSP treatment, I added soluble l-tocopherol analog, 2,2,5,7,8-pentamethyl-6-chromanol (PMC) that is amphipathic $^1O_2$ scavenger to reaction mixture, and conducted rSP treatment (Fryer, 1992; Grams and Inglett, 1972; Munné-Bosch, 2005).

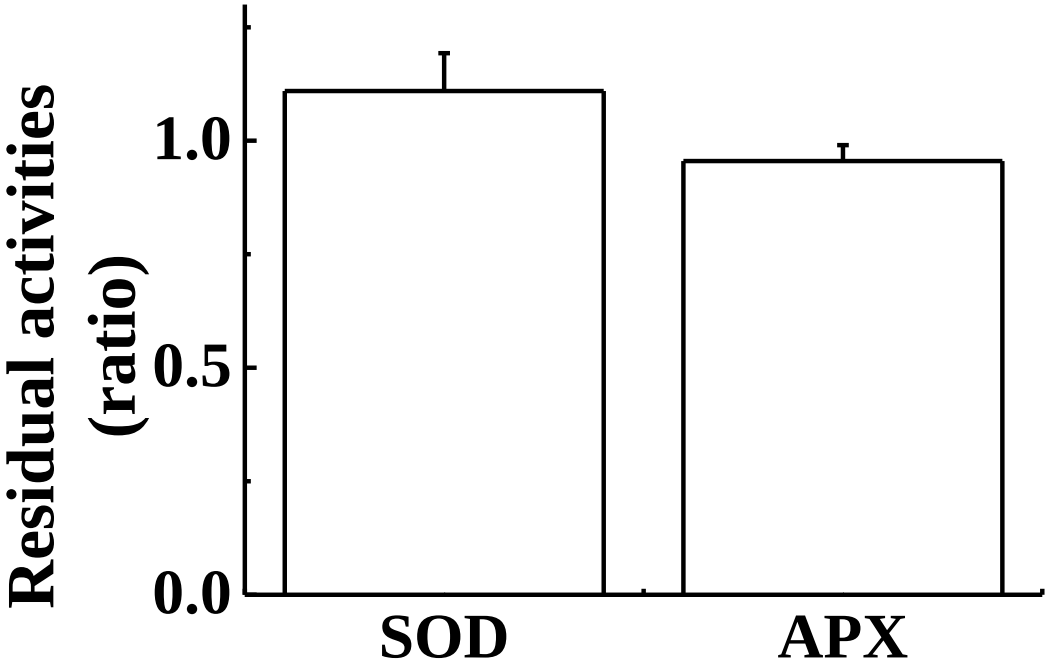

Figure II-7

The change in SOD and APX activities before and after rSP treatment. Chloroplastic SOD and APX activities were compared before and after rSP treatment and the residual activities are their ratio. Data are expressed as mean ± SEM of at least nine independent experiments.

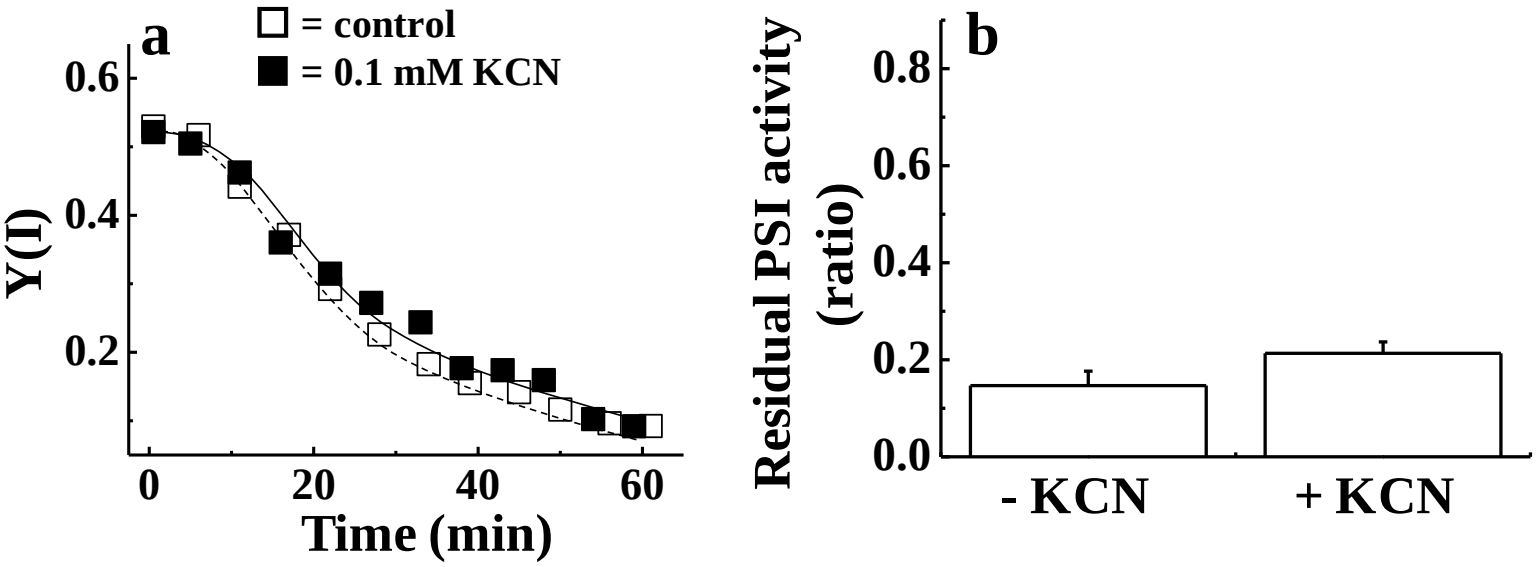

Figure II-8

The effect of KCN on PSI photoinhibition induced by rSP treatment. The reaction mixture contains 30 μg ml^{-1} isolated chloroplasts. (a) The time-course analysis of Y(I) in isolated chloroplasts in the absence (white square) and in the presence of KCN (0.1 mM) (black square). Experiments were repeated at least three times and representative data are shown. After rSP treatment, the reaction mixture was kept in the dark for 30 min, and the Pm was measured. Data were normalized to the Pm before rSP treatment, and the residual activity of PSI after rSP treatment were calculated (b). Data are expressed as mean ± SEM of three independent experiments.

The addition of PMC did not affect the decrease in Y(I) at the first part of rSP treatment (Fig. 5A). In contrast, PMC alleviated the decrease in Y(I) compared to control at the latter part of rSP treatment (Fig. II-9a). The residual activity of PSI after rSP treatment for 1h revealed that the addition of PMC was significantly alleviated the inactivation of PSI compared to control (Fig. II-9bB). In contrast, the residual activity of PSII was not different between in the absence and the presence of PMC (Fig. II-9c). To examine whether PMC acts as an electron acceptor like MV, I analyzed the kinetics of oxidized P700 chlorophyll during the short pulse illumination. I found that PMC did not affect the kinetics of oxidized P700 chlorophyll during short pulse illumination (Fig. II-10). Furthermore, I compared the O_2 absorption rate and Y(II) between in the absence and presence of PMC by using O_2-electrode and chlorophyll fluorescence. Under continuous actinic light illumination (500 μE m^{-2} s^{-1}), PMC did not affect O_2 absorption rate and Y(II) in isolated chloroplasts (Table II-1). From these results, I revealed that PMC does not act as an electron acceptor. When I doubled PMC concentration from 5μM to 10μM, the residual activity of PSI after rSP treatment for 1h was not increased [PSI residual activity = 0.35 ± 0.06 (n=3)]. This result indicated that 5 μM PMC is enough to protect PSI from photoinhibition induced by $^1O_2$.

Wheat plants have protective mechanisms against PSI photoinhibition induced by rSP treatment

To study whether the susceptibility of PSI photoinhibition responds to growth light environment and plant species *in vivo*, I applied the rSP treatment to two wheat cultivars [spring wheat, Chinese spring (CS); winter wheat, Mironovskaya 808 (M808)], which were grown under low-light (LL) and high-light (HL) conditions. First, I analyzed CS and M808 grown under HL conditions. The values for Fv/Fm [CS = 0.793 ± 0.005, M808 = 0.781 ± 0.022, (n = 3)] and Pm [CS = 3.1 ± 0.3, M808 = 4.1 ± 0.7 (n = 3)] were not significantly different between CS and M808. Furthermore, the dependency of Y(II), Y(NPQ), Y(I), Y(NA), and Y(ND) on light intensity was also not different between CS and M808 before rSP treatment (Fig. II-11a, c, e, and g).

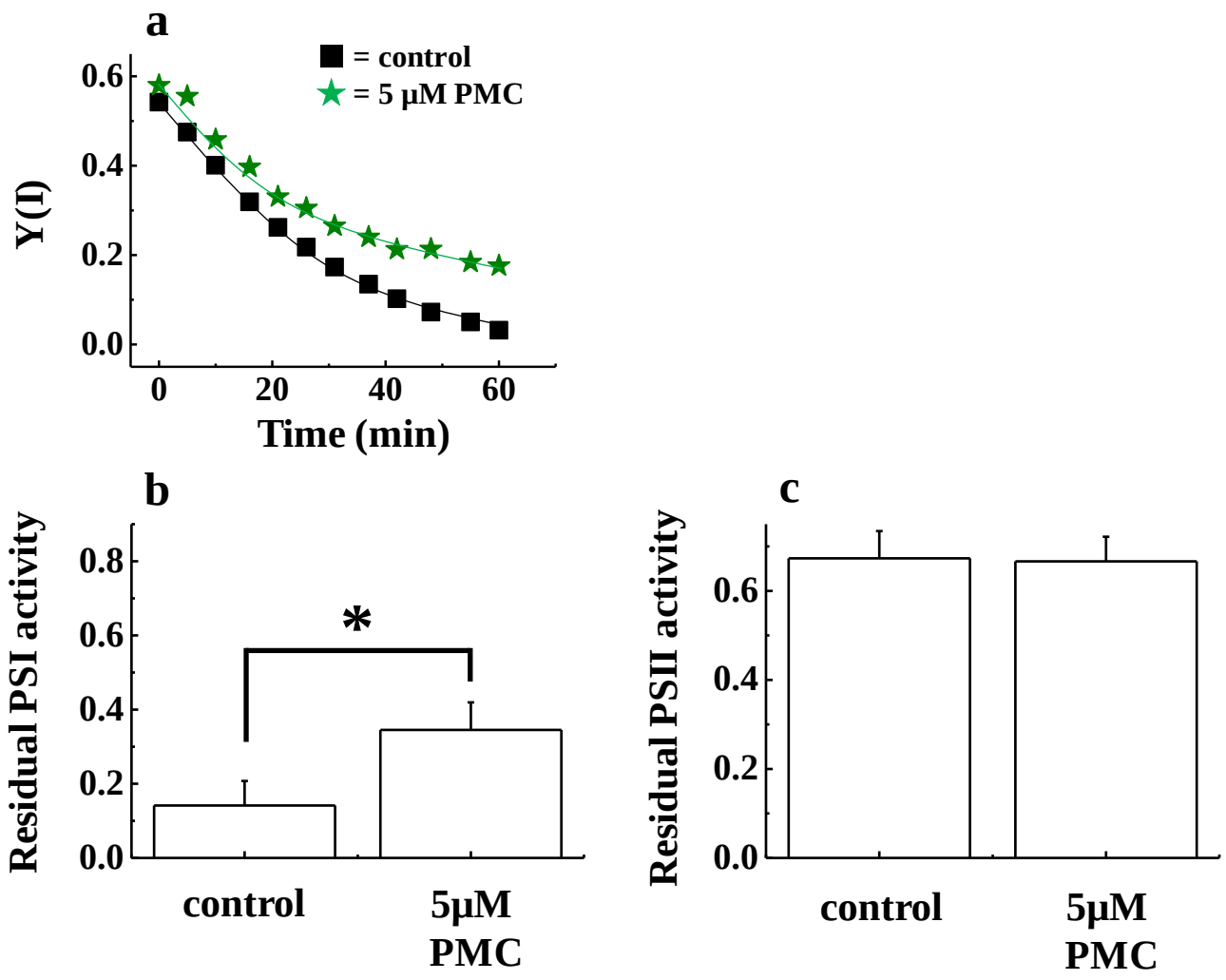

Figure II-9

The effect of PMC on PSI photoinhibition induced by rSP treatment. The reaction mixture contains 30 μg ml^{-1} isolated chloroplasts. (a) The time-course analysis of Y(I) in isolated chloroplasts in the absence (black square) and in the presence of PMC (5 μM) (green star). Experiments were repeated at least three times and representative data are shown. After rSP treatment, the reaction mixture was kept in the dark for 30 min, and the Pm and Fv/Fm were measured. Data were normalized to the Pm and Fv/Fm before rSP treatment, and the residual activity of PSI and PSII after rSP treatment were calculated (b, c). Data are expressed as mean ± SEM of three independent experiments.

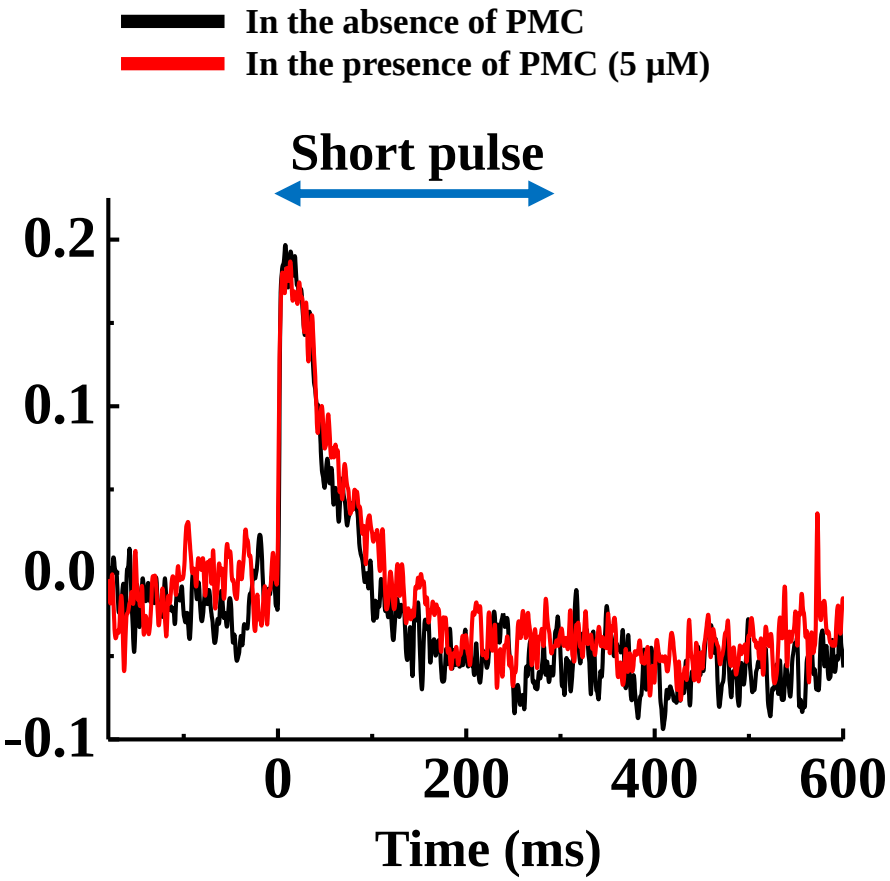

Figure II-10

The kinetics of oxidized P700 induced by a short-pulse in the absence of and in the presence of PMC (5 µM). The reaction mixture contained 30 µg ml^{-1} isolated chloroplasts. The data were obtained after rSP treatment was applied for 5 min. Black line shows the condition in the absence of PMC. Red line shows the condition in the presence of PMC. Experiments were at least three times. Short-pulse was illuminated every 10 s, and averaged data during three short-pulse illuminations were shown.

Table II-1
Oxygen evolution rate and Y(II) in the absence and in the presence of PMC

	control	+PMC (5 µM)
O_2 absorption rate **[µmol O_2 (mg Chl)$^{-1}$ h^{-1}]**	2.87 ± 0.69	2.65 ± 0.51
Y(II)	0.035 ± 0.022	0.035 ± 0.013

Isolated chloroplasts were illuminated by red light (500 µE m^{-2} s^{-1}) and steady state O_2 evolution rate and Y(II) were measured in the absence of and in the presence of PMC (5 µM) in the reaction mixture. The reaction mixture contained 30 µg ml^{-1} isolated chloroplasts. Data are expressed as mean ± SEM of three independent experiments.

In rSP treatment under atmospheric conditions, Y(I) in CS significantly decreased, compared to Y(I) in M808 (Fig. II-12a). The difference in the decrease of Y(I) between CS and M808 was caused by the difference in Y(NA) (Fig. II-13a and c). After rSP treatment for 1 h, the residual activities of PSII (Fv/Fm) and PSI (Pm) after rSP treatment were compared. The residual activity of PSI was significantly higher in M808 than in CS although there was no difference between CS and M808 in the residual activity of PSII (Fig. II-12b). I analyzed the change of PSI core protein content before and after rSP treatment in CS and M808. I found that PsaA protein content in leaf area basis did not change by rSP treatment (Fig. II-14). PSI photoinhibition induced by rSP treatment was alleviated under low O_2 conditions in both CS and M808 (Fig. II-15a). Therefore, these results indicated that the extent of O_2-dependent PSI photoinhibition induced by rSP treatment was different between CS and M808 when grown under HL conditions.

In contrast to the results obtained for HL-grown wheat plants, the decrease in Y(I) during rSP treatment under atmospheric conditions was similar between CS and M808 when they were grown under LL conditions (Fig. II-12c). Furthermore, there was no difference in the residual activities of PSII and PSI between CS and M808 grown under LL conditions after rSP treatment for 1 h (Fig. II-12d). When the rSP treatment was applied under low O_2 conditions, PSI photoinhibition was alleviated, compared to under atmospheric conditions (Fig. II-15b). When CS and M808 were grown under LL conditions, the values for Fv/Fm [CS = 0.773 ± 0.002, M808 = 0.779 ± 0.002, (n = 3); Student's *t*-test, $p > 0.05$] and Pm [CS = 3.2 ± 1.2, M808 = 3.3 ± 0.4 (n = 3)] were similar. Furthermore, the dependency of Y(II), Y(NPQ), Y(I), Y(NA), and Y(ND) on the light intensity was also similar between CS and M808 before rSP treatment (Fig. II-11b, d, f, and h). Compared to HL-grown wheat, LL-grown wheat suffered considerable damage to PSI in a shorter period of time (Fig. II-12). That is, HL acclimation alleviated PSI photoinhibition. Furthermore, I observed that the alleviation of PSI photoinhibition by HL acclimation has diversity between wheat cultivar. CS and M808 are spring and winter wheats, respectively (Kobayashi et al., 2004). Spring and winter wheats have different acclimation responses to cold temperatures or HL, and they have different

photosynthetic abilities after acclimation (Gray et al., 1996; Hurry et al., 1995; Savitch et al., 2000; Pocock et al., 2001; Dahal et al., 2012). For example, winter wheat cultivars grown under HL and low temperature conditions show higher tolerance to PSII photoinhibition than spring wheat cultivars grown under the same conditions (Pocock et al., 2001). To clarify whether susceptibility to PSI photoinhibition can be generally attributed to the difference in growth habits between spring and winter wheat cultivars, I analyzed four additional wheat cultivars (Bob White (Bob) and Haruyokoi (Haru) spring wheats; Norin 61 (N61) and Akadaruma (Aka) winter wheats). However, the susceptibility to PSI photoinhibition was not clearly separated between spring and winter wheat cultivars (Fig. II-16). Therefore, the difference in growth habits between spring and winter wheat cultivars is not necessarily related to the acclimatory responses to PSI photoinhibition susceptibility.

In these wheat plants, I analyzed chlorophyll and total carotenoid content in leaves. In HL-growth wheat plants, there is a variety about chlorophyll content in leaves, and N61 showed highest chlorophyll content, compared to other wheat cultivars, and CS and Aka showed lowest chlorophyll content (Table II-2). However, total carotenoid content was similar between wheat cultivars (Table II-2). On the other hand, there was no difference about chlorophyll and total carotenoids content among LL-grown wheat plants (Table II-3). To examine the relationship among chlorophyll content, chlorophyll *a/b* ratio, and the sensitivity toward PSI photoinhibition induced by rSP treatment, I plotted leaf chlorophyll content and chlorophyll *a/b* ratio against PSI residual activity after rSP treatment for 1h (Fig. II-17). I found that leaf containing high chlorophyll content tended to have higher tolerance toward PSI photoinhibition (Fig. II-17a). In contrast, chlorophyll *a/b* did not show any relationship with the sensitivity of PSI photoinhibition (Fig. II-17b).

I also analyzed PSII and PSI core protein content, and their antenna protein content in wheat cultivars. For this analysis, I examined the content of PsbA, PsaA, LHCb1, and LHCa1 protein content in leaves. In HL-grown wheat plant, clear differences in these protein compositions were not observed among wheat cultivar (Fig. II-18a). Similar to HL-grown wheat plants, the difference in photosynthetic protein composition among wheat cultivars grown under LL-conditions was not

observed (Fig. II-18b).

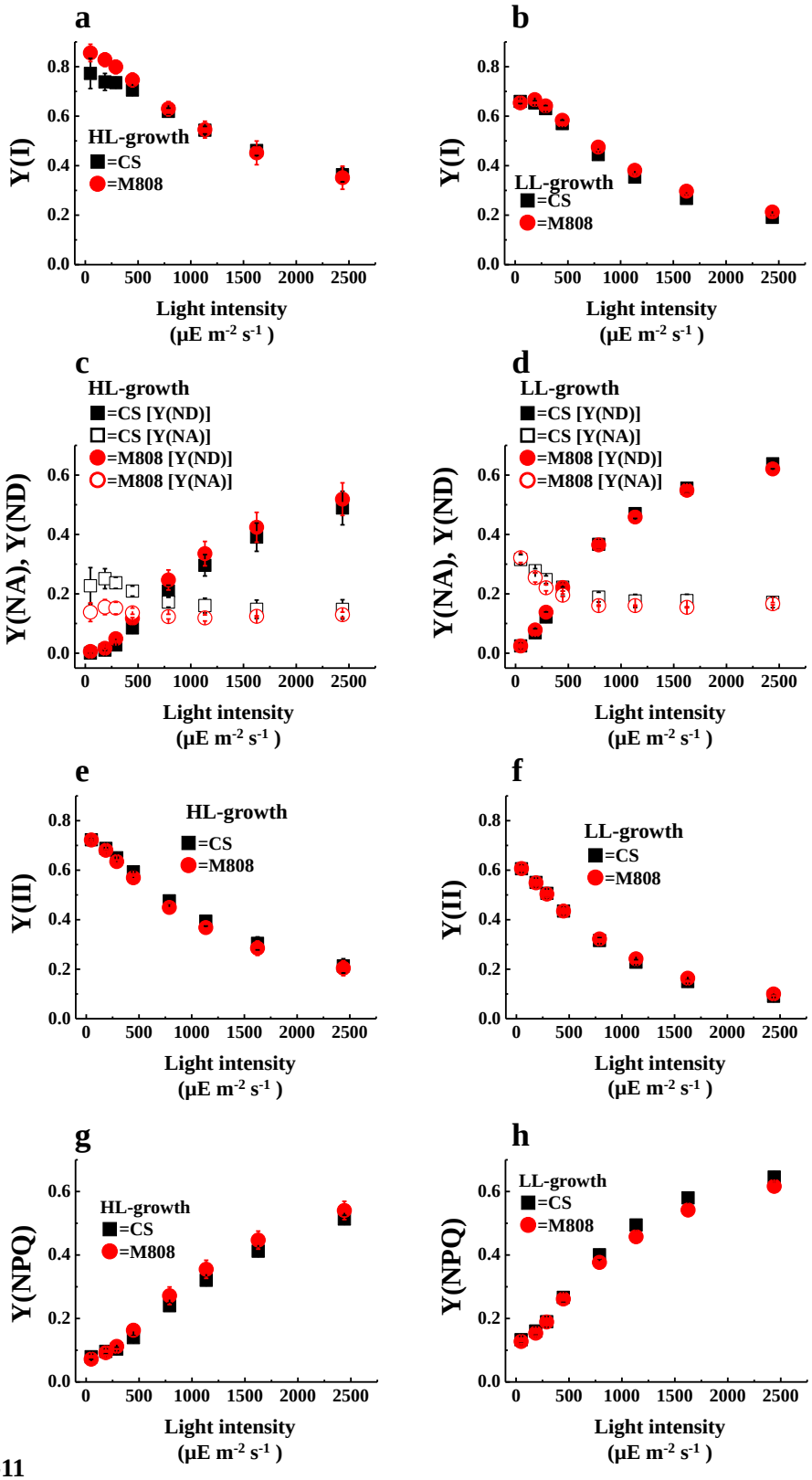

Figure II-11

The light response of Y(I), Y(NA), Y(ND), Y(NPQ), and Y(II) in CS and M808 grown under high-light (a, c, e, and g) and low-light (b, d, f, and h) conditions. The measurements were conducted under atmospheric conditions (21 kPa O_2, 40 Pa CO_2). Before the measurements, the plants were illuminated with AL (400 µE m^{-2} s^{-1}) for 30 min to activate the electron sink. Data are expressed as mean ± SEM of at least three independent experiments.

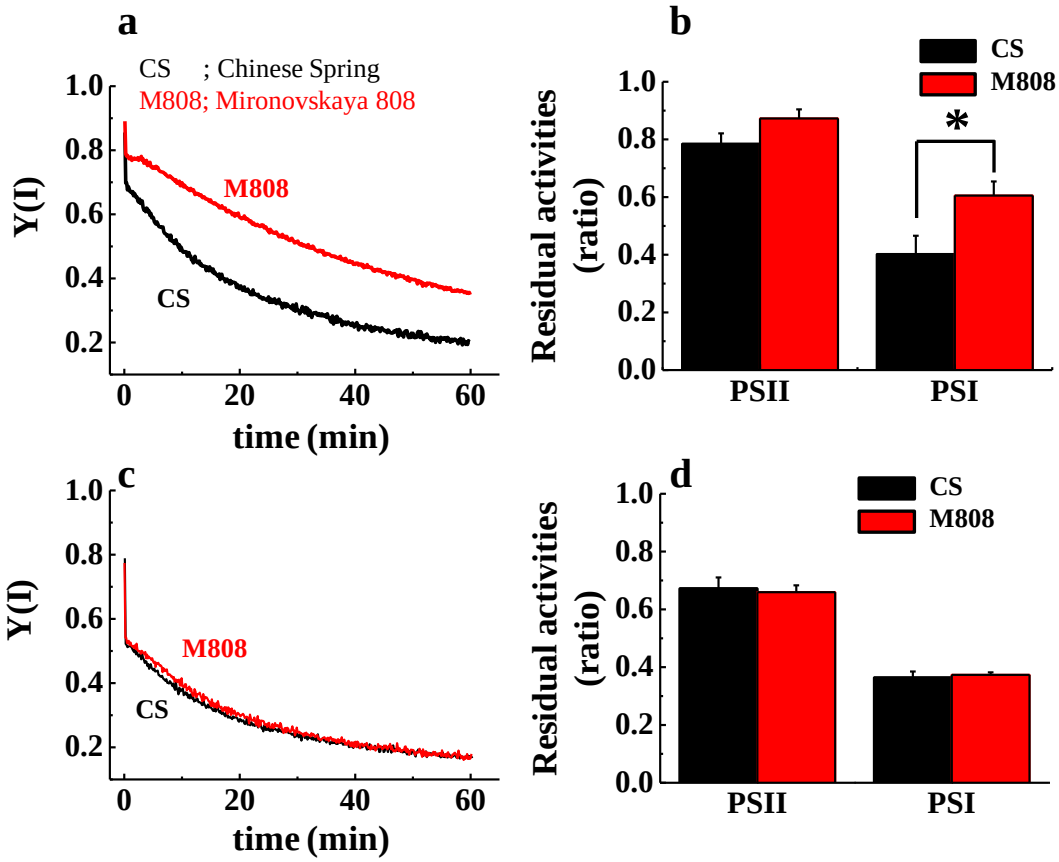

Figure II-12

The effect of growth light environment on PSI photoinhibition induced by rSP treatment. The time-course analyses of Y(I) in CS and M808 grown under HL conditions (a) and LL conditions (c) during rSP treatment under ambient conditions (21 kPa O_2, 40 Pa CO_2) are shown. Before rSP treatment, the plants were adapted in the dark for at least 1 h. Wheat leaves were illuminated every 10 s with a short-pulse (300 ms, 20,000 µE m^{-2} s^{-1}) and for 1 h without AL illumination. Experiments were repeated three times and representative data are shown. Black line, CS; Red line, M808. (b) and (d) indicate the effect of rSP treatment under atmospheric conditions (21 kPa O_2, 40 Pa CO_2) on PSI and PSII activities in CS and M808 grown under HL and LL conditions, respectively. After rSP treatment and photosynthesis measurements, the plants were kept in the dark for 30 min, and Fv/Fm and Pm were measured. Data were normalized to Fv/Fm and Pm before rSP treatment, and represents the residual activity of PSII and PSI after rSP treatment. Black bars, CS; Red bars, M808. Data are expressed as mean ± SEM of four independent experiments. Asterisks indicate a significant difference between CS and M808 (Student's *t*-test, $p < 0.05$).

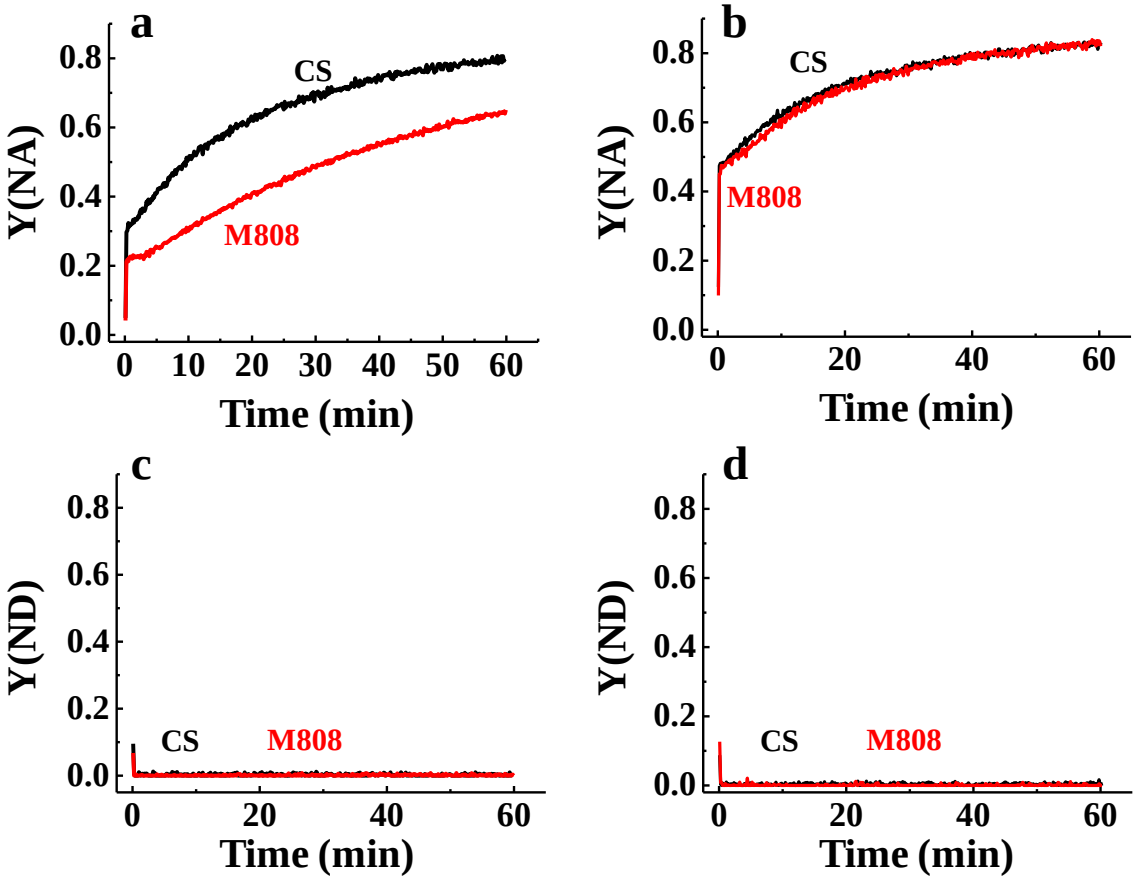

Figure II-13

The time-course analysis of Y(NA) and Y(ND) in CS and M808 grown under high-light conditions (a, c) and low-light conditions (b, d) during rSP treatment under ambient conditions (21 kPa O_2, 40 Pa CO_2). Before rSP treatment, the plants were adapted in the dark for at least 1 h. Wheat leaves were illuminated every 10 s with short-pulse AL (300 ms, 20,000 µE m^{-2} s^{-1}) and for 1 h without AL illumination. Experiments were repeated three times and representative data are shown. Black line, CS; Red line, M808.

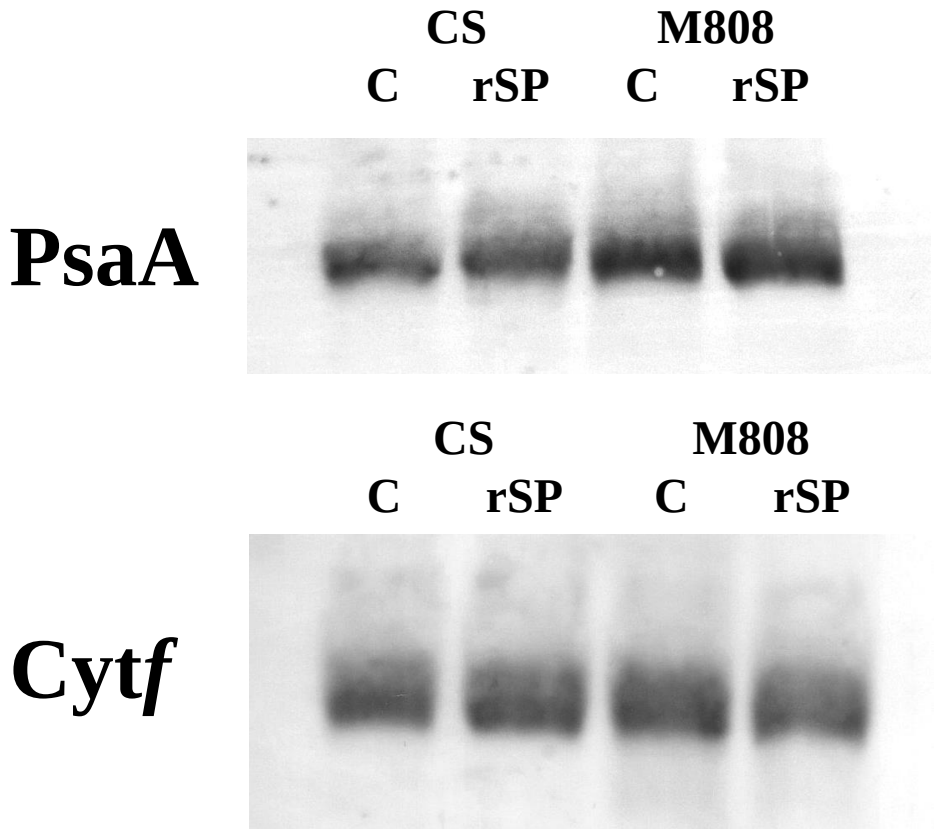

Figure II-14

The comparison of PSI core protein content in CS and M808 leaves between before and after SP treatment. Leaves were used in CS and M808 grown under HL-conditions. Leaves before rSP treatment were used as a control (C), and leaves treated rSP treatment for 1h were used as an rSP treated sample (rSP). I used antiserum specific to PsaA for quantifying PSI core protein content. In addition to PSI protein, Cyt *f* content in leaves was also analyzed as an internal standard. The protein corresponding to leaf area (0.016 cm^2) was loaded in each lane.

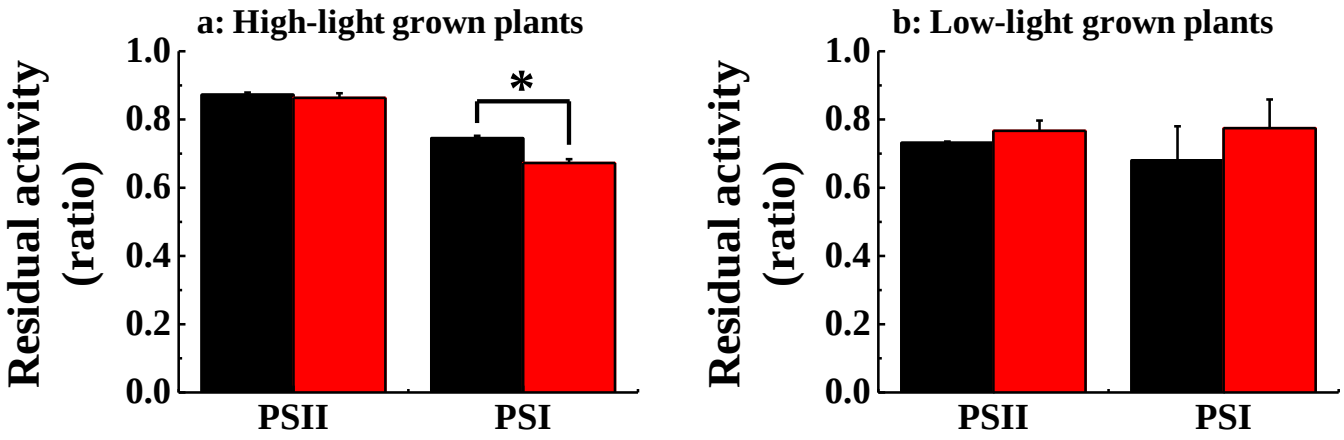

Figure II-15

The residual activities of PSII and PSI in high-light grown plants (a) and low-light grown plants (b) after rSP treatment under low O_2 conditions (1 kPa O_2, 40 Pa CO_2). After rSP treatment, the plants were kept in the dark for 30 min, and then Fv/Fm and Pm were measured. Data were normalized to Fv/Fm and Pm before rSP treatment. The data represents the residual activity of PSII and PSI after rSP treatment. Black bars, CS; Red bars, M808. Data are expressed as mean ± SEM of four independent experiments. The asterisk indicates a significant difference between CS and M808 (Student's *t*-test, $p < 0.05$).

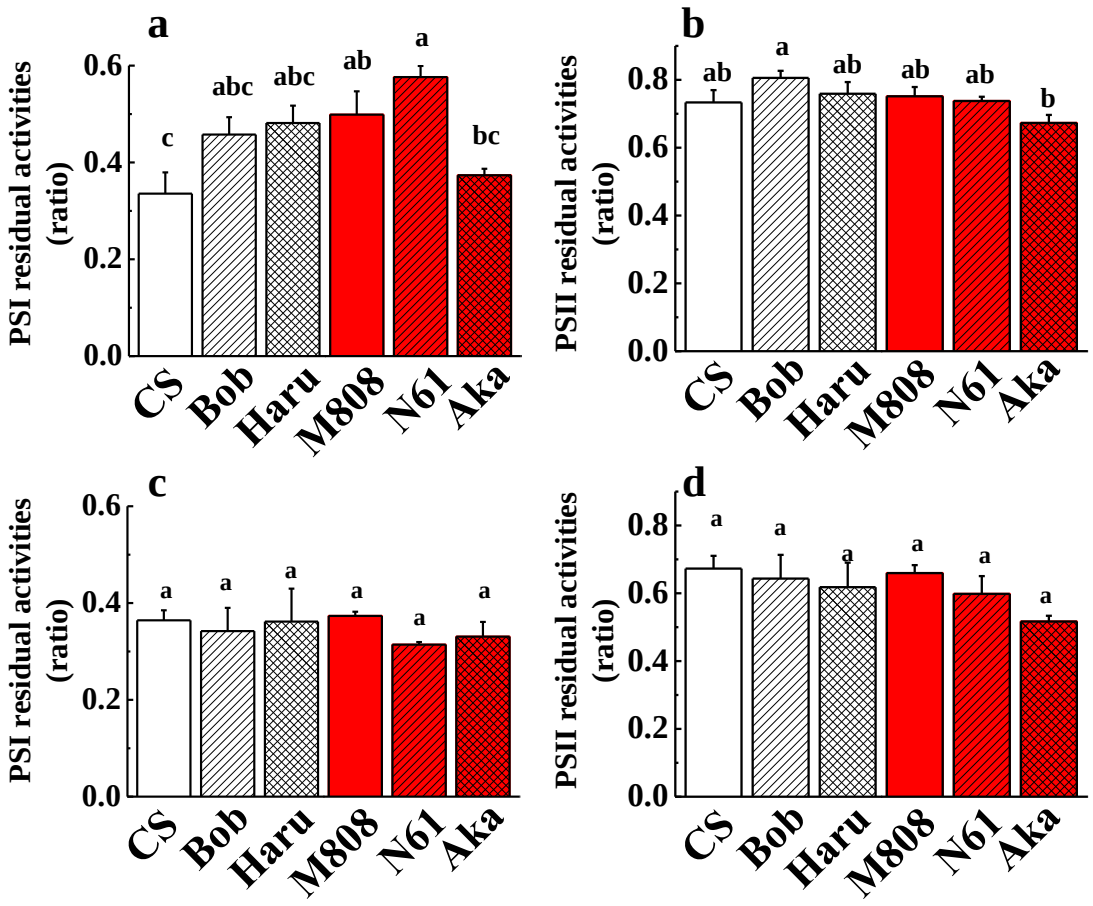

Figure II-16

The effect of rSP treatment under atmospheric conditions (21 kPa O_2, 40 Pa CO_2) on the PSI and PSII activities of six wheat cultivars grown under high-light (a, b) and low-light (c, d) conditions. Before rSP treatment, no difference was observed in Fv/Fm and Pm between the six wheat cultivars (data not shown). White columns (CS, Bob, Haru) indicate spring wheat cultivars, and red columns (M808, N61, Aka) indicate winter wheat cultivars. After rSP treatment and photosynthesis measurements, the plants were kept in the dark for 30 min, and then Fv/Fm and Pm were measured. Data were normalized to the Fv/Fm and Pm before treatment. The data represent the residual activity of PSII and PSI after rSP treatment and are expressed as mean ± SEM of three or four independent experiments. Different letters above the columns indicate a significant difference between the wheat cultivars (Tukey-Kramer HSD test, $p < 0.05$).

Table II-2
Chlorophyll content and chlorophyll *a/b* ratio in HL-growth wheat cultivars

	CS	Bob	Haru	M808	N61	Aka
Total Chl (mg m^{-2})	310.3±23.0^{b}	478.9±51.6^{ab}	459.6±88.2^{ab}	391.0±24.9^{ab}	585.4±62.3^{a}	325.2±18.2^{b}
Chl *a* (mg m^{-2})	234.2±13.8^{b}	393.9±23.0^{ab}	375.0±71.1^{ab}	294.7±22.0^{b}	479.3±49.9^{a}	265.3±15.1^{b}
Chl *b* (mg m^{-2})	49.4±4.9^{b}	85.0±9.7^{ab}	84.6±17.2^{ab}	72.8±6.5^{ab}	106.1±12.5^{a}	59.9±3.3^{ab}
Chl *a/b*	4.9±0.3^{a}	4.7±0.1^{ab}	4.5±0.1^{ab}	4.1±0.1^{b}	4.5±0.1^{ab}	4.4±0.1^{ab}
Carotenoids (mg m^{-2})	77.4±6.8	74.7±1.3	81.4±6.3	75.6±3.4	78.5±6.7	73.5±7.0

Chlorophyll content in HL-grown wheat cultivars was quantified in leaf area basis, and calculated chlorophyll *a/b* ratio. Data are expressed as mean ± SEM of three to six independent experiments. Different letters above the columns indicate a significant difference between the wheat cultivars (Tukey-Kramer HSD test, $p < 0.05$). No letter indicate no significant difference between wheat cultivars (one-way ANOVA $p > 0.05$)

Table II-3
Chlorophyll content and chlorophyll *a/b* ratio in LL-growth wheat cultivars

	CS	Bob	Haru	M808	N61	Aka
Total Chl (mg m^{-2})	224.4±22.3^{a}	286.2±24.4^{a}	190.2±48.6^{a}	319.0±39.2^{a}	240.3±21.9^{a}	230.7±13.4^{a}
Chl *a* (mg m^{-2})	180.6±17.6^{a}	235.4±20.1^{a}	157.4±39.8^{a}	242.4±58.5^{a}	196.6±18.0^{a}	192.8±9.0^{a}
Chl *b* (mg m^{-2})	43.8±4.6^{a}	50.8±3.9^{a}	32.8±9.0^{a}	77.1±24.4^{a}	43.8±4.3^{a}	37.9±7.1^{a}
Chl *a/b*	4.1±0.1^{a}	4.6±0.1^{a}	4.9±0.6^{a}	4.1±1.7^{a}	4.5±0.2^{a}	5.1±1.2^{a}
Carotenoids (mg m^{-2})	40.8±5.1	36.9±9.8	44.1±6.9	57.2±1.4	46.7±8.2	39.2±2.2

Chlorophyll content in LL-grown wheat cultivars was quantified in leaf area basis, and calculated chlorophyll *a/b* ratio. Data are expressed as mean ± SEM of three to six independent experiments. Same letters above the columns indicate no significant difference between the wheat cultivars (Tukey-Kramer HSD test). No letter indicate no significant difference between wheat cultivars (one-way ANOVA $p > 0.05$)

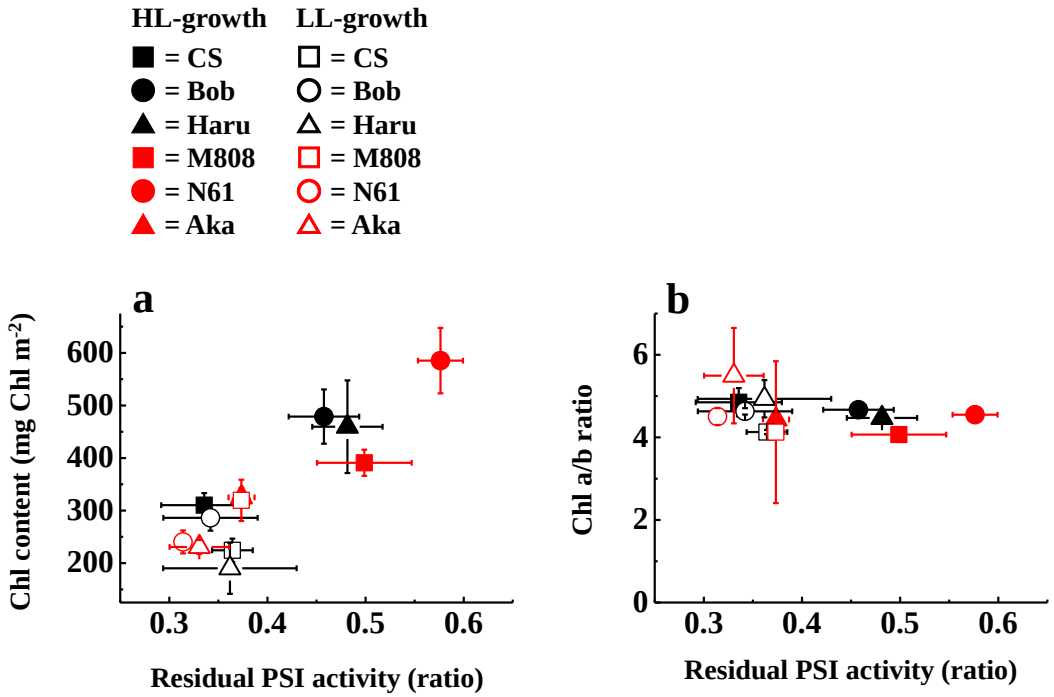

Figure II-17

The relationship between leaf chlorophyll content (A), chlorophyll *a/b* ratio (B) and the residual activity of PSI after rSP treatment for 1h. The value of chlorophyll content and chlorophyll *a/b* ratio was used in Table II-2, and II-3. The residual activity of PSI after rSP treatment was used in II-16.

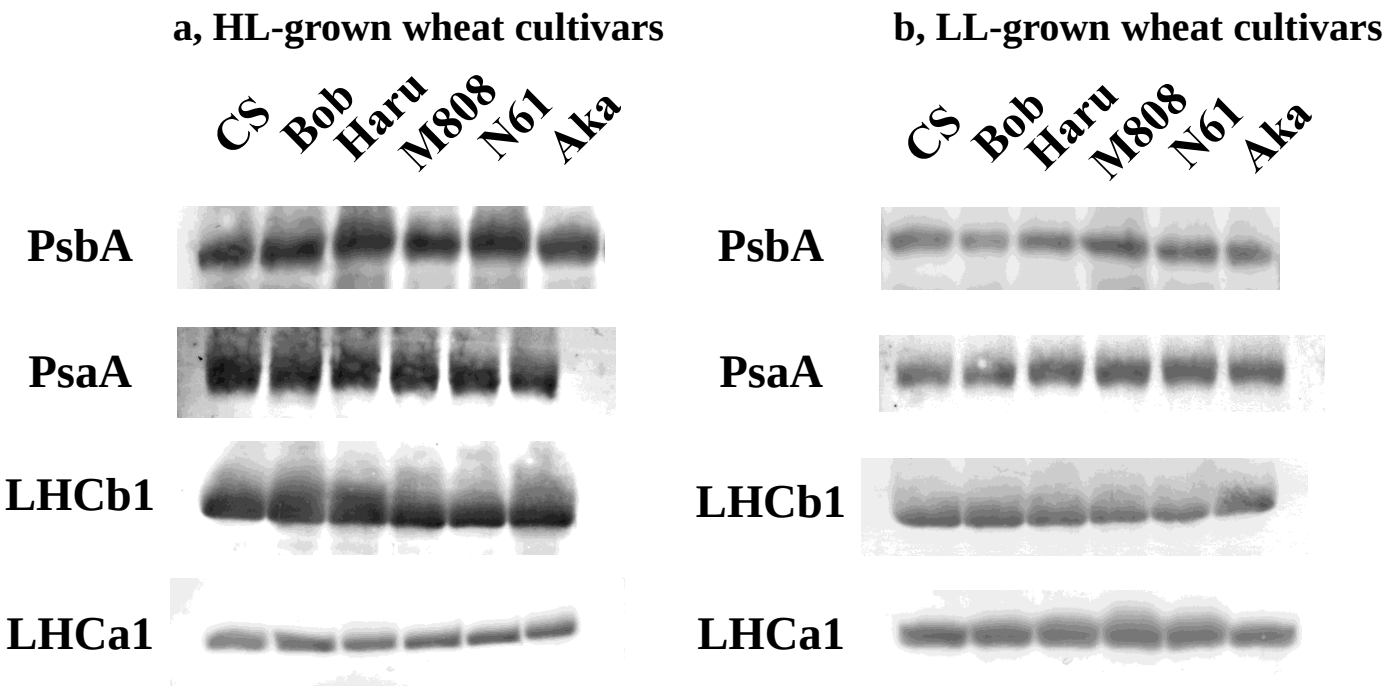

Figure II-18

The analysis of photosynthetic protein composition in HL- (A) and LL- (B) grown wheat cultivars. I used antiserum specific to PsbA, PsaA, LHCb1, and LHCa1 for quantifying PSII and PSI core protein, and their antenna protein content. The protein corresponding to 0.6 μg chlorophyll was loaded in each lane.

DISCUSSION

In this study, I aimed to reveal the mechanism by which rSP treatment induces photoinhibition specific to PSI by using isolated chloroplasts. I also investigated how growth light environment affects the PSI photoinhibition in wheat plants. First, I observed that rSP treatment induces PSI-specific photoinhibition in isolated chloroplasts when O_2 was present in a similar manner to leaves (Sejima et al., 2014). In addition, rSP treatment caused the limitation of the photosynthetic electron transport reaction at the acceptor side in PSI (Figs. II-1, II-2). These results suggest that rSP treatment critically affected chloroplasts, but other organelles were not involved in PSI photoinhibition.

I propose that PSI photoinhibition is triggered by ROS produced within the thylakoid membranes. Although several components of ROS production have been proposed in previous reports, the ROS production mechanism in PSI has not been clarified (Misra and Fridovich, 1971; Miyake et al., 1998; Asada, 2000; Voss et al., 2011; Kozuleva and Ivanov, 2010). ROS are known to trigger PSI photoinhibition and degrade its components because PSI photoinhibition requires O_2 (Allahverdiyeva et al., 2005; Sonoike and Terashima, 1994; Sonoike, 1996a). However, the production site of the ROS that trigger PSI photoinhibition has been not clarified. In this study, I observed that the addition of MV to isolated chloroplasts greatly alleviates PSI photoinhibition induced by rSP treatment (Fig. II-4). This result is consistent with a previous report on thylakoid membranes (Sonoike, 1996a). MV accepts electrons from PSI and stimulates the production of O_2^- (Babbs et al., 1989). O_2^- triggers the production of OH· through the Fenton reaction and the Haber–Weiss reaction. Furthermore, MV itself produces OH· via Winterbourn's reaction through the MV radical or MV^{2+} forms (Babbs et al., 1989). Here, I used 5 μM MV in the rSP treatment. Under these conditions, MV reacts with F_A/F_B at the stromal side in PSI (Sonoike and Terashima, 1994). Based on this report, MV should stimulate the production of ROS in the chloroplast stroma. Therefore, I suggest ROS produced in the stromal region does not contribute to PSI photoinhibition. In leaves, PSI photoinhibition induced by rSP treatment is suppressed under continuous AL illumination,

compared to dark conditions (Sejima et al., 2014). This is because constant AL illumination stimulates the oxidation of PSI by activating the electron sink in photosynthesis (like the Calvin cycle and photorespiration) and the formation of ΔpH across thylakoid membrane (Zaks et al., 2012). Indeed, I observed that ΔpH and electron donation from PSI to MV protect PSI photoinhibition in isolated chloroplasts (Fig. II-6). In Sejima et al. (2014), PSI photoinhbition was suppressed in accordance with the induction of Y(ND) under AL illumination. Based on this result, in leaves, the formation of large ΔpH across thylakoid membrane is more critical for the protection of PSI photoinhibition, compared to the consumption of electrons in electron sink in photosynthesis. Therefore, these results and those by Sejima et al. (2014) show that rSP treatment under dark conditions promotes the reduction of electron carriers in PSI without activating the electron sink and forming a large ΔpH, which suppresses the photosynthetic electron transport reaction from PSII to PSI *in vivo*. Accordingly, PSI photoinhibition would be triggered by the production of ROS within the thylakoid membrane *in vivo*, in the same way as in isolated chloroplasts.

I proposed that PSI photoinhibition proceeded with sequential two-step by the different kinds of ROS produced within thylakoid membrane (Fig. II-19). Firstly, the production of O_2^- and OH· at a secondary electron acceptor in PSI induced PSI photoinhibition (Takahashi and Asada 1988; Sonoike et al., 1995). PSI has four electron acceptors (A_0 as a primary acceptor, and A_1, Fx, and F_A/F_B as secondary acceptors). Ivanov's group suggests that the ROS production site in PSI is within the thylakoid membranes and that the secondary acceptor, A_1, is a major contributor to the Mehler reaction *in vivo* (Kozuleva and Ivanov, 2010; Kozuleva et al., 2014). Two types of A_1, which have different Em values (A_{1a}; –671 mV, A_{1b}; –844 mV), exist in PSI, and A_{1a} and A_{1b} are coupled with PsaA and PsaB, respectively (Rutherford et al., 2012). The degradation of PsaB is promoted during PSI photoinhibition without the degradation of PsaA, so A_{1b}, which has a lower Em value than A_{1a}, might be a primary ROS production site in PSI, and O_2^- produced at A_{1b} could trigger PSI photoinhibition (Sonoike and Terashima, 1994; Sonoike, 1996a). I suggest that ROS production and oxidative attack by ROS in PSI occur within thylakoid membranes.

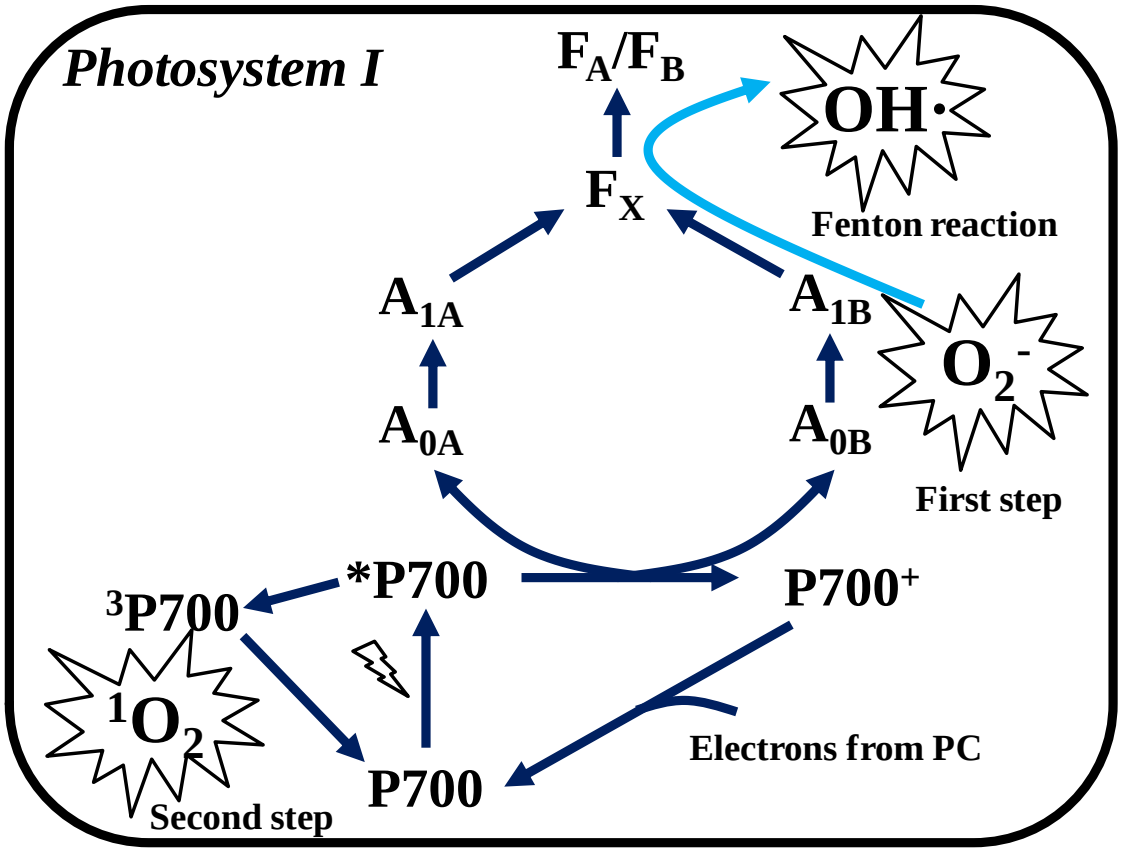

Figure II-19

The scheme of ROS production and photoinhbition in PSI. When electron carriers are highly reduced in PSI, the production of O_2^- is stimulated at A_1 site (Kozuleva and Ivanov, 2010; Kozuleva et al., 2014). O_2^- directly attacks peripheral component, or O_2^- is converted to OH· through Fenton reaction between iron-sulfur center in F_X, F_A, or F_B in the diffusing process (mentioned as first step) (Inoue et al., 1986; Sonoike et al., 1995; Takahashi and Asada, 1988). The destruction of F_X, F_A, and F_B are preceded by O_2^- and OH·, charge separation between P700 and chlorophyll A_0 would be limited (Shuvalov et l., 1986). Furthermore, the production of triplet-state of P700 (^{3}P700) is initiated (Rutherford et al., 2012; Shuvalov et al., 1986). ^{3}P700 react with O_2 to produce singlet O_2 ($^1O_2$). $^1O_2$ further attacks peripheral component in PSI, and proceeds PSI photoinhibition (mentioned as second step) (Cazzaniga et al. 2012). These all reactions proceed within the thylakoid membranes. Therefore, the decrease in P700 chlorophyll occurs, but protein degradation does not accompany with PSI photoinhibition. Blue arrows indicate energy transfer pathway in PSI, and light blue arrow indicates the diffusion of O_2^- in thylakoid membrane (Takahashi and Asada, 1988).

Therefore, chloroplastic SOD and APX cannot protect PSI from its photoinhibition (Figs. II-5, II-8). In fact, Takahashi and Asada (1982) reported that O_2 reduction detected by O_2^--dependent Cyt *c* reduction was stimulated in thylakoid membranes which were disintegrated by detergent. This means that O_2 reduction site does not exist in membrane surface. Furthermore, they revealed that high concentration of NH_4Cl, which induced the protonation of O_2^- stimulated the production of H_2O_2 in thylakoid membranes, and simultaneously NH_4Cl suppressed the O_2^- -dependent Cyt *c* reduction (Takahashi and Asada, 1988). From these observations, they concluded O_2^- was produced in aprotic region of thylakoid membrane, that is, interior of thylakoid membrane. Their conclusion is consistent with our observations.

Secondly, the production of singlet O_2 ($^1O_2$) by charge recombination in PSI proceeds further PSI photoinhibition (Fig. II-19). I revealed that PMC which acts as a $^1O_2$ scavenger, suppressed the decrease in Y(I) in isolated chloroplasts in the later part of rSP treatment, and PMC significantly protected PSI activity after rSP treatment for 1 h (Fig. II-9). In PSI photoinhibition, F_A, F_B, and F_X were primary destroyed and they lost electron transport activity (Inoue et al., 1986; Sonoike et al., 1995). Based on these reports, O_2^- produced at A_1 would diffuse in the thylakoid membrane and react with [Fe-S] cluster in F_X, F_A or F_B, furthermore OH· produced from O_2^- through Fenton reaction would inactivate their electron transfer activities (Takahashi and Asada, 1988; Sonoike et al., 1997). When electron transport reaction in PSI is limited after the destruction of F_X, F_A, and F_B, the charge separation of P700 chlorophyll would be suppressed, and then the charge recombination between $P700^+$ and A_0, A_1 would be stimulated (Shuvalov et l., 1986). In a similar way to P680 chlorophyll, the transient state of the excited P700 chlorophyll in PSI is de-excited to the triplet state (^{3}P700) through charge recombination, and then the ^{3}P700 reacts with O_2 to produce $^1O_2$ (Shuvalov et al., 1986; Rutherford et al., 2012). Cazzaniga et al. (2012) reported that $^1O_2$ is produced in the PSI-LHCI complex isolated from *A. thaliana*. Furthermore, they also reported that the *A. thaliana szl1* mutant, which contains less β-carotene than the wild-type, is susceptible to PSI photoinhibition under high light and low temperature conditions. This means that $^1O_2$ produced in

PSI caused PSI photoinhibition because β-carotene is major $^1O_2$ quencher (Telfer, 2014).

I observed that PSI core protein content did not decrease after PSI photoinhibition, even though P700 chlorophyll content and PSI activity were largely decreased in isolated chloroplast as well as leaves (Figs. II-3, II-14). Previous reports also reported that the decrease in PSI activity and P700 chlorophyll content do not correlate with the decrease in PSI protein content after PSI photoinhibition (Sonoike et al.,1997; Tjus et al., 1998; Zhang and Scheller, 2004). These results indicate that ROS do not stimulate PSI photoinhibition by stimulating PSI protein degradation. Therefore, these results support the idea that ROS produced within thylakoid membrane specifically target electron transport carriers in PSI and proceeds PSI photoinhibition.

Wheat plants acquire or strengthen their protection mechanisms against O_2-dependent PSI photoinhibition during HL acclimation, and the extent of this is dependent on cultivar type. In this study, I observed that CS and M808 had different susceptibilities to PSI photoinhibition when they were grown under HL conditions, but not under LL conditions (Fig. II-9). This result indicated that different HL acclimation responses between CS and M808 would be involved in susceptibility to PSI photoinhibition. In the light response analysis of photosynthetic parameters before rSP treatment, CS and M808 that had been grown under HL conditions increased their Y(II) and Y(I) under strong light intensity compared to those grown under LL conditions (Fig. II-7). This phenomenon is widely observed in higher plants (Bailey et al., 2001; Walters et al., 2003; Oelze et al., 2012). Thus, this result means that CS and M808 possess the ability to enhance their photosynthetic electron transport activity through HL acclimation. Based on these results, a HL inducible factor that protects PSI from its photoinhibition would be independent of photosynthetic electron transport activity.

PSI/PSII ratio in thylakoid membrane largely affects PSI photoinhibition. Brestic et al. (2015) reported that chlorophyll *b*-deficient wheat plant which has low PSI/PSII ratio is susceptible to PSI photoinhibition, compared to wild-type wheat plant. This is because that the increase in PSII per PSI would increase electrons which flow into single PSI complex, and this would cause highly reduced state in electron carriers of PSI (Brestic et al., 2015; Grieco et al., 2012; Kono et al., 2014).

In fact, the decrease in PSI/PSII ratio in leaves caused increase of Y(NA) (Brestic et al., 2015). However, in this study, I could not observe the difference in PSI/PSII ratio among wheat cultivars (Fig. II-18). Furthermore, when the alteration of PSI/PSII occurs, photosynthetic parameters estimated from chlorophyll fluorescence and $P700^+$ also modified (Andrews et al., 1995; Zhang and Scheller, 2004; Brestic et al., 2015). In contrast, I did not observed any difference in photosynthetic parameters between wheat cultivars in light response analysis although the susceptibility to PSI photoinhibition induced by rSP treatment was clearly different (Figs. II-11, II-12). These result indicated that cultivar difference in the susceptibility to PSI photoinhibition might not relate to the PSI/PSII ratio.

As mentioned in Cazzaniga et al. (2012), carotenoids is capable to protect PSI from photoinhibition. Total carotenoid content in leaf increased in accompanied with the increase in the growth light intensity (Demming-Adams and Adams III, 1996). Indeed, I observed total carotenoid content increased in HL-grown wheat cultivars, compared to LL-grown wheat cultivars (Tables II-2, II-3). However, I did not found the cultivar difference in the total carotenoid content in leaves. In addition to this, the dependency of Y(II) and Y(NPQ) on light intensity was similar between CS and M808 (Fig. II-11). The difference of xanthophyll content like zeaxanthin, violaxanthin, and antheraxanthin would affect the Y(II), and Y(NPQ) (Demming-Adams and Adams III, 1996; Nilkens et al., 2010). Based on these results, I assumed that the cultivar difference in the susceptibility of PSI photinhibition is independent of carotenoids. As a supporting results of this possibility, the decrease in Y(I) during the rSP treatment was faster in CS than M808 even at the first part of rSP treatment (Fig. II-12). Based on our scheme of PSI photoinhibition, PSI photoinhibition is stimulated by O_2^- or OH· at first (Fig. II-19). Therefore, the difference in the content of carotenoids which is capable to scavenge $^1O_2$ would not cause the decrease in Y(I) at the first part of rSP treatment.

Here, I could not identify the critical component to cause the cultivar difference in the susceptibility to PSI photoinhibition among wheat plant. However, I revealed that leaf chlorophyll content relates to the susceptibility to PSI photoinhibition (Fig. II-17a). Several studies reported that

the alteration of leaf chlorophyll content does not match the alteration of photosynthesis rate and wild-type plant considered to have excess chlorophyll for driving photosynthesis in general (Lin et al., 2003; Brestic et al., 2015). This fact might indicate that wild-type plants have excess chlorophylls in leaf for some protecting mechanism in thylakoid membranes, as being observed in this study (Fig. II-17a). Future studies are needed to reveal the unknown component to cause wheat cultivar difference in the susceptibility to PSI photoinhibition, and to relate the leaf chlorophyll content.

At the beginning of the rSP treatment, I observed a rapid decrease in Y(I) and Y(ND), and a quick increase in Y(NA) in both CS and M808, regardless of growth light environment (Fig. II-9a and c, Fig. II-10). Furthermore, the rapid decrease in Y(I) and Y(ND), and the fast increase in Y(NA) were reversed when the illumination interval of the rSP treatment was lengthened (Fig. II-20a and b). Although the causes of the rapid changes in the photosynthetic parameters for PSI and their recovery process are unknown, these changes are not due to PSI photoinhibition because the recovery from PSI photoinhibition takes a much longer time (about a day) (Sonoike, 2011; Zivcak et al., 2015a, b). Furthermore, I confirmed that these rapid changes occurred even under low O_2 conditions, thus these processes do not require O_2 (Fig. II-20c and d). This phenomenon might reflect the reduction of stromal electron acceptors, such as Fd, FNR, and $NADP^+$, caused by the illuminating pulse.

I have shown that rSP treatment stimulated specific PSI photoinhibition both *in vivo* and *in vitro*. Furthermore, the kinetics of Y(I) during rSP treatment were quite similar in the leaves and isolated chloroplasts (Fig. II-1a) (Sejima et al., 2014; Zivcak et al., 2015a, b). To date, there has not been a common method to assess the susceptibility of PSI photoinhibition *in vivo* and *in vitro*. This means that the rSP treatment improves PSI photoinhibition analysis efficiency. In addition, the rSP treatment clearly showed an acclimatory effect and cultivar differences in susceptibility to PSI photoinhibition. I have not yet identified the key factor that causes the difference in PSI photoinhibition between wheat cultivars. However, the rSP treatment should make it possible to reveal the protection mechanism against PSI photoinhibition through a forward or reverse genetic

approach, such as the selection of mutagenized plants that have a higher susceptibility or tolerance to PSI photoinhibition.

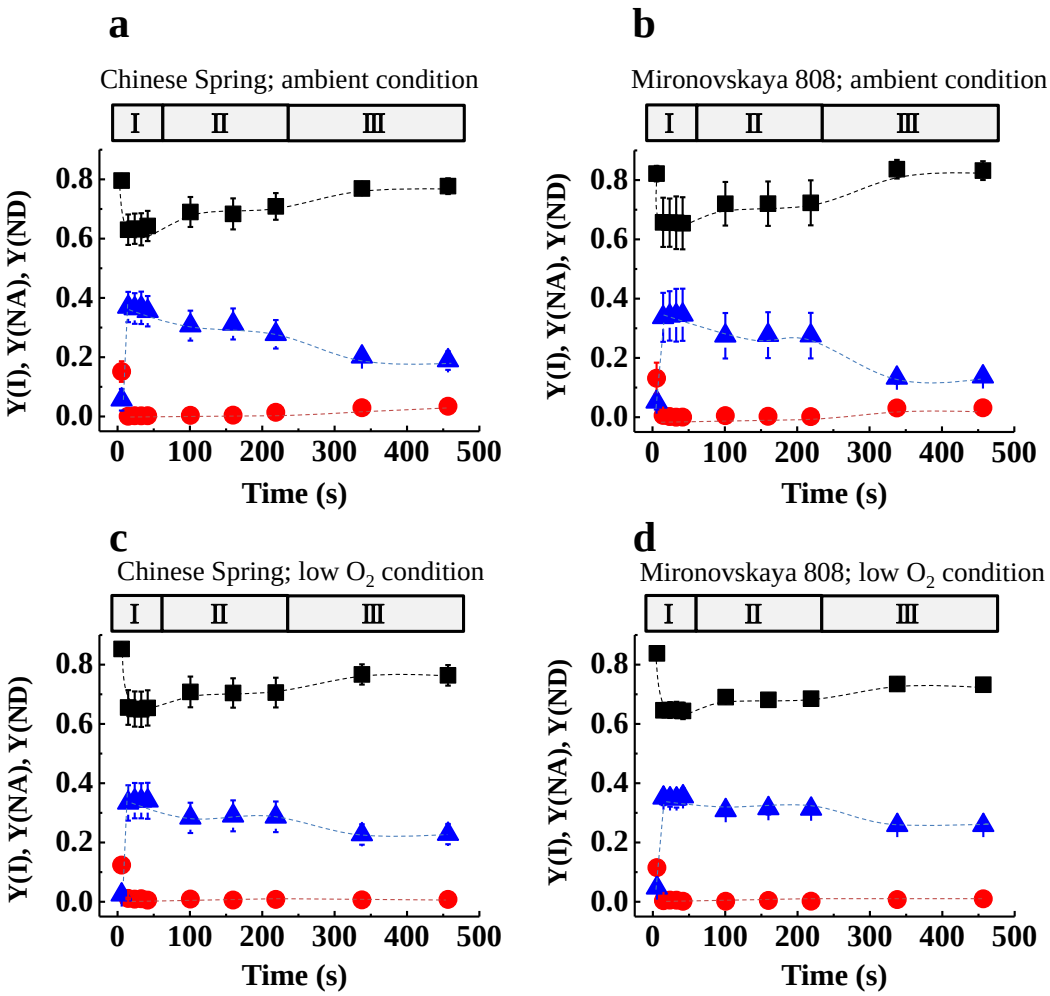

Figure II-20

Analysis of the rapid response of Y(I), Y(NA), and Y(ND) during rSP treatment under ambient conditions (a, b) and low O_2 conditions (c, d). Before rSP treatment, the plants were adapted in the dark for at least 1 h. In this experiment, the plants were illuminated with a short pulse at three different intervals (I, II, and III in the figures). (I); Wheat leaves were illuminated every 10 s with a short pulse of AL (300 ms, 20,000 µE m^{-2} s^{-1}) for 5 times. (II); the short pulse (300 ms, 20,000 µE m^{-2} s^{-1}) occurred 3 times every 60 s. (III); the short pulse (300 ms, 20,000 µE m^{-2} s^{-1}) occurred twice every 120 s. High-light grown CS and M808 were used. Black square indicates Y(I). Red circle indicates Y(ND). Blue triangle indicates Y(NA). Data are expressed as mean ± SEM of three independent experiments.

Chapter 3

Photorespiration, instead of alternative electron flow, determines the oxidized state of P700 at low CO_2 concentration in higher plants

~the importance of ATP-consumption pathway for the redox-regulation in photosynthesis ~

ABSTRACT

To elucidate the molecular mechanism involved in regulating the redox-state of P700 in PSI, I studied the effects of photorespiration, the Mehler-Ascorbate Peroxidase (MAP)-pathway (water-water cycle), and cyclic electron flow around PSI (CEF-I) in photosynthetic electron transport (PET) system, and photosynthetic CO_2-assimilation of sunflower (*Helianthus annuus* L.) leaves. At ambient partial pressure of CO_2 (pCO_2), a decrease in partial pressure of O_2 (pO_2) from 21 to 0 kPa did not affect the redox states of PSII or PSI, although the CO_2-assimilation rate increased. At 4 Pa pCO_2, the decrease in pO_2 slightly increased the CO_2-assimilation rate; however, the quantum yields of PSII [Y(II)] and PSI [Y(I)], the oxidation-state of PSII (qL), non-photochemical quenching (NPQ), and donor-side limitation parameters of PSI [Y(ND)] decreased depending on the decrease in pO_2. These responses were similar to that of the drought-stressed plants, which did not show any CO_2-assimilation or transpiration. In contrast, Y(I)/Y(II) and acceptor-side limitation parameters of PSI [Y(NA)] increased differently from Y(ND) during the decrease in pO_2 at 4 Pa CO_2. Therefore, CEF-I did not induce the oxidation of P700. Furthermore, I found that the H^+-consumption rate evaluated as the relaxation rate of electrochromic shift (ECS)-signal (V_H^+) had a positive linear relationship with the H^+-consumption rate estimated from photosynthesis and photorespiration rates (JgH^+). At 4 Pa pCO_2, qL and Y(ND) showed positive relationships with V_H^+, which was also observed in the drought-stressed plants. These results suggest that photorespiration induces the oxidation of P700, but not the MAP-pathway which does not consume ATP.

INTRODUCTION

As mentioned in chapter 2, the accumulation of electrons in the electron carriers in PSI caused ROS production and PSI photoinhibition. Therefore, to maintain oxidized state in PSI would be effective to avoid ROS production in PSI, and PSI photoinhibition in chloroplasts. Indeed, Sejima et al. (2014) first elucidated the physiological significance of P700 oxidation in higher plants. In Sejima et al. (2014), I regulated the redox-state of P700 by illuminating intact leaves with actinic light (AL) during rSP treatment, with the purpose of inducing the oxidation of P700 under steady-state photosynthesis. Then, an increase in oxidized P700 suppressed PSI photoinactivation. In higher plants, an increase in oxidized P700 is observed in response to exposure to high light and low CO_2 (Miyake et al. 2005b). This would be the regulative response of PET to suppress ROS production in PSI of thylakoid membranes.

Several candidates for the molecular mechanism to increase in Y(ND) are proposed. For the increase in Y(ND), two aspects should be considered: first, the electron sink in photosynthesis to consume electrons produced in PET; second, limitation of electron flow to P700 from PSII. The electron sink would have potential activity to alternate to CO_2 fixation activity in photosynthesis, and then photorespiration can be an electron sink (Brestic et al. 1995; Kozaki and Takeba 1996; Badger et al. 2000; von Caemmerer 2000; Sejima et al. 2015). The electron flow to P700 is regulated by acidification of the luminal side of the thylakoid membranes (Schreiber and Neubauer, 1990; Heber and Walker 1992; Kramer et al., 1999; Miyake 2010; Tikhonov et al. 2013). The Mehler-Ascorbate Peroxidase (MAP)-pathway (the water-water cycle) and cyclic electron flow around PSI (CEF-I) can induce acidification of the luminal side of the thylakoid membranes, which drives non-photochemical quenching (NPQ) of Chl fluorescence, decreases excitation efficiency of PSII, and suppresses PQH_2-oxidation activity in the Cyt b_6/f-complex (Miyake, 2010). MAP-pathway and CEF-I could therefore limit the electron flow to P700.

In the present work, I studied the effects of partial pressure of O_2 (pO_2) on Y(ND) in the leaves of sunflower (*Helianthus annuus* L.) plants. I found that lowering pO_2 decreased Y(ND) at

low CO_2. The decrease in Y(ND) accompanying the lowering pO_2 was also observed in plants suffering from drought stress. Furthermore, the decrease in pO_2 suppressed the formation of proton motive force and H^+-consumption rate for ATP production (V_H^+), which I evaluated by dark-interval relaxation kinetics (DIRK) analysis of the electrochromic shift (ECS) signal (Baker et al. 2007; Cruz et al. 2001; Sacksteder et al. 2000). ECS signal shows the accumulation of H^+ in the luminal side of thylakoid membranes (ΔpH) and the formation of membrane potential (ΔΨ) (Kramer et al., 2003). Both ΔpH and ΔΨ contribute to the synthesis of ATP catalyzed by ATPase as a proton motive force (Kramer et al., 2003). The decrease in Y(ND) paralleled with V_H^+ at low CO_2 or in drought stressed plants. That is, Y(ND) is regulated by a metabolic pathway that consumes both O_2 and ATP. On the other hand, the relative ratio of the quantum yield of PSI [Y(I)] to PSII [Y(II)] increased as pO_2 decreased, which indicates an increase in CEF-I activity. Here, I propose that photorespiration, instead of CEF-I and MAP-pathway, oxidizes P700 in PSI as electron sink, and contributes to the oxidation of P700 under drought stress, which would suppress the production of ROS.

MATERIALS AND METHODS

Plant materials

In this study, I used sunflower (*Helianthus annuus* L.) as a plant material. Seeds were imbibed using wet cotton at 4°C for 3 days to promote synchronized germination. The imbibed seeds were grown in a mixture of soil (Metro-Mix 350; Sun Gro Horticulture, Bellevue, WA, USA) and vermiculite (Konan, Osaka, Japan) in pots (12 cm × 12 cm in width and 9.5 cm in depth). The plants were placed in an environmentally controlled chamber with 14 h of light (25°C) and 10 h of darkness (23°C). The light intensity was 500 μE m^{-2} s^{-1}. The seedlings were watered every second day with 0.1% Hyponex solution (N:P:K = 5:10:5; Hyponex, Osaka, Japan). Analyses were carried out on fully expanded mature leaves of plants grown for at least 4 weeks. As a drought-stress treatment, I stopped irrigating for 3 days under growth conditions. After the measurement of drought-stressed sunflower plants, I irrigated again and used re-watered sunflower plants after irrigation for 3 days under growth conditions. Representative sunflower plants are shown in Figure III-1.

Measurement of gas exchange, chlorophyll fluorescence, and $P700^+$

Gas exchange analysis, chlorophyll fluorescence, and $P700^+$ were simultaneously measured with a Li-7000 (Li-Cor, Nebraska, USA) and Dual-PAM-100 (Heintz Walz GmbH, Effeltrich, Germany). Atmospheric gas (40 Pa CO_2/21 kPa O_2) and gas with the indicated mixture of pure O_2 and CO_2 were prepared by mixing 20.1% (v/v) O_2 in 79.9% (v/v) N_2, 1% (v/v) CO_2 in 99% N_2, and pure N_2 gas using a mass-flow controller (Kofloc model 1203; Kojima Instrument Co., Kyoto, Japan) was used in this study. The gases were saturated with water vapor at 18.0 ± 0.1°C and the leaf temperature was maintained at 25°C. The chlorophyll fluorescence parameters were calculated as described by Baker (2008), using the following parameters: F_o, minimum fluorescence yield; F_m, maximum fluorescence yield; and F_s, steady state fluorescence yield.

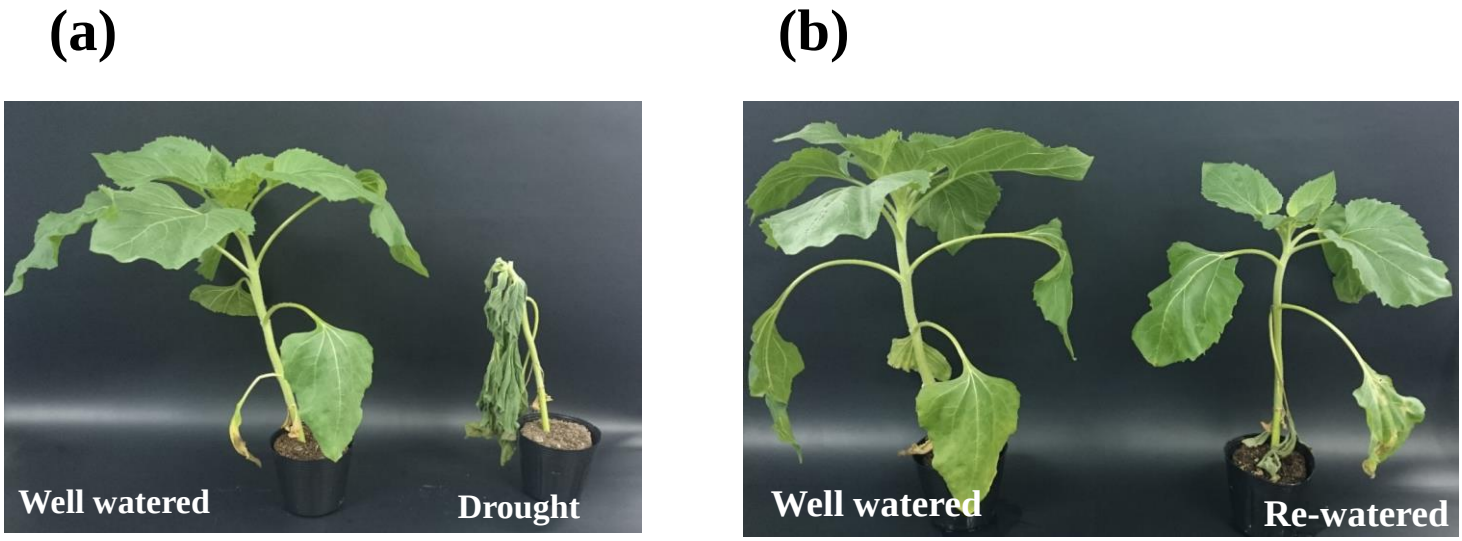

Figure III-1

(a) The phenotype of well-watered sunflower plant, and drought stressed plant. For drought stress, irrigation was stopped for 3 days under growth conditions. After the measurement of drought stressed plants, I irrigated to drought stressed plants for 3 days to confirm that sunflower plants were survived (b).

The maximum quantum efficiency of PSII photochemistry was calculated as $F_v/F_m = (F_m - F_o) / F_m$ and the quantum yield of photochemical energy conversion in PSII was calculated as $Y(II) = (F_m' - F_s) / F_m'$. Measuring light (0.1 μE m^{-2} s^{-1}) and saturated pulse (20,000 μE m^{-2} s^{-1}, 300 ms) were applied to determine Fo and Fm. H^+-consumption rate (JgH^+) estimated from the CO_2 assimilation rate (A), respiration rate (R_d), and electron transport rate (ETR) was calculated as described in Sejima et al. (2015). For this calculation, RuBP carboxylation rate (vc) and RuBP oxygenation rate (vo) were calculated as follows: $vc = (1/6) \times \{ETR - 4 \times (A + R_d)\}$, $vo = (1/6) \times \{ETR/2 + 4 \times (A + R_d)\}$. In this study, ETR was calculated as follows: ETR = AL intensity × Y(II) × 0.45. Using these parameters, JgH^+ was calculated as follows: $JgH^+ = 9.34 \times (vc + vo) \times \{3 + 3.5 \times (vo/vc)\} / \{2 + 2 \times (vo/vc)\}$ (Sejima et al. 2015). The oxidation-reduction state of $P700^+$ was determined according to the methods of Klughammer and Schreiber (1994) as follows: quantum yield of photochemical energy in PSI, $Y(I) = (P_m' - P) / P_m$; quantum yield of non-photochemical quenching due to the acceptor side limitation, $Y(NA) = (P_m - P_m') / P_m$; and quantum yield of non-photochemical quenching due to the donor side limitation, $Y(ND) = P / P_m$. The maximum oxidation level of P700 chlorophyll (P_m) was obtained using a saturated pulse under far-red light and reflected the maximum amount of photooxidized P700 chlorophyll. The parameter P reflects the steady-state oxidation level of $P700^+$, and P_m' was obtained by a saturated pulse at steady state. Actinic red light (AL) was used to measure the photosynthetic parameters.

Measurement of electrochromic shift

Gas exchange analysis and electrochromic shift were simultaneously measured with a Li-7000 and Dual-PAM equipped with a P515-analysis module (Klughammer et al. 2013). The gaseous phase was controlled as described in the previous section, "Measurement of gas exchange, chlorophyll fluorescence, and $P700^+$". The gases were saturated with water vapor at 18.0 ± 0.1°C and the leaf temperature was maintained at 25°C. The proton motive force, proton conductance (gH^+) in ATP

synthase, and H^+-consumption rate (V_{H^+}) were measured by dark interval relaxation kinetics (DIRK) analysis as described in Baker et al. (2007) and Sacksteder et al. (2000). The magnitude of proton motive force was normalized by dividing the magnitude of ECS decay in DIRK analysis by the magnitude of ECS induced by single turnover flash (10 μs) (Klughammer et al. 2013).

Isolation of intact chloroplasts from spinach leaves

Intact chloroplasts were isolated from spinach (*Spinacia oleracea* L.) leaves purchased from a local market and purified by Percoll density gradient centrifugation, as described previously (Takagi et al. 2012). The isolated chloroplasts were suspended in a reaction mixture [50 mM 4-(2-hydroxyethyl) piperazine-1-ethansulfonic acid-potassium hydrate (HEPES-KOH), pH 7.6; 0.33 M sorbitol; 10 mM sodium chloride (NaCl); 1 mM magnesium chloride ($MgCl_2$); 2 mM 2-({2-[bis(carboxymethyl)amino]ethyl-(carbonymethyl)}amino)acetic acid (EDTA); and 0.5 mM monopotassium phosphate (KH_2PO_4)]. The intactness of the purified chloroplasts was determined by the ferricyanide method (Heber and Santarius 1970), and 85–95% of the intact chloroplasts were used in our experiment. The chlorophyll content was determined as described previously (Arnon 1949).

Measurement of redox change in Cyt *f*

The redox change of Cyt *f* was measured by Kinetic LED array spectrophotometer (KLAS) (Klughammer et al., 1990; Takagi et al., 2012). The transmittance at three wavelengths (520 nm, 546 nm, and 554 nm) was measured, and the redox change of Cyt *f* was calculated as described in Joliot and Joliot, (2002):

$$\text{Oxidized Cyt } f\ (\times 10^3, \Delta I/I) = 546\text{ nm} - 554\text{ nm} - 0.11 \times (520\text{ nm} - 546\text{ nm})$$

RESULTS

I aimed to elucidate what molecular mechanism regulates the oxidation level of P700 [Y(ND)] in PSI of thylakoid membranes *in vivo*. As described in the Introduction, the electron sink and the limitation of electron flow to P700 may control Y(ND). To examine the importance of the electron sink and the limitation of electron flow to P700 for the induction of Y(ND), I studied the effects of pO_2 on photosynthesis characteristics in sunflower leaves, because photorespiration requires O_2 to function as an electron sink, and MAP-pathway also requires O_2 to induce ΔpH across thylakoid membranes. Simultaneously, I evaluated CEF activity. Furthermore, I used plants that suffered from drought stress, because Y(ND) would be required under the limited photosynthesis conditions during drought (Kohzuma et al. 2009). Then, I can evaluate what mechanism is functioning in the regulation of the redox state of P700.

Effects of pO_2 on photosynthetic CO_2-assimilation, transpiration, and stomatal conductance in sunflower leaves

At the ambient partial pressure of CO_2 (40 Pa pCO_2), pO_2 decreased from 21 to 0 kPa after the photosynthetic CO_2 assimilation rate reached steady state (Fig. III-2). With lowering pO_2, the CO_2 assimilation rate increased from 16 to 23 μmol CO_2 m^{-2} s^{-1} in well-watered plants (Fig. III-2a). This was due to the suppression of photorespiration activity (von Caemmerer 2000). At 4 Pa pCO_2 in well-watered plants, the CO_2 assimilation rate was lower than that at 40 Pa pCO_2 and 21 kPa pO_2. Because C_i was close to CO_2-compensation point and the electron sink capacity of photosynthetic CO_2 assimilation was limited, lower pCO_2 suppressed the CO_2 assimilation rate to near zero. At 4 Pa pCO_2, photorespiration activity was also suppressed with the lowering of pO_2, as observed in the increase of CO_2 assimilation rate to about 2 μmol CO_2 m^{-2} s^{-1} (Fig. III-2a). Furthermore, I used leaves of plants which suffered from drought stress (see "Materials and Methods", Fig. III-1). I observed that the leaves of drought-stressed plants responded somewhat differently from in well-watered leaves at 4 Pa pCO_2. At 40 Pa pCO_2, CO_2 assimilation rate was close to zero, and did

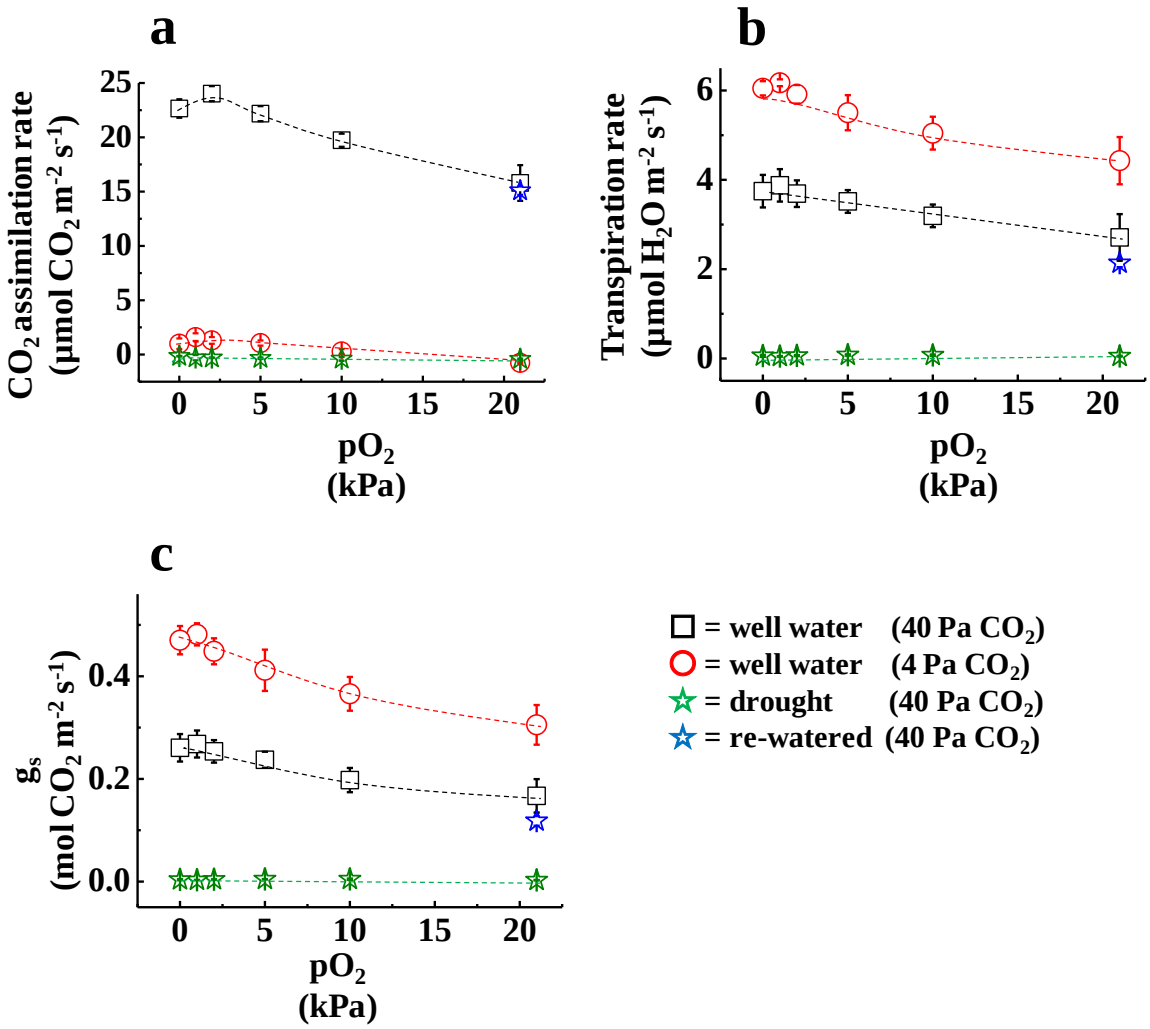

Figure III-2

Response to changes in the partial pressure of O_2 (pO_2) by CO_2 assimilation (a), transpiration rate (b), and stomatal conductance (c). Prior to analysis, plants were pre-illuminated at growth light intensity (500 µE m^{-2} s^{-1}) under ambient conditions [partial pressure of CO_2 (pCO_2) 40 Pa, pO_2 21 kPa] to activate electron sink in photosynthesis. After electron sink activation, pO_2 concentration was decreased in phases from 21 kPa to 0 kPa. For each pO_2, the parameters were obtained at steady state. Black square: well-watered leaves under 40 Pa pCO_2; Red circle: well-watered leaves under 4 Pa pCO_2; Green star: drought-stressed leaves under 40 Pa pCO_2; Blue star: re-watered leaves after drought stress under 40 Pa pCO_2. Data are expressed as mean ± SEM of three independent experiments.

not respond to the decrease in pO_2 in drought-stressed plants (Fig. III-2a). The drought-stressed plants after re-watering showed the same activity of photosynthetic CO_2 assimilation at 40 Pa pCO_2 and 21 kPa pO_2 (Fig. III-2a).

With lowering pO_2, transpiration rate increased from 3 to 4 μmol H_2O m^{-2} s^{-1} in well-watered plants at 40 Pa pCO_2 (Fig. III-2b). This was due to the stomatal opening, as observed in the increase in stomatal conductance (g_s) (von Caemmerer 2000). In fact, g_s also increased with lowering pO_2 (Fig. III-2c). At 4 Pa pCO_2, transpiration rate and g_s were higher than that at 40 Pa pCO_2 and 21 kPa pO_2 (Fig. III-2b, c). This result is consistent with many previous reports, which showed the increase of g_s under low pCO_2 conditions (e.g. Fujita et al. 2013). Lowering pO_2 also increased transpiration rate from 4.5 to about 6 μmol CO_2 m^{-2} s^{-1} at 4 Pa pCO_2 (Fig. III-2b). Then, g_s increased with lowering pO_2, accompanied by an increase in transpiration rate (Fig. III-2c). In contrast, the drought-stressed plants did not show any transpiration in the tested range of pO_2 at 40 Pa pCO_2, which corresponded with closure of the stomata, as shown in g_s (Fig. III-2b, c) (Mizokami et al. 2015). The drought-stressed plants after re-watering showed the same transpiration rate and g_s at 40 Pa pCO_2 and 21 kPa pO_2 (Fig. III-2b).

Effects of pO_2 on parameters on PSI

At 40 Pa pCO_2, Y(I), Y(ND), and Y(NA) responded little to the decrease in pO_2 in well-watered plants (Fig. III-3). That is, PET would not be limited by a change in photorespiration activity. At 4 Pa pCO_2, Y(I) was lower than that at 40 Pa pCO_2, and Y(I) decreased with lowering pO_2 from 10 kPa (Fig. III-3a). The drought-stressed plants showed the same behavior as the well-watered plants at 4 Pa pCO_2, except that Y(I) below 10 kPa pO_2 was lower than that of the well-watered plants at 4 Pa CO_2. This would be the lower photosynthetic CO_2-assimilation rate in drought-stressed plant than in well-watered plants at 4 Pa CO_2 because this corresponds to the response of photosynthetic CO_2 assimilation rate observed in Figure III-2a. At 4 Pa pCO_2, Y(ND) was higher than that at 40 Pa pCO_2

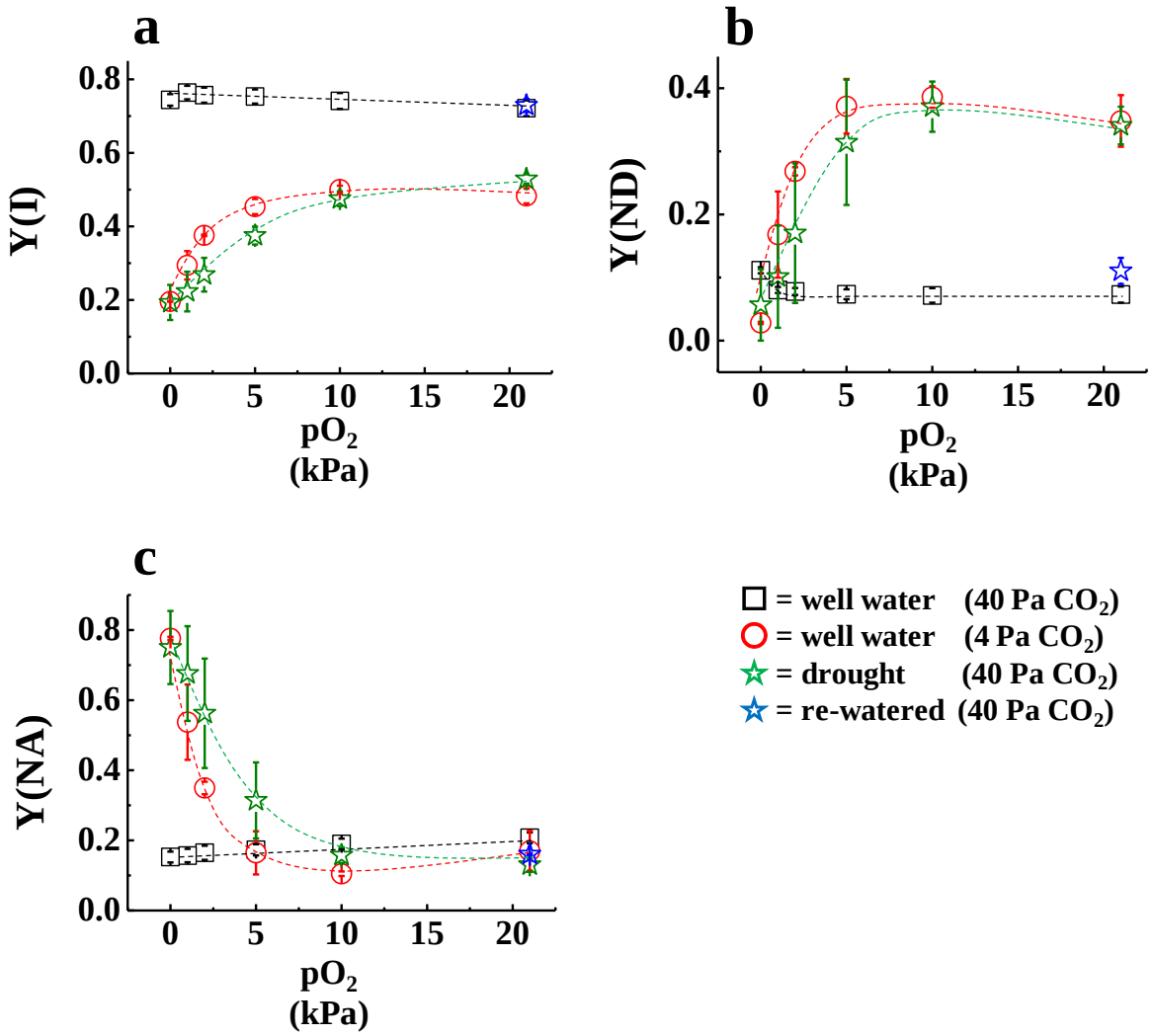

Figure III-3

pO_2 response of Y(I) (a), Y(ND) (b), and Y(NA) (c). Prior to analysis, plants were pre-illuminated at growth light intensity (500 µE m^{-2} s^{-1}) under ambient conditions (pCO_2 40 Pa, pO_2 21 kPa) to activate electron sink in photosynthesis. After electron sink activation, pO_2 concentration was decreased in phases from 21 kPa to 0 kPa. For each pO_2, the parameters were obtained at steady state. Black square: well-watered leaves under 40 Pa pCO_2; Red circle: well-watered leaves under 4 Pa pCO_2; Green star: drought-stressed leaves under 40 Pa pCO_2; Blue star: re-watered leaves after drought stress under 40 Pa pCO_2. Data are expressed as mean ± SEM of three independent experiments.

and Y(ND) decreased with lowering pO_2 from 10 kPa (Fig. III-3b). The behavior of Y(ND) resembled Y(I) (Fig. III-3a). The drought-stressed plants showed the same behavior with the well-watered plants at 4 Pa pCO_2 (Fig. III-3b). At 4 Pa pCO_2, Y(NA) was the same as that at 40 Pa pCO_2; however, Y(NA) increased with lowering pO_2 from 10 kPa (Fig. III-3c). The behavior of Y(NA) was roughly the inverse of Y(I) and Y(ND) (Fig. III-3a, b). The drought-stressed plants showed the same behavior with the well-watered plants at 4 Pa pCO_2 (Fig. III-3c). The drought-stressed plants after re-watering showed similar Y(I), Y(ND), and Y(NA) values to well-watered plants at 40 Pa pCO_2 and 21 kPa pO_2 (Fig. III-3).

Effects of pO_2 on parameters of PSII

At 40 Pa pCO_2, Y(II) and qL of well-watered plants showed minor response to the decreased pO_2 (Fig. III-4a, b). At 4 Pa pCO_2, Y(II) was lower than that at 40 Pa pCO_2, and Y(II) decreased with lowering pO_2 from 10 kPa (Fig. III-4a). The drought-stressed plants showed the same behavior with the well-watered plants at 4 Pa of pCO_2 (Fig. III-4a). However, Y(II) below 10 kPa pO_2 was lower than that of the well-watered plant leaves at 4 Pa pCO_2. As with Y(I), this corresponds to the lower photosynthetic CO_2 assimilation rate observed in Fig. 1A. At 4 Pa pCO_2, qL was lower than that at 40 Pa pCO_2, and qL decreased as pO_2 was lowered from 10 kPa (Fig. III-4b). The behavior of qL resembled Y(II) (Fig. III-4a). The drought-stressed plants showed the same behavior with the well-watered plants at 4 Pa of pCO_2 (Fig. III-4b). However, qL below 10 kPa pO_2 was lower than that of the well-watered plant leaves at 4 Pa pCO_2, similarly to Y(II) (Fig. III-4a). Just as for Y(II), this corresponds to the lower photosynthetic CO_2 assimilation rate in drought-stressed plants compared to well-watered plants at 4 Pa pCO_2 (Figs. III-2a, III-4a). NPQ slightly increased with the decrease in pO_2 at 40 Pa pCO_2 in well-watered plants (Fig. III-4c). NPQ showed higher value at 4 Pa pCO_2 compared to 40 Pa pCO_2, and NPQ decreased when pO_2 was below 2 kPa (Fig. III-4c). The drought-stressed plants again showed the same behavior at 4 Pa pCO_2. The drought-stressed plants

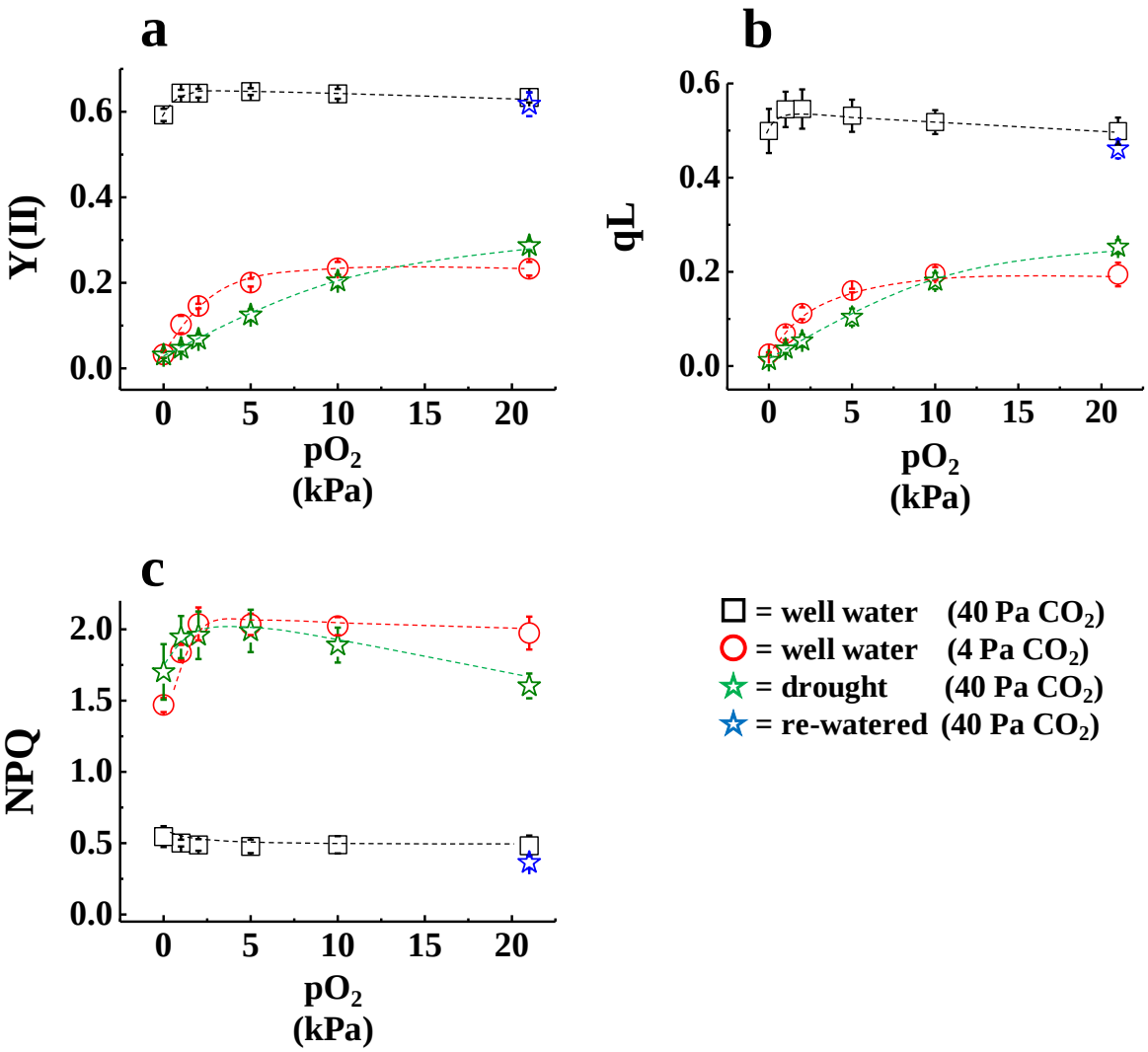

Figure III-4

pO_2 response of Y(II) (a), qL (b), and NPQ (c). Prior to analysis, plants were pre-illuminated at growth light intensity (500 µE m^{-2} s^{-1}) under ambient conditions (pCO_2 40 Pa, pO_2 21 kPa) to activate electron sink in photosynthesis. After electron sink activation, pO_2 concentration was decreased in phases from 21 kPa to 0 kPa. For each pO_2, the parameters were obtained at steady state. Black square: well-watered leaves under 40 Pa pCO_2; Red circle: well-watered leaves under 4 Pa pCO_2; Green star: drought stressed leaves under 40 Pa pCO_2; Blue star: re-watered leaves after drought stress under 40 Pa pCO_2. Data are expressed as mean ± SEM of three independent experiments.

after re-watering showed the same Y(II), qL, and NPQ at 40 Pa pCO_2 and 21 kPa pO_2 (Fig. III-4).

Effects of pO_2 on relative activity of CEF-I

The ratio of Y(I) to Y(II) gives a relative activity of cyclic electron flow around PSI (CEF-I) (Miyake et al. 2004). Values of Y(I)/Y(II) above 1 indicate the turnover and magnitude of CEF-I. At 40 Pa pCO_2, Y(I)/Y(II) of well-watered plants responded little to decreases in pO_2 (Fig. III-5). That is, CEF-I would not be limited by changes in photorespiration activity at 40 Pa pCO_2. At 4 Pa pCO_2, Y(I)/Y(II) was higher than that at 40 Pa pCO_2, and Y(I)/Y(II) increased as pO_2 decreased from 10 kPa (Fig. III-5). The drought-stressed plants showed the same behavior at 4 Pa pCO_2. These data suggest that lowering photorespiration activity induced CEF-I activity when photosynthetic CO_2 fixation activity was severely suppressed. The drought-stressed plants after re-watering showed the same Y(I)/Y(II) at 40 Pa pCO_2 and 21 kPa pO_2 (Fig. III-5). The behavior of Y(I)/Y(II) was inverse to that of Y(ND) at 4 Pa pCO_2, and in the drought-stressed plants (Figs. III-3b, III-5). That is, CEF-I did not contribute to the regulation of the redox-state of P700.

Effects of pO_2 on H^+-consumption rate

Photorespiration and the MAP-pathway require O_2 to express their activities (Badger et al. 2000; Brestic et al. 1995; Kozaki and Takeba 1996; Schreiber and Neubauer 1990; von Caemmerer 2000). However, in contrast to MAP-pathway, photorespiration uses ATP to regenerate RuBP from phosphoglycolate, which is produced by the oxygenation of RuBP catalyzed by Rubisco (Sejima et al. 2015; von Caemmerer 2000). Therefore, if photorespiration functions, consumption rate of H^+ should be modified based upon the ATP requirement for the regeneration of RuBP in the given range of pO_2 (Sejima et al. 2015). Accumulation of H^+ on the luminal side of thylakoid membranes, H^+-conductance, and H^+-consumption rate were evaluated as proton motive force, gH^+, and V_{H^+}, following the methods of Baker et al. (2007), Cruz et al. (2001), and Sacksteder et al. (2000). At 40

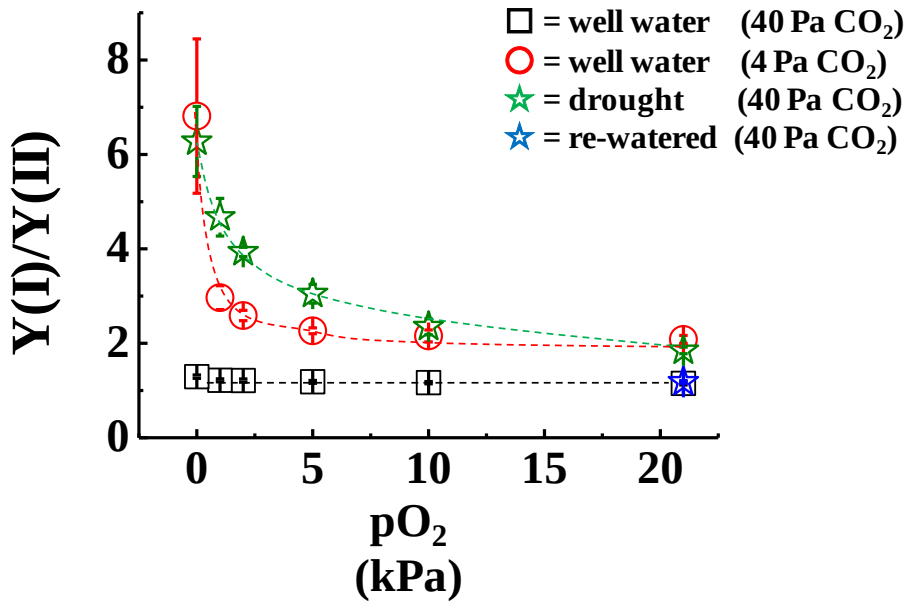

Figure III-5

pO_2 response of CEF activity estimated from the ratio of Y(I) and Y(II). CEF activity was calculated from Y(I) and Y(II) obtained in Fig. III-3 and III-4. Black square: well-watered leaves under 40 Pa pCO_2; Red circle: well-watered leaves under 4 Pa pCO_2; Green star: drought stressed leaves under 40 Pa pCO_2; Blue star: re-watered leaves after drought stress under 40 Pa pCO_2. Data are expressed as mean ± SEM of three independent experiments.

Pa pCO_2, proton motive force responded very little to decreased pO_2 in well-watered leaves (Fig. III-6a). At 4 Pa pCO_2, proton motive force was larger than that above 21 kPa pO_2 at 40 Pa pCO_2, and proton motive force decreased with decreasing pO_2 (Fig. III-6a). The drought-stressed plants showed the same behavior with the well-watered plants at 4 Pa pCO_2. gH^+ did not respond to the decrease in pO_2 in well-watered leaves at 40 Pa pCO_2, except below 2 kPa pO_2 (Fig. III-6b). V_H^+ also responded to decreased pO_2 only below 2 kPa pO_2 (Fig. III-6c). In contrast, at 4 Pa pCO_2, gH^+ was lower than that at 40 Pa pCO_2, and gH^+ decreased with lowering pO_2 (Fig. III-6b). V_H^+ at 4Pa pCO_2 was also lower than at 40 Pa pCO_2, and V_H^+ decreased with lowering pO_2 (Fig. III-6c). gH^+ and V_H^+ in the drought-stressed plants showed similar behavior with the well-watered plants at 4 Pa pCO_2. However, gH^+ and V_H^+ were slightly lower than that of the well-watered plant leaves at 4 Pa pCO_2. This again corresponds to the lower photosynthetic CO_2 assimilation rate in drought-stressed plants, compared to well-watered plants (Fig. III-2a). The drought-stressed plants after re-watering were close in value to the proton motive force, gH^+, and V_H^+ at 40 Pa pCO_2 and 21 kPa pO_2 (Fig. III-6).

As expected above, I detected V_H^+ in the range of pO_2 I set. That is, at lower pO_2 at 4 Pa pCO_2, the metabolic pathway to consume H^+ accumulated on the luminal side of the thylakoid membranes functioned, and the activity of H^+-consumed metabolic pathway was decreased as pO_2 decreased (Fig. III-6c). Based on these results, I propose that the metabolic pathway is driven by photorespiration, not by the MAP-pathway (Sejima et al. 2015).

Relationship of V_H^+ to qL, Y(ND), Y(II), and JgH^+

I tested whether the metabolic pathway accompanying H^+-consumption regulates the redox-state of PET components (Fig. III-7). I found that qL showed the strong relationship with V_H^+ (Fig. III-7a). Increase in V_H^+ oxidized the primary electron acceptor, Q_A, in PSII of thylakoid membranes (Kramer et al., 2004b). Y(ND) also showed a positive dependence on V_H^+ below 30 s^{-1} (Fig. III-7b). Above 30 s^{-1} of V_H^+, Y(ND) decreased with the increase in V_H^+. As V_H^+ showed a positive linear relationship

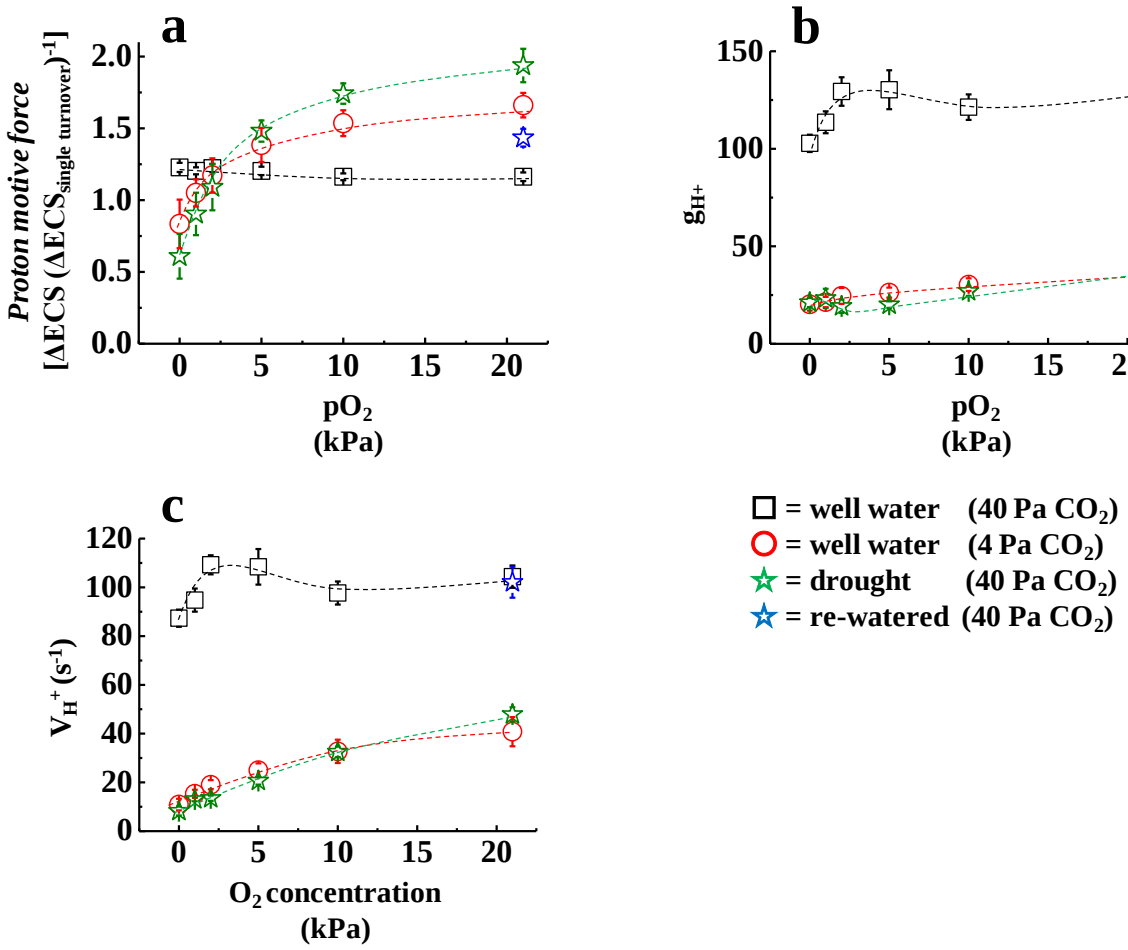

Figure III-6

pO_2 response of proton motive force (a), gH^+ (b), and V_H^+ (c). Before this analysis, plants were pre-illuminated at growth light intensity (500 µE m^{-2} s^{-1}) under ambient condition (pCO_2 40 Pa, pO_2 21 kPa) for activating electron sink. After the electron sink activation, pO_2 concentration was decreased in phases from 21 kPa to 0 kPa. For each pO_2, the parameters were obtained at steady state. Black square: well-watered leaves under 40 Pa pCO_2; Red circle: well-watered leaves under 4 Pa pCO_2; Green star: drought stressed leaves under 40 Pa pCO_2; Blue star: re-watered leaves after drought stress under 40 Pa pCO_2. Data are expressed as mean ± SEM of three independent experiments.

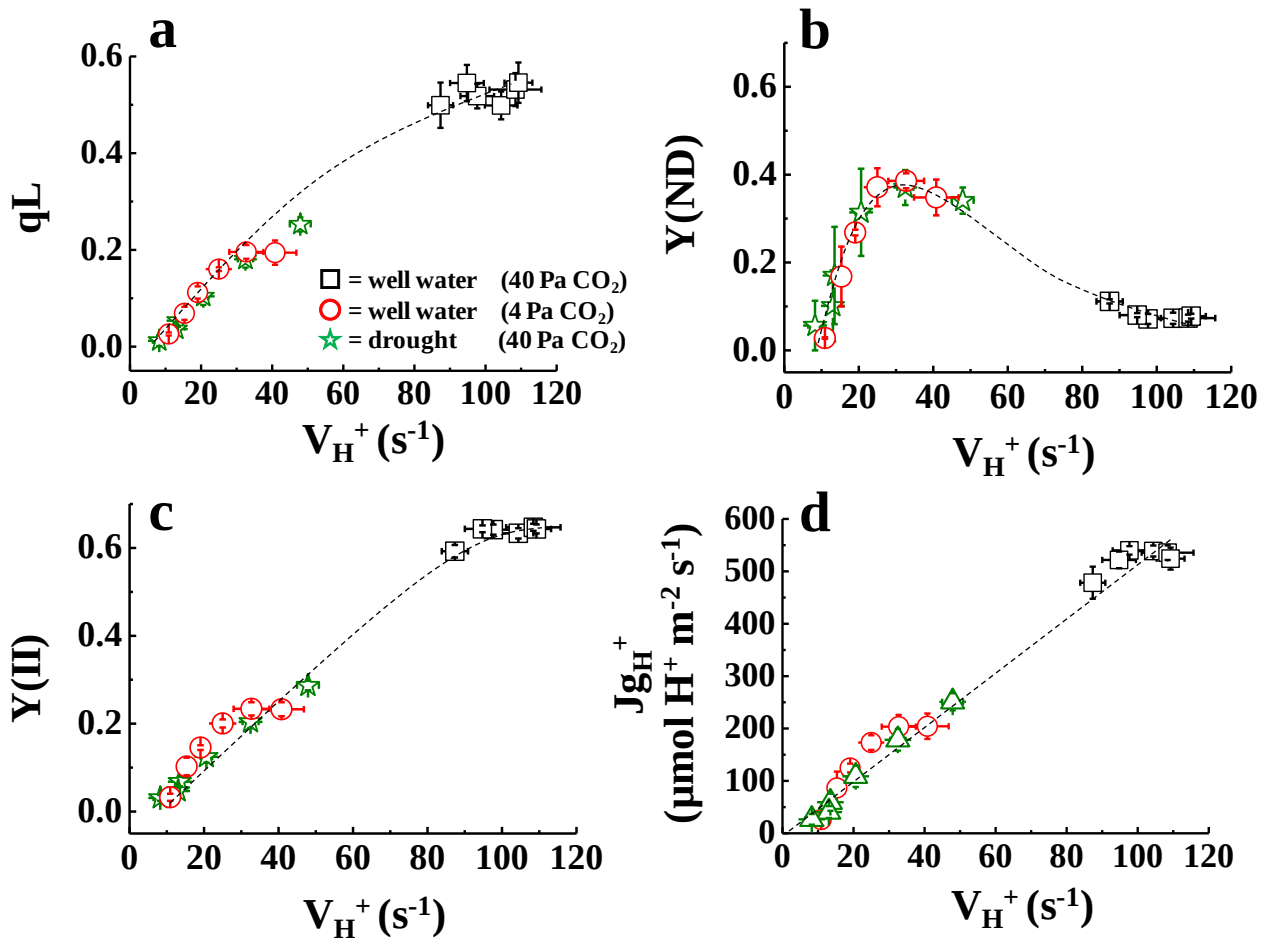

Figure III-7

The effect of proton consumption rate (V_H^+; estimated from ECS) on qL (a), Y(ND) (b), Y(II) (c), and JgH^+ (d) was shown. The values of V_H^+, qL, Y(ND), and Y(II) are those from Fig. III-3, III-4, and III-6. JgH^+ was calculated from the CO_2 assimilation rate and the value of Y(II) presented in Fig. III-2a and III-4a, respectively.

with Y(II) (Fig. III-7c), the stimulation of LEF consuming H^+ would suppress the acidification of luminal side of thylakoid membranes and decrease Y(ND) (Fig. III-7b). If V_H^+ reflects the H^+-consumption by photorespiration, the H^+-consumption rate, JgH^+, calculated by both carboxylation rate (vc) and oxygenation rate (vo) of RuBP catalyzed by Rubisco would show a positive linear relationship with V_H^+ (Sejima et al. 2015). Both vc and vo were estimated from Y(II) and CO_2-assimilation rate (see "Materials and Methods) (Sejima et al. 2015). I found that JgH^+ clearly showed a positive linear relationship with V_H^+ (Fig. III-7d). Statistical analysis showed that the intercept (2.6 ± 10.1, $p > 0.8$) of the linear regression line was zero, and the slope (5.19 ± 0.16, $p < 0.0001$) was above zero. The correlation coefficient (r^2) was 0.9844. This relationship is the same as that shown by Sejima et al. (2015). In C3-plants, such as tobacco and sunflower, V_H^+ reflects the H^+-consumption rate, which is given by photosynthesis and photorespiration. From these facts, I conclude that the metabolic pathway to consume H^+ is driven by photorespiration under low CO_2 or drought stress conditions. As observed in Figure III-7b, Y(ND) increased with the increase in photorespiration activity, where photorespiration functions as an electron sink.

DISCUSSION

In the present study, I aimed to elucidate the molecular mechanism that regulates the redox-state of P700, especially the oxidized form of P700, using intact leaves of sunflower. Under steady-state conditions, photo-oxidoreduction cycle of P700 occurs. Light excites the ground state of P700 to the excited state of P700, P700*. P700* donates an electron to the secondary electron acceptor in PSI and is oxidized to $P700^+$. Then, $P700^+$ is reduced to P700 by the electron from PSII through the Cyt b_6/f-complex and PC. The amount of $P700^+$ is determined by the balance between the input efficiency of electrons from PSII and the output efficiency of electrons from P700*. CEF-I and the MAP-pathway have been proposed to regulate the proton gradient (ΔpH) across the thylakoid membranes (Heber and Walker 1992). The acidification of the luminal side of thylakoid membranes suppresses electron flow from the Cyt b_6/f-complex (Tikhonov, 2013), which can contribute to oxidizing P700. However, I eliminated the possibility that CEF-I and MAP-pathway to regulate the redox-state of P700 in the present research (Figs. III-5, III-6c). I found that photorespiration functioned at lower pO_2, albeit with lower activity (Figs. III-6c, III-7d). Furthermore, photorespiration oxidized Q_A in PSII and P700 (Fig. III-7a, b). These results support the role of photorespiration as an electron sink in regulation of the redox-state of P700. At higher V_H^+ activity, Y(ND) decreased due to the activation of ATP consumption as photosynthesis is stimulated (Fig. III-7b, c, d).

Photorespiration has been proposed to protect PSII from photoinhibition in C3-plants (Brestic et al. 1995; Kozaki and Takeba 1996; Osmond and Grace 1995; Takahashi and Badger 2011; Wu et al. 1991). As a protector of PSII, photorespiration with the Calvin cycle has been considered as an electron sink. Photorespiration oxidizes PQH_2 to PQ, by stimulating electron consumption, and prevents the production of ROS in PSII to cause the oxidative degradation of D1 protein and the PSII-repair system (Aro et al. 1993; Nishiyama et al., 2004). In the present study, I add another physiological function to photorespiration: oxidizing P700 in PSI at the thylakoid membrane, which lowers the possibility of photoreduction of O_2 to produce ROS in PSI (Sejima et al. 2014).

In C4-plants (e.g. maize), photorespiration is suppressed in the mature leaves, where photorespiratory CO_2 release is estimated to be 2% of photosynthesis (De Veau and Burris 1989). The CO_2-compensation point in C4-plants is much lower than that in C3-plants because phosphoenol pyruvate carboxylase (PEPC) fixes HCO_3^-, which is converted from CO_2 by carbonic anhydrase (CA) (von Caemmerer 2000). Thus, C4-plants show a higher affinity to CO_2, and concentrate CO_2 in the bundle sheath cells to suppress photorespiration activity. In fact I could not observe any photorespiratory activity in maize leaves even at CO_2-compensation point in previous work (Sejima et al. 2015). However, the young leaves of maize plant show a higher activity of photorespiration, compared to the mature leaves (De Veau and Burris 1989, Dai et al. 1993). How the redox level of P700 is regulated in C4 plants remains to be clarified.

The MAP-pathway (the Water-Water cycle) can drive O_2-dependent electron flow in chloroplasts, with a magnitude ranging from 10 to 40 μmol O_2 (mg Chl)$^{-1}$ h^{-1} (Asada et al. 1974; Furbank and Badger 1983; Heber et al. 1978; Hormann et al. 1994; Miyake et al. 1998; Takahashi and Asada 1982, 1988). Chloroplasts have a scavenging system for ROS: superoxide dismutase (SOD), ascorbate peroxidase (APX), monodehydroascorbate reductase (MDAR), dehydroascorbate reductase (DHAR), and glutathione reductase (GR) (Asada 1999, Miyake et al. 1998). These scavenging enzymes support O_2-dependent electron flow. The MAP-pathway can induce ΔpH across thylakoid membranes, which can contribute to the production of ATP in chloroplasts (Schreiber and Neubauer 1990; Schreiber et al. 1991; Forti and Elli 1995, 1996; Takagi et al., 2012). These physiological functions were proposed on the basis of results obtained from *in vitro* experiments using intact chloroplasts. Contrary to these proposals, Ruuska et al. (2000) insisted that the MAP-pathway is a minor flux in LEF, even though photosynthetic activity was suppressed using Rubisco-antisense tobacco plants. Driever and Baker (2011) also insisted that the MAP-pathway is a minor flux in LEF. With our present study, I suggest that photorespiration can occupy a major electron flux in LEF, which regulates the redox-state of P700 to suppress the production of ROS in PSI *in vivo*.

Cyclic electron flow around PSI (CEF-I) can drive the induction of ΔpH across thylakoid membranes, and contribute to the production of ATP (Heber and Walker 1992). The concept of CEF-I was first proposed some decades ago (Arnon 1959, Allen 2002, 2003). The CEF-I story was developed in *in vitro* experiments, similarly to the MAP-pathway (Okegawa et al. 2008; Munekage et al. 2002; Nishikawa et al. 2012; Shikanai 2007; Yamamoto et al. 2011; Yamamoto and Shikanai 2013; Wang et al. 2014). Recently, molecular mechanisms to drive CEF-I were proposed using mutants of *A. thaliana* by Shikanai's group (Yamamoto et al. 2011; Wang et al. 2014). NADH dehydrogenase-like complex (NDH) functioned as a ferredoxin (Fd)-PQ oxidoreductase, where PGR5 protein might be required to regulate its activity. However, doubt is cast on this story by several studies (Fisher and Kramer 2014; Nandha et al. 2007; Laisk et al. 2007; Joliot et al. 2004). NDH and PGR5 contribute to the reduction of PQ using Fd as an electron donor, which activities has been shown as the increase in minimal Chl (F_o) fluorescence (DalCorso et al., 2008; Munekage et al. 2002; Okegawa et al. 2008; Yamamoto et al. 2011; Yamamoto and Shikanai 2013). These reduction activities were too small to explain the levels of *in vivo* activity (Laisk et al. 2007). Furthermore, antimycin A, the famous inhibitor of *in vitro* CEF-I activity, inhibits the reduction of Q_A in PSII (Fisher and Kramer 2014). These *in vitro* stories of CEF-I are covered by mysterious clouds; thus far, nobody can yet give a satisfactory answer as to its role.

Turning to the *in vivo* story of CEF-I, many researchers tried to identify its activity (Breyton et al. 2006; Clarke and Johnson 2001; Cornic et al. 2000; Golding and Johnson 2003; Johnson 2005; Joliot and Joliot 2002, 2005; Joliot et al. 2004; Laisk et al. 2007; Miyake et al. 2004, 2005a, 2005b). The turnover rate of CEF-I *in planta* is capable to reach about 100 s^{-1} per PSI (Joliot and Joliot 2002; Joliot et al. 2004; Laisk et al. 2005, 2007), which is much higher than NDH and PGR5-dependent CEF activity *in vitro* (0.035 s^{-1}, Fisher and Kramer 2014) or *in vivo* (1 s^{-1}, Gotoh et al. 2010; 0.1 s^{-1}, Trouillard et al. 2012). I also found lower activity of Fd-dependent Cyt *f*-reduction, using thylakoid membranes isolated from spinach leaves (Fig. III-8). When thylakoid membranes were exposed to far-red (FR) light, Cyt *f* was oxidized in the presence of Fd (Fig. III-8a).

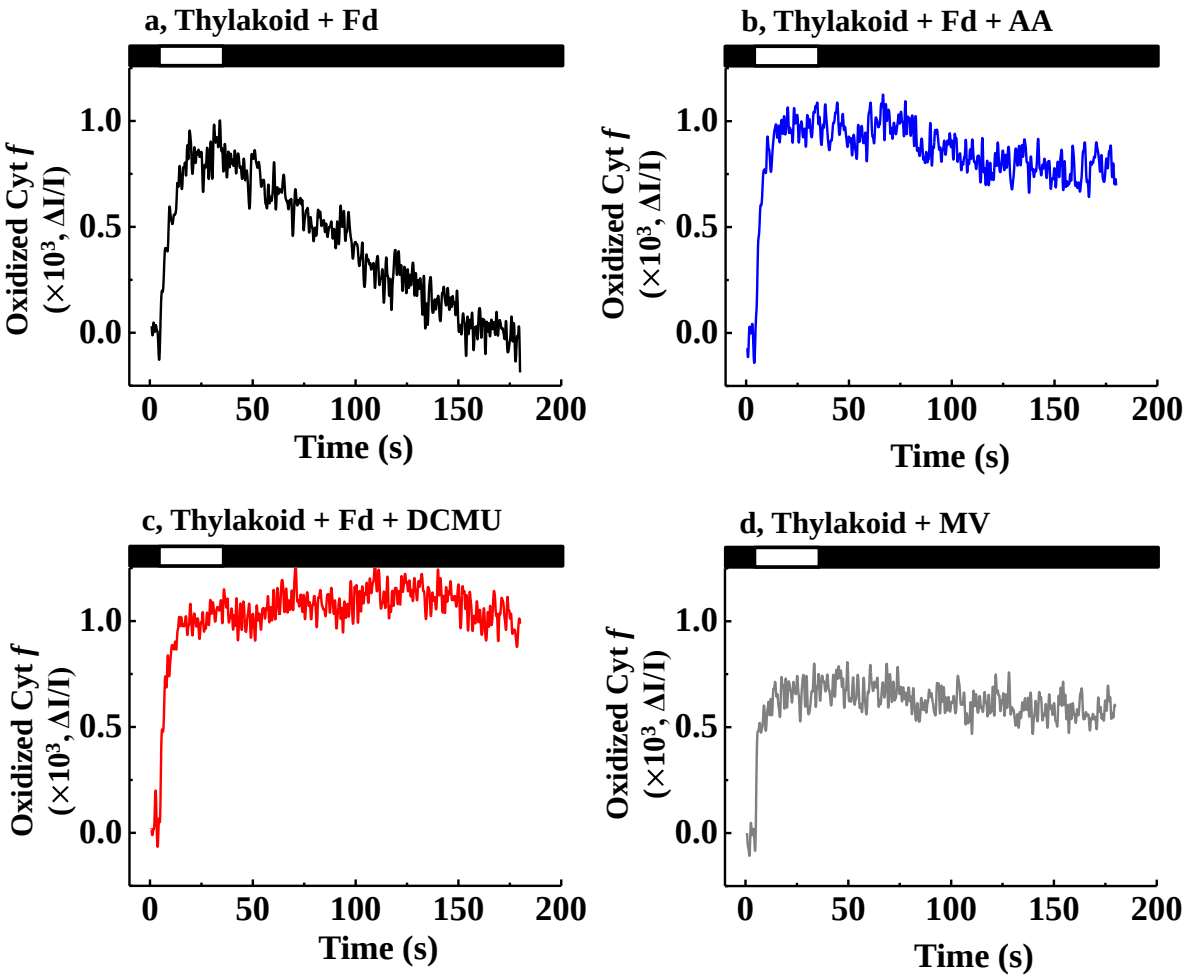

Figure III-8

The activity of cyclic electron flow estimated from the redox change of Cyt *f* in thylakoid membranes isolated from spinach leaves. The reaction mixture contained thylakoid membranes (30 µg Chl ml^{-1}) was used for this experiment. FR light was illuminated to the reaction mixture in the presence of Fd (5 µM) (A), Fd and antimycin A (10µM) (B), Fd and DCMU (10 µM) (C), or MV (50µM) (D). Typical data were shown in this figure. FR was illuminated for 30 s. The black bar indicates the duration of dark condition, and white bar indicates the duration of FR illumination.

Furthermore, after turning off of FR light, Cyt *f* was reduced quite slowly (time to half-reduction ~1 min; Fig. III-8a). The presence of antimycin A did not affect the oxidation of Cyt *f*; however, the reduction of Cyt *f* was suppressed (Fig. III-8b). Furthermore, the reduction of Cyt *f* was inhibited by the presence of DCMU (Fig. III-8c). To examine whether Fd is required for the reduction of Cyt *f*, I added methylviologen (MV) as an electron acceptor. The oxidation of Cyt *f* was then observed under FR illumination; however, the reduction of Cyt *f* was not observed after turning off FR illumination (Fig. III-8d). This observation corresponds to those reported by Fisher and Kramer (2014). From these results, I proposed the *in vitro* route of electron flow in CEF-I, as follows: the reduced Fd donates electrons to PSII directly, possibly to Q_A, and the electrons flow to PQ through Q_B (Fisher and Kramer, 2014). FR-dependent Cyt *f* reduction was also observed in intact chloroplasts (Fig. III-9a). Furthermore, AA and DCMU showed the same effects in thylakoid membranes (Fig. III-9b, c). I found the reduction rate of Cyt *f* to be quite slow, similar to the half-time of F_o increase of Chl fluorescence (Okegawa et al. 2008; Munekage et al. 2002; Yamamoto et al. 2011; Yamamoto and Shikanai 2013). Fd-dependent F_o increase *in vitro* and F_o increase after turning off AL *in vivo* showed a half-life of 10 s at least (Okegawa et al. 2008; Munekage et al. 2002; Yamamoto et al. 2011; Yamamoto and Shikanai 2013). These values were considerably small compared to CEF-I activity observed *in vivo*.

I also observed the increase in CEF-I activity *in vivo* estimated from the ratio of Y(I)/Y(II) at 4Pa pCO_2, and in the drought-stressed plants (Fig. III-5). Laisk et al. (2010) reported that CEF-I functions *in vivo*, where electrons from the reduced Fd flow to heme *c* in the Cyt b_6/*f*-complex (Kurisu et al. 2003, Stroebel et al. 2003). The reduced heme *c* donates electrons to high-potential heme *b* in the Cyt b_6/*f*-complex, where the reduced heme *b* donates electrons to Cyt *f* directly and does not contribute to the induction of ΔpH across thylakoid membranes (Laisk et al. 2010). I propose the possibility that this heme *c*-dependent CEF-I function under conditions of suppressed photosynthesis, such as drought stress. The photoreduction rate of O_2 in PSI is far smaller than that of heme *c*-dependent CEF-I *in vivo* (Asada et al. 1974; Furbank and Badger 1983; Heber et al., 1978;

Hormann et al. 1994; Laisk et al., 2010; Miyake et al. 1998; Takahashi and Asada, 1982, 1988). Therefore, heme *c*-dependent CEF-PSI could inhibit the photreduction of O_2 in PSI to produce ROS, and protect PSI from oxidative damages by ROS *in vivo*.

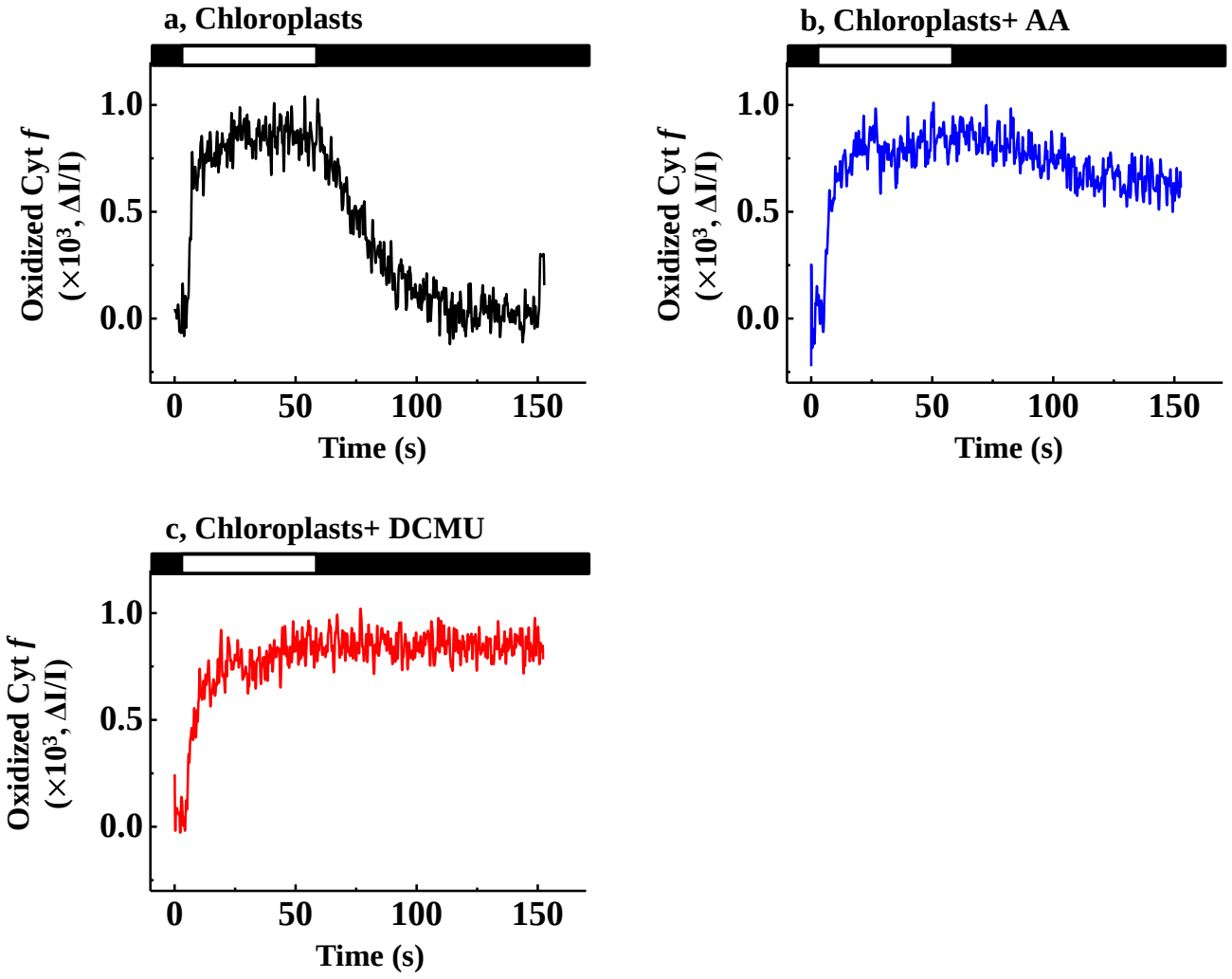

Figure III-9

The activity of cyclic electron flow by the redox change of Cyt *f* in intact chloroplasts isolated from spinach leaves. The reaction mixture contained intact chloroplasts (30 μg Chl ml^{-1}) was used for this experiment. FR light was illuminated to the reaction mixture (A), in the presence of antimycin A (10μM) (B), and in the presence of DCMU (10 μM) (C). Typical data were shown in this figure. FR was illuminated for 50 s. The black bar indicates the duration of dark condition, and white bar indicates the duration of FR illumination.

Chapter 4

Proton-management by chloroplastic CF_0CF_1-ATPsynthase is critical for the redox-regulation in Photosystem I in *A. thaliana* ~Electron sink and electron source communicate together by ATP requirement~

ABSTRACT

Over-reduction of photosynthetic electron transport chain should be avoid because the accumulation of reducing electron carriers produces reactive oxygen species (ROS), and reduces plant fitness through ROS-dependent oxidative damages in plant cell. Therefore, for improving the plant fitness, the mechanisms to regulate the redox-state in photosynthetic electron transport chain have to be elucidated. In this study, I isolated new allelic mutant which carries missense mutation in γ-subunit of chloroplast-localized CF_0CF_1-ATPase, named *hope2*. *hope2* showed high H^+-efflux activity, and highly reduced-state in photosystem I (PSI), compared to wild-type plant (WT). Furthermore, *hope2* was vulnerable to PSI photoinhibition under illumination, compared to WT. Here, I demonstrate that chloroplastic ATPase regulates the redox-state in photosynthetic electron transport chain, especially in PSI through the management of H^+-efflux.

INTRODUCTION

In many studies, the management of ΔpH is referred to the H^+-influx regulation in photosynthetic electron transport (Munekage et al., 2002; Shikanai, 2007; DalCorso et al., 2008; Miyake, 2010; Soursa et al., 2012). Alternative electro flow (AEF) is believed to stimulate the formation of ΔpH without producing NADPH, therefore AEF is considered to have important role to adjust ΔpH during photosynthetic electron transport (Miyake, 2010). Among AEF, Fd and NAD(P)H dehydrogenase like complex (NDH)-dependent cyclic-electron flow around PSI (CEF-I) and water-water cycle (WWC) have been well focused (Heber and Walker, 1992; Asada, 1999; Munekage et al., 2002; Shikanai, 2007; DalCorso et al., 2008; Yamamoto et al., 2011; Yamamoto and Shikanai, 2013). However, recent reports indicate that the activities of these AEFs hardly compete with LEF in higher plants. For example, compared to the rate of LEF (about 100 s^{-1}), Fd/NDH-dependent cyclic electron flow can proceed at the rate up to 1 s^{-1} (Gotoh et al., 2010; Joliot et al., 2004; Fisher and Kramer, 2014; Trouillard et al., 2012). WWC also shows quite lower electron transport activity than LEF (Driever and Baker, 2011; Shirao et al., 2013). Based on these reports, it is doubtful whether AEF truly important to control ΔpH in the photosynthetic electron transport reaction. Indeed, I demonstrated that major AEF, cyclic electron flow and water-water cycle does not contribute to the formation of *pmf* and the redox-regulation in PSI during photosynthesis (chapter 3). Then, what is the critical regulator of ΔpH across the thylakoid membranes during photosynthesis?

In this study, I showed that H^+-efflux regulation, but not H^+-influx regulation, by chloroplastic CF_0CF_1-ATPase (ATPase) is critical component to management ΔpH in photosynthetic electron transport reaction. I isolated ethyl methane sulfonate (EMS) mutant in *A.thaliana*, named *hope2*, which carried missense mutation in γ-subunit of ATPase. In *hope2*, H^+-efflux in ATPase increased compared to WT. The high H^+-efflux in ATPase caused lower *proton motive force* (*pmf*), furthermore, the highly reduced state in PSI. Due to the highly reduced state in PSI, *hope2* was vulnerable to PSI photoinhibition under illumination, compared to WT. Here, I proposed ATPase carries a central role in the regulation of photosynthetic electron transport reaction through the management of ΔpH.

MATERIALS AND METHODS

Plant Material and Plant growth conditions

In this study, I used *Arabidopsis thaliana* (Col). *Arabidopsis thaliana* mutagenized with ethyl methane sulfonate was purchased from LEHEL SEEDS (Texas, USA). Seeds were imbibed using wet cotton at 4°C for 3 days to promote synchronized germination. The imbibed seeds were grown in a mixture of soil (Metro-Mix 350; Sun Gro Horticulture, Bellevue, WA, USA) and vermiculite (Konan, Osaka, Japan) in pots (7.5 cm × 7.5 cm in width and 6 cm in depth). The plants were placed in an environmentally controlled chamber with 16 h of light (23 °C) and 8 h of darkness (21 °C). The light intensity was 150μE m^{-2} s^{-1}. The seedlings were watered every second day with 0.1% Hyponex solution (N:P:K = 5:10:5, Hyponex, Osaka, Japan). Analyses were carried out on fully expanded rosette leaves of plants grown for at least 3 weeks.

The quantification of leaf chlorophyll and nitrogen content

The chlorophyll and total carotenoids content was measured by the method of Porra et al. (1989). Leaf segments were incubated in N, N-dimethylformamide at 4^{o}C overnight. Absorbance at 750 nm, 663.8 nm, and 646.8 nm were measured to calculate chlorophyll content. Chlorophyll content in leaves was represented by leaf area base. Total leaf nitrogen content was determined with Nessler's reagent in a digestion solution after the addition of sodium-potassium tartrate (Makino and Osmond, 1991). Detached leaves were kept in a drying machine (60^{o}C) and dehydrated over-night. Sulfuric acid 60 % (v/v) (100 µl) and dehydrated leaves were mixed in the glass tube and incubated at 150^{o}C in a heating block thermostat bath for 40 min. After cooling the glass tube in the air, 30 % (v/v) H_2O_2 (50 µl) was added to the mixture. The mixture was incubated at 180^{o}C for 40 min in the heating block, subsequently H_2O_2 (50 µl) was added after the mixture was cooled. The incubation in the heating block and the addition of H_2O_2 were repeated another two times, but the incubation temperature was changed to 220^{o}C and 260^{o}C in each incubation respectively. The incubation at

260°C and the addition of H_2O_2 were continued until the color of the mixture turned clear from brown. When the color turned clear, distilled water (4.95 ml) was added to the mixture and mixed vigorously. The mixture (500 µl), distilled water (4.25 ml), 10 % (w/v) potassium sodium tartrate ($KNaC_4H_4O_6$) solution (100 µl) and 2.5 N sodium hydroxide (NaOH) (50 µl) were mixed and Nessler's reagent (100 µl) was immediately added to the mixture. Nitrogen content was determined by the absorbance change at 420 nm.

Measurement of gas exchange, chlorophyll fluorescence, and $P700^+$

Gas exchange analysis, chlorophyll fluorescence, and $P700^+$ were simultaneously measured with a Li-7000 (Li-Cor, Nebraska, USA) and Dual-PAM-100 (Heintz Walz GmbH, Effeltrich, Germany). Atmospheric gas (40 Pa CO_2/21 kPa O_2) and gas with the indicated mixture of pure O_2 and CO_2 were prepared by mixing 20.1% (v/v) O_2 in 79.9% (v/v) N_2, 1% (v/v) CO_2 in 99% N_2, and pure N_2 gas using a mass-flow controller (Kofloc model 1203; Kojima Instrument Co., Kyoto, Japan) was used in this study. The gases were saturated with water vapor at 18.0 ± 0.1°C and the leaf temperature was maintained at 25°C. The chlorophyll fluorescence parameters were calculated as described by Baker (2008), using the following parameters: F_o, minimum fluorescence yield; F_m, maximum fluorescence yield; and F_s, steady state fluorescence yield. Measuring light (0.1 µE m^{-2} s^{-1}) and saturated pulse (20,000 µE m^{-2} s^{-1}, 300 ms) were applied to determine Fo and Fm. The oxidation-reduction state of P700 chlorophyll was determined according to the methods of Klughammer and Schreiber (1994). The maximum oxidation level of P700 chlorophyll (P_m) was obtained using a saturated pulse under far-red light and reflected the maximum amount of photooxidized P700 chlorophyll. Actinic red light (AL) was used to measure the photosynthetic parameters.

Measurement of electrochromic shift

Gas exchange analysis and electrochromic shift were simultaneously measured with a Li-7000 and Dual-PAM equipped with a P515-analysis module (Klughammer et al. 2013). The gaseous phase was controlled as described in the previous section, "Measurement of gas exchange, chlorophyll fluorescence, and $P700^{+}$". The gases were saturated with water vapor at 18.0 ± 0.1°C and the leaf temperature was maintained at 25°C. The proton motive force, proton conductance (gH^{+}) in ATP synthase were measured by dark interval relaxation kinetics (DIRK) analysis as described in Baker et al. (2007) and Sacksteder et al. (2000). The magnitude of proton motive force was normalized by dividing the magnitude of ECS decay in DIRK analysis by the magnitude of ECS induced by single turnover flash (10 µs) (Klughammer et al. 2013). The measurement of ΔΨ and ΔpH was conducted as described in Cruz et al. (2001). The magnitude of ΔΨ and ΔpH was also normalized by dividing their magnitude by the magnitude of ECS induced by single turnover flash.

rSP-treatment

The rSP treatment was applied to *A.thaliana* leaves that had been dark-adapted for at least 1 h, as described previously (Sejima et al., 2014). Plants were illuminated with short-pulses (20,000 µE m^{-2} s^{-1}, 300 ms) every 10 s in the absence of AL, or in presence of AL (1,000 µE m^{-2} s^{-1}) for 1 h under the ambient conditions (40 Pa CO_2, 21 kPa O_2). After rSP treatment, the photosynthetic residual activities of PSII and PSI were determined as described in the figure legends.

SDS-PAGE and Western-blot analysis

For protein analysis, thylakoid membranes were isolated from WT and *hope2* leaves as described in Hisabori et al. (1993). Proteins were separated basis on chlorophyll content (5 µg), and chlorophyll content was evaluated as described in Arnon (1949). The proteins were electrophoresed on 12.5 % (w/v) SDS-polyacrylamide gels containing 6M urea (Laemmli, 1970). The Proteins were separated by SDS-PAGE, transferred onto polyvinylidene difluoride (PVDF) membrane (Merk Millipore,

Massachusetts , USA), and then blocked with blocking one reagent (Nakalai Tesque, Kyoto, Japan) for 30 min at room temperature (25 ^{o}C). The PVDF membrane was subsequently incubated with specific peptide antibody for 1 h at room temperature (25 ^{o}C). The PVDF membrane was washed 3 times with TBS tween buffer (10 mM Tris-HCl (pH 7.4), 0.14 M NaCl, 0.1 % (v/v) Tween-20) and incubated with ECL^{TM} peroxidase labeled anti-rabbit antibody (GE Healthcare, Buckinghamshire, UK) for 1 h at room temperature (25 ^{o}C). The PVDF membrane was washed three times with TBS tween buffer. Proteins were detected with an alkaline phosphatase labeling.

Map-based cloning

I conducted mapping for *HOPE2* gene as described in Okumura et al. (2013). I crossed *hope2* (Col) and WT (Ler), and isolated individual *hope2*-type F_2 plants. DNA was extracted from these plant leaves and searched *HOPE2* gene by using various cleaved amplified polymorphic sequence (CAPS) and simple sequence length polymorphism (SSLP) makers. Table IV-1 showed primers used for mapping.

Re-sequencing and detection of SNPs

Genome DNA was extracted by DNeasy Plant Mini Kit (QIAGEN, Germany). Each DNA sample (~1.5 µg in 130 µl solution) was sheared using Covaris S2 (Covaris, USA) with the following settings: duty cycle 10%, intensity 5, cycles/burst 100, 600 seconds. A half amount of the sheared DNA was applied to library construction using SPARK DNA Sample Prep Kit, Illumina Platform (Enzymatics Inc., USA). For adaptor and primers, NEBNext Singleplex Oligos for Illumina (NEB, USA) was used. PCR reactions for library amplification were performed using Kapa HiFi 2 x mastermix (Kapa Biosystems, USA), with 8 cycles of the recommended cycle condition. The amplified library was separated with 2% agarose gel, and 200-400 bp range of gel was sliced out to recover the library DNA. All libraries were quantified by real-time PCR using LightCycler480II (Roche Diagnostics, Germany) and SYBR Fast Illumina Library Quantification Kit (Kapa

Biosystems) to adjust the library concentration. Sequencing was conducted on GAIIx (illumina, USA), using TruSeq reagents (Cluster Kit v2 and SBS Kit v5) with 10 pM denatured libraries.

FASTQ data was imported into StrandNGS software (Agilent), and mapping of 75 nt reads to Arabidopsis Col-0 genome was done COBweb algorithm as following parameters; Minimum alignment score : 95, Number of gaps allowed : 5, Number of matches to be output for each read : 1, Ignore reads with alignment length less than : 25, Trim 3'end with average base quality less than : 10. Baysian-based SNPs were extracted in StrandNGS as following parameters; Ignore reference locations with coverage below : 6, Ignore reference locations with variants below : 4, Confidence score cutoff : 30. Effects by SNPs were detected on annotated genes (Ensemble Transcripts at 2012.12.16), then further analyzed with Excel. Candidate SNPs were selected following criteria; specific line had specific SNPs and sequence on same position for other lines were same to reference genome, percentage of mutated SNP sequence was more than 60% for coverage, only typical conversions of nucleotide by EMS, G to A / C to T, were selected.

Plant Transformation

Plant transformation was performed as described in Okumura et al. (2013). For generating complementation lines of *hope2*, genomic DNA of *ATPC1* containing 2kb of the 5'-and 2kb of 3'-flanking sequence was amplified by KOD-FX NEO (Toyobo, Osaka, Japan), and this amplified sequence was subcloned into pDONR 221 (Invitrogen, California, USA). Primers used for plant transformation were as follows; *ATPC1* forward, 5'-AAAAAGCAGGCTTGTAATTTCGATATGAAATT-3'; *ATPC1* reverse, 5'-AGAAAGCTGGGTGAGTTTGGCGCTATTTTGGA -3'. I used Gate-way technology (Invitrogen, California, USA), and subcloned sequence was transferred to pGWB401 (Nakagawa et al., 2007). The transformation of *hope2* was performed by floral dipping using *Agrobacterium tumefaciens* (strain C58pMP90) (Clough and Bent 1998).

Table IV-1 Primers list for *HOPE2* mapping

Name	Forward primer	Reverse primer	Type	Restriction enzyme
F6N15	5'-CATTCAAAGTGTCATCCTTGAG-3	5'-GGCCTTTTAAGTCATGGATTG-3'	SSLP	
F3D13	5'-GCCATTCTCGATCTTCTCATC-3	5'-CATCGCACGATCTTCTCTAC-3	CAPS	EcoRI
T25H8	5'-AACCCAATCCTTCGAGTGAGC-3	5'-GGATGGACCATCCTTTCAGCC-3'	CAPS	EcoRI
T32N4	5'-ATCTGCATTTGTCTTTACGTC-3	5'-AGATGATGAAGTTGGTAGGTC-3'	CAPS	EcoRV
C6L9	5'-GTCTCTCATGCCTTTGTTCA-3'	5'-TAACTCTCTCTCGATCTCCGT-3'	SSLP	EcoRI
T1J24	5'-GGACAAGACTGGCCTACAAC-3'	5'-CGGATACGGCAATTGTATCC-3'	CAPS	EcoRI
T14G16	5'-TCGACTAGATTTATTATTTCTCTCAG-3'	5'-GTTTGGCTTGACTCTGTGAAC-3'	SSLP	
F9M13	5'-TTCTCCATAAGACACACGACG-3	5'-AACGCTTCCTTCTCAGTACC-3'	CAPS	EcoRI
T15F16	5'-CAGCACCACAAACTTCTTTCG-3'	5'-AAGGGCTATGACAAAGACAACG-3'	CAPS	XhoI

RESULTS

Isolation of *hope2* mutant from ethyl methane sulfonate treated *A. thaliana*

To identify the critical component to manage ΔpH in photosynthetic electron transport reaction, I tried to isolate a mutant which impaired ΔpH-dependent regulation in photosynthesis from A.thaliana mutagenized by ethyl methanesulfonate (EMS). For the isolation, I set specific gaseous conditions for this screening. Under the gas conditions where CO_2 and O_2 are present, the Calvin-cycle and photorespiration act as an electron sink which has large electron consumption capacity during photosynthesis in higher plants (Badger et al., 2000). Then, electron sink itself regulates the redox state of photosynthetic electron transport chain. Therefore, under such conditions, ΔpH-dependent redox regulation of photosynthetic electron transport chain would be elusive. Based on these considerations, I set low O_2 conditions (0 Pa CO_2, 2 kPa O_2) where the Calvin-cycle and photorespiration are largely suppressed as screening conditions. The redox-state of photosynthetic electron transport chain was evaluated steady-state chlorophyll fluorescence (Fs) which is regulated by photochemical and non-photochemical quenching under red actinic light (AL) illumination (150 μE m^{-2} s^{-1}) monitored by two-dimensional chlorophyll fluorescence analyzer (Baker, 2008). In WT plant, chlorophyll fluorescence was largely induced when AL was illuminated, but chlorophyll fluorescence was successfully quenched over time, and approached Fo level under low O_2 conditions (Fig. IV-1a). In contrast, under anoxia conditions (0 Pa CO_2, 0 k Pa O_2), WT failed to quenched Fs under illumination (Fig. IV-1b). That is, even under low O_2 condition, WT can operate the redox regulatory system in photosynthetic electron transport chain under the illumination. For the isolation of the target mutant, I screened approximately 10,000 EMS treated *A. thaliana* [ecotype; Columbia-0 (Col)]. Then, I isolated about 40 mutant lines which showed higher Fs level, compared to WT under low O_2 conditions. To eliminate the mutant lines that impaired electron sink capacity, I monitored the kinetics of chlorophyll fluorescence under ambient conditions (40 Pa CO_2, 21 kPa O_2) where the Calvin-cycle and photorespiration can operate, and ambient O_2 conditions (0 Pa CO_2, 21 kPa O_2) where photorespiration can operate. Then, I isolated the mutant lines that are capable to quench Fs.

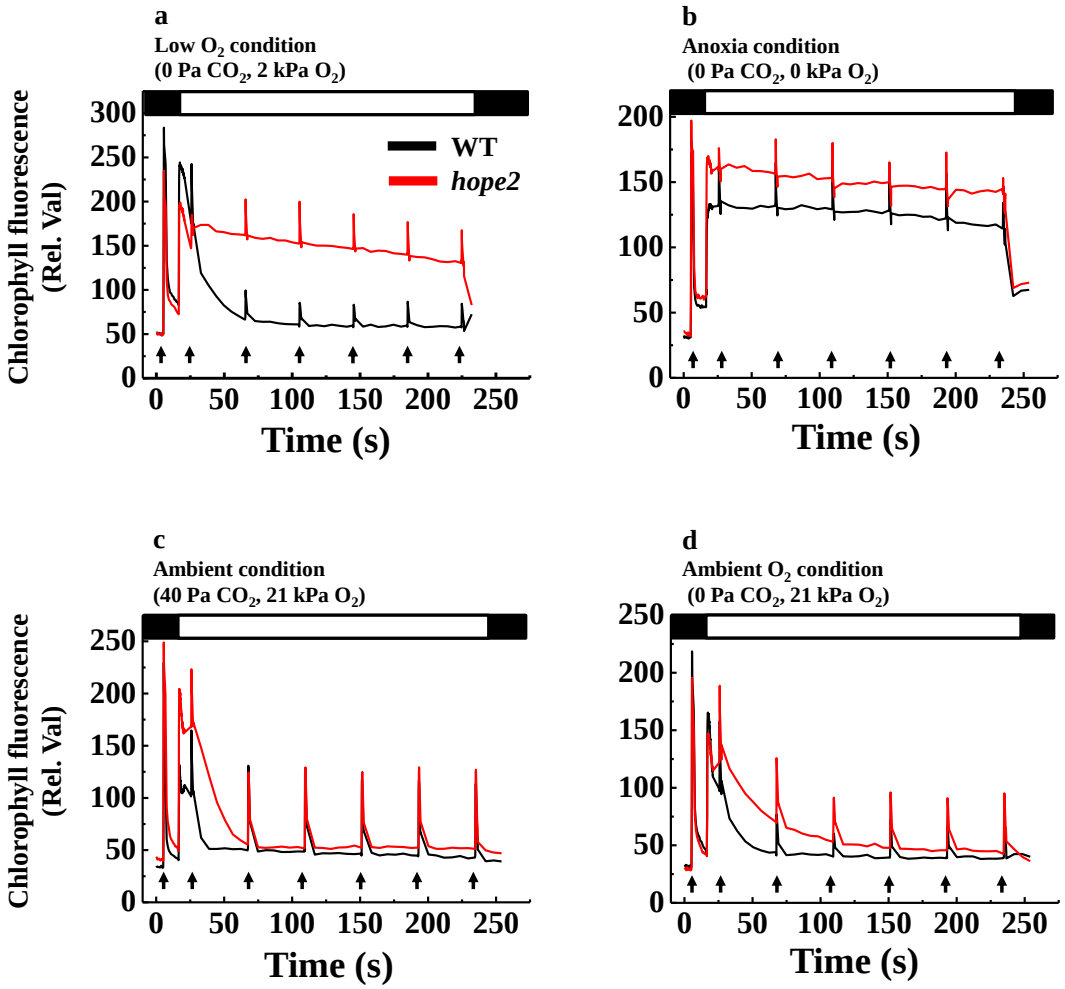

Figure IV-1

Isolation of *hope2* mutant by using chlorophyll fluorescence analysis. The typical kinetics of chlorophyll fluorescence under (a) low O_2 conditions (0 Pa CO_2, 2 kPa O_2), (b) anoxia conditions (0 Pa CO_2, 0 kPa O_2), (c) ambient condition (40 Pa CO_2, 21 kPa O_2), and (d) ambient O_2 conditions (0 Pa CO_2, 21 kPa O_2) were shown. Black lines indicate the kinetics of WT, and red lines indicate the kinetics of *hope2* mutant. Plants were adapted in the dark at least 1h. Black bars represented above the figures indicate dark conditions, and white bars represented above the figure indicate AL illumination (150 µE m^{-2} s^{-1}). Arrows in the figure indicate the illumination of saturation pulse (10,000 µE m^{-2} s^{-1}; 1s) at that time.

During this screening, I obtained recessive mutant in *A. thaliana* M2 seedling, named *hunger for oxygen in electron transport reaction 2* (*hope2*). *hope2* showed greatly higher Fs level under low O_2 conditions, compared to WT (Fig. IV-1a). In contrast, *hope2* quenched Fs under ambient conditions and ambient O_2 conditions (Fig. IV-1c, d). Under anoxia conditions, *hope2* showed high Fs level, similar to WT (Fig. IV-1b). These results showed that the redox-state regulatory system in photosynthetic electron transport chain independent of electron sink activity is disturbed in *hope2*. To confirm whether the redox regulatory system disturbed in *hope2* relates to ΔpH, I analyzed *pmf*, ΔΨ, and ΔpH under low O_2 conditions by using electrochromic shift (Cruz et al., 2001). Under ambient condition, *pmf*, ΔΨ, and ΔpH were not significantly different (Fig. IV-2a). In contrast, *pmf*, and ΔpH were significantly lower in *hope2* compared WT under low O_2 conditions (Fig. IV-2b). These results indicate that *hope2* exactly collapsed the management of ΔpH under the condition where electron sink activity is severely suppressed.

Next, I evaluated the growth in *hope2*. Under our growth conditions [16 h light (150 μE m^{-2} s^{-1}), 25 ^{o}C, and 8 h dark 23 ^{o}C], *hope2* grew normally, similar to WT (Fig. IV-3). Furthermore, leaf chlorophyll content, chlorophyll *a*/*b* ratio, and N content were similar between WT and *hope2* (Table IV-2). These results indicate that the mutation carried in *hope2* is not essential for plant growth.

The light response analysis of photosynthetic performance in *hope2* at the steady state

I studied photosynthetic activity in *hope2* at steady state under ambient conditions. I simultaneously analyzed gas exchange, chlorophyll fluorescence, and $P700^{+}$ by Li-7000 (Li-Cor, USA) and Dual-PAM (Walz, Germany). Maximum quantum yield of PSII showed similar value between WT and *hope2* [WT; 0.813±0.006, *hope2*; 0.808 ±0.005 (n = 3)]. The light response analysis of CO_2 fixation rate showed that *hope2* has similar CO_2-fixation activity to WT (Fig. IV-4a). Then, stomatal conductance (g_s) and the partial pressure of intercellular CO_2 (Ci) also showed similar value between WT and *hope2* (Fig. IV-4b, c). In both WT and *hope2*, quantum yield of PSII [Y(II)], and the redox-state of Q_A in PSII (qL) similarly decreased with the increase in light intensity (Fig. IV-4d, e).

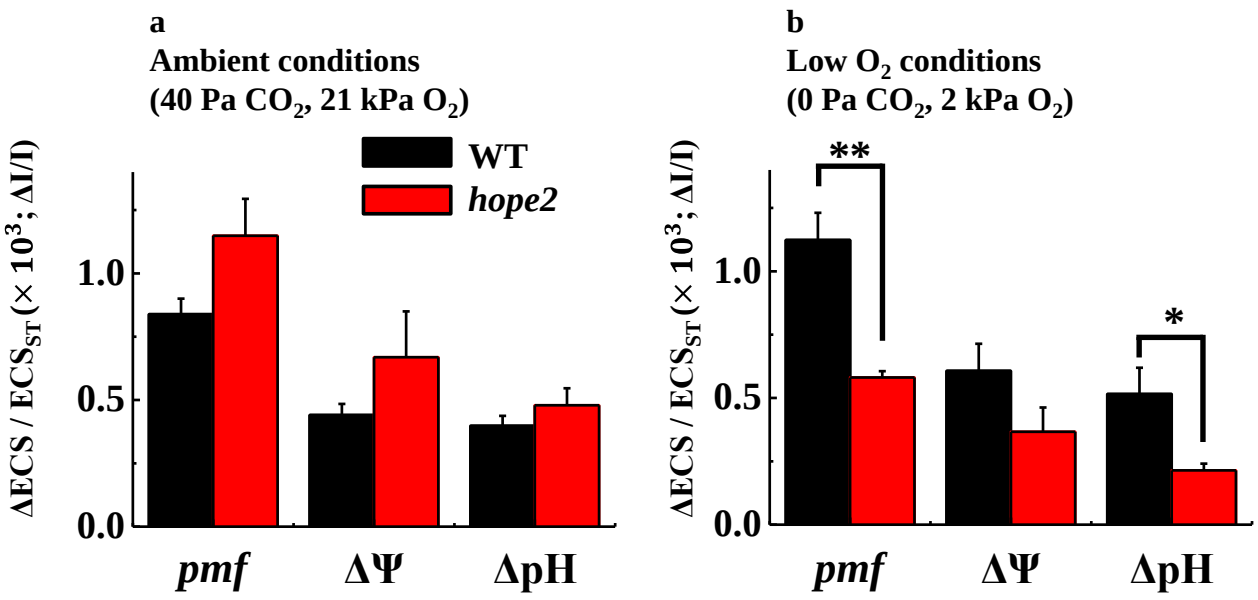

Figure IV-2

The comparison of *pmf*, ΔpH, and ΔΨ between WT and *hope2* at steady-state photosynthesis. AL (150 µE m^{-2} s^{-1}) was illuminated under ambient conditions (40 Pa CO_2, 21 kPa O_2) (a), and low O_2 conditions (0 Pa CO_2, 2 kPa O_2) (b). Black bars indicate WT and red bars indicate *hope2* mutant. Data are expressed as mean ± SEM of at least three independent experiments. The asterisk indicates a significant difference between WT and *hope2* (Student's t-test; *, $p < 0.05$; **, $p < 0.01$).

Figure IV-3

Phenotype of WT and *hope2* under growth conditions. Typical plants were photographed at 3 weeks after germination. WT and *hope2* were grown under day (16 h, 23 ^{o}C) /night (8 h, 20 ^{o}C) cycle conditions. The growth light intensity during the day was set 150μE m^{-2} s^{-1}. Atmospheric condition was kept ambient (40 Pa CO_2, 21 kPa O_2) and relative humidity was kept about 60 %. White bar drawn in the picture indicates a length, 1 cm.

Table IV-2
Chlorophyll and Nitrogen content in WT and *hope2* leaves

	WT	*hope2*
N (μmol m^{-2})	78.9 ± 4.3	78.4 ± 1.8
Chl *a* (mg m^{-2})	186.3 ± 1.9	174.1 ± 4.8
Chl *b* (mg m^{-2})	51.0 ± 0.7	44.8 ± 2.9
Total (mg m^{-2})	237.3 ± 2.4	218.8 ± 7.6
Chl *a/b*	3.6 ± 0.1	3.9 ± 0.1

Data are expressed as mean ± SEM of at least three independent experiments.

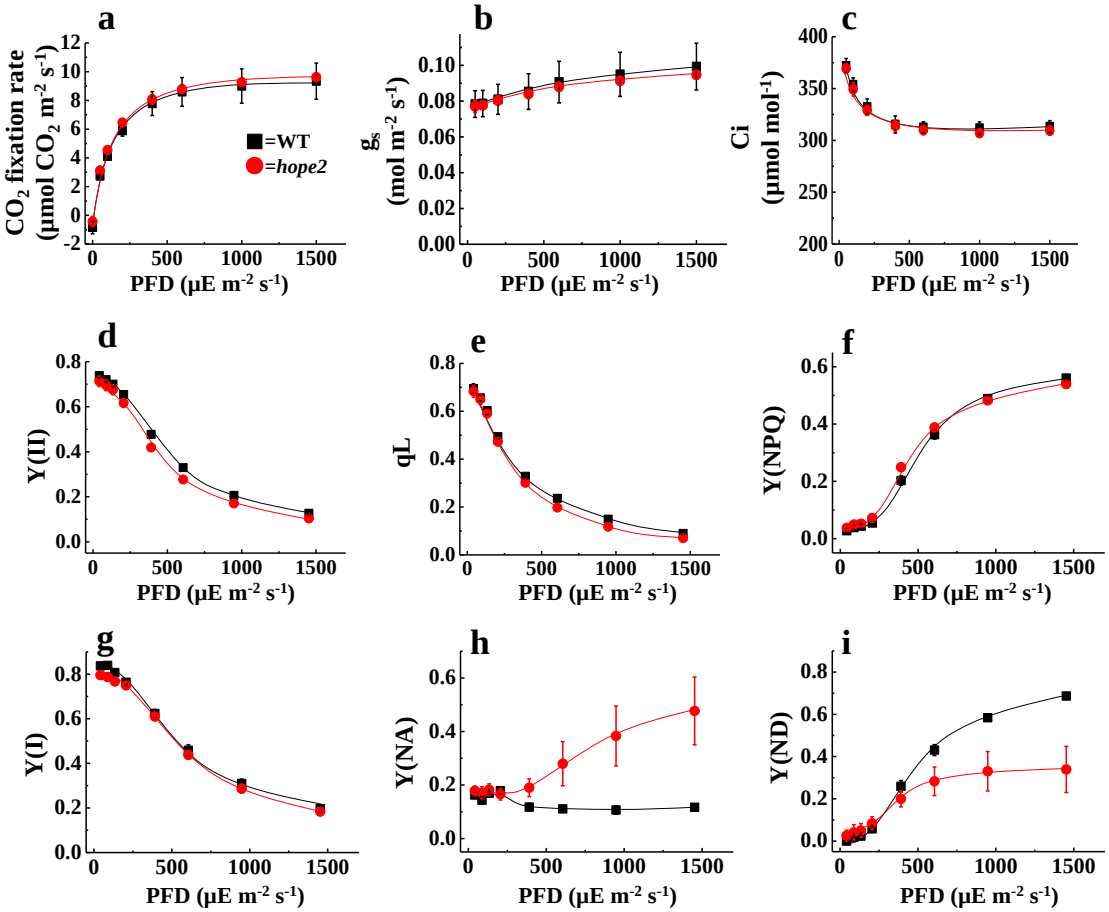

Figure IV-4

Light response of photosynthetic parameters evaluated from gas exchange, chlorophyll fluorescence, and the kinetics of $P700^{+}$ in WT and *hope2*. The measurements were conducted under ambient conditions (40 Pa CO_2, 21 kPa O_2). Before this analysis, AL (150μE m^{-2} s^{-1}) was illuminated in leaves for 10min to activate the electron sink in photosynthesis. (a) CO_2 assimilation rate, (b) stomatal conductance (g_s), and (c) intercellular CO_2 concentration (Ci) were determined by gas-exchange analysis. (d) Y(II), (e) qL, and (f) Y(NPQ) were determined by chlorophyll florescence. (g) Y(I), (h) Y(NA), and (i) Y(ND) were determined by absorbance change of 830 nm. Black squares indicate WT and red circles indicate *hope2*. Data are expressed as mean ± SEM of at least three independent experiments.

Quantum yield of light-induced NPQ [Y(NPQ)] increased with the increase in light intensity, but there was no difference between WT and *hope*2 (Fig. IV-4f). In addition to chlorophyll fluorescence parameters, I calculated quantum yield of PSII [Y(I)], and quantum yield of non-photochemical energy dissipation in reaction center which are limited due to a shortage of electrons [Y(ND)] and electron acceptors [Y(NA)] (Klughammer and Schreiber, 1994). Y(I) in *hope2* decreased with the increase in light intensity, similar to that in WT (Fig. IV-4g). In contrast, Y(NA) in WT hardly respond to the increase in the light intensity, however Y(NA) in *hope2* largely increased under high light conditions (Fig. IV-4h). Furthermore, Y(ND) in *hope2* was suppressed to increase under high light conditions, compared to that in WT (Fig. IV-4i). From these results, I found that *hope2* maintains photosynthetic electron transport activity over the range of the light intensity. However, unlike WT which photosynthetic electron transport is limited at the donor-side of PSI, photosynthetic electron transport in *hope2* is highly limited at the acceptor side of PSI under high light conditions. This means that PSI in *hope2* becomes the reduced state compared to WT under high light conditions.

Photosystem I becomes extremely reduced state in *hope2* under low Ci conditions

I studied the response of photosynthetic parameters in WT and *hope2* to the change of Ci under high light conditions. CO_2 -fixation rate increased with the increase in Ci, and CO_2 -fixation rate was similar between WT and *hope2* over the range of Ci (Fig. IV-5a). Similar to the response of CO_2 fixation rate to the change of Ci, Y(II) both in WT and *hope2* increased with the increase in Ci (Fig. IV-5b). From these results, I found that *hope2* can operate LEF under the condition where CO_2 -fixation is limited in both the carboxylation of RuBP by Rubisco and RuBP regeneration (von Caemmerer and Farquhar 1981). Then, qL and Y(NPQ) showed similar response in both WT and *hope2* similarly over the range of Ci (Fig. IV-5c, d). Therefore, the change of Ci does not affect the redox-state in PQ and thermal dissipation in PSII in *hope2*.

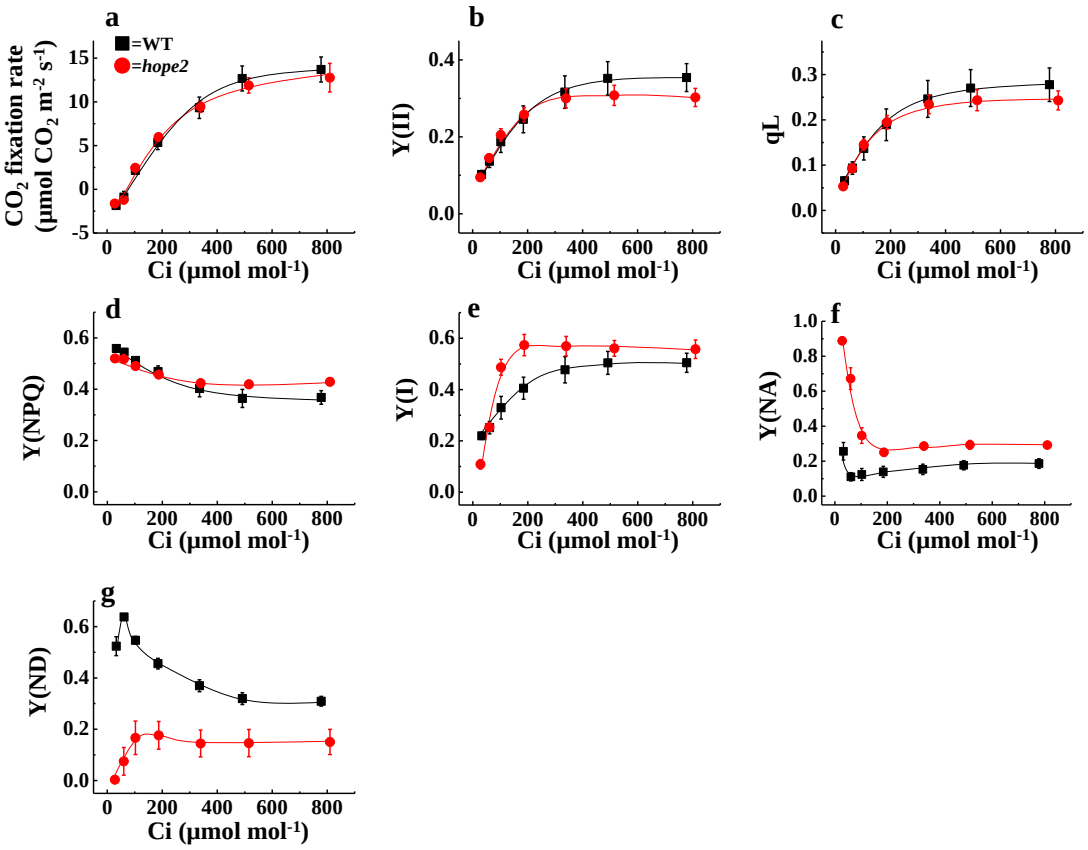

Figure IV-5

CO_2 response of photosynthetic parameters evaluated from gas exchange, chlorophyll fluorescence, and the kinetics of $P700^+$ in WT and *hope2*. In this analysis, AL intensity was set 1,000 μE m^{-2} s^{-1}. Before this measurement, AL (400μE m^{-2} s^{-1}) was illuminated in leaves for 10min to activate the electron sink in photosynthesis under ambient conditions (40 Pa CO_2, 21 kPa O_2). (a) CO_2 assimilation rate was determined by gas-exchange analysis. (b) Y(II), (c) qL, and (d) NPQ were determined by chlorophyll florescence. (e) Y(I), (f) Y(NA), and (g) Y(ND) were determined by absorbance change of 830 nm. Black squares indicate WT and red circles indicate *hope2*. Data are expressed as mean ± SEM of at least three independent experiments.

Y(I) increased with the increase in Ci in WT (Fig. IV-5e). On the other hand, Y(I) in *hope2* also increased with the increase of Ci, however, the kinetics was different from WT (Fig. IV-5e). Although *hope2* showed lower Y(I) compared to WT under very low Ci condition (40 μmol mol^{-1}), *hope2* showed higher Y(I) under the range of Ci between 100 to 300 μmol mol^{-1}, compared to WT (Fig. IV-5e). Y(NA) in WT was slightly increased under low Ci conditions, however Y(NA) was stable to the change of Ci in WT (Fig. IV-5f). In contrast, Y(NA) in *hope2* showed extremely higher value under low Ci conditions (Fig. IV-5f). Although Y(NA) in *hope2* relaxed with the increase in Ci, Y(NA) was higher in *hope2* than WT even under high Ci conditions. Y(ND) in WT marked higher value under low Ci conditions, and Y(ND) was relaxed with the increase in Ci (Fig. IV-5g). On the contrary to the kinetics in WT, *hope2* hardly induced Y(ND) under low Ci conditions (Fig. IV-5g). The increase in Ci partially induced Y(ND) in *hope2*, however the values were lower than WT (Fig. IV-5g). There results indicate that, in *hope2*, the limitation of photosynthetic electron transport reaction at the acceptor-side in PSI is more pronounced under low Ci condition where CO_2-fixation was largely restricted. That is, *hope2* cannot regulate the redox-state in PSI when electron sink capacity is limited.

Photosynthetic electron transport reaction is highly limited at the acceptor-side of PSI in *hope2* during the induction phase in photosynthesis

In our preceding section, I found that the regulation of the redox-state in PSI is disturbed in *hope2* when photosynthetic electron sink capacity is limited. Based on these observations, the induction phase in photosynthesis should affect the redox-state in *hope2* because electron sink is inactivated in the dark. To confirm this possibility, I analyzed the kinetics of photosynthetic parameters during the induction phase in WT and *hope2*, which were adapted in the dark to inactivate the electron sink. After AL onset, CO_2-fixation rate was increased and reached steady-state at about 3 min in WT (Fig. IV-6a). This was also observed in *hope2*, and CO_2-fixation rate was similar between WT and *hope2*. Then, g_s and Ci showed same kinetics in WT and *hope2* (Fig. IV-6b, c). Y(II) and qL in WT and

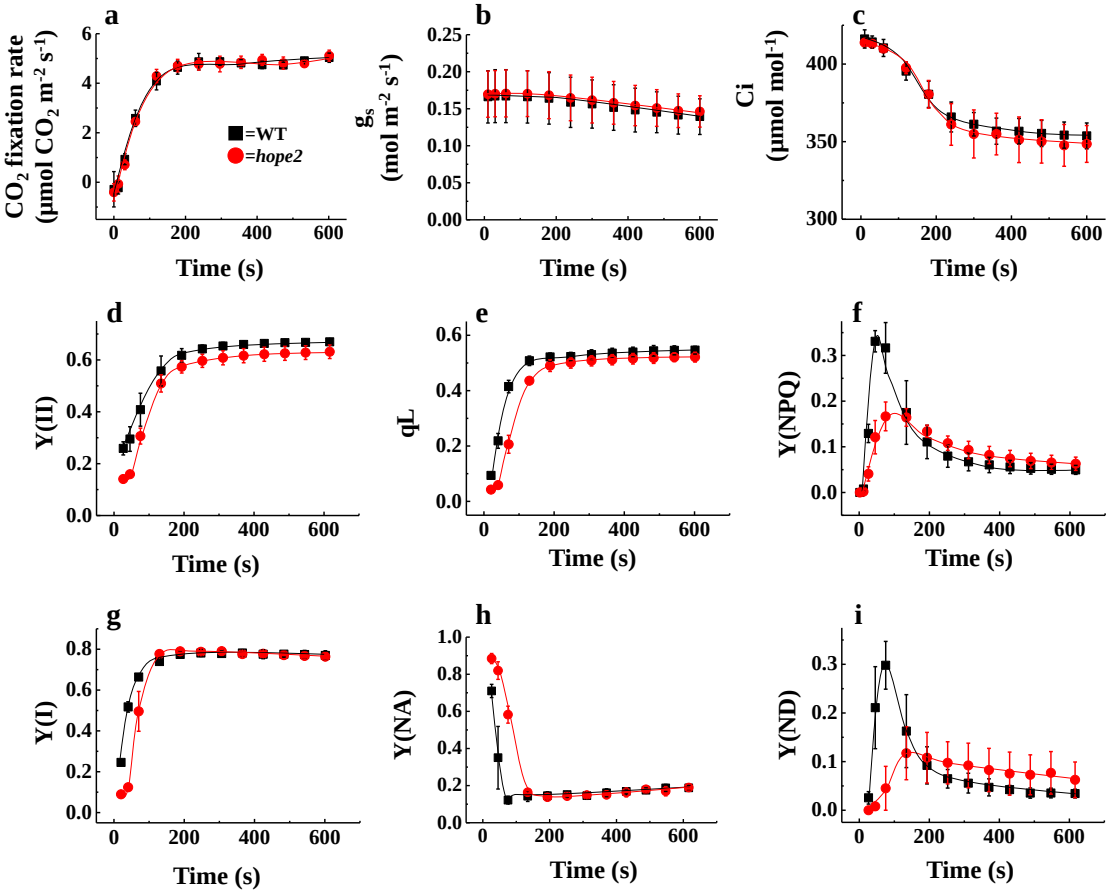

Figure IV-6

Comparison of photosynthetic parameters evaluated from gas exchange, chlorophyll fluorescence, and the kinetics of $P700^{+}$ in WT and *hope2* during photosynthetic induction phase. Plants were adapted in the dark at least 1h before this analysis. In this analysis, AL intensity was set 150 μE m^{-2} s^{-1}. (a) CO_2 assimilation rate, (b) stomatal conductance (g_s), and (c) intercellular CO_2 concentration (Ci) were determined by gas-exchange analysis. (d) Y(II), (e) qL, and (f) Y(NPQ) were determined by chlorophyll florescence. (g) Y(I), (h) Y(NA), and (i) Y(ND) were determined by absorbance change of 830 nm. Black squares indicate WT and red circles indicate *hope2*. Data are expressed as mean ± SEM of at least three independent experiments.

hope2 were increased over time after illumination, however *hope2* showed lower values in both Y(II) and qL just after AL onset (Fig. IV-6d, e). I also evaluated the PQ redox-state as described in Suorsa et al. (2012). I found that PQ was more reduced in compared to WT just after AL onset independent of the calculation methods (Fig. IV-7). The *hope2* kinetics of Y(NPQ) in WT transiently increased just after AL onset, and Y(NPQ) was relaxed over time (Fig. IV-6f). This kinetics of Y(NPQ) was consistent with previous reports, and this type of NPQ is recognized as qE (Kalituho et al., 2007; Armbruster et al., 2014). In *hope2*, the transient increase in Y(NPQ) was suppressed compared to WT (Fig. IV-6f). These results indicate that CO_2-fixation is not disturbed in *hope*2, however photosynthetic electron transport chain, even in PQ, becomed reduced, and the induction of qE was suppressed in *hope2* before CO_2-assimilation reached the steady state.

The kinetics to Y(I) was similar to the kinetics of Y(II), and Y(I) in *hope2* showed lower value compared to WT just after AL onset (Fig. IV-6g). At the same time, Y(NA) was greatly higher in *hope2* compared to WT although Y(NA) was relaxed and showed similar value to WT over time (Fig. IV-6h). The kinetics of Y(ND) was similar to the kinetics of Y(NPQ), and the transient increase in Y(ND) was suppressed in *hope2* compared to WT (Fig. IV-6i). From these results, I found that photosynthetic electron transport reaction is highly limited at the acceptor-side in PSI in *hope2* when electron sink capacity is limited consistent with the previous results (Fig. IV-5). Furthermore, in the induction phase in photosynthesis, I found that the limitation of photosynthetic electron transport reaction in PSI also caused PQ redox-state and qE in *hope2*.

hope2 is new allele in ATPC1which encodes γ-subunit of chloroplastic ATPase

To isolate the *HOPE2* gene, I conducted detailed mapping by using F2 generation of *hope2* which was generated by crossing with accession Landsberg *erecta* (Ler). *HOPE2* gene was identified in the short arm of chromosome 4 (Fig. IV-8). Following this, I resequenced chromosome 4 in *hope2* by using next generation DNA sequencer (see Materials and Methods). Then, I found *hope2* carried a single base pair substitution in At4g04640 (*ATPC1*) which encodes γ-subunit of chlorplastic ATPase.

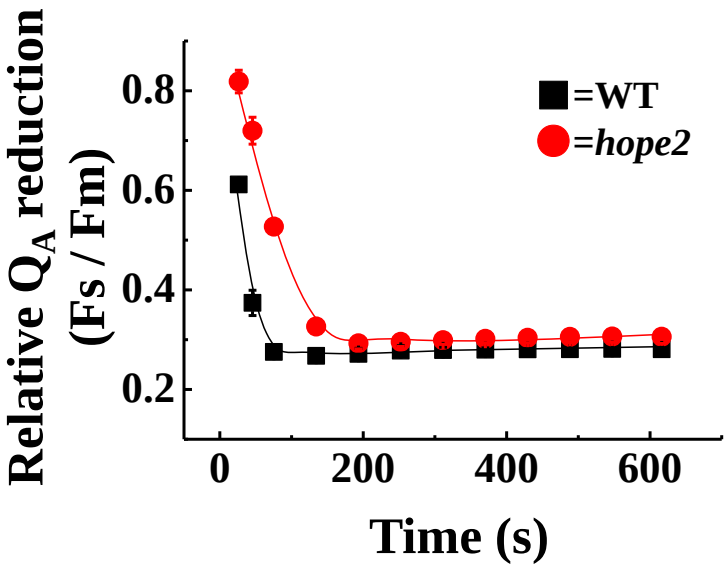

Figure IV-7

Comparison of Q_A reduction level in WT and *hope2* duing photosynthetic induction phase. Plants were adapted in the dark at least 1h before this analysis. In this analysis, AL intensity was set 150 µE m^{-2} s^{-1}. Black squares indicate WT and red circles indicate *hope2* mutant. Data are expressed as mean ± SEM of at least three independent experiments.

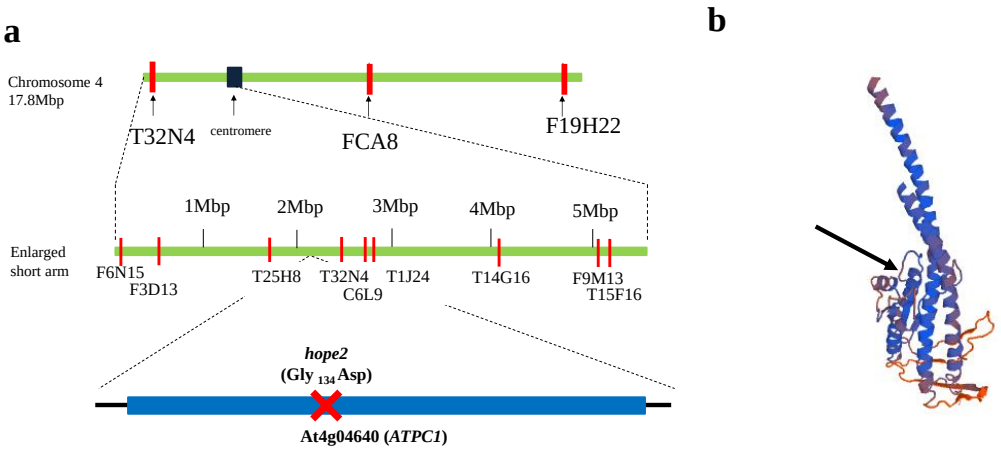

c

hope2	VEVLYNINEQLQTDDVDVPLTKVRPVKKVALVVVTDDRGLCGGFNNFIIK
Atabidopsis	VEVLYNINEQLQTDDVDVPLTKVRPVKKVALVVVTGDRGLCGGFNNFIIK
Oryza sativa	VEVLYNMNQEIQTEDIDLPLTRIRPVKKVALVVLTGERGLCGSFNNNVLK
Zea mays	VEVLYNMNQEIQTEDIDLPLTRTRPVKKVALVVLTGERGLCGSFNNNVLK
Eucalyptus grandis	VEVLYNINEQLQIEDVDAPLTSVRPVKKVALVVVTGDRGLCGGFNNNIIK
Glycine max	VEVLYNINEQLLTEDVDIPLTKVRPVKKVALVVVTGDRGLCGGFNNAIIK
Chlamydomonas reinhardtii	VKVLYGVNQRVRQEDVDSPLCAVRPVKSVLLVVLTGDRGLCGGYNNFIIK
Synechocystis sp. PCC 6803	AQVLYNLQNRLSFAETELPLFEQREPKAVALLVVTGDRGLCGGYNVNAI

Figure IV-8

hope2 carried missense mutation in *ATPC1*. (a) Identification of *HOPE2* gene by map-based cloning and next generation sequencer. In chromosome, DNA makers which were used for map-based cloning were shown. Maker sequences were shown in Table IV-1. The blue region of At4g04640 (*ATPC1*) indicates exon, and red cross indicates a mutation point in *hope2*. (b) Structural prediction of ATPC1 in WT. The Structure of ATPC1 was predicted by using SWISS-MODEL (http://swissmodel.expasy.org/). In this prediction, N-terminal transit-peptide to chloroplasts (60 amino acids) was eliminated. Black arrows indicate the 134th Gly in the structure. (c) The comparison of amino acid alignment of ATPC1 between photosynthetic organisms. Red belt indicates the mutation point in *hope2*.

This single base pair substitution caused missense mutation (C to T) and modified 134th amino acid from Gly to Asp in ATPC1 (Fig. IV-8a). By using SWISS-MODEL (http://swissmodel.expasy.org/), I identified the missense mutation in hope2 exists in Rossmann fold structure in ATPC1 (Fig. IV-8b). Furthermore, I found that this Gly is highly conserved in γ-subunit in ATPase among photosynthetic organisms (Fig. IV-8c).

To confirm whether the phenotype of *hope2* was caused by the missense mutation in *ATPC1*, I performed molecular complementation test in *hope2* by introducing genomic *ATPC1* in *A.thaliana*, and expressed under the control of native *ATPC1* promoter. The complementation line (*hope2*/*ATPC1*) showed similar kinetics in chlorophyll fluorescence quenching to WT under our screening conditions (Fig. IV-9). I also analyzed photosynthetic parameters in light response analysis and the induction phase of photosynthesis in *hope2*/*ATPC1*. These analyses revealed that the limitation of photosynthetic electron transport reaction at the acceptor side in PSI observed in *hope2* was rescued in *hope2*/*ATPC1* (Figs. IV-10,11). From these results, I concluded that *hope2* is a new allele in γ-subunit of chloroplastic ATPase which is modified the redox-state in photosynthetic electron transport chain, especially in PSI.

Based on these above results, I quantified ATPase content in WT and *hope2* in thylakoid membranes. Wester-blot analysis revealed that β and γ-subunit of ATPase decreased in *hope2* compare to WT, however, PsbB and PsaA were showed similar content between WT and *hope2* (Fig. IV-12). This result showed that CF_1-complex in ATPase on the thylakoid membranes decreased in *hope2* compared to WT.

hope2 shows higher H^+-conductance in ATPase

I analyzed the regulation of *pmf* and H^+-conductance in ATPase (gH^+) during photosynthesis in WT and *hope2* by using electrochromic shift (Baker et al., 2007; Klughammer et al., 2013; Sacksteder et al., 2000). First, I studied the kinetics of *pmf* and gH^+ to the change of light intensity. In WT, *pmf* increased with the increase in the light intensity, and *pmf* was saturated around 300 μE

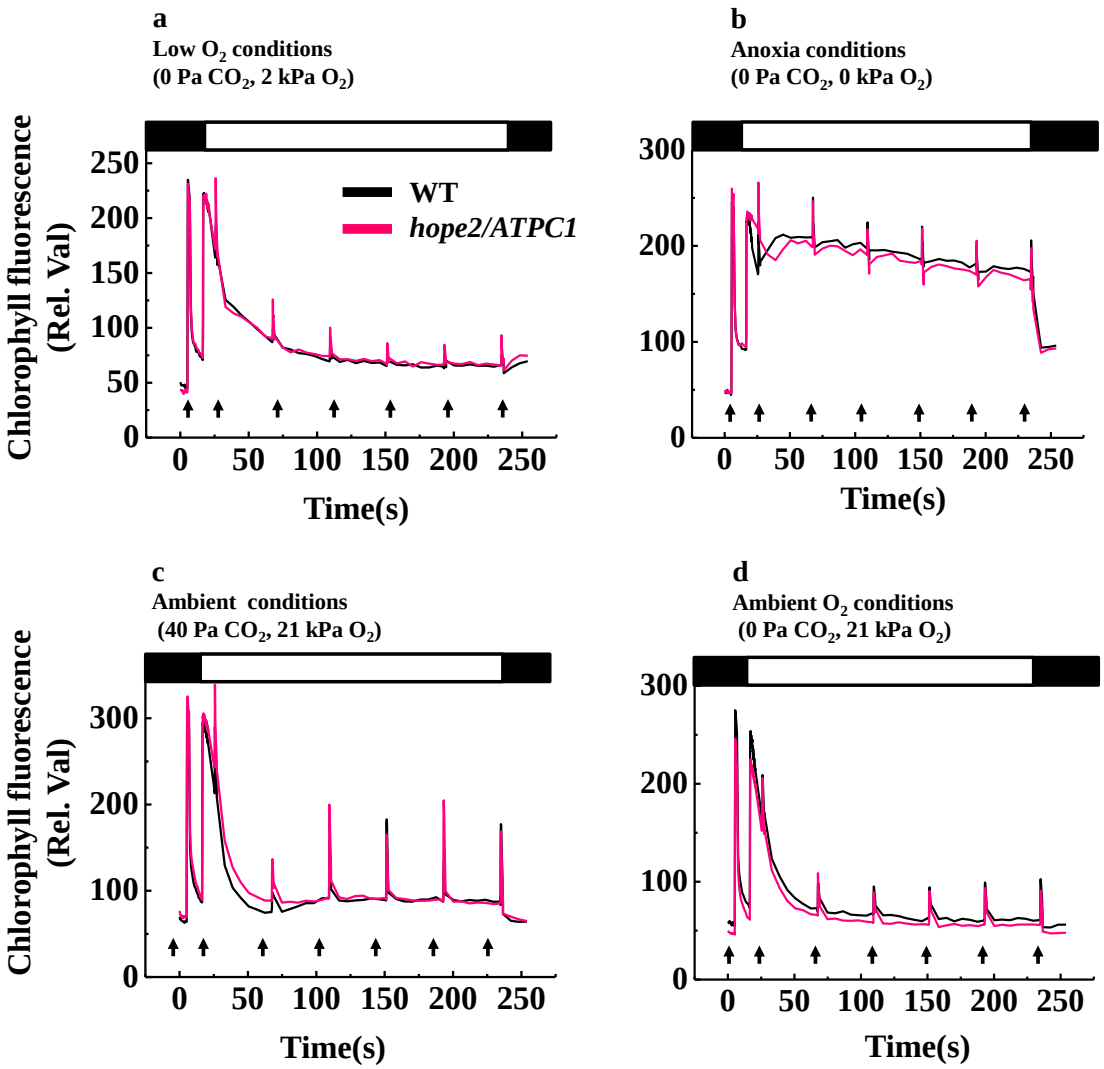

Figure IV-9

Chlorophyll fluorescence analysis of *hope2*/*ATPC1* complementation line. The typical kinetics of chlorophyll fluorescence under (a) low O_2 conditions (0 Pa CO_2, 2 kPa O_2), (b) anoxia conditions (0 Pa CO_2, 0 kPa O_2), (c) ambient condition (40 Pa CO_2, 21 kPa O_2), and (d) ambient O_2 conditions (0 Pa CO_2, 21 kPa O_2) were shown. Black lines indicate the kinetics of WT, and pink lines indicate the kinetics of *hope2*/*ATPC1* complementation line. Plants were adapted in the dark at least 1h. Black bars represented above the figures indicate dark conditions, and white bars represented above the figure indicate AL illumination (150 µE m^{-2} s^{-1}). Arrows in the figure indicate the illumination of saturation pulse (10,000 µE m^{-2} s^{-1}; 1s) at that time.

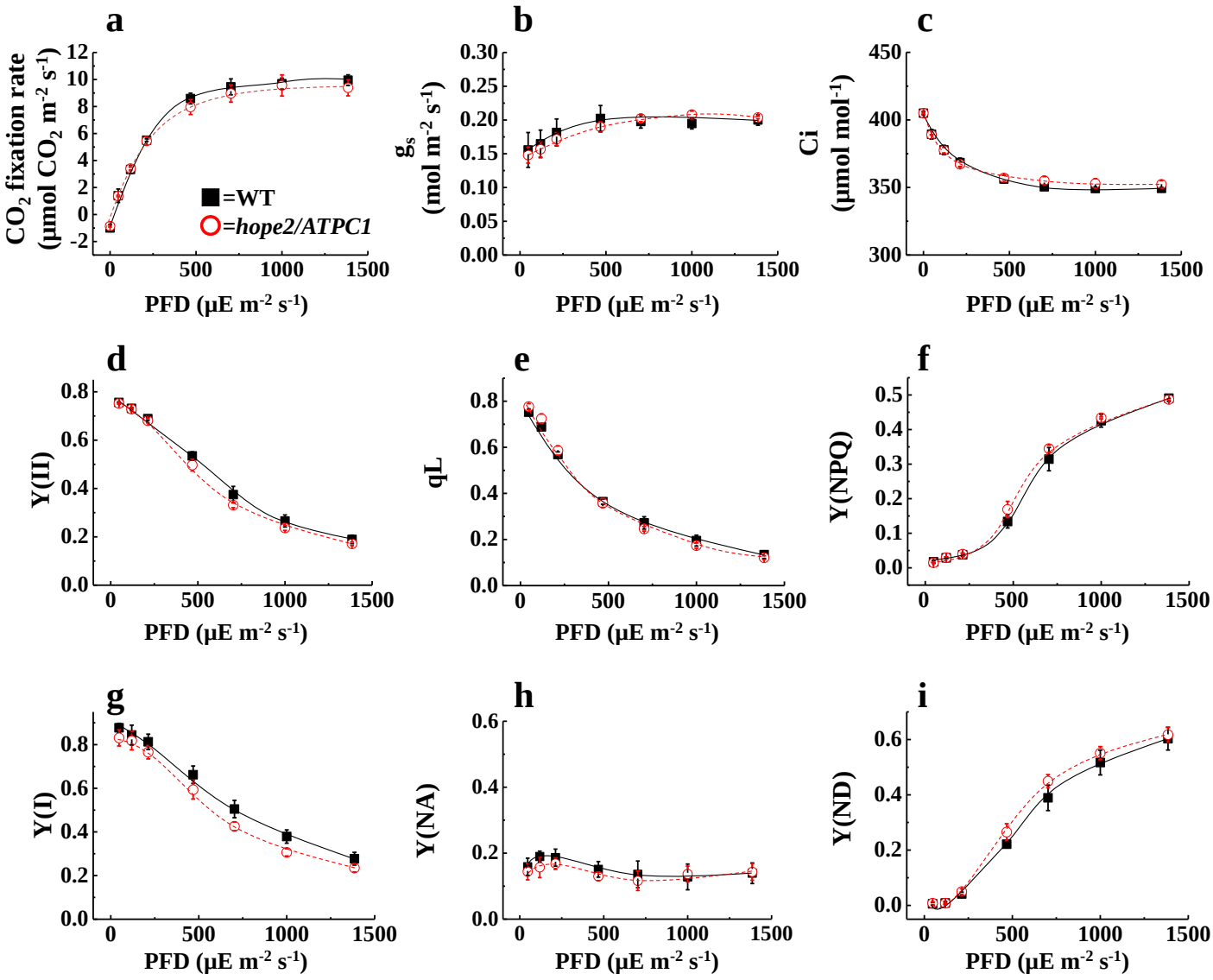

Figure IV-10

Light response of photosynthetic parameters evaluated from gas exchange, chlorophyll fluorescence, and the kinetics of $P700^{+}$ in WT and *hope2*/*ATPC1*. The measurements were conducted under ambient conditions (40 Pa CO_2, 21 kPa O_2). Before this analysis, AL (150µE m^{-2} s^{-1}) was illuminated in leaves for 10min to activate the electron sink in photosynthesis. (a) CO_2 assimilation rate, (b) stomatal conductance (g_s), and (c) intercellular CO_2 concentration (Ci) were determined by gas-exchange analysis. (d) Y(II), (e) qL, and (f) Y(NPQ) were determined by chlorophyll florescence. (g) Y(I), (h) Y(NA), and (i) Y(ND) were determined by absorbance change of 830 nm. Black filled squares indicate WT and red open circles indicate *hope2*/*ATPC1*. Data are expressed as mean ± SEM of at least three independent experiments.

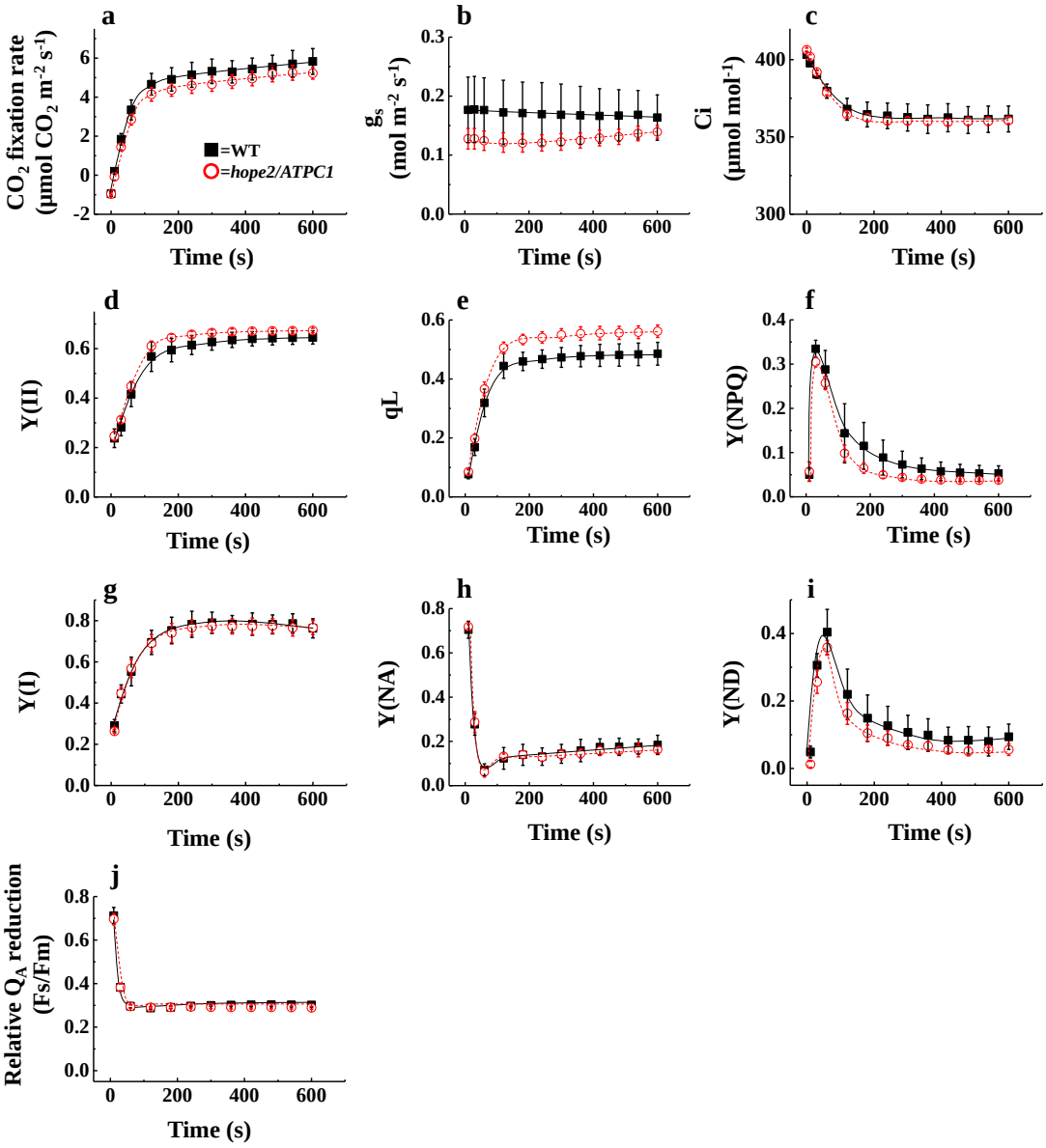

Figure IV-11

Comparison of photosynthetic parameters evaluated from gas exchange, chlorophyll fluorescence, and the kinetics of $P700^{+}$ in WT and *hope2/ATPC1* during photosynthetic induction phase. Plants were adapted in the dark at least 1h before this analysis. In this analysis, AL intensity was set 150 μE m^{-2} s^{-1}. (a) CO_2 assimilation rate, (b) stomatal conductance (g_s), and (c) intercellular CO_2 concentration (Ci) were determined by gas-exchange analysis. (d) Y(II), (e) qL, (f) Y(NPQ), and (j) relative Q_A reduction were determined by chlorophyll florescence. (g) Y(I), (h) Y(NA), and (i) Y(ND) were determined by absorbance change of 830 nm. Black squares indicate WT and red circles indicate *hope2/ATPC1*. Data are expressed as mean ± SEM of at least three independent experiments.

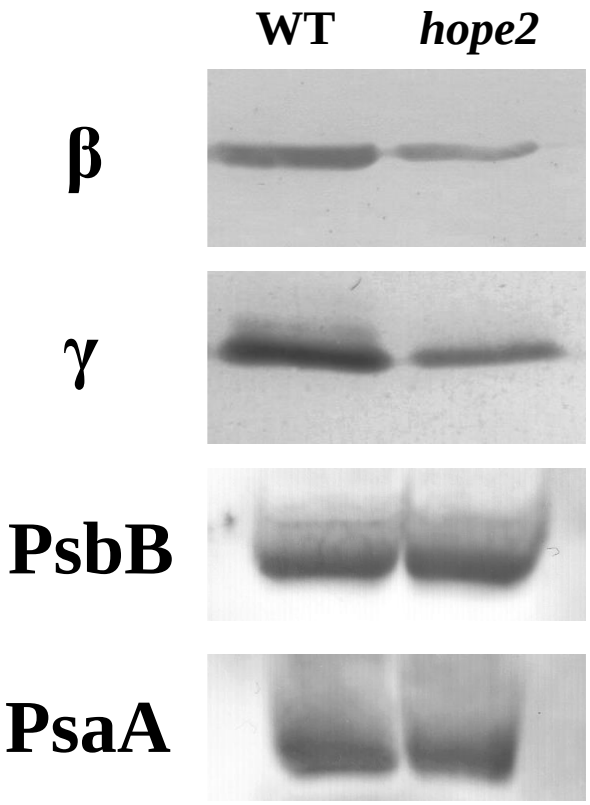

Figure IV-12

Western-blot analysis in WT and *hope2*. Thylakoid membranes were isolated from rosette leaves in WT and *hope2* (see Materials and Methods). The protein corresponding to 5 µg chlorophyll was loaded in each lane.

m^{-2} s^{-1} in WT (Fig. IV-13a). In contrast, the steady-state level of *pmf* in *hope2* was lower than WT, although *pmf* increased with the increase in the light intensity (Fig. IV-13a). When, I divided pmf into ΔpH and ΔΨ, ΔΨ was similar between WT and *hope2* over the range of the light intensity (Fig. IV-14a, b). However, Δ pH was lower in *hope2* compared to WT under high light conditions (Fig. IV-14c). These results indicate that the decrease in pmf caused by the decrease in ΔpH in *hope2*. gH^+ increased up to around 100 μE m^{-2} s^{-1} in WT, subsequently gH^+ decreased and reached steady state (Fig. IV-13b). In *hope2*, gH^+ also increased similar to WT up to 100 μE m^{-2} s^{-1}, however, *hope2* maintained higher gH^+ compared to WT under high light conditions (Fig. IV-13b). These results showed that H^+-efflux through ATPase is stimulated in *hope2* under high light conditions.

Next, I studied the response of *pmf* and gH^+ toward the change of Ci under high light conditions. *pmf* in *hope2* was lower compared to WT, and the difference was emphasized under low Ci condition (Fig. IV-13c). gH^+ was increased with the increase in Ci in WT, however, gH^+ in *hope2* was hardly respond to the change of Ci, and *hope2* kept higher gH^+ compared to WT over the range of Ci (Fig. IV-13d).

In the induction phase of photosynthesis, WT immediately formed *pmf* after the AL onset, and *pmf* was relaxed over time (Fig. IV-13e). In contrast, *hope2* showed lower *pmf* after the AL onset compared to WT, and *pmf* increased over time (Fig. IV-13e). gH^+ after onset of AL was low in WT, and gH^+ increased over the illumination time (Fig. IV-13f). Unlike gH^+ in WT, gH^+ in *hope2* showed higher after the AL onset, moreover gH^+ increased faster than WT over illumination time (Fig. IV-13f). From these results, I found *hope2* showed higher gH^+ than WT when *hope2* showed lower *pmf* than WT.

Chloroplastic ATPase maintains the light-dependent thiol regulatory system in hope2

The activity of chloroplastic ATPase is regulated by thiol-modulation in γ-subunit via thioredoxin (Yoshida et al., 2014). I studied whether *hope2* affects thioredoxin-dependent regulatory system in γ-subunit of ATPase. In this analysis, I illuminated single-turnover (ST) flash (100μs) to leaves,

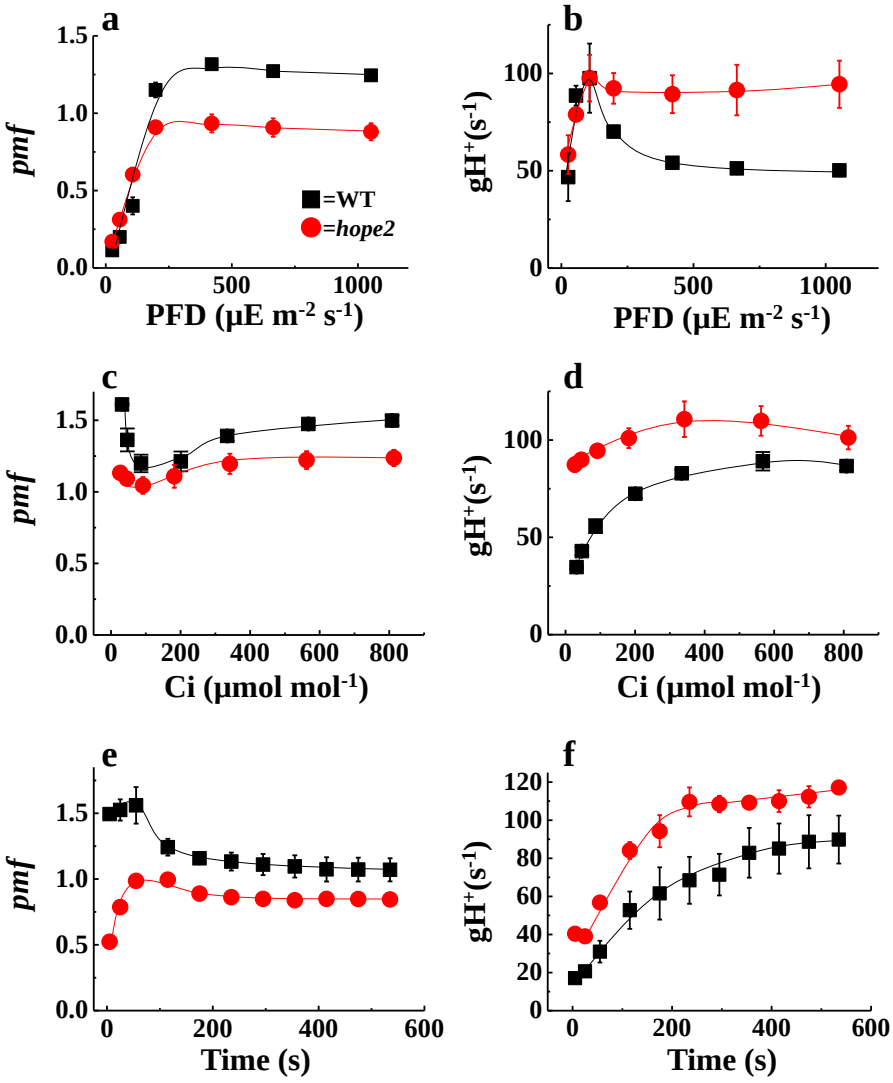

Figure IV-13

The comparison of *pmf* and gH^+ between WT and *hope2*. (a) and (b) showed the response of *pmf* and gH^+ toward the change of light intensity. This analysis was conducted under ambient conditions (40 Pa CO_2, 21 kPa O_2). Before this analysis, AL (150µE m^{-2} s^{-1}) was illuminated in leaves for 10min to activate the electron sink in photosynthesis. (c) and (d) showed the response of *pmf* and gH^+ toward the change of Ci. Before this measurement, AL (400µE m^{-2} s^{-1}) was illuminated in leaves for 10min to activate the electron sink in photosynthesis under ambient conditions (40 Pa CO_2, 21 kPa O_2). (e) and (f) showed the response of *pmf* and gH^+ at the induction phase in photosynthesis. Plants were adapted in the dark at least 1h before this analysis. In this analysis, AL intensity was set 150 µE m^{-2} s^{-1}. Black squares indicate WT and red circles indicate *hope2*. Data are expressed as mean ± SEM of at least three independent experiments.

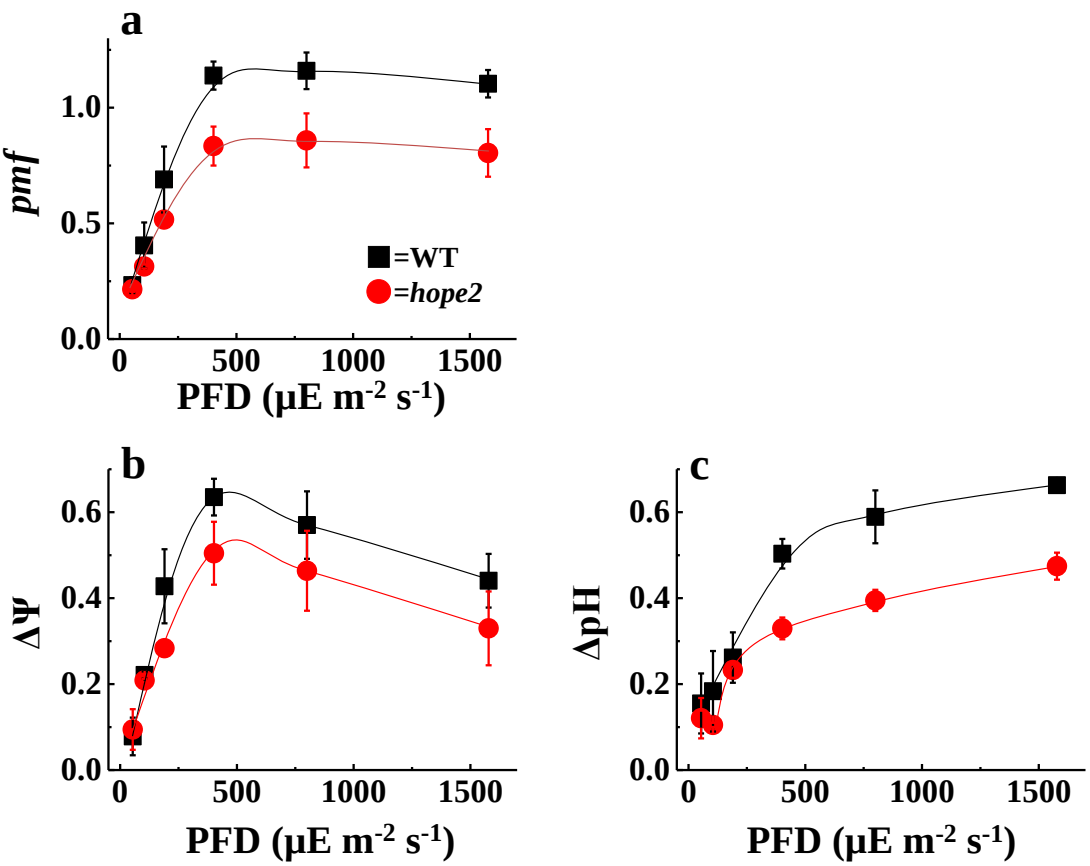

Figure IV-14

Light response of *pmf* (a), ΔΨ(b), and ΔpH (c) in WT and *hope2* under ambient conditions (40 Pa CO_2, 21 kPa O_2). Before this analysis, AL (150µE m^{-2} s^{-1}) was illuminated in leaves for 10min to activate the electron sink in photosynthesis. Black squares indicate WT and red circles indicate *hope2*. Data are expressed as mean ± SEM of at least three independent experiments.

and gH^+ was evaluated by the decay of ECS-signal (Wu et al., 2008 Kohzuma et al., 2013). As shown in Figure IV-15a and b, the decay of ECS-signal was activated by AL in both WT and *hope2*, compared to dark adapted their leaves. Moreover, I studied the de-activation kinetics of gH^+ under dark condition after gH^+ activation by AL (Kramer and Crofts, 1989). gH^+ decreased over the time of dark adaptation, then, WT and *hope2* showed similar decrease in gH^+ (Fig. IV-15c). These results indicate *hope2* maintained light-dependent thiol-regulatory system in γ-subunit of ATPase like WT.

PSI redox regulation by ATPase is essential to protect from photoinhibition in PSI under illumination

In previous study, I found that repetitive short-pulse illumination damaged specifically PSI in vivo and *in vitro* [termed as repetitive short-pulse (rSP)-treatment] (Sejima et al, 2014; Zavicak et al., 2015; Chapter 1). rSP-treatment stimulates the reduction of electron carriers in PSI, and ROS production in PSI (Sejima et al., 2014; Chapter 1). I applied rSP-treatment to WT and *hope2*. Under dark conditions, rSP-treatment for 1h largely decreased Y(I) in WT and *hope2* (Fig. IV-16a). Then, there was no difference between WT and *hope2*. During rSP-treatment Y(ND) did not induced in both WT and *hope2* (Fig. IV-16b). In contract, Y(NA) greatly increase similarly in both WT and *hope2* (Fig. IV-16c). Y(II) also decreased in both WT and *hope2*, however, the magnitude was slightly larger in *hope2* than WT (Fig. IV-16d). The kinetics of these photosynthetic parameters during rSP-treatment was consistent with the previous reports (Sejima et al, 2014; Zavicak et al., 2015; Chapter 1). After rSP-treatment, I evaluated the residual activities in PSII and PSI from the change of Fv/Fm, and maximum photo-oxidizable P700 content (Pm) (Sejima et al., 2014). Then, the residual activities in PSII and PSI were similar between WT and *hope2* after rSP-treatment for 1h (Fig. IV-16e).

Subsequently, I applied rSP-treatment to WT and *hope2* under high light conditions. For activating the electron sink in photosynthesis, rSP-treatment was started after AL illumination for 5 min. In WT, Y(I), Y(ND), Y(NA), and Y(II) were stable during rSP-treatment for 1h (Fig. IV-16f, g,

h, and i). Y(I) in *hope2* decreased during rSP-treatment although *hope2* kept similar Y(I) to WT at the beginning of rSP-treatment (Fig. IV-16f). *hope2* showed lower Y(ND) than WT, and Y(ND) slightly decreased during rSP-treatment (Fig. IV-16g). In contrast, *hope2* showed higher Y(NA) than WT, furthermore, Y(NA) increased during rSP-treatment (Fig. IV-16h). As well as Y(I), Y(II) in *hope2* slightly decreased during rSP-treatment although *hope2* kept similar Y(II) to WT at the beginning of rSP treatment (Fig. IV-16i). After rSP-treatment under high light conditions, PSI activity in WT decreased only by 10%, however, PSI photoinhibition was stimulated in *hope2*, and PSI activity decreased by 45% (Fig. IV-16j). There results indicate that the protection mechanism for PSI photoinhibition was lowered in *hope2* under illumination. Moreover, PSII activity also significantly decreased in *hope2*, compared to WT (Fig. IV-16j). This would be caused by accumulation of electrons at acceptor-side in PSII because of PSI photoinhibition (Vass, 2011).

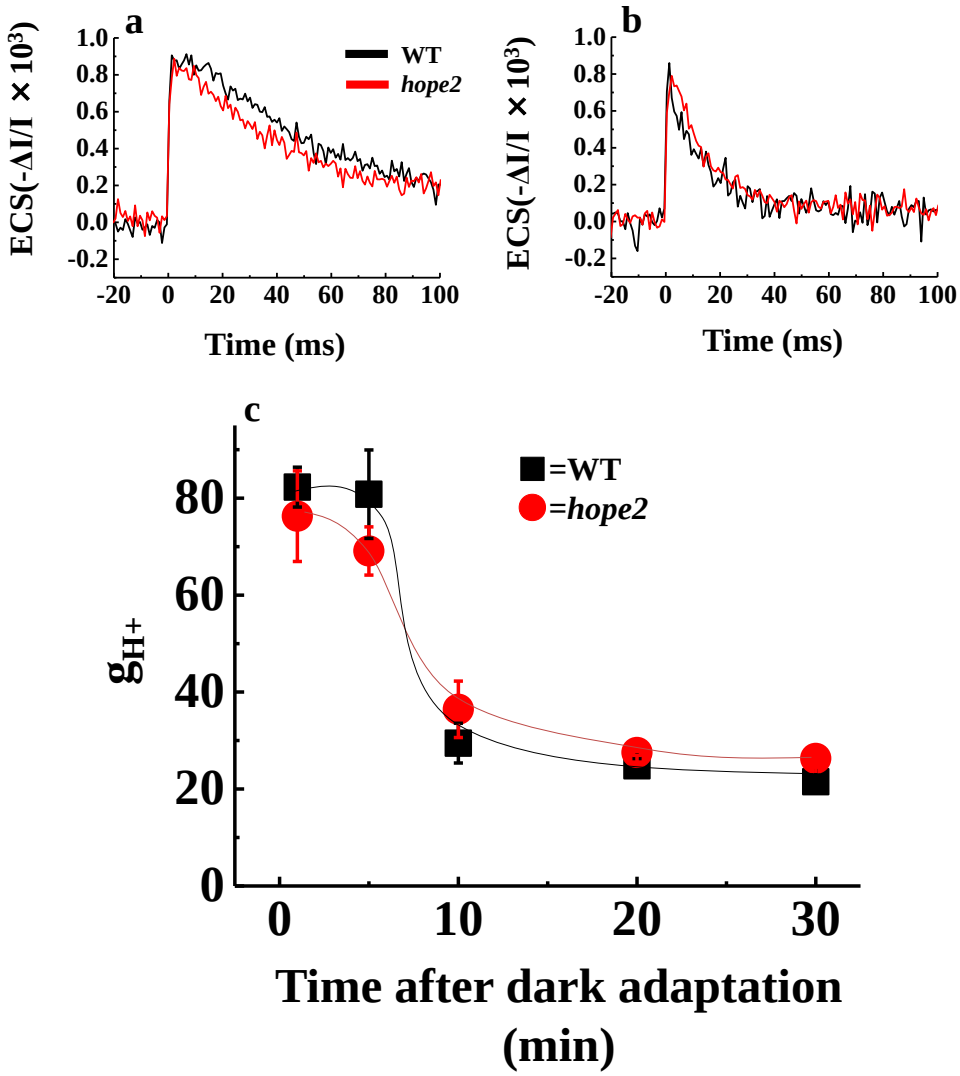

Figure IV-15

The analysis of activation/inactivation regulatory system in ATPase. (a) showed ECS-signal in WT and *hope2* when single-turnover flash (100 µs) was applied to their leaves which were adapted in the dark at least 1 h. (b) showed ECS-signal in WT and *hope2* when single-turnover flash (100 µs) was applied to their leaves which were adapted in the dark after AL illumination (150 µE m^{-2} s^{-1}) for 10min. Black lines indicates WT, and red lines indicates *hope2*. (c) showed the relaxation of gH^+ in the dark. Plants were illuminated AL (150µE m^{-2} s^{-1}) for 10min. After the illumination, gH^+ was calculated by ECS decay induced by single-turnover flash (100 µs), and gH^+ was plotted by indicated the time after dark adaptation. Black squares indicate WT and red circles indicate *hope2* mutant. Data are expressed as mean ± SEM of at least three independent experiments.

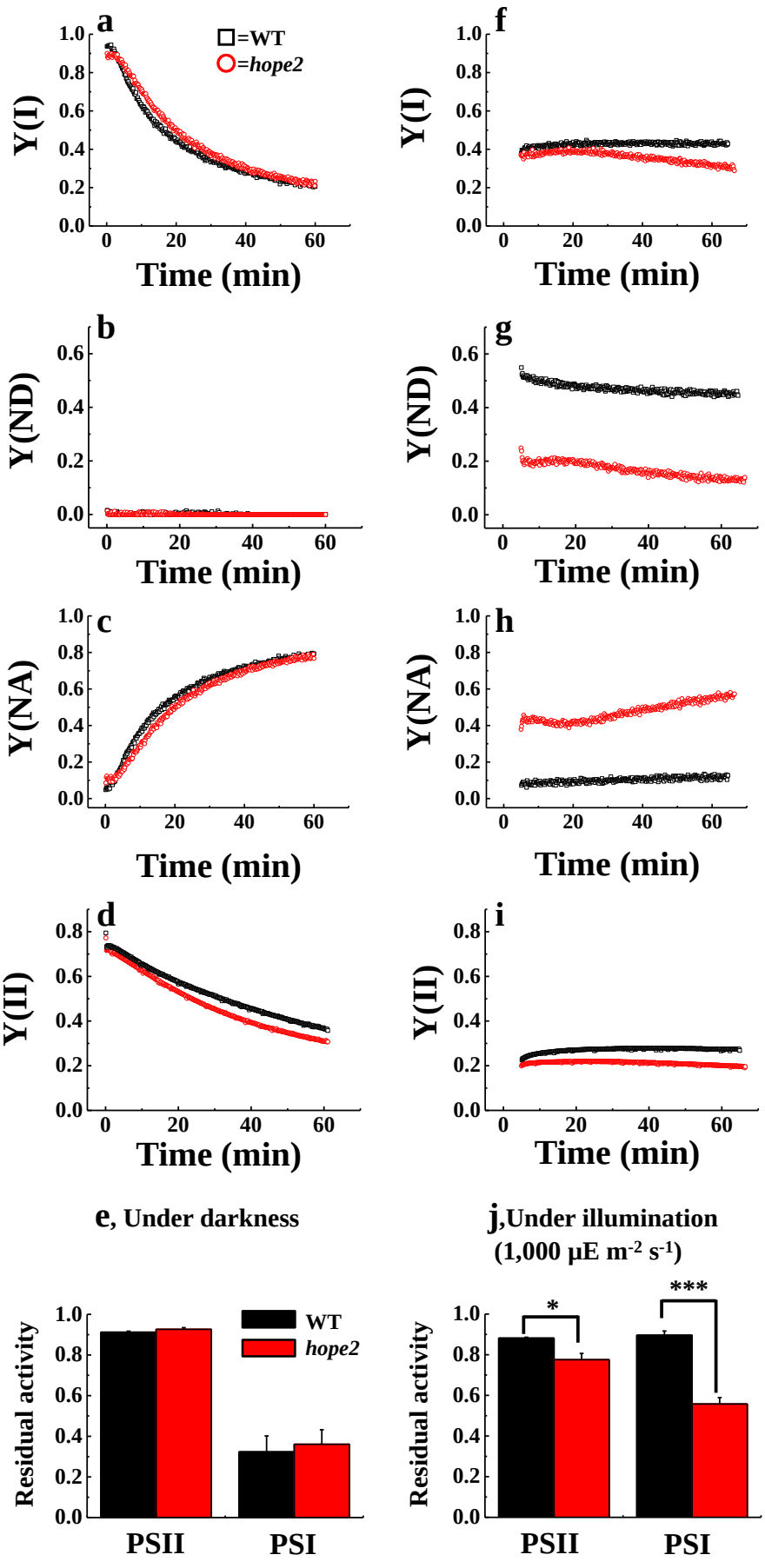
a
□=WT
○=hope2
Y(I)
Time (min)
f
Y(I)
Time (min)
b
Y(ND)
Time (min)
g
Y(ND)
Time (min)
c
Y(NA)
Time (min)
h
Y(NA)
Time (min)
d
Y(II)
Time (min)
i
Y(II)
Time (min)
e, Under darkness
Residual activity
WT
hope2
PSII
PSI
j,Under illumination
(1,000 μE m-2 s-1)
*
***
Residual activity
PSII
PSI

Figure IV-16

The kinetics of photosynthetic parameters in WT and *hope2* during rSP-treatment, and residual activity in PSII and PSI. WT and *hope2* leaves were illuminated every 10 s with a short-pulse (300 ms, 20,000 μE m^{-2} s^{-1}) and for 1 h. The time-course analyses of Y(I) (a, e), Y(ND) (b, f), Y(NA) (c, g), and Y(II) (d, h) in WT and *hope2* during rSP treatment under ambient conditions (21 kPa O_2, 40 Pa CO_2) are shown. The results of (a) to (d) were obtained by rSP-treatment in the dark, and the results of (f) to (h) were obtained by rSP-treatment under the AL illumination (1,000 μE m^{-2} s^{-1}). The experiment was conducted at least three times, and typical data were shown. Black squares indicate WT and red circles indicate *hope2*. (e), and (j) showed the effect of rSP-treatment under atmospheric conditions (21 kPa O_2, 40 Pa CO_2) on PSI and PSII activities in WT and *hope2*. (e) showed the result of rSP-treatment in the dark, and (j) showed the result of rSP-treatment under the AL illumination. After rSP treatment and photosynthesis measurements, the plants were kept in the dark for 30 min, and Fv/Fm and Pm were measured. Black squares indicate WT and red circles indicate *hope2*. Black bars indicate WT and red bars indicate *hope2*. Data are expressed as mean ± SEM of at least three independent experiments.

DISCUSSION

In this study, I aimed to identify the regulatory mechanism of ΔpH during photosynthesis, and I screened EMS-treated *A. thaliana*, which is impaired the ΔpH-dependent redox regulation in photosynthetic electron transport chain under our screening condition (low O_2 conditions). Then, I isolated *hope2*, which carries missense mutation in γ-subunit of chloroplastic ATPase. In higher plants, chloroplastic ATPase is consisted of stroma exposed CF_1complex which have five different proteins (α, β, γ, δ, and ε) and membrane embedded CF_0 complex which have four different proteins (a, b, b',and c) (Groth and Strotmann, 1999; Hisabori et al., 2002; Schöttlet et al., 2015). γ-subunit possess thiol-regulatory Cys resides, and the reduction of the disulfide bond by thioredoxin activates ATP synthesis under illumination (Hisabori et al., 2002; Yoshida et al., 2014). Previous studies showed that T-DNA tagged or antisense mutant of chloroplastic ATPase γ-subunit decreases the amount of choroplastic ATPase, and H^+-efflux from luminal side to stromal side in thylakoid membranes is greatly suppressed (Dal Bosco et al., 2004; Fristedt et al., 2015; Rott et al., 2011). In contrast to these previous studies, *hope2* showed high H^+-efflux at ATPase especially under the conditions where electron source activity is accelerated compared to electron sink capacity (Schöttler et al., 2015). Based on the characterization of new *ATPC1* allele, *hope2*, I concluded that chloroplastic ATPase plays an important role in the redox regulation of photosynthetic electron transport chain through the management of H^+-efflux.

hope2 impair the regulation of Δ pH by disturbing the H^+-efflux management in ATPase during photosynthesis. *hope2* showed similar CO_2-fixation rate and Y(II) at steady-state photosynthesis (Figs. IV-4, IV-5). This means that *hope2* have similar LEF activity to WT. In addition, I compared CEF activity estimated from the relationship between Y(I) and Y(II) (Miyake et al., 2004). Then, WT and *hope*2 showed similar relationship between Y(I) and Y(II) (Fig. IV-17). These results indicated that H^+-influx activity operated by LEF and CEF is similar between WT and *hope2*. In contrast, gH^+ was higher in *hope2* than WT under the conditions where *pmf* decreased in *hope2* compared to WT (Fig. IV-13). Therefore, the lower *pmf* in *hope2* is caused by high H^+-efflux

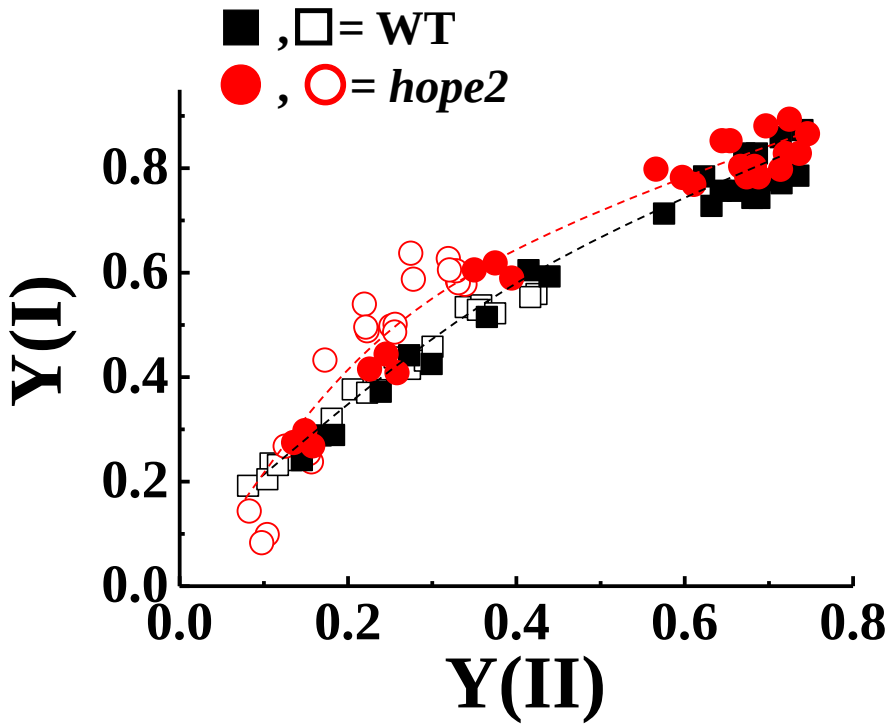

Figure IV-17

Comparison of PSI cyclic electron flow activity estimated from Y(I) and Y(II) in WT and *hope2* mutant. Data of Y(I) and Y(II) were used in light response analysis under ambient conditions (40Pa CO_2, 21 kPa O_2) (solid black square= WT, solid red circle= *hope2*) and CO_2 response analysis that AL intensity was set 1,000 µE m^{-2} s^{-1} (open black square= WT, open red circle= *hope2*).

efficiency in ATPase during photosynthesis.

I proposed that ATPase-dependent H^+-efflux management is critical for the ΔpH-dependent regulation in photosynthetic electron transport chain, especially in PSI. This idea strongly support the previous studies (Avenson et al., 2004, 2005; Kanazawa and Kramer, 2002; Kramer et al., 2004a; Rott et al., 2011; Takizawa et al, 2007, 2008). In WT, gH^+ showed lower value when Y(ND) increased under high light condition or low CO_2 condition at steady-state photosynthesis (Figs. IV-4, IV-5). Under ambient conditions, photosynthesis is limited by photon capture under low light conditions, however the limitation shits to the carboxylation rate of ribulose-1,5-bisphosphate (RuBP) by RuBP carboxylase/oxygenase (Rubisco) under high light condition (von Caemmerer and Farquhar, 1981). This limitation is emphasized under high light and low CO_2 conditions, because CO_2 for carboxylation by Rubisco is less (von Caemmerer and Farquhar, 1981). That is, photosynthesis is limited by the consumption rate of NADPH and ATP, but not those synthesis rates, under such conditions (Schöttler et al., 2015). Then, the content of ADP and Pi in chloroplasts decreases because of slow turnover of ATP, and H^+-efflux in ATPase is decelerated (Takizawa et al., 2007, 2008). Based on these reports, in WT, the decrease in gH^+ would be caused by the substrate limitation in ATPase under high light and low CO_2 conditions (Fig. IV-13) (Kanazawa and Kramer, 2002; Avenson et al., 2005; Kohzuma et al, 2009; Takizawa et al., 2008; Dietz and Heber, 1984, 1986). Therefore, ATPase is capable to form large *pmf* by decreasing gH^+ in response to ADP, and Pi availability in chloroplasts. This response contributes to limit electron flow from PSII to PSI at Cytb_6f , and oxidize P700 Chl in PSI when electron sink activity decreases relative to electron source activity (Figs. IV-4, IV-5) (Kramer et al., 1999; Takizawa et al., 2008; Tikhonov, 2013; Schöttler et al., 2015). In contrast to WT, *hope2* showed higher Y(NA), and then gH^+ in *hope2* were higher than WT (Fig. IV-13). These results indicate that ATPase-dependent ΔpH regulation is disturbed in *hope2*, and PSI in *hope2* became highly reduced state, compared to WT by accelerating electron transport from PSII to PSI. In fact, I observed that oxidized P700 induced by far-red illumination was relaxed faster in *hope2* than WT, when multiple-turnover flash was applied (Fig. IV-18a).

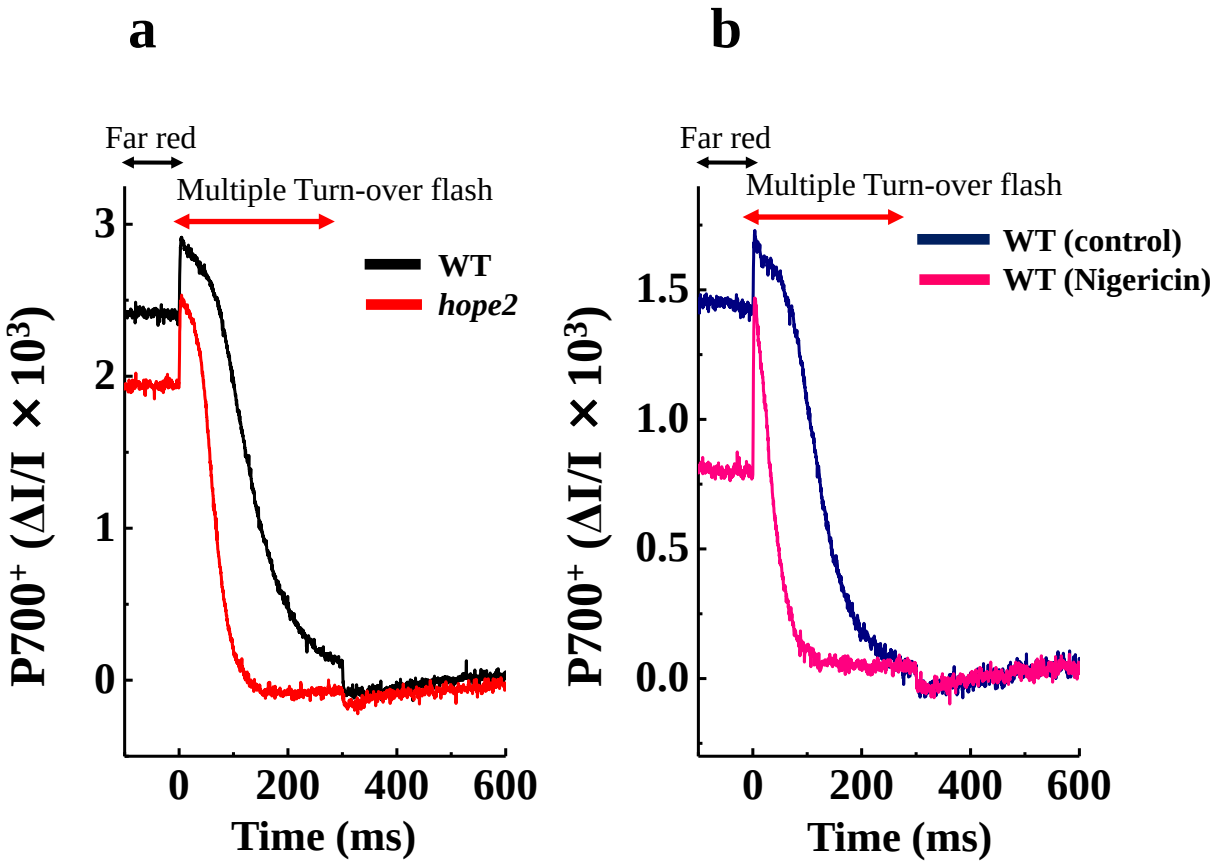

Figure IV-18

P700$^+$ relaxation kinetics in WT, *hope2*, *hope2*/*ATPC1* and the effect of nigericin in P700$^+$ relaxation. Far-red light was preilluminated in leaves to induce P700$^+$. Multiple-turnover flash (15,000 μE m^{-2} s^{-1}, 300ms) was illuminated at the time 0, and then far-red light was turned off simultaneously. Black line indicates the kinetics of WT, and red line indicates the kinetics of *hope2* in (a). In (b), dark blue line indicates the kinetics of WT infiltrated 150 mM sorbitol solution, and pink line indicates the kinetics of WT infiltrated the solution containing 150 mM sorbitol and 0.1 mM nigericin.

The kinetics of the relaxation of oxidized P700 in *hope2* was similar to WT leaf infiltrated the uncoupler nigericin (Fig. IV-18b). In contrast to our high gH^+ mutant, Rott et al. (2011) reported that ATPase mutant which shows lower gH^+ formed considerably large *pmf* and slowed electron transport from PSII to PSI, compared to WT. Based on the results by high gH^+ and low gH^+ mutant in ATPase, H^+-efflux management in ATPase well-adjusts the redox state in PSI depending on metabolic state in chloroplasts.

I clearly showed that H^+-efflux management in ATPase is required for protecting PSI photoinhibiton (Fig. IV-16). PSI photoinhibition is caused by accumulating the reduced electron carriers in PSI, and producing ROS like O_2^-, OH·, and $^1O_2$ within the thylakoid membranes (Terashima et al., 1994; Sejima et al., 2014; Cazzaniga et al., 2012; Chapter 2). I found that rSP-treatment in the dark conditions similarly damaged PSI in both WT and *hope2* (Fig. IV-16). In the previous study, I suggest that ΔpH-dependent regulation for protecting PSI photoinhibition is hardly induced in the dark because the formation of ΔpH by short-pulse illumination is insufficient (Chapter 2). Thus, high gH^+ in *hope2* did not affect the magnitude of PSI photoinhibiton in the dark. These results also indicate that the susceptibility in PSI itself is the same between WT and *hope2* (Takagi and Miyake, 2014). In contrast, rSP-treatment under the illumination hardly stimulated PSI photinhibiton in WT; however *hope2* failed to protect PSI from its photoinhibition (Fig. IV-16). This is because ΔpH-dependent limitation of photosynthetic electron transport is disturbed in *hope2*, and electron carriers in PSI become reduced state compared to WT (Figs. IV-13, IV-16, IV-18) (Sonoike, 1996a; Sejima et al., 2014). To confirm whether the PSI photoinhibition observed in *hope2* under illumination is caused by the highly reduced state of electron carriers in PSI, we used *pgr5* which showed higher reduced state in PSI, and I analyzed the effect of rSP-treatment in the dark and under illumination (Munekage et al., 2002; Soursa et al., 2012). Then, *pgr5* showed similar magnitude of PSI photoinhibition to WT in the dark; however *pgr5* caused PSI photoinhibition compared to WT by rSP-treatment under the illumination (Fig. IV-19). *pgr5* showed lower Y(ND) and higher Y(NA) than WT under the illumination.

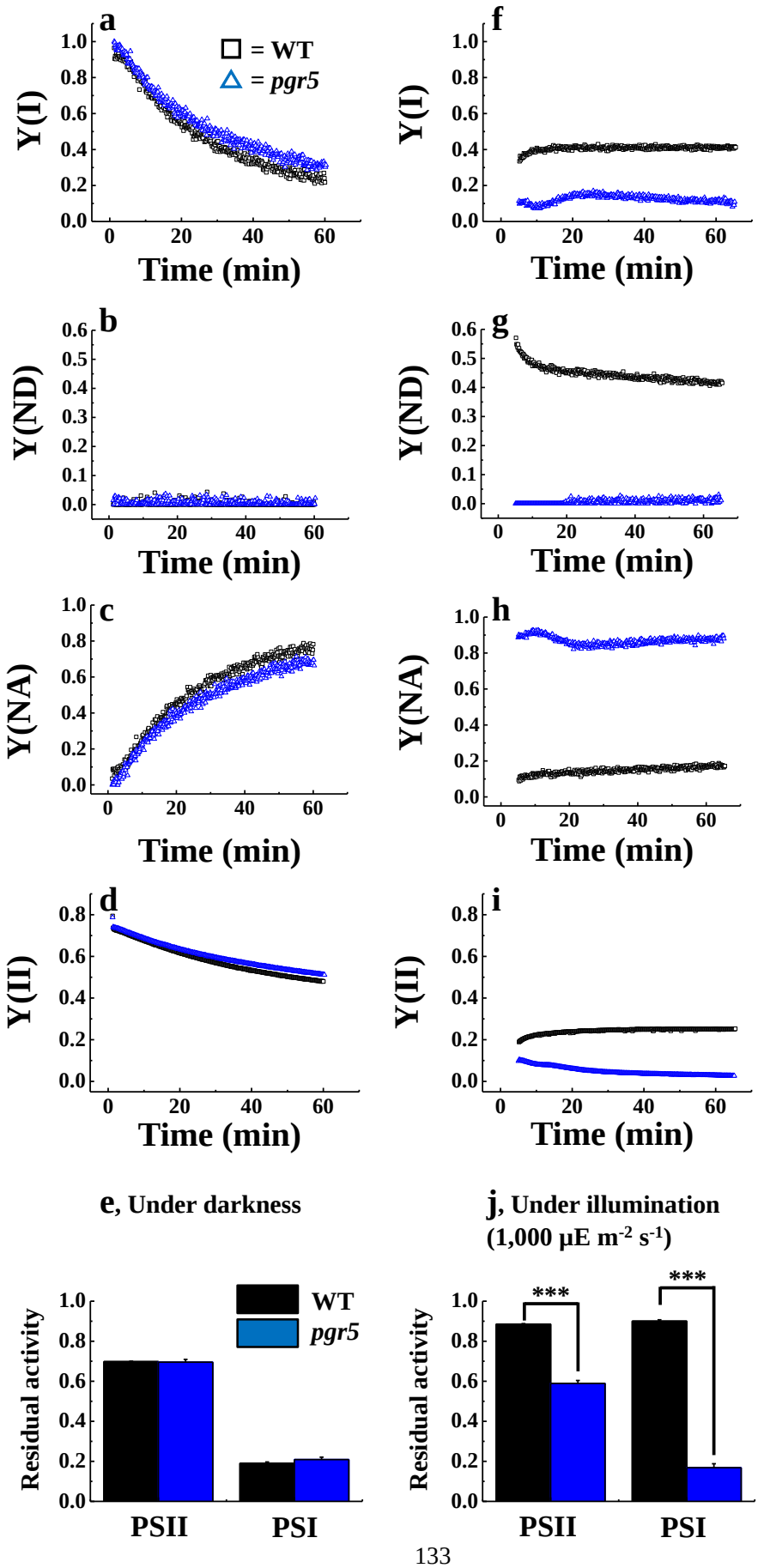
a
= WT
= pgr5
Y(I)
Time (min)
f
b
Y(ND)
g
c
Y(NA)
h
d
Y(II)
i
e, Under darkness
j, Under illumination
(1,000 µE m-2 s-1)
Residual activity
WT
pgr5
PSII
PSI
***

Figure IV-19

The kinetics of photosynthetic parameters in WT and *pgr5* during rSP-treatment, and residual activity in PSII and PSI. WT and *pgr5* leaves were illuminated every 10 s with a short-pulse (300 ms, 20,000 μE m^{-2} s^{-1}) and for 1 h. The time-course analyses of Y(I) (a, e), Y(ND) (b, f), Y(NA) (c, g), and Y(II) (d, h) in WT and *pgr5* during rSP treatment under ambient conditions (21 kPa O_2, 40 Pa CO_2) are shown. The results of (a) to (d) were obtained by rSP-treatment in the dark, and the results of (f) to (h) were obtained by rSP-treatment under the AL illumination (1,000 μE m^{-2} s^{-1}). The experiment was conducted at least three times, and typical data were shown. Black squares indicate WT and blue triangles indicate *hope2*. (e), and (j) showed the effect of rSP-treatment under atmospheric conditions (21 kPa O_2, 40 Pa CO_2) on PSI and PSII activities in WT and *hope2*. (e) showed the result of rSP-treatment in the dark, and (j) showed the result of rSP-treatment under the AL illumination. After rSP treatment and photosynthesis measurements, the plants were kept in the dark for 30 min, and Fv/Fm and Pm were measured. Black squares indicate WT and red circles indicate *pgr5*. Black bars indicate WT and blue bars indicate *pgr5*. Data are expressed as mean ± SEM of at least three independent experiments.

The tendency in Y(ND) and Y(NA) is similar between *pgr5* and *hope2* although the magnitude of these value were different. These results indicate that PSI photoinhibition in *pgr5* and *hope2* is caused by the impairment of ΔpH-dependent photosynthetic electron transport regulation, and large influx of electrons in PSI compared to WT. As is well known, cold sensitive cucumber leaves suffer from PSI photoinhibition under low temperature and illumination (Terashima et al., 1994). Interestingly, under the same conditions, Tershima et al (1991a, 1991b) reported that CF_1-complex reversibly dissociated from CF_0-complex of ATPase, and this causes high H^+-efflux from luminal side in thylakoids. Combining our results, PSI might be caused in cucumber leaves as follows: first, CF_1-dissociation dissipates ΔpH across the thylakoid membrane, second the dissipation of ΔpH accelerates electron transport from PSII to PSI, and the accumulation of electron carriers produce ROS within PSI. Based on these results, I suggest that the increase in the stability of ATPase, and rapid H^+-efflux management would improve the plant robustness toward the environmental stresses. In *pgr5*, PSII photoinhibition was also stimulated by rSP-tratment under AL illumination (Fig IV-19). Similar to *hope2*, this would be caused by accumulation of reducing electron carriers in PSII because of PSI photoinhibition (Vass, 2011).

Chloroplastic ATPase also affects NPQ in addition to the redox state in PSI. In this study, I observed that *hope2* failed to induce NPQ at the induction phase of photosynthesis, and low O_2 conditions (Figs. IV-1a, IV-6f). In dark adapted leaves, electron sink activity depending on Rubisco and the Calvin-cycle enzyme is repressed, and the activating processes are needed depending on Rubisco activase and thioredoxins for full activation of electron sink (Yamori et al.,2012; Yoshida et al., 2014). Indeed, I observed that CO_2 -fixation rate did not reach steady state in dark adapted leaves just after AL onset (Fig. IV-6a). On the other hand, under low O_2 conditions, photosynthetic electron transport is greatly suppressed because the Calvin-cycle and photorespiration served as electron sink are restricted, although partial O_2-dependent electron transport would occur in the thylakoid membrane (Miyake et al., 1998; Chapter 3). Under these conditions, H^+-influx depending on photosynthetic electron transport is also suppressed. Therefore, *hope2* would fail to

maintain ΔpH because of high H^+-efflux compared to low H^+-influx, and the induction of NPQ would be collapsed in *hope2* at the induction phase and low O_2 conditions (Figs. IV-13; IV-20). In contrast to these conditions, *hope2* induce NPQ similar to WT at steady state in photosynthesis (Figs. IV-4, IV-5). Under these conditions, H^+-influx activity is also high because of opening electron sink. Thus, *hope2* would satisfy the luminal pH required for the protonation of PsbS and VDE (Niyogi et al., 1998; Li et al., 2000). In fact, NPQ was rapidly relaxed after off-set AL illumination in *hope2* similar to WT (Fig. IV-21). This result indicates that the composition of NPQ is similar between WT and *hope2* (Müller et al., 2001). Furthermore, pK for the induction of NPQ by PsbS and VDE is around 6.8, and these values are higher than luminal pH under high light conditions (Takizawa et al., 2007; Zaks et al., 2012; Tikhonov, 2013). Therefore, the increase in luminal pH in *hope2*, compared to WT, might not affect NPQ induced by the protonation of PsbS and VDE at steady state photosynthesis. Based on these results, under high light conditions, pH-dependent photosynthetic regulation at Cytb_6f, which widely responds to luminal pH is important for maintaining the redox state in PSI, compared to NPQ, and PSI redox state is not maintained only by NPQ in PSII.

I cannot explain the high H^+-efflux in *hope2* by referring to the change of ATPase content (Fig. IV-12). In higher plants, the decrease in chloroplastic ATPase content suppresses H^+-efflux from luminal side, and forms large ΔpH across the thylakoid membrane (DalBosco et al., 2004; Rott et al., 2011; Fristedt et al., 2015). Furthermore, these situations induce growth defect (Dal Bosco et al., 2004; Rott et al., 2011 Fristedt et al., 2015). However, *hope2* did not show these phenotypes (Figs. IV-3, IV-13). Does CF_1-complex dissociate from CF_0-complex, and accelerate H^+-efflux uncoupled with ATP synthesis in *hope2*? (Terashima et al., 1991a, 1991b). I proposed it would be also unlikely because thiol-dependent regulation is functional in ATPase in *hope2* (Fig. IV-15). If CF_1-complex dissociates from CF_0-complex and H^+-efflux is accelerated, H^+-efflux would not respond to dark/light cycle. Moreover, I observed CO_2-fixation rate is not suppressed in *hope2*, compared to WT (Figs. IV-4, IV-5, IV-6). This means that ATPase in *hope2* is capable to synthesis ATP. From these results, I suggest that amino acid substitution of ATPase in *hope2 d*ecreases the stability of

CF_1-complex, and disturbs H^+-efflux regulation responding to stromal ATP/ADP ratio during photosynthesis.

This study demonstrated that H^+-management by ATPase is critical for regulating ΔpH during photosynthesis (Avenson et al., 2004, 2005; Kanazawa and Kramer, 2002; Kramer et al., 2004a; Kohzuma et al. 2009; Rott et al., 2011). Even now, the knowledge about physiological regulation of chloroplastic ATPase during photosynthesis and its H^+-efflux regulations are limited (e.g. the physiological meaning of the phosphorylation of β-subunit of CF_1-complex, and binding 14-3-3 protein) (Bunney et al., 2001; del Riego et al., 2006; Kanekatsu et al, 1998). Because *hope2* lose H^+-efflux regulation during photosynthesis, the future investigation of ATPase structure or the protein interaction in *hope2* could reveal the physiological regulation of ATPase and the perspective ΔpH-dependent regulation of photosynthesis.

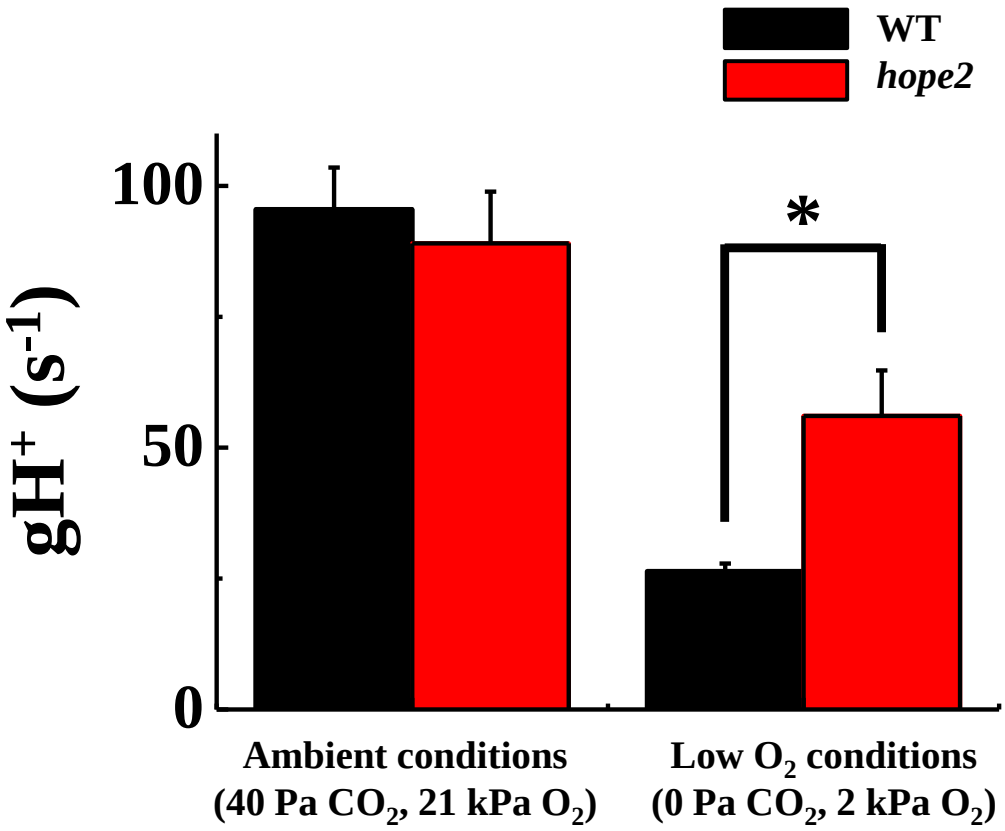

Figure IV-20

H^+-conductance in ATPase under ambient conditions and low O_2 conditions at steady-state photosynthesis. Leaves were illuminated by AL (150 µE m^{-2} s^{-1}), and gH^+ was calculated from ECS decay in DIRK-analysis. Black bars indicate WT and red bars indicate *hope2*. Data are expressed as mean ± SEM of at four independent experiments. The asterisk indicates a significant difference between WT and *hope2* (Student's t-test; *, $p < 0.05$).

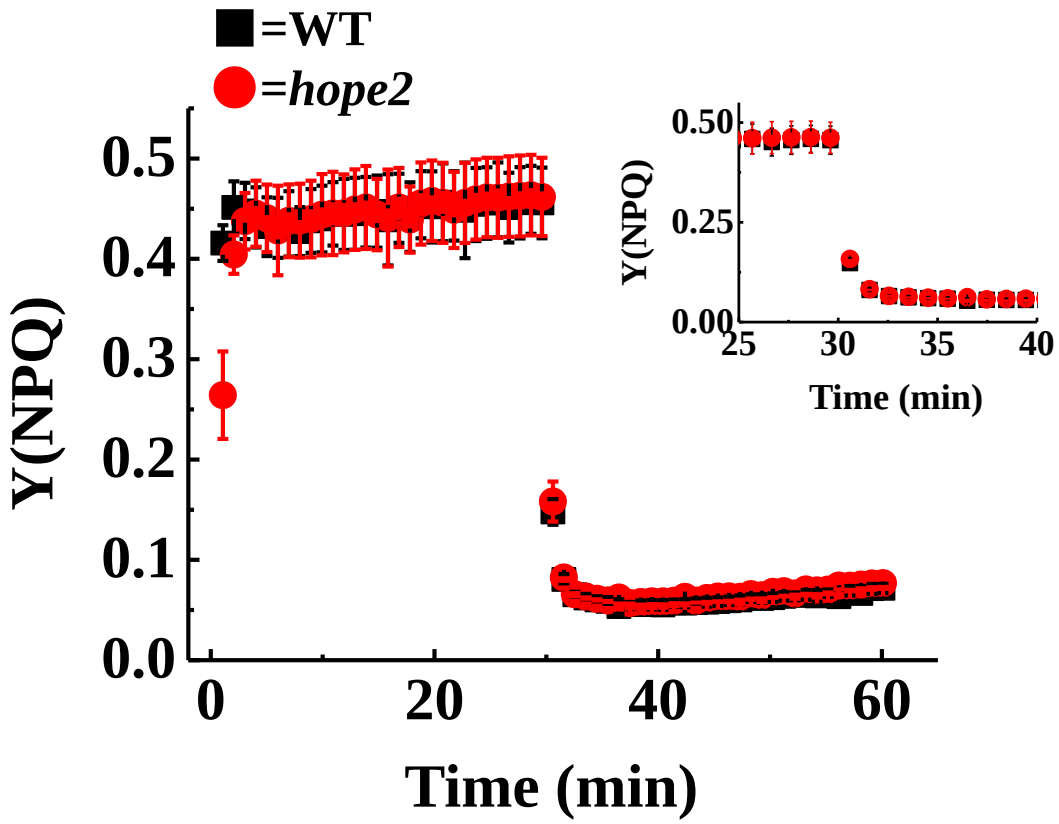

Figure IV-21

The induction and relaxation kinetics of Y(NPQ) in WT and *hope2*. Plants were adapted in the dark at least 1 h, and illuminated AL (1,000 μE m^{-2} s^{-1}) for 30 min. After the illumination, the relaxation of Y(NPQ) in the dark was monitored. Black squares indicate WT and red circles indicate *hope2*. Inlet showed enlarged figure around the off-set of AL. Data are expressed as mean ± SEM of at least three independent experiments.

Chapter 5

The Calvin Cycle Inevitably Produces Sugar-Derived Reactive Carbonyl Methylglyoxal during Photosynthesis: A Potential Cause of Plant Diabetes

ABSTRACT

Sugar-derived reactive carbonyl species (RCS) including methylglyoxal (MG) are aggressive by-products of oxidative stress known to impair the functions of multiple proteins. These advanced glycation end-products accumulate in patients with diabetes mellitus and cause major complications including arteriosclerosis and cardiac insufficiency. In the glycolytic pathway, the equilibration reactions between DHAP and GAP were recently shown to generate MG as by-products. Since plants produce vast amounts of sugars and support the same reaction in the Calvin cycle, I hypothesized that MG also accumulates in chloroplasts. The incubation of isolated chloroplasts with excess 3-PGA as the GAP precursor drove the equilibration reaction toward MG production. The rate of O_2 evolution was used as an index of 3-PGA-mediated photosynthesis. The 3-PGA- and time-dependent accumulation of MG in chloroplasts was confirmed by HPLC. In addition, MG production increased with increased light intensity under the conditions where chloroplasts operate the Calvin cycle depending on 3-PGA. I also observed a positive linear relationship between the rates of MG production and O_2 evolution ($R = 0.88$; $p < 0.0001$). These data provide the evidence that MG is produced by the Calvin cycle and that sugar-derived RC production is inevitable during photosynthesis. Furthermore, I found that the production of MG was enhanced under high-CO_2 conditions in the illuminated wheat leaves, compared to under ambient CO_2 conditions.

INTRODUCTION

Plant leaves accumulate high concentrations of sugars in their cells during photosynthesis (Qiu et al. 2008), which indicates that the threat by sugar-derived reactive carbonyl species (RCS) and ROS would be stronger in autotrophs than in heterotrophs. Qiu et al. (2008) reported that the carbonylated proteins due to RCS and ROS accumulated in the leaves of plants that are exposed to high CO_2 concentrations. They first did not expect the accumulation of the modified proteins under high CO_2 concentrations when photosynthesis was stimulated because the enhanced photosynthesis suppressed the production of ROS in chloroplasts (Asada 1999). In the illuminated chloroplasts, the photoreduction of O_2 to O_2^- at PSI of thylakoid membranes is inevitable (Asada 1999). The photoreduction of O_2 competes with that of $NADP^+$ at PSI. Therefore, the stimulated photosynthesis suppresses the production of ROS under high CO_2 concentrations, which indicates that the oxidative modification of proteins by RCS and ROS was suppressed under high CO_2 concentrations. Thornalley et al. (2009) first detected AGEs in plant leaves. The concentrations of many AGEs fluctuated in day/night cycles. Based on these results, I proposed the hypothesis that carbon metabolism in plant leaves, which photosynthesize and fix CO_2 to sugars, always accompanied RCS production. In particular, in environments wherein photosynthesis is enhanced at high light or high CO_2 concentrations, even in organisms that carry on photosynthesis, the risk of suffering from diabetes mellitus would be high.

Higher plants also possess the detoxification enzymes of RCS, similar to vertebrates (Mundree et al. 2000, Paulus et al. 1993, Saito et al. 2013). As observed in human beings, aldo-keto reductase (AKR) functions in the scavenging of MG in higher plants. AKR is found as a family, which comprises 14 subfamilies and the AKR4C subfamily scavenges methylglyoxal (MG) (Saito et al. 2013). Furthermore, other detoxification enzymes of RCS were proposed to function in stress environments. The gene expressions in the glyoxalase (GLX) system and AKR subfamilies were enhanced under abiotic stresses such as salinity, osmotic pressure, and heat (Singla-Pareek et al. 2003). Under drought conditions, the activity of the AKR subfamily increased (Simpson et al. 2009).

Furthermore, genetically modified plants that have a higher activity of AKR showed tolerance against the above stress conditions (Sunkar et al. 2003). It has been observed increases in the gene expressions of the AKR4C subfamily in the leaves of plants, which were exposed to high CO_2 concentrations and high light environments (Saito et al. 2013). These facts support the hypothesis that, even for photosynthesis organisms, the risk of diabetes mellitus increases when photosynthesis is enhanced.

In this chapter, to prove my hypothesis, I tried to elucidate the production mechanism of MG during photosynthesis and the physiological function of photosynthetic activity on MG production. I used MG as an index of RCS production during the Calvin cycle in isolated chloroplasts. During glycolysis, MG is a by-product obtained during the equilibration reaction between dihydroxyacetone phosphate (DHAP) and glyceraldehydes phosphate (GAP) catalyzed by triosephosphate isomerase (TPI) (Richard 1991). Since this enzyme regulates the same reactions in the Calvin cycle, we expected MG to be generated as a by-product of the Calvin cycle in higher plants. In this study, I initiated 3-phosphoglycerate (3-PGA)-dependent O_2 evolution in the isolated chloroplasts. 3-PGA is metabolized to GAP, which is sequentially catalyzed by PGA kinase and GAP dehydrogenase (GAPDH). GAP is equilibrated with DHAP, which is catalyzed by TPI. I observed MG production only in the presence of 3-PGA in the illuminated chloroplasts. The production rate of MG depended on light intensity. MG production showed a positive linear relationship with 3-PGA-dependent O_2 evolution. Furthermore, I found the enhanced production of MG under high-[CO_2] in the illuminated wheat leaves. These facts demonstrate that enhanced MG production is inevitable for stimulated photosynthesis under high CO_2 concentrations.

MATERIALS AND METHODS

Plant materials and growth conditions

Wheat (*Triticum aestivum* L. cv. Mironovskaya 808) was grown in soil (commercial peat-based compost) for 4-5 weeks under 14 h light (25^{o}C) / 10 h dark (20^{o}C) and 500 µE m^{-2} s^{-1}.

Isolation of intact chloroplasts from spinach leaves

Spinach leaves from a local market were processed to isolate intact chloroplasts, as described previously (Takagi et al. 2012). The chloroplasts were suspended in a reaction buffer containing 50 mM HEPES–KOH (pH 7.4), 0.33 M sorbitol, 10 mM NaCl, 1 mM $MgCl_2$, 2 mM EDTA, 0.5 mM KH_2PO_4, and 1 mM ascorbate. This chloroplast suspension was purified on a Percoll gradient. The purified chloroplasts were approximately 80–90% intact based on the ferricyanide method (Heber and Santarius 1970). Chlorophyll content was determined by the method of Arnon (1949).

O_2 exchange in isolated chloroplasts

The rate of 3-PGA-dependent O_2 evolution was measured in isolated chloroplasts, as described previously. In brief, the chloroplast suspension was placed in different O_2 electrode cuvettes (DW2/2; Hansatech Ltd, King's Lynn, UK) with actinic red light (> 640 nm), in the absence or presence of 3-PGA. At specific time intervals, aliquots of the chloroplast solution were collected for the analysis of sugar-derived RCs. During the assay, temperature-controlled water was circulated through the water jacket, and was maintained at 25 or 35°C.

Gas-exchange analysis

The rates of CO_2 and H_2O vapor exchange were measured with an open gas-exchange system using a temperature-controlled chamber. The system was detailed in Makino et al. (1988). Differences in the partial pressures of CO_2 and H_2O entering and leaving the chamber were measured with an IRGA

(LI-7000, Li-COR, USA). Gas with the incidated mixture of pure O_2 and CO_2 was prepared by mixing 20.1% (v/v) in 79.9% (v/v) N_2 and 1% (v/v) CO_2 in 99% (v/v) N_2 using a mass-flow controller (Kofloc model 1203; Kojima Instruments Copr., Kyoto, Japan). The mixture of gases was saturated with water vapor at 13.5 ± 0.1^{o}C. The PPFD at the position of the leaf in the chamber was adjusted to 1,060 µmol photons m^{-2} s^{-1}. Leaf temperature was controlled at 25^{o}C. Gas-exchange parameters were calculated according to the equations in von Caemmerer and Farquhar (1981). For the analysis of sugar-derived RCs, leaf in the chamber was rapidly moved out and frozen in the liquid-N_2 solution until RCs-analysis. It took about 1 s for freezing.

Analysis of sugar-derived RCS

The sugar-derived RCS (1,2-dicarbonyls) generated by 3-PGA-dependent O_2 evolution were identified as the corresponding quinoxalines after derivatization with o-phenylenediamine (OPD), as described previously (Mavric et al. 2008). The aliquots of isolated intact chloroplasts (1 ml) were mixed with 1 ml sodium phosphate buffer [50 mM NaH_2PO_4, 0.2% (w/v) OPD, pH 6.5] and incubated at room temperature for 12 h in the absence of light. During this incubation, the intact chloroplasts were disrupted by hypotonic shock and the released sugar-derived RCs reacted with OPD to produce quinoxaline derivatives. Next, the suspension was centrifuged (10,000 ×g; 10 min) and the supernatant was filtered through a 0.45-µm membrane. The quinoxaline derivatives were identified by HPLC. In brief, 40 µl samples were injected, and the elution was performed at a flow rate of 1 ml/min. Solvent A contained 0.150% (v/v) acetic acid, and solvent B comprised 80% (v/v) aqueous methanol containing 0.150% (v/v) acetic acid. The gradient started with 60% solvent B, followed by a linear increase to 100% solvent B over 20 min and a linear decrease to 60% solvent B over 3 min, followed by equilibration with 60% solvent B for 7 min. The analytical column was a Knauer Eurospher 100 C18 (5 mm; 4.6 × 250 mm). The wavelength was set at 312 nm. External calibration was performed using a linear calibration curve with MG (0.1–300 µg/ml) purchased from Nacalai Tesque (Japan).

The sugar-derived RCS (1, 2-dicarbonyls) generated during the photosynthesis of intact leaves were identified as described above. The frozen leaf was mixed in a chilled mortar and pestle in the sodium phosphate buffer (1 ml) [50 mM NaH_2PO_4, 0.2% (w/v) OPD, pH 6.5], and furthermore incubated at room temperature for 12 h in the absence of light. Next, the suspension was centrifuged (10,000 ×g; 10 min) and the supernatant was filtered through a 0.45-µm membrane. The quinoxaline derivatives were identified by HPLC, as described above.

RESULTS

PGA-dependent O_2 evolution accompanied the production of methylglyoxal and glyoxal in intact chloroplasts

The mechanism of sugar-derived RCS production during photosynthesis was elucidated by studying MG/GLO metabolisms. During glycolysis, MG and glyoxal (GLO) are produced by enzymatic or non-enzymatic equilibrium reactions between DHAP and GAP (Thornalley 2006). Since these reactions are also a part of the Calvin cycle in chloroplasts, I hypothesized that the production of GAP would stimulate the equilibration reaction between GAP and DHAP catalyzed by TPI, and the productions of MG and GLO would be enhanced in chloroplasts.

The production of GAP by the Calvin cycle was induced by adding 3-PGA to the intact chloroplast suspension, which enters the stroma through the phosphate-triose phosphate-phosphoglycerate translocator (Flügge and Heldt 1984). 3-PGA is then sequentially converted into 1,3-bisphosphoglycerate and then into GAP, by PGA kinase and GAP dehydrogenase, respectively. These reactions consume NADPH and ATP, which are regenerated by photosynthetic linear electron flow. Since the addition of 3-PGA to actinic red-illuminated chloroplasts induces O_2 evolution, the rate of O_2 evolution reflects the production rate of GAP in chloroplasts (Takagi et al. 2012).

Dicarbonyl compounds (MG, GLO, and 3-DG) react with o-phenylenediamine (OPD) to produce quinoxaline derivatives (Mavric et al. 2008). The OPD-derived compounds were separated by HPLC and quantitatively detected by spectrophotometry (Mavric et al. 2008). The illumination of intact chloroplasts (400 μmol photons m^{-2} s^{-1}) in the absence of 3-PGA did not induce the production of sugar-derived RCS: MG, GLO, and 3-DG (Fig.V-1, Fig. V-2) or O_2 evolution (data not shown). The incubation of intact chloroplasts with 10 mM PGA in the dark did not induce the production of sugar-derived RCS: MG (Fig.V-3), and GLO (data not shown). In contrast, the addition of 3-PGA to intact chloroplasts under illumination induced the productions of MG and GLO

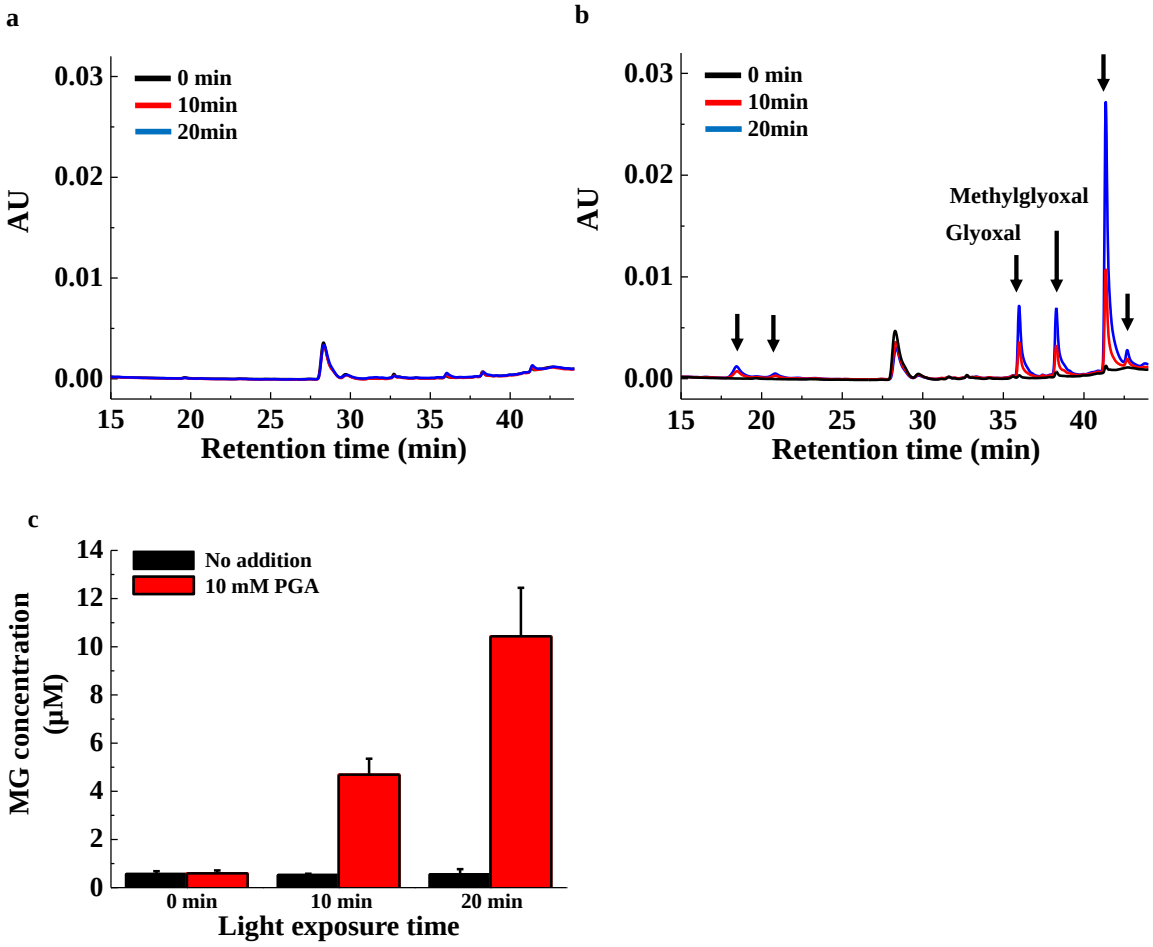

Figure V-1

Chromatograms of OPD derivatives of sugar-derived RCS. 3-PGA was absent (a) and present (b) in the reaction mixtures. The reaction mixtures (1 ml) that contains chloroplasts (40 µg Chl) in the absence and presence of 10 mM 3-PGA are illuminated in red light (>640 nm, 400 µmol photons m^{-2} s^{-1}) at 25°C. Typical chromatograms of sugar-derived RCs are shown. AU shows the relative absorbance unit at 312 nm. Three lines indicate different light exposure time (black, 0 min; red, 10 min; and blue, 20 min). Arrows indicate sugar-derived RCS, the levels of which increased in the presence of 3-PGA. Glyoxal (GLO) and methyglyoxal (MG) were identified from the retention times of the commercially purchased compounds. (c) MG was quantified at the indicated time after illumination in the absence (black bars) or presence (red bars) of 3-PGA. HPLC of sugar-derived RCs is described in the Materials and Methods section. Values are expressed as mean ± SD of three independent experiments.

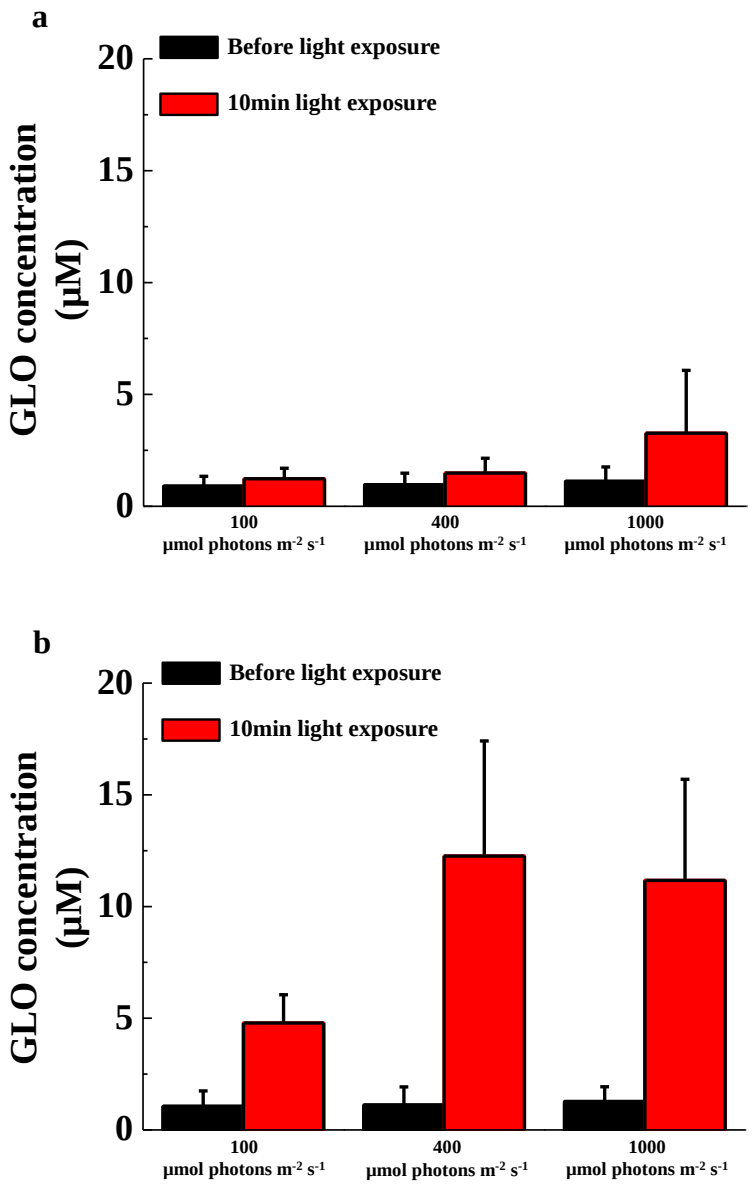

Figure V-2

Light dependency of glyoxal (GLO) production in isolated chloroplasts. Reaction mixtures (1 ml) containing chloroplasts (40 µg Chl) in the absence (a) and presence (b) of 10 mM 3-PGA were illuminated (100, 400, or 1000 µmol photons m^{-2} s^{-1} red light) during the 10-min period. Black bar, in the dark; red bars, light exposure; AU, arbitrary units of absorbance at 312 nm. GLO concentrations were estimated from the peak area on the chromatograms and expressed as AU relative to the baseline level in the dark. Values are expressed as mean ± SD of three independent experiments.

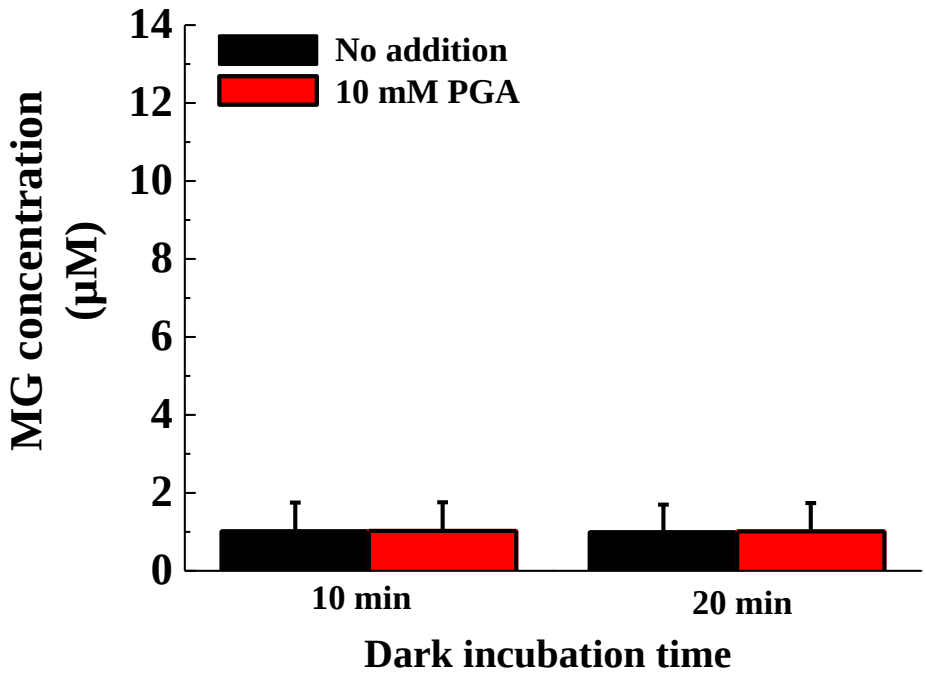

Figure V-3

Requirement of light on the production of MG in isolated chloroplasts. MG was quantified at the indicated time after incubation with the isolated chloroplasts in the absence (black bars) or presence (red bars) of 3-PGA. HPLC of sugar-derived RCs is described in the Materials and Methods section. Values are expressed as mean ± SD of three independent experiments.

(Figs. V-1B, V-2) and induced O_2 evolution (data not shown). The amounts of these RCS increased linearly with prolonged illumination (Fig. V-1C). Under dark conditions, no RC was observed even in the presence of 3-PGA (data not shown). Furthermore, I confirmed that 3-PGA did not react with OPD to produce the quinoxaline form (data not shown). I also found four peaks (R.T: 17, 21, 41, and 42 min) in the chromatography profile, which were not identified in the present work (Fig. V-1B). As a result, I found six compounds which accumulated in the presence of 3-PGA. These results indicated that the turnover of TPI reaction in the Calvin cycle produced MG and GLO, similarly to that observed in the glycolysis pathway.

Next, I tested the effect of intensity of light illuminated to intact chloroplasts on the production of MG (Fig. V-4A). With the increase in light intensity, the content of MG increased in the presence of 3-PGA. In contrast, this increase was not observed in the absence of 3-PGA (Fig. V-4B). I also observed that the increase in the light intensity enhanced GLO production (Fig. V-2).

Relationship between photosynthetic activity and MG production in intact chloroplasts

I calculated the rates of O_2 evolution and MG production and plotted them against light intensity (Fig. V-5). Both O_2 evolution and MG production rates increased with increasing light intensity at 25°C. At 100 μmol photons m^{-2} s^{-1} and a saturated intensity of 1000μmol photons m^{-2} s^{-1}, MG production rates corresponded to 3% of the O_2 evolution rates. Furthermore, there was a positive linear relationship between the rates of MG production and O_2 evolution (Fig. V-6A).

Finally, I tested the impact of temperature on MG production during photosynthesis. I plotted the MG production rate against the O_2 evolution rate at 35°C (Fig. V-6B). The MG production rate showed a positive linear relationship with the O_2 evolution rate, similarly to that observed at 25°C. However, the slope of the positive line at 35°C was larger than that at 25°C. Therefore, these data show that high temperature enhances MG production in chloroplasts, which could be due to an increase in TPI activity. As a result, the production rate of a by-product, MG, would be increased.

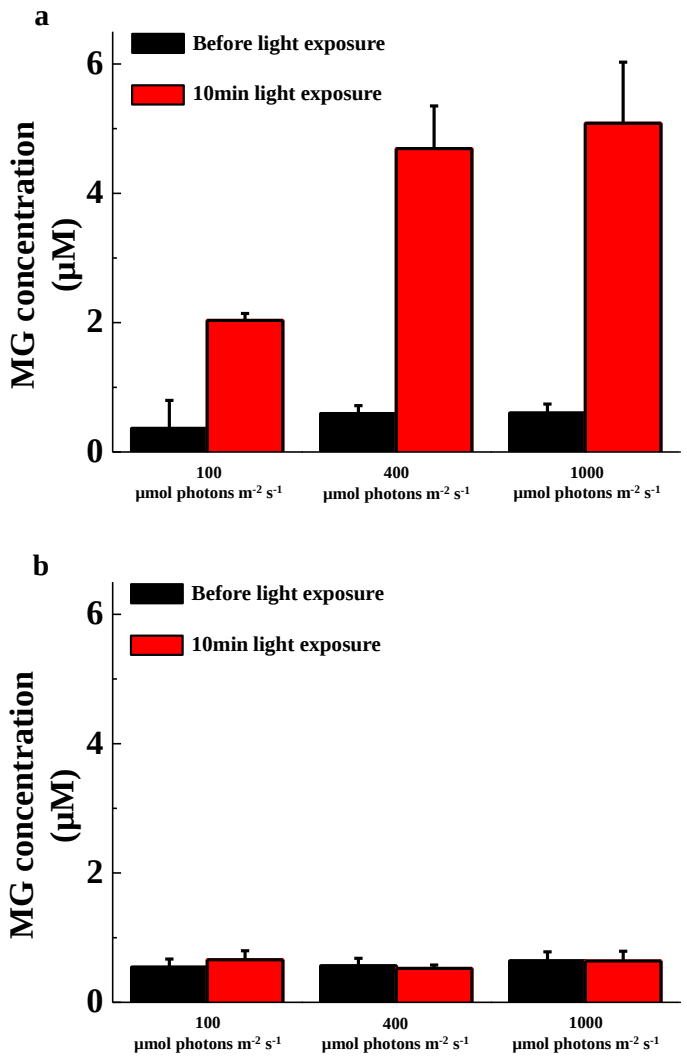

Figure V-4

Light dependency of MG production in chloroplasts. The reaction mixtures (1 ml) that contain chloroplasts (40 μg Chl) in the presence (a) and absence (b) of 10 mM 3-PGA were illuminated at the indicated intensity of red light for 10 min. Black bar, in the dark; red bars, exposure at the indicated intensity of light. Values are expressed as mean ± SD of three independent experiments.

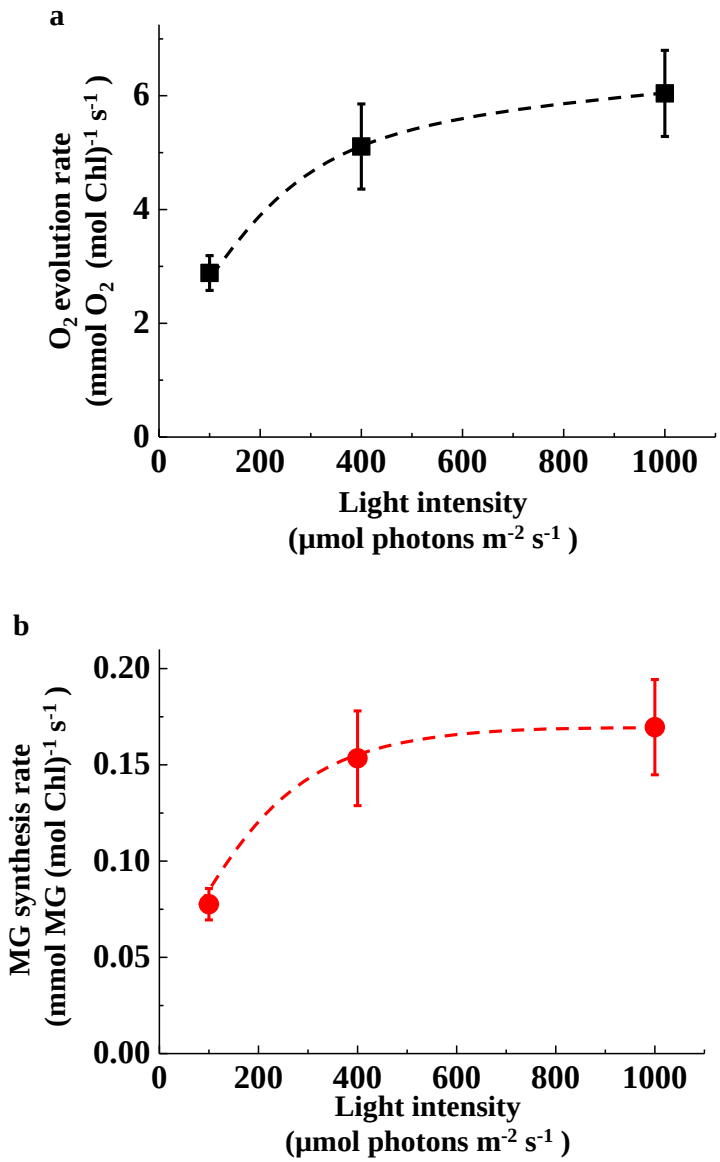

Figure V-5

Dependence of O_2 evolution rate (a) and MG synthesis rate (b) on the intensity of red light in chloroplasts. The reaction mixture (1 ml) containing 40 µg chloroplasts and 10 mM 3-PGA illuminated at the indicated light intensity. O_2 evolution rate was calculated from the steady-state increase in [O_2] at 10 min. MG synthesis rate was calculated from the concentration of MG at 10 min. Values are expressed as mean ± SE of five independent experiments.

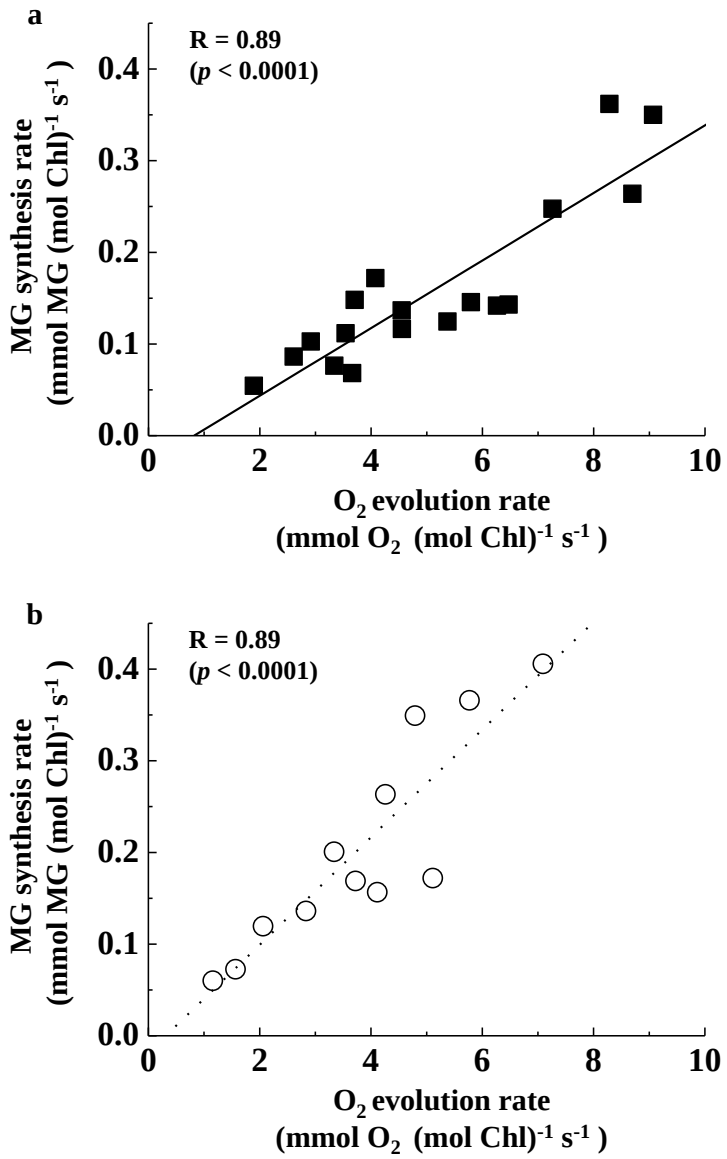

Figure V-6

The relationship between O_2 evolution rate and MG synthesis rate. The O_2 evolution rate and MG synthesis rate were obtained from Figure 3. (a) The O_2 evolution rates were plotted against MG synthesis rates. These rates were estimated at 25°C. The positive linear line was the fitted line with the linear regression model. (b) Both the O_2 evolution rate and MG synthesis rate were estimated at 35°C (data not shown), and the O_2 evolution rates were plotted against MG synthesis rates. The positive linear dotted line was the fitted line with the linear regression model. The correlation coefficient (R) and its statistical significance value (*p*) were shown. Values are obtained by five independent experiments.

High-[CO_2] stimulated the photosynthesis with the enhanced production of MG in wheat leaves

As shown above, the presence of 3-PGA stimulated the production of MG in the intact chloroplasts. These results show that the stimulation of the turnover of the Calvin cycle enhanced the production of MG. Next, I tested whether the stimulation of photosynthesis accompanied the enhanced production of MG in the intact leaves of higher plants. I compared the production of MG in the illuminated wheat leaves under the different concentration of CO_2.

I illuminated wheat leaves at 1,060 μmol photons m^{-2} s^{-1}, 20% O_2, and 40 Pa CO_2 for 1 hr. The steady-state rate of photosynthetic CO_2-fixation was 15 ± 3 μmol CO_2 m^{-2} s^{-1} (n = 3). Then, I analyzed dicarbonyl compounds in the illuminated leaves (Fig. V-7). I found the productions of MG and GLO in the intact leaves of wheat (Fig. V-7). The concentrations of MG and GLO were 1.9 ± 0.2 μmol m^{-2} (n=3) and 117 ± 19 μmol m^{-2} (n=3) (Table V-1).

Next, I illuminated wheat leaves at high-[CO_2] (1,060μmol photons m^{-2} s^{-1}, 20% O_2, and 90 Pa CO_2) for 1 hr. The steady-state rate of photosynthetic CO_2-fixation was 21 ± 2 μmol CO_2 m^{-2} s^{-1} (n = 3), which was larger than that at 40 Pa CO_2. Then, I analyzed dicarbonyl compounds (Fig. V-7). I found a lot of peaks in the HPLC chromatograph, some of which were larger than those at 40 Pa CO_2. These results indicated that the stimulated photosynthesis induced the production of dicarbonyl compounds. The concentrations of MG and GLO were 2.8 ± 0.3 μmol m^{-2} (n=3) and 150 ± 40 μmol m^{-2} (n=3), which were larger than those at 40 Pa CO_2.

I found a lot of peaks in the HPLC chromatograph, some of which were different from those found in the intact chloroplasts. In the present work, I did not identify these peaks, which remain to be clarified for elucidating the physiological function of these dicarbonyl compounds.

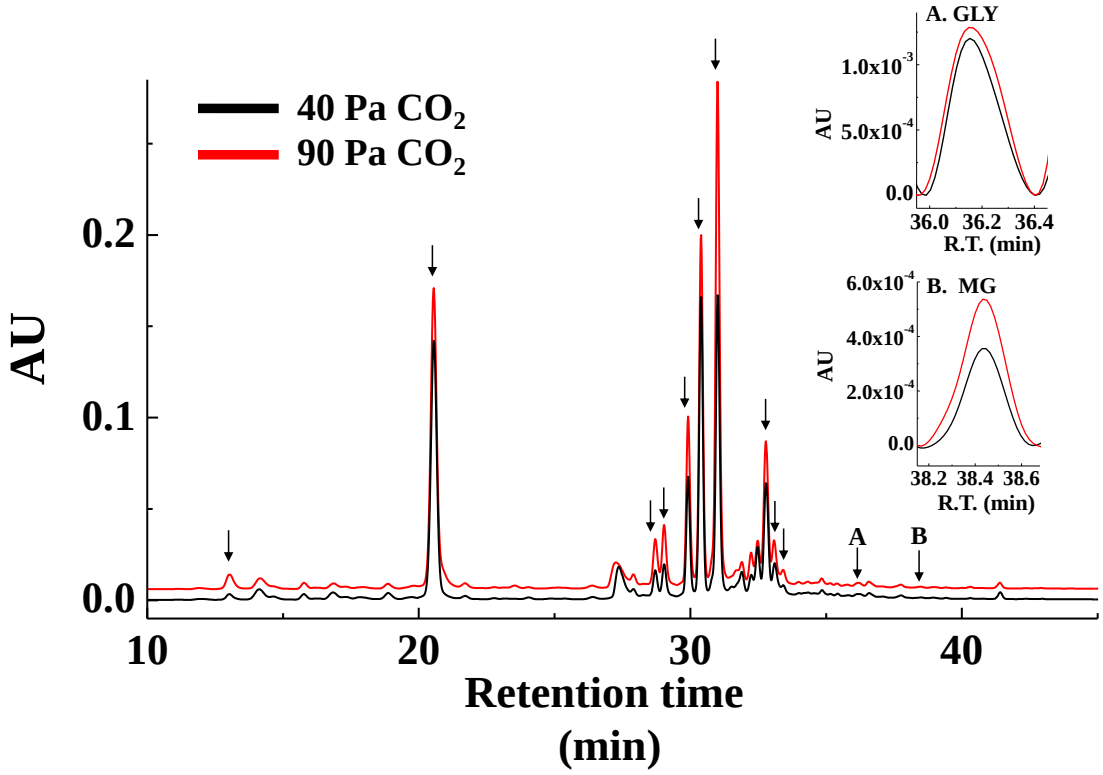

Figure V-7

Chromatograms of OPD derivatives of sugar-derived RCS. Red line, 40Pa CO_2; green line, 90 Pa CO_2. Typical chromatograms of sugar-derived RCS are shown. AU shows the relative absorbance unit on the basis of leaf area at 312 nm. Arrows indicate sugar-derived RCs, the levels of which increased at 90Pa CO_2, compared to 40Pa CO_2. Glyoxal (GLO) and methyglyoxal (MG) were identified from the retention times of the commercially purchased compounds. Inlets showed typical MG and GLO peaks, which were normalized with the base line. HPLC of sugar-derived RCS is described in the Materials and Methods section. "R.T." means retention time.

Table V-I

Effect on an increase in CO_2 partial pressure on net CO_2 assimilation rate (A) and concentration of MG and GLO in wheat leaves

Partial pressure of CO_2 (Pa)	A (µmol CO_2 m^{-2} s^{-1})	MG (µmol m^{-2})	GLO (µmol m^{-2})
40	**15 ± 3**	**1.9 ± 0.2**	**117 ± 19**
90	**21 ± 2**	**2.8 ± 0.6**	**150 ± 40**

DISCUSSION

I hypothesized that 3-PGA-dependent O_2 evolution initiated the production of MG in the isolated chloroplasts. 3-PGA was metabolized to GAP, which was sequentially catalyzed by PGA kinase and GAPDH, and GAP was equilibrated with DHAP, which was catalyzed by TPI. MG and GLO were detected only in the presence of 3-PGA (Figs. V-1 and V-4). The production rate of MG increased with the illumination time and light intensity. MG production showed a positive linear relationship with 3-PGA-dependent photosynthesis (Fig. V-6). These facts evidenced that the production of MG via the Calvin cycle was the same as that observed in glycolysis, and MG and GLO productions were inevitable during photosynthesis. I furthermore found that the productions of MG and GLO were enhanced under high-[CO_2] in the intact leaves. Photosynthetic activity was increased at high-[CO_2], That is, the stimulated turn-over of the Calvin cycle induced the productions of the by-products, MG and GLO.

I observed the production of the other RCS in the isolated chloroplasts and the intact leaves (Fig. V-1). Furthermore, I found a lot of RCS, some of which were different from those found in the intact chloroplasts. The production mechanisms of these RCS were unknown. MG and GLO produced in the Calvin cycle may induce their production by affecting the metabolism during photosynthesis, or the inactivation of the enzymes during oxidative attacks on lipid metabolism (Vistoli et al. 2013).

I evaluated the steady-state concentration of MG in chloroplasts. Plant chloroplasts showed AKR activity (Saito et al. 2011). Vmax and Km for MG in the AKR reaction of chloroplasts were 3 μmol NAPDH (mg Chl)$^{-1}$ h^{-1} and 5 mM, respectively (Saito et al. 2011). In 3-PGA-dependent O_2 evolution, the maximum production rate of MG was approximately 0.6 μmol MG (mg Chl)$^{-1}$ h^{-1} (Fig. V-5). Next, the steady-state concentration of MG was estimated to be approximately 1.3 mM. At steady state, the production rate of MG was equal to the scavenging rate by AKR, which followed the Michaelis−Menten-type reaction.

$$0.6\ \mu\text{mol MG (mg Chl)}^{-1}\ \text{h}^{-1} = [3\ \mu\text{mol NAPDH (mg Chl)}^{-1}\ \text{h}^{-1} \times (\text{MG})\text{st}] / [5\ \text{mM} + (\text{MG})\text{st}].$$

(MG)st was the steady-state concentration of MG (mM) and was estimated to be 1.3 mM.

During the light phase of photosynthesis, MG catalyzes the photoreduction of O_2 to O_2^- mediated in the photosystem I (PSI) complex (Saito et al. 2011). The Km for MG is approximately 0.2 mM. In 3-PGA-dependent O_2 evolution, MG may catalyze the photoreduction of O_2 at PSI. When MG is univalently reduced, it forms a MG radical (see figure below; Yim et al. 1995) with a mid-point redox potential (E'm) of −330 mV (Kalapos 2008). If this reaction occurs at PSI, the reduced MG presumably donates electrons to O_2, producing O_2^-.

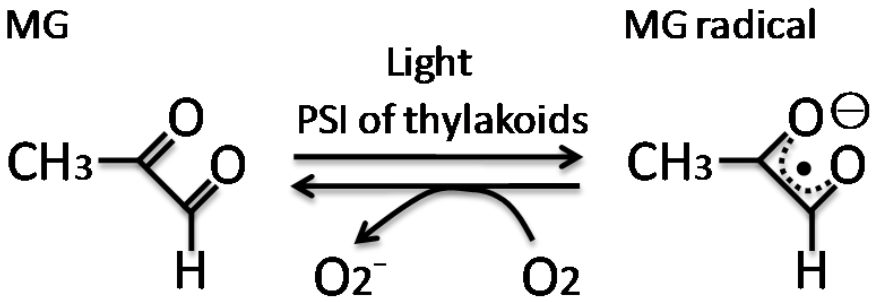

The candidates for electron transport components that catalyze the univalent reduction of MG at the PSI are phylloquinone (E'm: −800 mV), Fx, an interpolypeptide (4 Fe-4 S cluster) (E'm −705 mV), FA (E'm −520 mV), FB (E'm −580 mV), which are 4 Fe-4 S clusters bound to the extrinsic subunit PsaC (Nelson and Yocum 2006), and ferredoxin (E'm −430 mV). O_2^- disproportionate to H_2O_2 and H_2O. That is, the photoreduction of O_2 at PSI stimulates the production of H_2O_2. Furthermore, the accumulation of O_2^- and H_2O_2 stimulates the production of hydroxyl radicals (OH·) by the transition metal-catalyzed Fenton reaction. OH· has a higher redox potential than O_2^- and H_2O_2, and can fragment DNA, proteins, and lipids (Asada and Takahashi 1987). In particular, the stimulated production of OH· in chloroplasts fragments ribulose 1,5-bisphosphate carboxylase/oxygenase (Rubisco) and glutamine synthase, and these enzymes degrade oxidatively (Fucci et al. 1983, Ishida et al. 1997, 1998). In addition, at low temperature, OH· decomposes the PSI complex (Sonoike, 1996b, Tjus et al. 2001). These oxidative attacks by OH· would be one of the reasons why the carbonylated proteins accumulated in plants cultivated at high CO_2 concentrations (Qiu et al. 2008).

In the present work, I first showed that MG and GLO productions in chloroplasts depended on light and 3-PGA, indicating that MG and GLO were produced by the Calvin cycle during photosynthesis. As is the case in glycolysis, MG and GLO would be generated as a by-product of the TPI reaction in the Calvin cycle. Therefore, if photosynthesis is enhanced by high-[CO_2] levels, the metabolic turnover of the Calvin cycle accelerates, resulting in enhanced MG and GLO production. In fact, I observed the enhanced productions of MG and GLO at high-[CO_2]. I also observed higher rates of MG production at 35°C compared with that observed at 25°C. As global warming proceeds, the temperature on Earth will continue to increase. This increases the activity of TPI, resulting in an increased production rate of MG. Research on the production mechanisms of sugar-derived RCS is indispensable for the elucidation of the physiological functions of RCS in crop productivity exposed to the global warming environments.

Chapter 6

Suppression of chloroplastic alkenal/one oxidoreductase represses the carbon catabolic pathway in *Arabidopsis thaliana* leaves during night

ABSTRACT

Lipid-derived reactive carbonyls species (RCS) have electrophilic moieties and cause oxidative stress by reacting with cellular components. *Arabidopsis thaliana* has a chloroplast-localized alkenal/one oxidoreductase (AtAOR) for the detoxification of lipid-derived RCS, especially α, β-unsaturated carbonyls. In this study, I aimed to evaluate the physiological importance of AtAOR, and analyzed AtAOR mutants (*aor*) including T-DNA knock-out, *aor* (T-DNA), and RNAi knock-down, *aor* (RNAi) lines. I found that both *aor* mutants showed smaller plant sizes than WT, when they were grown under day/night cycle conditions. To elucidate the cause of the *aor* mutant phenotype, I analyzed the photosynthetic rate and respiration rate by gas-exchange analysis. Subsequently, I found that WT and *aor* (RNAi) showed similar CO_2 assimilation rate; however, respiration rate was lower in *aor* (RNAi) than in WT. Furthermore, I revealed that phosphoenolpyruvate carboxylase activity decreased and starch degradation during night was suppressed in *aor* (RNAi). In contrast, the phenotype of *aor* (RNAi) was rescued when *aor* (RNAi) were grown under constant light conditions. These results indicate that smaller plant sizes observed in *aor* mutants grown under day/night cycle conditions were attributable to the decrease in carbon utilization during the night. Here, I propose that the detoxification of lipid-derived RCS by AtAOR in chloroplasts contributes to the protection of dark respiration and supports plant growth during night.

INTRODUCTION

To avoid the risk of accumulation of lipid-derived reactive carbonyls species (RCS) in plant cells and the consequent oxidative modification of biomolecules, plants have detoxification enzymes like aldo-keto reductase (AKR), aldehyde dehydrogease (ALDH), aldose/aldehyde reductase (ALR), alkenal reductase (AER), and alkenal/one reductase (AOR) (Oberschall et al., 2000; Mano et al., 2002; Kirch et al., 2004; Yamauchi et al., 2011; Saito et al., 2013). AKR and ALR reduce aldehyde groups to alcohol groups by using NAD(P)H, and ALDH oxidizes aldehyde groups to carboxylic acid groups by using $NAD(P)^+$ (Oberschall et al., 2000; Kirch et al., 2004; Saito et al., 2013). AER and AOR detoxify α, β-unsaturated carbonyls through the reduction of a highly electrophilic α, β-unsaturated bond by using NAD(P)H (Mano et al., 2002; Yamauchi et al., 2011). Overexpression of these detoxification enzymes in higher plants reduces the content of lipid-derived RCS in cells, compared to WT. Moreover, these overexpressing plants acquire tolerance toward oxidative damage under drought and salt stress conditions, where ROS production in chloroplasts is stimulated (Sunkar et al., 2003; Mano et al., 2005; Rodrigues et al., 2006; Turóczy et al., 2011). On the other hand, transgenic plants that have suppressed activities of these detoxification enzymes show higher sensitivity to oxidative stress than WT (Kotchoni et al., 2006; Shin et al., 2009; Stiti et al., 2011; Yamauchi et al., 2012). However, the methods to evaluate the risk of lipid-derived RCS in higher plants are limited to maximum quantum yield of PSII (Fv/Fm) or the content of chlorophyll in leaves in many studies. Therefore, the mechanisms how lipid-derived RCS affect plant physiological reactions such as photosynthesis or respiration are less clarified *in vivo*.

In this study, I aimed to elucidate the physiological importance of the detoxification of lipid-derived RCS in chloroplasts that is the source of ROS and lipid-derived RCS in higher plants. First, I grew the *Arabidopsis thaliana* T-DNA insertion mutant of chloroplast localized AOR [*aor* (T-DNA)], and analyzed plant growth. I found that *aor* (T-DNA) showed growth retardation, compared to WT, under day/night cycle conditions. This result conflicted with previous results (Yamauchi et al., 2012). To confirm whether AOR is related to growth in *Arabidopsis thaliana*, I

constructed RNA interference mutants of AOR in *Arabidopsis thaliana*, *aor* (RNAi), and checked their growth. I observed that *aor* (RNAi) also showed growth retardation, compared to WT, under day/night cycle conditions. Furthermore, I found that the growth retardation in *aor* (RNAi) was relieved under constant light conditions. These results indicated that the detoxification of lipid-derived RCS in chloroplasts is required for plant growth under day/night conditions, which are normal growth conditions on earth. Furthermore, I observed a suppressed activity of dark respiration and an accumulation of starch in chloroplasts at the end of the night in *aor* (RNAi). These results suggest that AtAOR can function to protect the catabolic pathway of starch and contribute to supporting plant growth under day/night cycle conditions.

MATERALS AND METHODS

Plant growth conditions

Arabidopsis thaliana wild type [ecotype Columbia-0 (Col-0)] and *aor* mutants were grown for 3-4 weeks under day/night cycle growth conditions [16 h light (23^{o}C, 150 µE m^{-2} s^{-1}) / 8 h dark (20^{o}C)] or constant light conditions [24 h light (23^{o}C, 150 µE m^{-2} s^{-1})] in a plant growth chamber. Relative humidity was kept at 50-60%. Seeds were sown in soil (commercial peat-based compost) and kept at 4^{o}C for 3 days to stimulate their germination, before seeds were transferred to the plant growth chamber. A 0.1 % Hyponex solution (N-P-K = 5-10-5, Hyponex, Osaka, Japan) was used to irrigate plants every other day.

Production of the RNAi transgenic line for *AtAOR*

The cDNA region of *AtAOR* (At1g23740) that triggers silencing was selected using the dsCheck program (Naito et al. 2005) to avoid off-target effects. The PCR primers used to amplify the selected 387-bp fragment of the *AtAOR* cDNA were 5'-caccGAGCGAGAAAGCATTGGAAG-3' and 5'-GCGTCAAAGACAACATCGTA-3'. The PCR products were cloned into the pENTR/D-TOPO vector and then transferred into the pHellsgate8 vector (Helliwell et al. 2003) by an LR recombination reaction (Gateway, Invitrogen, Carlsbad, CA, USA). Arabidopsis Col-0 was transformed with the pHellsgate8-At1g23740 plasmid using Agrobacterium tumefaciens strain GV3101 and the floral-dip method. Seeds were collected and transformants were selected on media containing Murashige and Skoog salt mix, 50 µg ml^{-1} kanamycin, and 0.8 % agar. The selected transgenic lines (T1 generation) were transferred to soil, and T1 lines showing a strong silencing phenotype were selected by RT-PCR, cultivated until they flowered, and self-fertilized. The lines that showed stable silencing effects in T2 were further analyzed.

Transient expression in *Arabidopsis thaliana* mesophyll protoplasts

Preparation of protoplasts from *Arabidopsis thaliana* rosette leaves and PEG-calcium transfection

was performed according to a method described previously (Yoo et al., 2007). The coding region of AtAOR in both transit and non-transit forms obtained by PCR using the KOD-FX Neo (Toyobo, Osaka, Japan) was sub-cloned into Sal I and Nco I sites of a pCaMV35S_GFP vector (Chiu et al., 1996) using the In Fusion HD Cloning Kit (Takara, Osaka, Japan). The primers used in this experiment were 5'- GTCGACATGAACGCAGCGCTTGCAAC-3' and 5'- CCATGGCAGGAATGGGATAAACAACGACC-3'. For transformation, 10 µg of each plasmid DNA was transfected into 2 × 104 protoplasts, and GFP and chlorophyll fluorescence were observed using a fluorescence microscope (BZ-8000, KEYENCE, Japan). The field of cells was excited at 480 nm and fluorescence emission was detected at 510 nm.

Measurements of chlorophyll content in leaves.

The chlorophyll content was measured by the method of Porra et al., (1989). Leaf segments were incubated in N, N-dimethylformamide at 4^{o}C overnight. Absorbance at 750, 663.8, and 646.8 nm were measured to calculate chlorophyll content. Chlorophyll content in leaves was represented by leaf area base.

Measurements of nitrogen content in leaves.

Total leaf nitrogen content was determined with Nessler's reagent in a digestion solution after the addition of sodium-potassium tartrate (Makino and Osmond, 1991). Detached leaves were kept in a drying machine (60^{o}C) and dehydrated over-night. Sulfuric acid 60 % (v/v) (100 µl) and dehydrated leaves were mixed in the glass tube and incubated at 150^{o}C in a heating block thermostat bath for 40 min. After cooling the glass tube in the air, 30 % (v/v) H_2O_2 (50 µl) was added to the mixture. The mixture was incubated at 180^{o}C for 40 min in the heating block, subsequently H_2O_2 (50 µl) was added after the mixture was cooled. The incubation in the heating block and the addition of H_2O_2 were repeated another two times, but the incubation temperature was changed to 220^{o}C and 260^{o}C in each incubation respectively. The incubation at 260^{o}C and the addition of H_2O_2 were continued until

the color of the mixture turned clear from brown. When the color turned clear, distilled water (4.95 ml) was added to the mixture and mixed vigorously. The mixture (500 µl), distilled water (4.25 ml), 10 % (w/v) potassium sodium tartrate ($KNaC_4H_4O_6$) solution (100 µl) and 2.5 N sodium hydroxide (NaOH) (50 µl) were mixed and Nessler's reagent (100 µl) was immediately added to the mixture. Nitrogen content was determined by the absorbance change at 420 nm.

SDS-PAGE

For protein analysis, an amount of leaf tissue was homogenized with a pestle in 3 ml extraction buffer (50 mM HEPES-KOH, pH 7.6, 1 mM dithiothreitol (DTT), 2 % (w/v) polyvinylpolypyrolidone, 1 mM PMSF, 10 mM leupeptin). The homogenate was centrifuged at 15,000 × g for 15 min at 4^{o}C. The supernatant was treated as the soluble fraction. The proteins were electrophoresed on 12.5 % (w/v) SDS-polyacrylamide gels, as described by Laemmli (1970). The proteins (5 µg) were loaded on each lane and the gels stained with Coomassie Brilliant Blue R-250.

Western blotting

The Proteins were separated by SDS-PAGE, transferred onto polyvinylidene difluoride (PVDF) membrane (Millipore), and then blocked with blocking one reagent (Nakalai Tesque, Kyoto, Japan) for 30 min at room temperature (25 ^{o}C). The PVDF membrane was subsequently incubated with AtAOR-specific peptide antibody for 1 h at room temperature (25 ^{o}C). The PVDF membrane was washed 3 times with TBS tween buffer (10 mM Tris-HCl (pH 7.4), 0.14 M NaCl, 0.1 % (v/v) Tween-20) and incubated with ECLTM peroxidase labeled anti-rabbit antibody (GE Healthcare, Buckinghamshire, UK) for 1 h at room temperature. The PVDF membrane was washed three times with TBS tween buffer. AtAOR protein was detected with a Chemi-Lumi One Super (Nakarai Tesque, Kyoto, Japan) and scanned with Ez-Capture MG (ATTO, Tokyo, Japan).

Gas-exchange and chlorophyll fluorescence analysis

The rates of CO_2 and H_2O vapor exchange were measured with Dual-PAM-100 (Heintz Walz, Effeltrich, Germany) and IRGA measuring systems (LI-7000, Li-COR, Lincoln, NE, USA) equipped with the 3010-DUAL gas exchange chamber (Heintz Walz, Effeltrich, Germany). The system is detailed in Makino et al. (1988). Gas with the indicated mixture of pure O_2 and CO_2 was prepared by mixing 20.1 % (v/v) in 79.9 % (v/v) N_2 and 1 % (v/v) CO_2 in 99 % (v/v) N_2 using a mass-flow controller (Kofloc model 1203; Kojima Instruments Co., Kyoto, Japan). The mixture of gases was saturated with water vapor at 13.5 ± 0.1^{o}C. The leaf temperature was controlled at 25^{o}C. In the experiments that analyze the photosynthetic activity in Arabidopsis leaves, chlorophyll fluorescence analysis was simultaneously conducted by Dual-PAM 101 (Walz, Effeltrich, Germany). Gas-exchange parameters were calculated according to the equations in von Caemmerer and Farquhar (1981), and chlorophyll fluorescence parameters (Fv/Fm and quantum yield of PSII) were calculated according to the equations in Butler and Kitajima (1975) and Genty et al., (1989). Leaves were illuminated (150 μE m^{-2} s^{-1}) for 10 min and photosynthetic parameters determined. For the calculation of chlorophyll fluorescence parameters, measured light intensity (0.1 μE m^{-2} s^{-1}) and saturating pulse (300 ms, 10,000 μE m^{-2} s^{-1}) were applied to determine Fo, Fm, Fs, and Fm'.

Oxygen-exchange analysis

Leaf segments were placed in a cuvette (LD2/2; Hansatech Ltd, King's Lynn, UK). O_2 uptake was measured in the dark, according to the method of Deliu and Walker (1981). Temperature-controlled water was circulated through the water jacket, and leaf temperature was maintained at 25°C.

Enzyme assays

AtAOR activity was determined in a reaction mixture (1 ml) that contained 50 mM potassium phosphate (pH 7.0), 0.2 mM NADPH, and 20 mM acrolein. The acrolein-dependent oxidation of NADPH was followed by monitoring the decrease in absorbance at 340 nm, assuming an absorption

coefficient of 6.2 mM cm^{-1}.

For evaluation of Rubisco activity, leaf protein was extracted in buffer [100 mM Tris-HCl (pH 7.8), 5 mM $MgCl_2$, 2 mM EDTA, 5 mM DTT, 1 mM reduced glutathione, (GSH) 0.5 % (v/v) Triton X-100, 5 % (w/v) polyvinylpyrrolodone] and leaf protein solution was obtained by centrifugation (15,000 x g ,2 min, 4^oC). Rubisco activity was measured as the decrease in absorbance at 340 nm by coupling the activity of Rubisco to NADH oxidation using phosphoglycerate kinase and NAD^+-GAPDH (Sawada et al. 1990). To measure the total Rubisco activity, 1 ml of the leaf protein solution was transferred to a new tube, the $MgCl_2$ concentration was brought to 20 mM, and the NaHCO3 concentration was brought to 10 mM. This mixture was kept on ice for 10 min before assaying for total Rubisco activity. The reaction mixture contained 50 mM HEPES-KOH (pH 8.0), 15 mM $MgCl_2$, 20 mM NaCl, 10 mM DTT, 0.5 mM ATP, 0.2 mM NADH, 5 mM phosphoenolpyruvate, 5 mM creatine phosphate, 10 mM $NaHCO_3$, 20 units of pyruvate kinase, 2 units of phosphocreatine kinase, 18 units of NAD-GAPDH, 18 units of phosphoglyceratekinase, 1 mM ribulose 1, 5-bisphosphate, and leaf protein solution. The reaction was started by addition of ribulose 1, 5-bisphosphate after pre-incubation for 2 min, and monitored by following the absorbance at 340 nm.

For evaluation of FBPase, PRK, and $NADP^+$-GAPDH activities, leaf protein was extracted in buffer [100 mM Tris-HCl (pH 7.8), 10 mM $MgCl_2$, 1 mM EDTA, 2.5 mM DTT, 1mM GSH, 0.5 % (v/v) Triton X-100, 5 %(w/v) polyvinylpyrrolodone] and leaf protein solution was obtained by centrifugation (15,000 x g , 2 min, 4^oC). FBPase activity was determined in a reaction mixture (1 ml) that contained 100 mM Tris–HCl (pH 8.0), 10 mM $MgCl_2$, 0.5 mM EDTA, 0.4 mM $NADP^+$, 0.1 mM fructose 1,6-bisphosphate, 0.5 units of glucose 6-phosphate dehydrogenase, 1.5 units of phosphoglucose isomerase, and the leaf protein solution. The reaction was started by addition of fructose 1, 6-bisphosphate after pre-incubation for 2 min and absorbance at 340 nm was monitored (Tamoi et al., 1996a).

PRK activity was determined in a reaction mixture (1 ml) that contained 100 mM Tris-HCl

(pH 8.0), 100 mM KCl, 10 mM $MgCl_2$, 0.2 mM NADH, 2 mM ATP, 2.5 mM phosphoenolpyruvate, 2 mM ribose 5-phosphate, lactate dehydrogenase (5 units), pyruvate kinase (2 units), phosphoriboisomerase (1 unit) and the leaf protein solution. The reaction was started by addition of ribose 5-phosphate after pre-incubation for 2 min and was followed by monitoring absorbance at 340 nm (Kobayashi et al. 2003).

$NADP^+$-GAPDH activity was determined in a reaction mixture (1 ml) that contained 100 mM Tris-HCl buffer (pH 8.0), 10 mM $MgCl_2$, 5 mM ATP, 0.2 mM NADPH, 2 units of phosphoglycerate kinase, 3 mM 3-phosphoglycerate and the leaf protein solution. The reaction was started by addition of 3-phosphoglycerate after pre-incubation for 2 min and absorbance at 340 nm was monitored (Tamoi et al., 1996b).

For evaluation of PEPC, citrate synthase, aconitase, and PDH activities, leaf protein was extracted in buffer [50 mM KH_2PO_4-K_2HPO_4 (pH 7.6), 10 mM $MgSO_4$, 1 mM EDTA, 5 mM DTT, 0.05 % (v/v) Triton X-100, 5 % (w/v) polyvinylpyrrolodone, and one tablet of protein cocktail (Roche, Basel, Switzerland)] described in Watanabe et al., (2013), and leaf protein solution was obtained by centrifugation (15,000 x g, 2 min, 4^oC).

PEPC activity was determined in a reaction mixture (1 ml) that contained 100 mM HEPES-NaOH buffer (pH 7.5), 10 mM $MgCl_2$, 1 mM $NaHCO_3$, 5 mM glucose-6-phosphate, 0.2 mM NADH and 12 units of malate dehydrogenase at 35^oC. The reaction was started by adding 400 mM phosphoenolpyruvate to 10 µl after pre-incubation for 2 min and absorbance at 340 nm was monitored (Fukayama et al., 2003).

Citrate synthase activity was determined in a reaction mixture (1 ml) that contained 82 mM Tris-HCl buffer (pH 7.9), 0.05 % Triton X-100, 2.8 mM malate, 20 mM 3-acethylpyridine adeninedinucleotide and 12 units of malate dehydrogenase at 30^oC. The reaction was started by adding 17 mM acetyl-CoA for 10 µl after pre-incubation for 2 min and absorbance at 365 nm was monitored (Jenner et al., 2001).

Aconitase activity was determined in a reaction mixture (1 ml) that contained 80 mM

HEPES-NaOH buffer (pH 7.5), 0.42 mM $MnCl_2$, 0.05 % Triton X-100, 0.5 mM $NADP^+$ and 1 unit NADP isocitrate dehydrogenase at 30°C. The reaction was started by adding 800 mM aconitate to 10 µl reaction mixture after pre-incubation for 2 min and absorbance at 340 nm was monitored (Jenner et al., 2001).

Pyruvate dehydrogenase activity was determined in a reaction mixture (1 ml) that contained 75 mM TES-NaOH buffer (pH 7.5), 0.5 mM $MgCl_2$, 2 mM NAD^+, 0.2 mM CoA, 0.2 mM thiamine diphosphate (TPP) and 2.5 mM cysteine-HCl at 25°C. The reaction was started by adding 100 mM pyruvate to 10 µl reaction mixture after pre-incubation for 2 min and absorbance at 340 nm was monitored (Millar et al.,1999).

Isolation of RNA, RT-PCR and real-time RT-PCR

Total RNA was isolated from plants using the RNeasy Plant Mini Kit (QIAGEN, Hilden, Germany). For detection of mRNAs, first-strand cDNA was synthesized from 1 µg of total RNA using a primer mix (Random primer and Oligo (dT) primer) and an enzyme mix (Rever Tra Ace and RNase inhibitor) (Toyobo, Osaka, Japan). PCR was performed in 50 µl reaction solution containing 1 µl cDNA mixture, 0.4 µM of each primer, and TaKaRa Ex Taq (Takara, Osaka, Japan). The PCR reaction cycles consisted of denaturation at 95℃ for 10 s, annealing at 55℃ for 30 s and extension at 72℃ for 15 s. Quantitative real-time PCR was performed with SYBR Premix Ex Taq (Takara, Osaka, Japan) using LightCycler 1.5 (Roche, Basel, Switzerland), and the comparative threshold cycle method was applied to determine the relative levels of mRNAs. Primers used in RT-PCR and real-time PCR are listed in Table VI-1.

Detection of H_2O_2 in leaves

H_2O_2 was visually detected in *Arabidopsis* leaves by using 3, 3-diaminobenzidine (DAB) (Ren et al., 2002). Leaves were infiltrated with 10 mM MES (pH 5.5) containing 0.1 % (w/v) DAB for 3 h. Then, leaves were transferred to dark or light conditions (150 µE m^{-2} s^{-1}, 23°C) and incubated for 3 h. After

Table VI-1

Genes and primers used for RT-PCR and real-time PCR.

Locus	Description	Forward primer	Reverse primer	Reference
FBA1 (At2g21330)	Fructose 1,6- bisphosphate aldolase 1	5'-CCGGAATCATGTTCTTGTCT-3	5'-GCTGAGCCAGCGAATTGGCT-3'	Watanabe et al., (2013)
PK (At2g36580)	Pyruvate kinase	5'-GGACTCTAGGTCCGAAATCT-3	5'-AACTTGCAACTCAGGTCCTA-3'	Watanabe et al., (2013)
PDH E1 alpha (At1g59900)	Pyruvate dehydrogenase E1 alpha subunit	5'-CATACAGGTACCACGGTCAC-3'	5'-GGCTCTGGCATTGGGCAATC-3'	Watanabe et al., (2013)
CSY4 (At2g44350)	mitochondrion targeted citrate synthase 4	5'-CGTGGCCAAATGTTGATGCT-3'	5'-CTTCAAGCCAGTCCATGGTA-3'	Watanabe et al., (2013)
ACO3 (At2g05710)	Aconitase 3	5'- GGCGTTGTTGGAAAGTTTGT-3'	5'- GCACCATACTCGGGAGACAT-3'	
PEPC1 (At1g53310)	Phosphoenolpyruvate carboxylase 1	5'-GAGTACTTCCGCCTCGCTAC-3'	5'-TGCTGATCCGAATCCAAGCC-3'	
CI76 (At5g37510)	Complex I76 kDa subunit	5'-ACAAGGTGTGTACGATTTGC-3	5'-TTTGAGGTCAAGGCTCCAAC-3'	Michalecka et al., (2003)
COX6a (At4g37830)	Cytochrome c oxidase subunit 6A	5'-TCTTTCCCGAGCAGTGAC-3'	5'-GATAGGCAGGAGGGTCTTCG-3'	Watanabe et al., (2013)
AOX1a (At3g22370)	Alternative oxidase 1a	5'-AAGGCGGCGAAATCGCTGTT-3'	5'-TCCTCCTTCATCGGAGTTTTCTC-3'	Watanabe et al., (2013)
Rps15aA (At1g07770)	40S ribosomal protein subunit S15A	5'- GGTGTTATCAGCCCACGTTT -3'	5'- GGTCCATAATGCCAGCAGAT-3'	
ACT2 (At3g18780)	Actin 2	5'- CCGTACAGATCCTTCCTGATATCC -3	5'- CCGTACAGATCCTTCCTGATATCC -3	
AtAOR (At1g23740)	Alkenal/one oxidoreductase	5'- GACTACGGCGGAGTTGATGT -3'	5'- CCTTGCCGTCTCTTAGCATC -3'	

the incubation, leaves were boiled in 96 % ethanol until brown color was visible.

Transmission Electron Microscopy

Rosette leaves harvested at the end of day and the end of night were trimmed into small pieces (2 × 3 mm^2) with a razor blade; these pieces were pre-fixed with 2.5 % glutaraldehyde (Nisshin EM, Tokyo, Japan) in 0.1 M phosphate-buffered saline (PBS, pH 7.4) at 4°C overnight. Leaf pieces were then rinsed with PBS three times at intervals of 10 min and post-fixed with 1 % PBS-buffered osmium tetroxide (Nisshin EM, Tokyo, Japan) at room temperature for 1 h. After the samples had been rinsed briefly with distilled water, they were immediately dehydrated in ethanol series (50 %, 70 %, 90 %, and 100 %). They were then immersed in an intermediate solvent (propylene oxide; Nisshin EM, Tokyo, Japan) for 10 min and in a mixture (1:1, v/v) of propylene oxide and Spurr's resin (Spurr, 1969) (Polysciences, Warrington, PA, USA) for 6 h at room temperature (25 ^{o}C). Following this they were placed in pure Spurr's resin at 4°C for 3 days, and then embedded in plain embedding plates and polymerized at 70°C for 24 h. Blocks of leaves were cut with a Porter-Blum MT-1 ultramicrotome (Ivan Sorvall, Norwalk, CT, USA) and a diamond knife (Diatome, Bienne, Switzerland). Ultrathin sections about 80 nm were prepared; these were stained with 4 % aqueous uranyl acetate for 10 min and Sato's lead for 10 min (Sato, 1968) at room temperature (25 ^{o}C). Every staining step was succeeded by a step of washing with water three times for 3 min. The stained sections were observed under a JEM-1400 electron microscope (JEOL, Akishima, Japan) at an accelerating voltage of 75 kV.

Point counting method

Chloroplasts in leaves were photographed at random at the magnification of 4000 X using a CCD camera. The photographs were printed with a printer using images of chloroplasts. The photographs were examined by using point lattice counting methods (Weibel, 1979; Ylä-Anttila et al., 2009). A square lattice was placed on the photographs, and the lattice line intersections that were placed on

the chloroplasts and starch granules, were counted.

Statistical analysis

All measurement data were expressed as mean values ± SEM of at least three independent analyses. We used Student's t-test, and the Tukey-Kramer HSD test to detect differences between WT and *aor* mutants. All statistical analyses were performed using Microsoft Excel 2010 (Microsoft, Washington, USA) and JMP8 (SAS Institute Inc., Tokyo, Japan).

RESULTS

aor-mutants show growth retardation compared to WT under day/night cycle conditions

To study the importance of the detoxification of lipid-derived RCS in higher plants, I grew the T-DNA tagged knock-out mutant of *AtAOR* [*aor* (T-DNA)] (Yamauchi et al., 2012) under day/night conditions (16 h light and 8 h dark), and analyzed the phenotype. First, I checked the mRNA expression of AtAOR in *aor* (T-DNA) by RT-PCR. The expression of AtAOR was successfully inhibited in *aor* (T-DNA) (Fig. VI-1a). Under day/night cycle conditions, *aor* (T-DNA) showed smaller growth, compared to WT (Fig. VI-1b). Growth rate, as evaluated by maximum rosette diameter was slower in *aor* (T-DNA) than in WT (Fig. VI-1c). Furthermore, dry weight of *aor* (T-DNA) 3 weeks after germination was significantly lower than WT (Fig. VI-1d). These results conflicted with the previous report that the growth of *aor* (T-DNA) was the same as that of WT (Yamauchi et al., 2012).

To confirm whether the growth retardation in *aor* (T-DNA) observed in our analysis depends on the malfunction of AtAOR, I generated RNAi mutants in Arabidopsis, which specifically suppressed the mRNA expression of AtAOR. I isolated two RNAi lines [*aor* (RNAi)s], *aor-1* and *aor-4*. The mRNA expression levels of AtAOR decreased to approximately 2% and 50% in *aor-1* and *aor-4* respectively, as compared to WT (Fig. VI-2a). Subsequently, the accumulation of AtAOR proteins in *aor-1* and *aor-4* leaves was compared with those of WT by western blot analysis. AtAOR protein in WT leaves was detected at a molecular weight of approximately 38 kDa (Fig. VI-2b). According to ExPASy (http://www.expasy.org/), the molecular weight of full length AtAOR protein was estimated as 41 kDa. However, AtAOR protein was reported to possess a transit peptide sequence to chloroplasts (Yamauchi et al., 2011). Thus, it was speculated that the true molecular weight of AtAOR protein is smaller than its full length protein. To clarify whether AtAOR protein is localized in the chloroplasts of *Arabidopsis* cells, I expressed a translational fusion protein between AtAOR protein and green fluorescence protein (GFP) in protoplasts isolated from *Arabidopsis*. Green fluorescence from GFP was observed in protoplasts and the location emitting

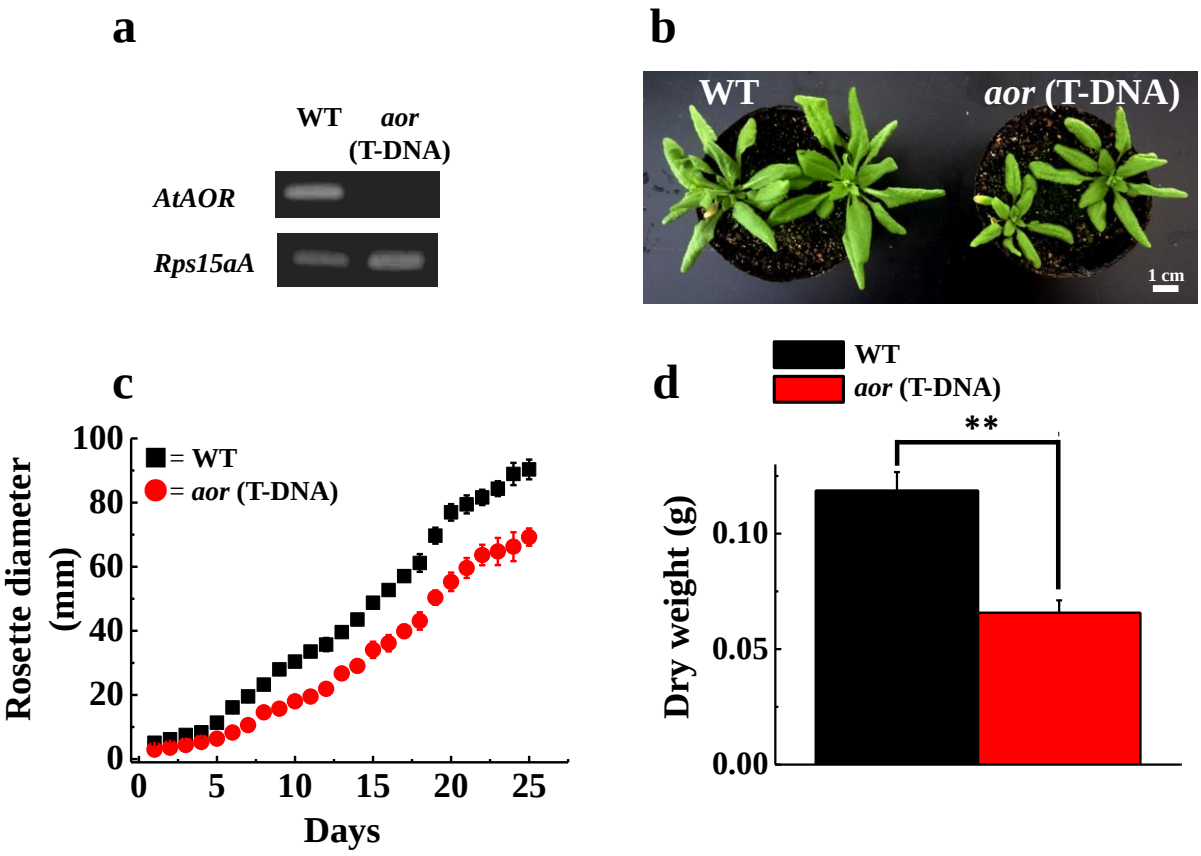

Figure VI-1

Phenotype analysis of *aor* (T-DNA) grown under day/night cycle growth conditions. (a) The confirmation of mRNA expression of *AtAOR* in WT and *aor* (T-DNA) leaves by RT-PCR. As a positive control, mRNA expression of *Rps15aA* (40 S ribosomal protein S15A) was shown. (b) The plant phenotype of WT and *aor* (T-DNA). These plants are 3-weeks old after germination. Representable plants were shown. White bar shows the length, 1cm. (c) The plant growth evaluated as an increase in maximum rosette diameter was shown. Data are expressed as means ± SEM of four independent plants. Black square indicates WT, and red circle indicates *aor* (T-DNA). (d) Dry weight of plants was compared between WT and *aor* (T-DNA). Black bar indicates WT, and red bar indicates *aor* (T-DNA). Data are expressed as mean ± SEM of four independent experiments. Asterisks indicate a significant difference between WT and *aor* (T-DNA) (Student's t-test, $p < 0.01$).

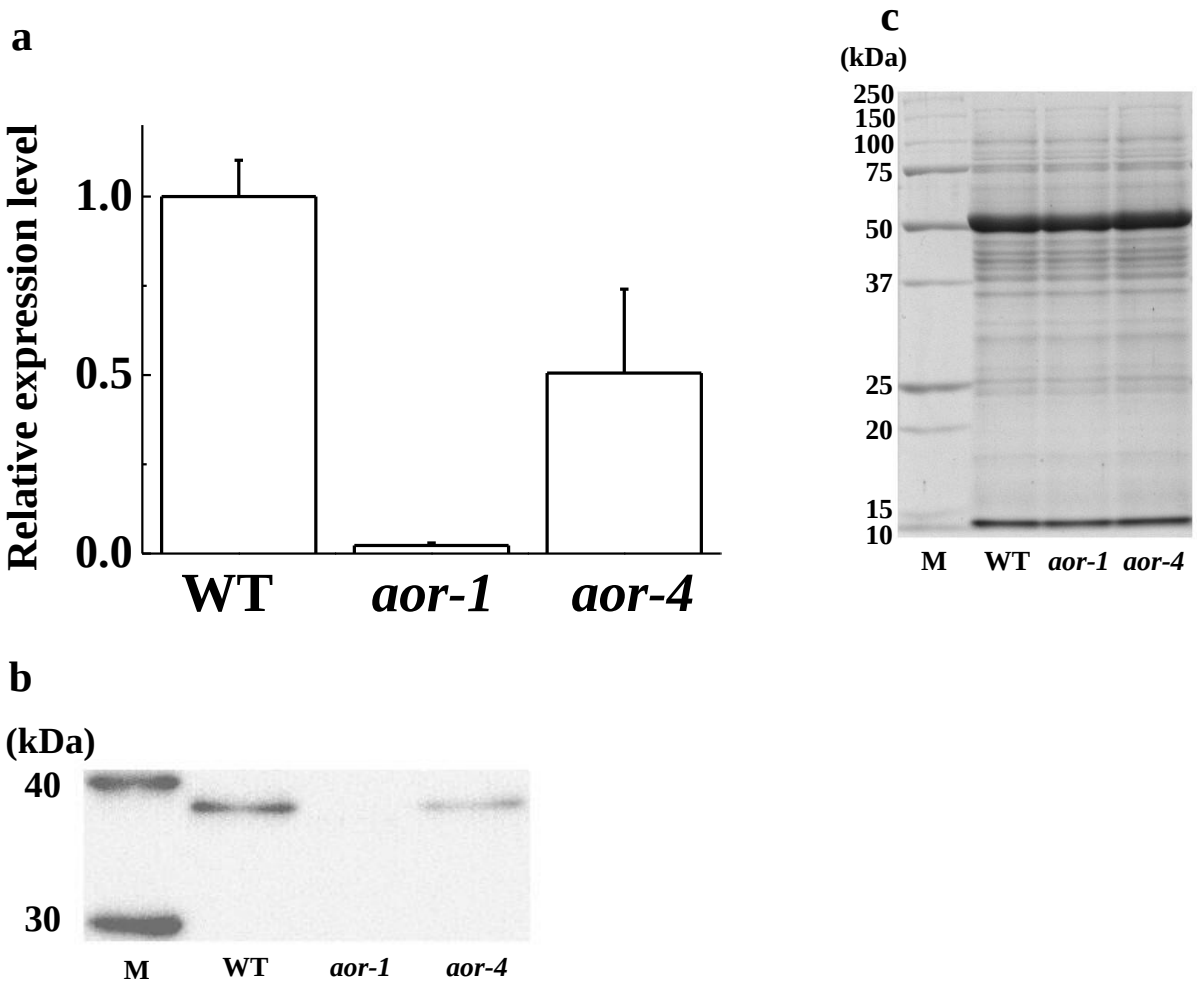

Figure VI-2

mRNA expression analysis of *AtAOR* and the detection of AtAOR protein in WT and *aor* (RNAi) mutant leaves. (a) Relative expression levels of *AtAOR* mRNA in WT and *aor* (RNAi) mutant leaves were shown. Expression level was quantified by real-time PCR. Data are expressed as mean ± SEM of three independent experiments. (b) AtAOR protein extracted from WT and *aor* (RNAi) mutants leaves were detected by western-blot analysis. The protein corresponding to 5 μg was loaded in each lane. (c) The separation of proteins extracted from WT and *aor* (RNAi) mutant leaves by SDS-PAGE were shown, as a loading control. 5 μg proteins were loaded in each lane.

green fluorescence overlapped with red fluorescence emitted from chloroplasts (Fig. VI-3). These results indicated that AtAOR protein was localized in chloroplasts. From these results, I concluded that AtAOR protein exists in the chloroplast as the 38 kDa protein. In *aor-1*, no AtAOR protein was detected, whereas a small amount of AtAOR protein was detected in *aor-4* (Fig.VI-2b). Fig. VI-2c showed the protein profile on SDS-PAGE that correlates with the western blot analysis shown in Fig. VI-2b.

Next, I evaluated the acrolein-reducing activity in crude leaf extracts of *aor* (RNAi) mutants. The activity decreased to about 60 % and 75 % in *aor-1* and *aor-4* respectively, compared to WT (Table VI-2). Because higher plants have a cytosolic acrolein detoxification enzyme, *aor-1* would show residual activity regardless of the undetectable AtAOR protein, as mentioned in previous reports (Mano et al., 2005; Papdi et al., 2008; Yamauchi et al., 2012).

I evaluated the growth rates in *aor-1* and *aor-4* under day/night cycle conditions. As well as the *aor* (T-DNA), *aor-1* and *aor-4* showed growth retardation, and dry weights of *aor-1* and *aor-4* at 3 weeks after their germination decreased to about 49 % and 54 % respectively, compared to WT (Fig. VI-4a, b). From these facts, I concluded that AtAOR protein function is required for plant growth.

Suppression of AtAOR decreases dark respiration rate, but not the photosynthesis rate under day/night cycle conditions

To elucidate the cause of growth retardation in *aor* mutants, I analyzed the activities of photosynthesis and dark respiration rate in *aor-1* and *aor-4* under their growth conditions. First, I quantified the nitrogen and chlorophyll contents in *aor-1* and *aor-4*. Compared to WT, chlorophyll content in *aor-1* and *aor-4* mutants decreased by about 14 % and 20 % respectively, and nitrogen content also decreased by about 18 % in both *aor* mutants (Table VI-3). These decreases in chlorophyll and nitrogen contents were also observed in the *aor* (T-DNA) (Table VI-4). Next, I evaluated the photosynthetic activity and dark respiration rate in WT and *aor* (RNAi) mutants. CO_2

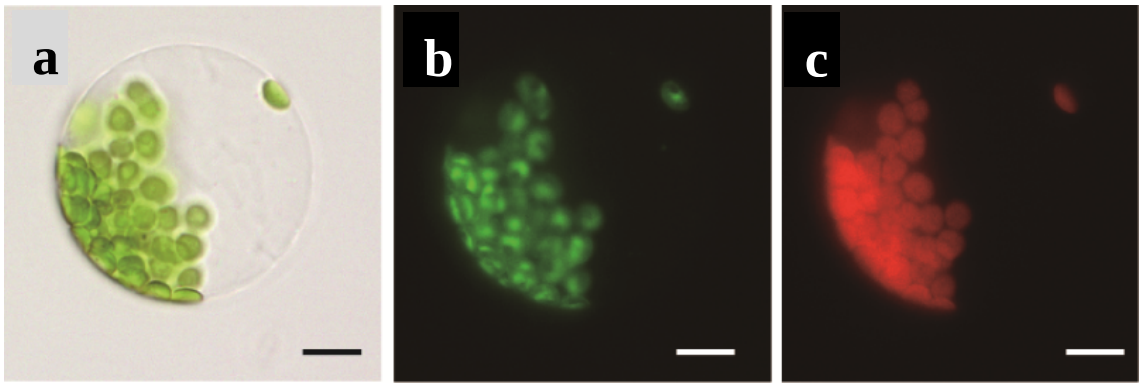

Figure VI-3

Subcellular localization of AtAOR in plant cell. (a) shows a picture of protoplast isolated from *Arabidopsis* leaves. (b) shows the localization of AtAOR fused GFP by green fluorescence. (c) shows chlorophyll autofluorescence in red. Black and white bars in this picture indicate the length, 10 μm.

Table VI-2 The reduction activity of acrolein in crude leaf extract

Line	Activity (μmol mg protein^{-1} h^{-1})	
WT	**4.5 ± 0.6**	**(100)**
aor-1	**2.7 ± 0.1**	**(60)**
aor-4	**3.0 ± 0.3**	**(75)**

The acrolein reduction activities in the crude protein extraction of leaves in WT and *aor* (RNAi) mutants were determined. In this experiment, 3- to 4- weeks old plants were used. Data are expressed as mean ± SEM of three independent experiments. The values in parenthesis indicate the relative activity for WT.

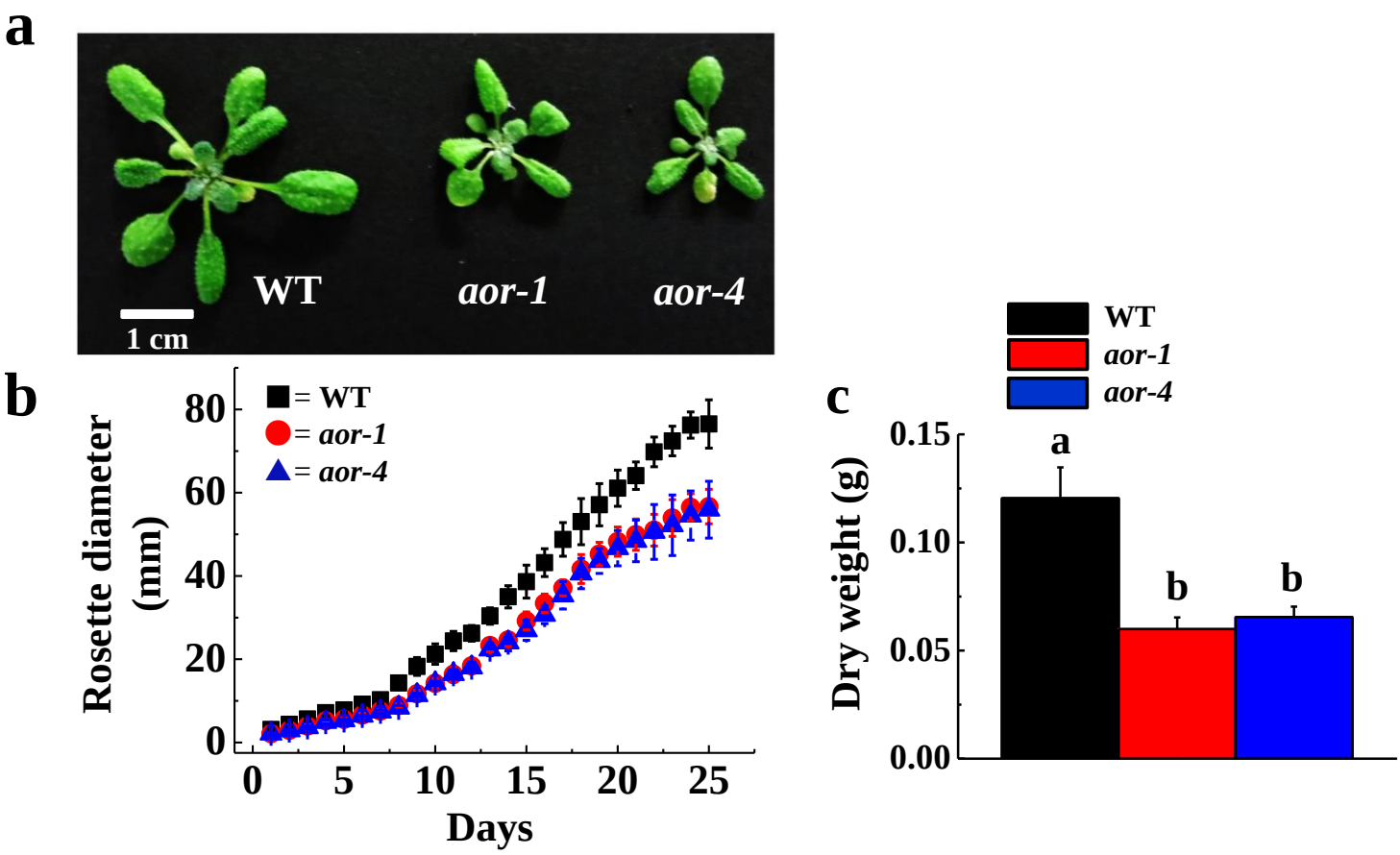

Figure V-4

Characterization of *aor* (RNAi) mutants grown under day/night cycle conditions. (a) The plant phenotype of WT, *aor-1* and *aor-4*. These plants were 2-weeks old after germination. Representable plants were shown. White bar shows the length, 1cm. (b) The plant growth evaluated as an increase in maximum rosette diameter was shown. Data are expressed as mean ± SEM of six independent plants. Black square indicates WT, red circle indicates *aor-1*, and blue triangle indicates *aor-4*. (c) Dry weight of plants was compared between WT and *aor* mutants. Black bar indicates WT, red bar indicates *aor-1*, and blue bar indicates *aor-4*. Data are expressed as mean ± SEM of sixteen independent experiments. Different alphabets indicate a significant difference between WT and *aor* (RNAi) mutants (Tukey-Kramer HSD test, $p < 0.05$).

Table VI-3

Chlorophyll and nitrogen content in WT and *aor* (RNAi) mutants grown under day/night cycle growth conditions

Line	Chl (µmol m^{-2})	N (mmol m^{-2})
WT	**219.0 ± 7.4**	**75.6 ± 3.0**
aor-1	**189.9 ± 6.4 ****	**63.0 ±4.1 ***
aor-4	**177.3 ± 6.6 ****	**62.4 ± 4.2 ***

Chlorophyll and nitrogen content in WT and *aor* (RNAi) mutant leaves. WT and *aor* (RNAi) mutants were grown under day/night cycle growth conditions. Chlorophyll and nitrogen contents were determined on leaves in 3- to 4-weeks old plants. Data are expressed as mean ± SEM of six independent experiments. Asterisks indicate a significant difference between WT and *aor* (RNAi) mutants (Student's t-test: *, $p < 0.05$; **, $p < 0.01$).

Table VI-3
Chlorophyll and nitrogen content in WT and *aor* (T-DNA) grown under day/night condition

Line	Chl (mg m^{-2})	N (mmol m^{-2})
WT	**253.7 ± 6.2**	**61.0 ± 4.3**
***aor* (T-DNA)**	**221.8 ± 6.5 ***	**47.8 ± 1.7***

Chlorophyll and nitrogen content in WT and *aor* (T-DNA) mutant leaves. WT and *aor* (T-DNA) were grown under day/night cycle conditions. Chlorophyll and nitrogen contents were determined on leaves in 3- to 4-weeks old plants. Data are expressed as mean ± SEM of three independent experiments. Asterisks indicate a significant difference between WT and *aor* (T-DNA) (Student's t-test: *, $p < 0.05$).

assimilation rates in *aor-1* and *aor-4* showed similar values to WT under atmospheric conditions, where actinic light (AL) intensity was the same as growth-light intensity (150 μE m^{-2} s^{-1}) (Table VI-4). Furthermore, internal partial pressure of CO_2 (Ci) and stomatal conductance (g_s) were also similar amongst WT, *aor-1*, and *aor-4* (Table VI-4). Simultaneously, I evaluated the maximum quantum yield of PSII (Fv/Fm) and the incident quantum yield of PSII [Y(II)] under growth light conditions. The values of Fv/Fm and Y(II) were similar amongst WT, *aor-1*, and *aor-4* (Table VI-4). These results indicated that *aor-1* and *aor-4* have similar photosynthetic activities, compared to WT.

In contrast to the photosynthetic activity, the dark respiration rates evaluated from CO_2 - gas exchange analysis decreased in *aor-1* and *aor-4*, compared to WT (Table VI-4). I also evaluated the dark respiration rate by using an O_2-electrode; *aor-1* and *aor-4* also showed lower respiration rates, compared to WT (Fig. VI-5). Furthermore, I also evaluated the photosynthetic activities and the dark respiration rate in the *aor* (T-DNA) grown under day/night conditions. Both Y(II) and g_s tended to be lower than WT, however CO_2 assimilation rate and Ci were the same between WT and *aor* (T-DNA) (Table VI-5). In contrast, the dark respiration rate in *aor* (T-DNA) was lower compared to WT, but similar to both *aor-1* and *aor-4* (Table VI-5). These results suggested that the growth retardations in *aor* mutants were caused by a decrease in the dark respiration rate.

mRNA expression analysis of respiration related gene by real-time PCR

In the previous chapter, I observed that *aor* mutants showed lower respiration rates in the dark, but not CO_2 assimilation rates in the light. These observations indicated that the utilization efficiency of carbon acquired during photosynthesis decreased in *aor* mutants during the night. Thus, mRNA expression of genes related to respiratory metabolism enzymes, such as those involved in starch degradation, glycolysis, tricarboxylic acid (TCA)-cycle, and respiratory electron transport reactions, was analyzed. In the following experiments, I used *aor-1* as the *aor* mutant. For this analysis, mRNA was extracted from leaves in WT and *aor-1* at three different times [at the end of the day (1 h before night period started), at midnight (4 h after night period started), and the end of the night (7 h

Table VI-4
Dark respiration rate and photosynthetic parameters in WT and *aor* (RNAi) grown under day/night cycle

	Fv/Fm	Respiration ($\mu mol\ CO_2\ m^{-2}\ s^{-1}$)	CO_2 assimilation ($\mu mol\ CO_2\ m^{-2}\ s^{-1}$)	Y(II)	g_s ($\mu mol\ CO_2\ m^{-2}\ s^{-1}$)	Ci ($\mu mol\ mol^{-1}$)
WT	**0.827±0.002**	**1.41±0.34**	**4.72±0.20**	**0.631±0.004**	**0.076±0.008**	**386.1±12.4**
aor-1	**0.821±0.003**	**0.54±0.14 †**	**4.87±0.22**	**0.625±0.016**	**0.070±0.014**	**374.1±9.3**
aor-4	**0.817 ± 0.003**	**0.51±0.15†**	**4.49 ± 0.10**	**0.627±0.025**	**0.086±0.003**	**384.9±4.4**

Photosynthesis activity was determined under growth light conditions (light intensity = 150 µE m^{-2} s^{-1}), and respiration was determined in the dark. Data are expressed as mean ± SEM of three independent experiments. Dagger indicates a significant difference between WT and *aor* (RNAi) mutants (Student's t-test: †, $p < 0.1$).

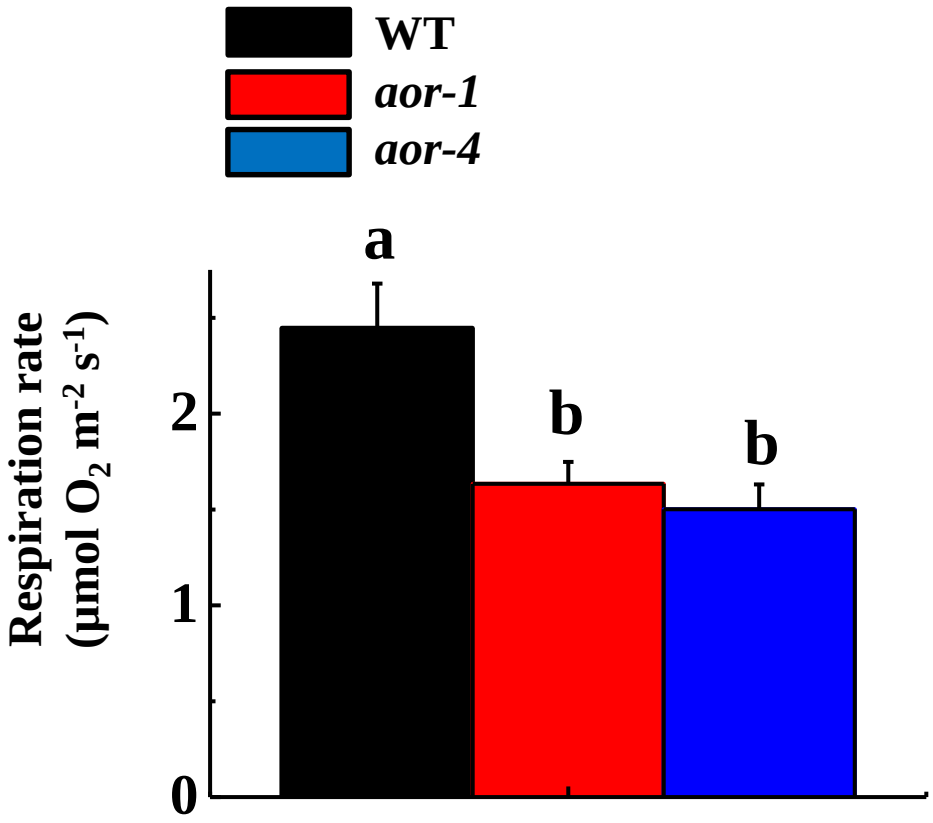

Figure VI-5

The comparison of respiration rate in WT and *aor* (RNAi) mutants evaluated by O_2 electrode. In this experiment, WT and *aor* (RNAi) mutants grown under day/night cycle were used. Black bar indicates WT, red bar indicates *aor-1*, and blue bar indicates *aor-4*. Data are expressed as mean ± SEM of four to nine independent experiments. Different alphabets indicate a significant difference between WT and *aor* (RNAi) mutants (Tukey-Kramer HSD test, $p < 0.05$).

Table VI-5
Dark respiration rate and photosynthetic parameters in WT and *aor* (T-DNA) grown under day/night cycle conditions

	Fv/Fm	Respiration ($\mu mol\ CO_2\ m^{-2}\ s^{-1}$)	CO_2 assimilation ($\mu mol\ CO_2\ m^{-2}\ s^{-1}$)	Y(II)	g_s ($\mu mol\ CO_2\ m^{-2}\ s^{-1}$)	Ci ($\mu mol\ mol^{-1}$)
WT	**0.809±0.003**	**1.51±0.18**	**4.76±0.09**	**0.701±0.004**	**0.147±0.007**	**389.5±6.7**
***aor* (T-DNA)**	**0.812±0.001**	**0.75±0.06 ****	**4.52±0.39**	**0.680±0.007†**	**0.112±0.015†**	**382.3±10.6**

Photosynthesis activity was determined under growth light conditions (light intensity = 150 µE m^{-2} s^{-1}), and respiration was determined in the dark. Data are expressed as mean ± SEM of three independent experiments. Dagger indicates a significant difference between WT and *aor* (T-DNA) (Student's t-test: † $p < 0.1$; * $p < 0.05$).

after night period started)]. As an internal standard, I used *Rps15aA* (encoding 40S ribosomal protein S15A; Watanabe et al., 2013), and the mRNA expression level in WT at the end of the day was set to 1 (Fig. VI-6). First, I analyzed the expression level of mRNAs relating to glycolysis. The mRNA expression level of *FBA1* (encoding fructose 1,6-bisphosphate aldolase 1) decreased from the end of the day to midnight, and subsequently increased until the end of the night in both WT and *aor-1* (Fig. VI-6a). For the mRNA expression level of *PK* (encoding pyruvate kinase), a significant difference between WT and *aor-1* was not observed; however the behavior of change in the amount of mRNA was different, that is, the mRNA expression level tended to decrease in *aor-1* at midnight, compared to WT (Fig. VI-6b). The change in mRNA expression level of *PDH* (encoding pyruvate dehydrogenase E1 alpha subunit) increased at midnight and subsequently decreased at the end of the night in WT (Fig. VI-6c). In contrast, the mRNA expression level of *PDH* did not increase at midnight in *aor-1* (Fig. VI-6c). The mRNA expression level of *PEPC1* (encoding phosphoenolpyruvate carboxylase 1) also increased from the end of the day to midnight, and subsequently decreased to the end of the night in WT (Fig. VI-6d). However, the mRNA expression level of *PEPC1* in *aor-1* decreased linearly from the end of the day to the end of the night (Fig. VI-6d).

Next, I analyzed the mRNA expression level of TCA-cycle enzymes and respiratory electron transport chain components. The mRNA expression level of *ACO3* (encoding aconitase 3) and *CSY4* (encoding mitochondrion targeted citrate synthase 4) showed similar changes to that of *PEPC1* from the end of the day to the end of the night, and the mRNA expression level of *ACO3* was significantly lower in *aor-1* at midnight, as compared to WT (Fig. VI-6e, f). In contrast, the mRNA expression levels of *CI76* (encoding complex I 76 kDa subunit), *COX6a* (encoding cytochrome *c* oxidase subunit 6A) and *AOX1a* (Alternative oxidase 1a) showed similar changes in WT and *aor-1* (Fig. VI-6g, h and i).

In addition, I analyzed mRNA expression levels of enzymes involved in starch degradation, *GWD1* (encoding glucan water dikinase 1), *SEX4* (encoding phosphoglucan phosphatase), *BAM1*

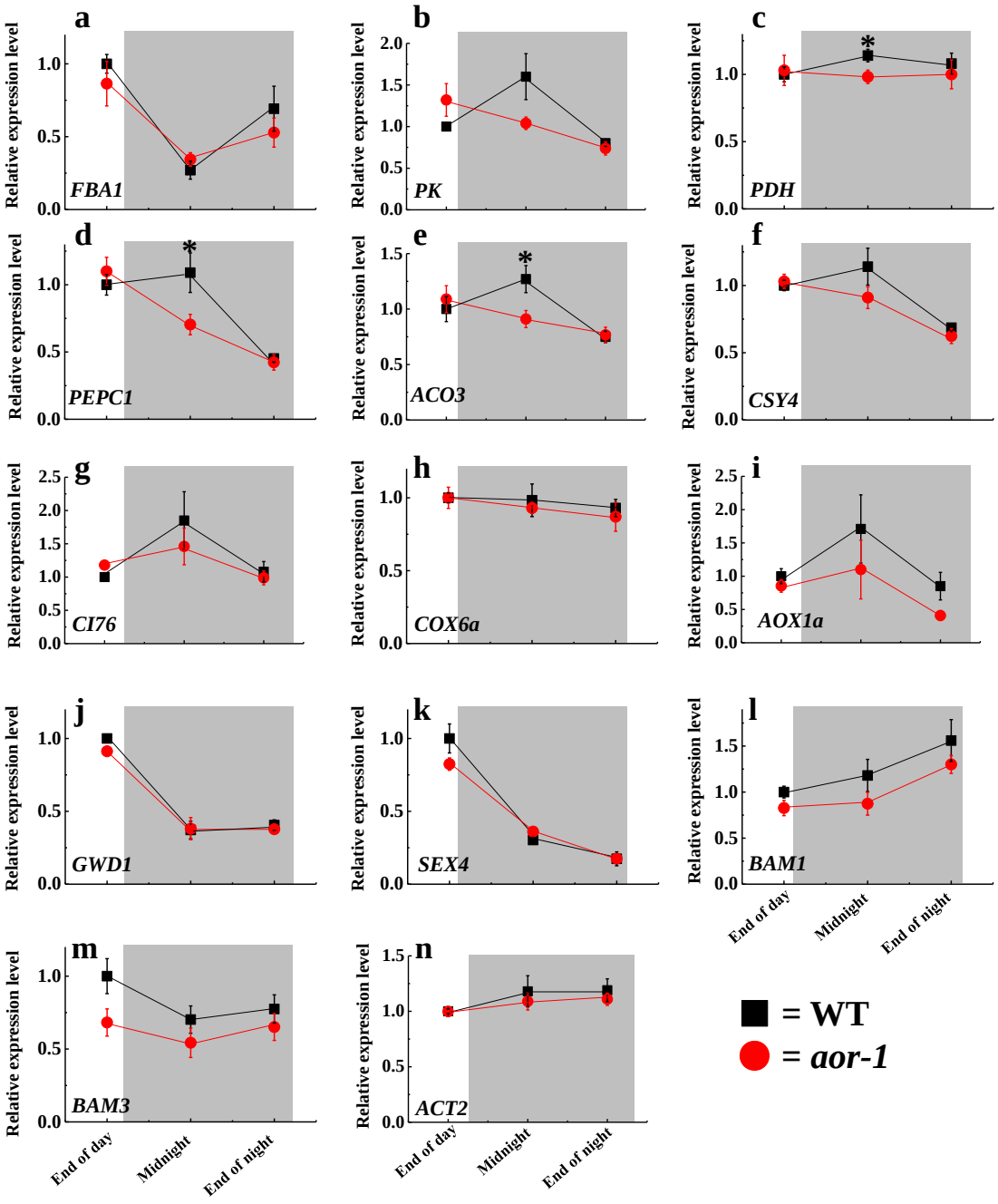

Figure VI-6

mRNA expression analysis related to respiration and starch degradation in leaves. mRNA was extracted from WT and *aor-1* mutant leaves at end of day (1 h before night period started), midnight (4 h before night period started), and end of night (7 h before night period started). In each gene, mRNA expression levels in WT at the end of the day was set to 1, and relative expression change was shown. Black square indicates WT, and red circle indicate *aor-1*. Data are expressed as mean ± SEM of three to six independent experiments. Asterisks indicate a significant difference between WT and *aor-1* mutant (Student's t-test: *, $p < 0.05$).

(encoding β-amylase 1), and *BAM3* (encoding β-amylase 3). In these starch degradation-related genes, no differences in mRNA expression levels were observed between WT and *aor-1* (Fig. VI-6j, k, l, m). The expression patterns of these genes during the night period were consistent with previous reports (Smith et al., 2004; Santelia et al., 2011). To confirm that the mRNA expression level of each gene was independent from the expression levels of an internal standard, I also analyzed *ACT2* (encoding actin 2) expression each time. Both in WT and *aor-1*, *ACT2* hardly showed any change in mRNA expression level during the night and no difference was observed in *ACT2* expression between WT and *aor-1* (Fig. VI-6n). Therefore, these results indicated that the mRNA expression of each gene normalized by *Rps15Aa* showed unique changes during the night. Based on these observations, it was indicated that the functions of glycolysis and TCA-cycle during the night period were modified in *aor-1*.

Enzyme activities of pyruvate dehydrogenase, phosphoenolpyruvate carboxylase, aconitase and citrate synthase in WT and *aor-1* leaves

Based on the mRNA expression analysis, I evaluated the enzyme activities of pyruvate dehydrogenase (PDH), phosphoenolpyruvare carboxylase (PEPC), aconitase, and citrate synthase in WT and *aor-1* leaves, which were sampled at the night period. PDH activities in WT and *aor-1* were similar (Fig. VI-7a). In contrast, PEPC activity in *aor-1* significantly decreased to about 75 %, as compared to WT (Fig. VI-7b). The activities of aconitase and citrate synthase were similar between WT and *aor-1* (Fig. VI-7c, d).

Starch degradation in WT and *aor-1* leaves during the night-period

During the night period, plants degrade starch through respiratory metabolism (Zeeman et al., 2010). I quantified the amount of starch in chloroplasts in WT and *aor-1*. For this measurement, leaves in WT and *aor-1* were harvested at the end of day and night. The starch in chloroplasts was observed by transmission electron microscopy, and the amount of starch in chloroplasts was quantified by the

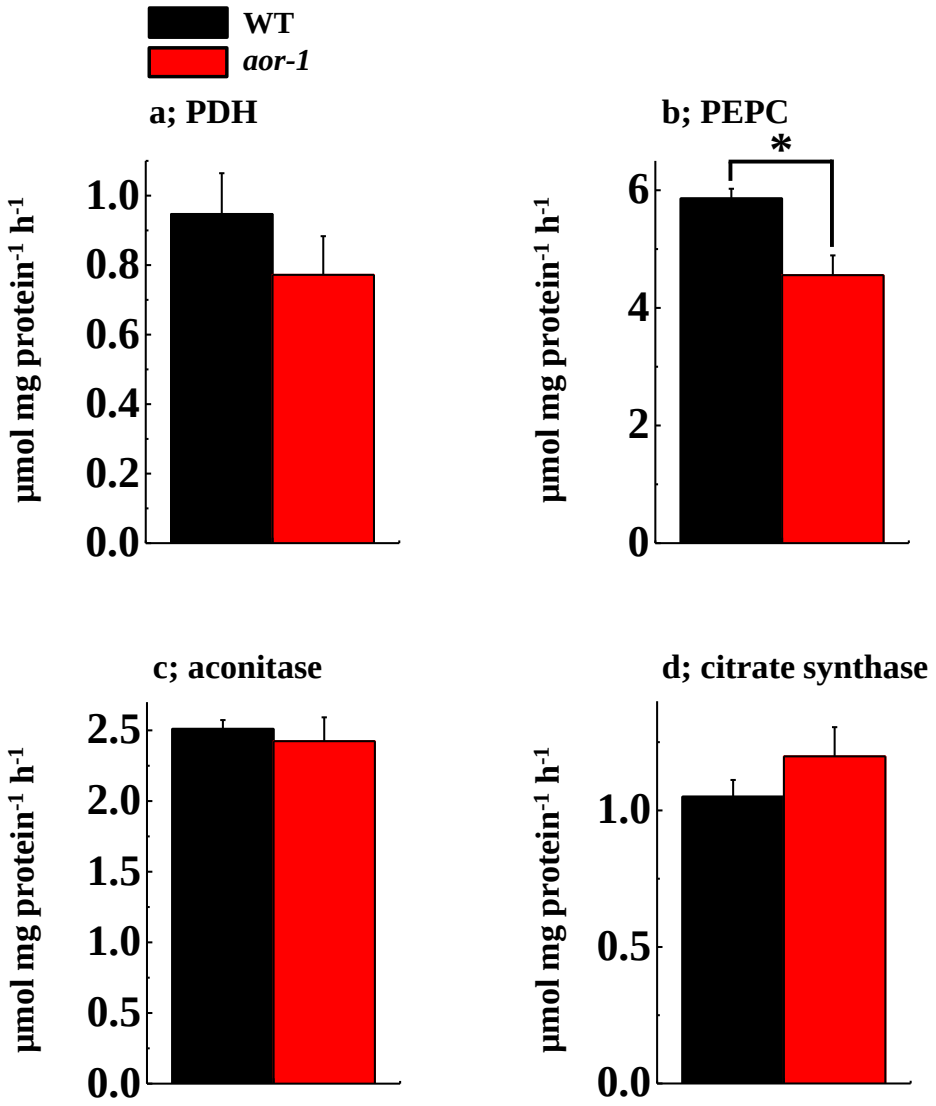

Figure VI-7

Evaluation of enzyme activity of pyruvate dehydrogenase (a), phosphoenolpyruvate carboxylase (b), aconitase (c), and citrate synthase (d) in WT and *aor-1* leaves. Leaves were harvested from WT and *aor-1* grown under day/night cycle growth conditions, and these enzyme activities were evaluated in leaves harvested during the night period. Black bar indicates WT, and red bar indicates *aor-1*. Data are expressed as mean ± SEM of four independent experiments. Asterisks indicate a significant difference between WT and *aor-1* (Student's t-test: *, $p < 0.05$).

point counting method (Weibel, 1979). In WT leaves, starch accumulated in chloroplasts at the end of the day was hardly detected at the end of the night (Fig. VI-8a). This result showed that about 98 % of the starch accumulated during the day was consumed during the night in chloroplasts of WT (Fig. VI-8b). In contrast, starch remained in chloroplasts of *aor-1* at the end of the night, although the starch content significantly decreased at the end of the night, compared to the end of the day (Fig. VI-8). This result showed that about 62 % of the starch accumulated in the day was consumed in *aor-1* chloroplasts during the night-period. Compared to WT, starch content in *aor-1* was significantly higher at the end of both day and night (Fig. VI-8b). These results indicated that starch degradation was suppressed in *aor-1* during the night, resulting in the accumulation of starch in chloroplasts.

Growth of WT and *aor-1* under constant light conditions

I grew WT and *aor-1* under constant light conditions and analyzed their growth. I found that WT and *aor-1* grew similarly (Fig. VI-9a). Dry weight at 3 weeks after germination was also similar between WT and *aor-1* under continuous light conditions (Fig. VI-9b). Furthermore, nitrogen and chlorophyll contents were also at similar values for WT and *aor-1* mutant (Table VI-6). These results indicate that constant light conditions rescued the growth in *aor-1*.

Next, I analyzed the photosynthetic activities in WT and *aor-1* grown under constant light growth conditions. CO_2 assimilation rate and Y (II) were not different between WT and *aor-1* (Table VI-7). The values of Fv/Fm, Ci, and g_s were also not different between WT and *aor-1* (Table VI-7). These results showed that WT and *aor-1* have similar photosynthetic activities, similar to the day/night cycle growth conditions. In contrast, the dark respiration rate in *aor-1* was lower, compared to WT (Table VI-7). I also checked the phenotype of *aor* (T-DNA) grown under continuous light condition. As well as *aor-1*, *aor* (T-DNA) grew similar to WT (Fig. VI-10). Chlorophyll and nitrogen contents were similar between WT and *aor* (T-DNA), furthermore, photosynthetic activities estimated by CO_2 assimilation rate and Y(II) were not different between

WT and *aor* (T-DNA) (Tables VI-8, VI-9). However, the dark respiration rate was lower in *aor* (T-DNA) than in WT, as well as *aor-1* (Table VI-9).

Next, I analyzed mRNA expressions of *PDH*, *PEPC1*, *ACO3*, and *CSY4* in both WT and *aor-1* grown under constant light growth conditions. The mRNA expression levels of these genes were not different between WT and *aor-1* (Fig. VI-11).

I also evaluated the enzyme activities of PDH, PEPC, aconitase, and citrate synthase in both WT and *aor-1* grown under constant light conditions. PEPC activity in *aor-1* decreased, compared to WT (Fig. VI-12b). In contrast, PDH, aconitase, and citrate synthase activities were similar between WT and *aor-1* (Fig. VI-12a, c, d). These results indicated that PEPC activity decreased in *aor-1*, although the growth in *aor-1* was similar to WT.

a

WT end of day

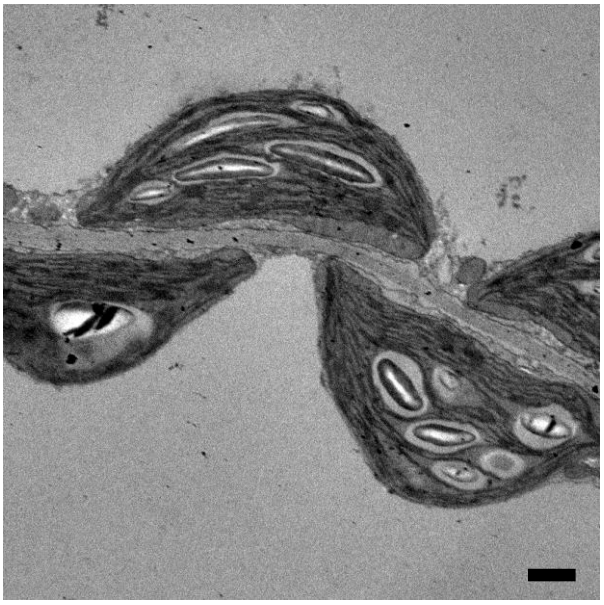

WT end of night

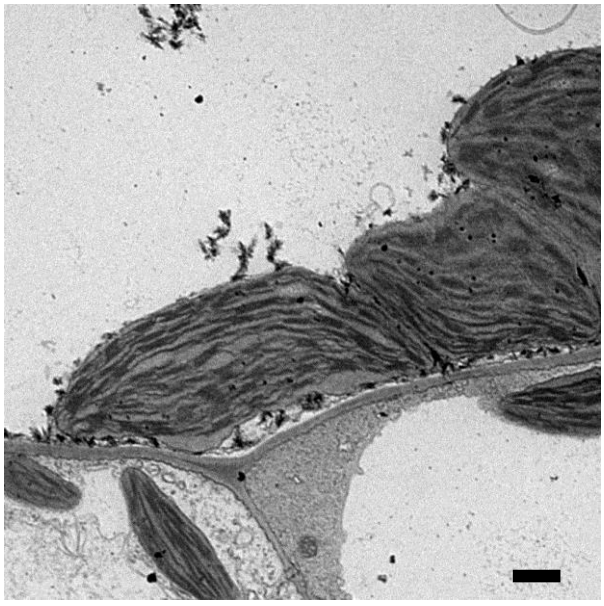

***aor-1* end of day**

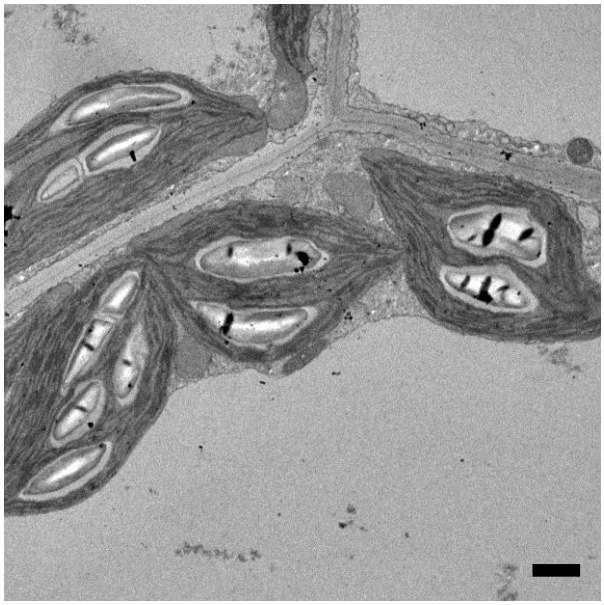

***aor-1* end of night**

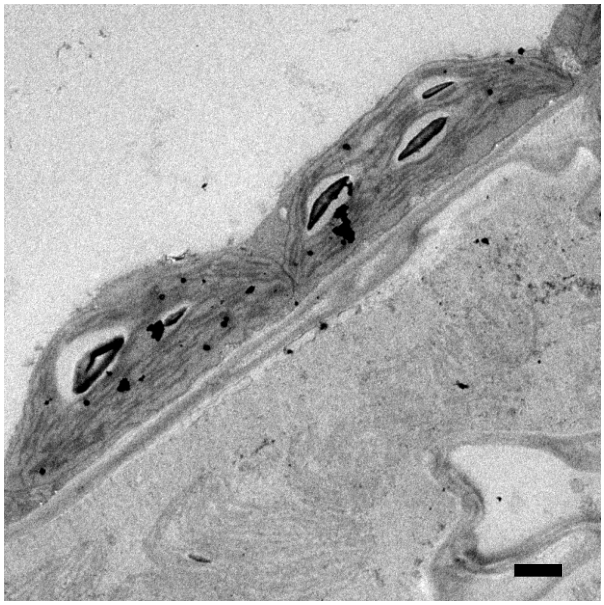

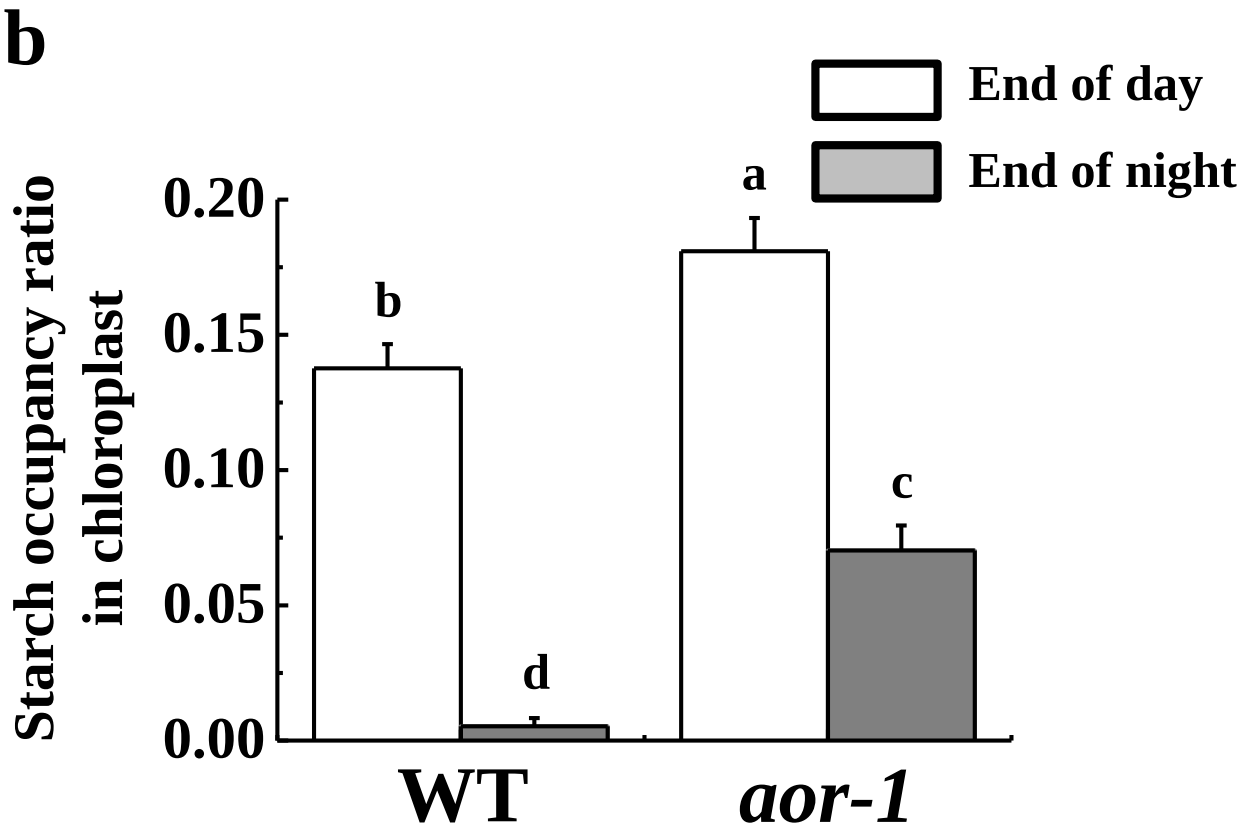

Figure VI-8

The evaluation of starch metabolism in WT and *aor-1* leaves during night. (a) Ultrastructural observation of chloroplasts in WT and *aor-1* leaves. Leaves were harvested at end of the day (start night period before 1 h), and end of the night (start night period after 7 h) for this analysis. Representative pictures are shown. Black bar shown in pictures indicates the length, 2 μm. (b) Starch occupancy in chloroplasts in WT and *aor-1* evaluated by point counting method (see Materials and Methods). Data are expressed as mean ± SEM. More than sixteen chloroplasts were observed in each treatment. Different alphabets indicate a significant difference between WT and *aor-1* (Tukey-Kramer HSD test, $p < 0.05$).

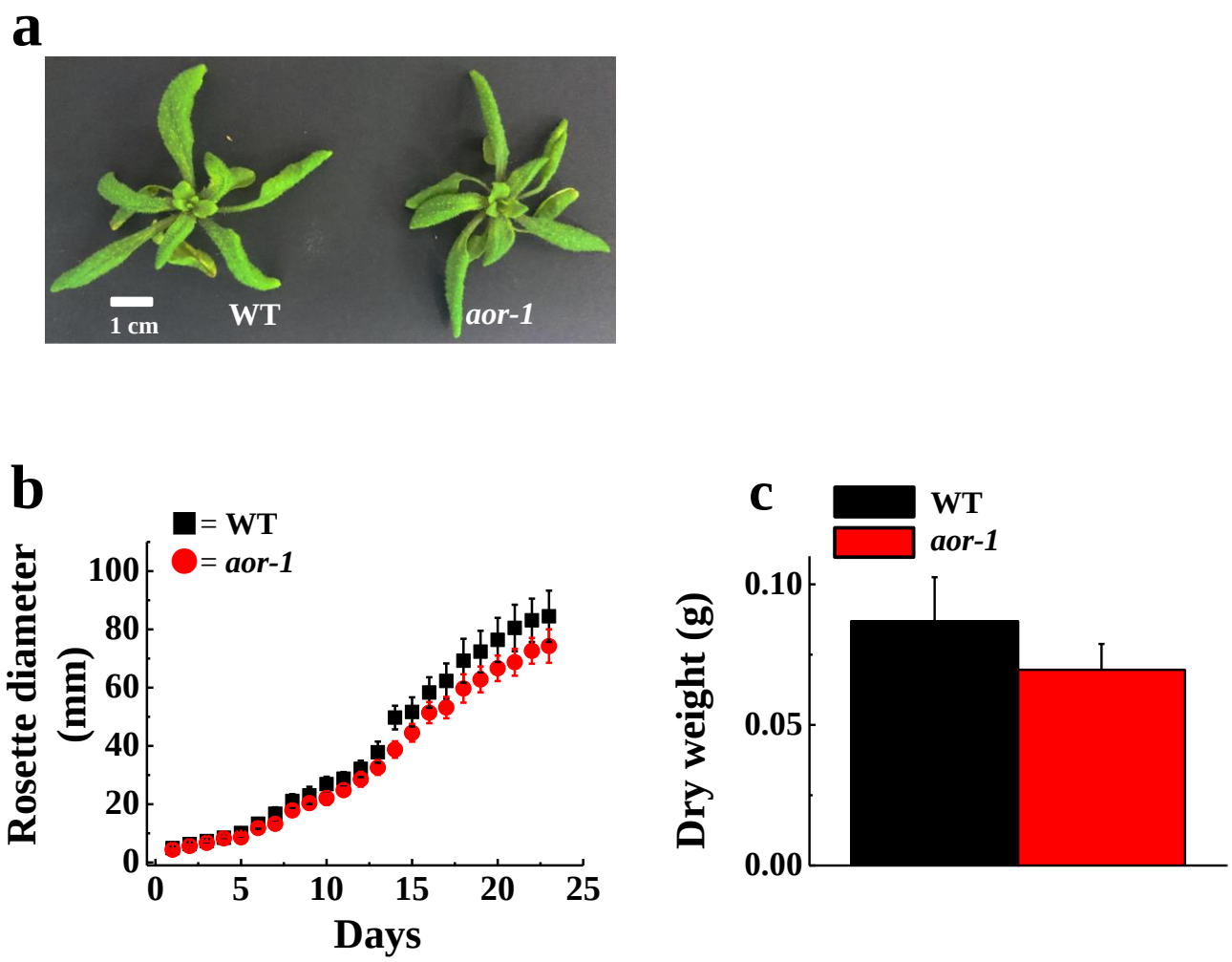

Figure VI-9

Characterization of *aor-1* grown under constant light growth conditions. (a) The plant phenotype of WT and *aor-1*. These plants are 3-weeks old after germination. Representative plants were shown. (b) The plant growth evaluated as an increase in maximum rosette diameter was shown. Data are expressed as means ± SEM of nine to ten independent plants. (c) Dry weight of plants was compared between WT and *aor-1*. Data are expressed as mean ± SEM of nine to ten independent experiments.

Table VI-6

Chlorophyll and nitrogen content in WT and *aor* mutants grown under continuous light conditions

Line	Chl (mg m^{-2})	N (mmol m^{-2})
WT	**261.3 ± 9.7**	**75.1 ± 4.8**
aor-1	**288.3 ± 8.4 †**	**83.5 ± 6.5**
aor-4	**290.2±20.0**	**78.8±3.5**

Chlorophyll and nitrogen content in WT and *aor-1* leaves. WT and *aor-1* were grown under constant light growth conditions. Chlorophyll and nitrogen content were determined on leaves in 3- to 4-weeks old plants. Data are expressed as mean ± SEM of six independent experiments. Dagger indicates a significant difference between WT and *aor-1* (Student's t-test: †, $p < 0.1$).

Table VI-7
Dark respiration rate and photosynthetic parameters in WT and *aor-1* grown under constant light conditions

	Fv/Fm	Respiration (μmol CO_2 m^{-2} s^{-1})	CO_2 assimilation (μmol CO_2 m^{-2} s^{-1})	Y(II)	g_s (μmol CO_2 m^{-2} s^{-1})	Ci (μmol mol^{-1})
WT	**0.822±0.003**	**0.46±0.18**	**4.69±0.44**	**0.685±0.016**	**0.097±0.008**	**378.8±9.1**
aor-1	**0.818±0.003**	**0.25±0.07**	**4.40±0.19**	**0.682±0.020**	**0.092±0.008**	**369.7±7.4**

Photosynthesis activity was determined under growth light condition (light intensity = 150 μE m^{-2} s^{-1}), and respiration was determined in the dark. Data are expressed as mean ± SEM of three independent experiments.

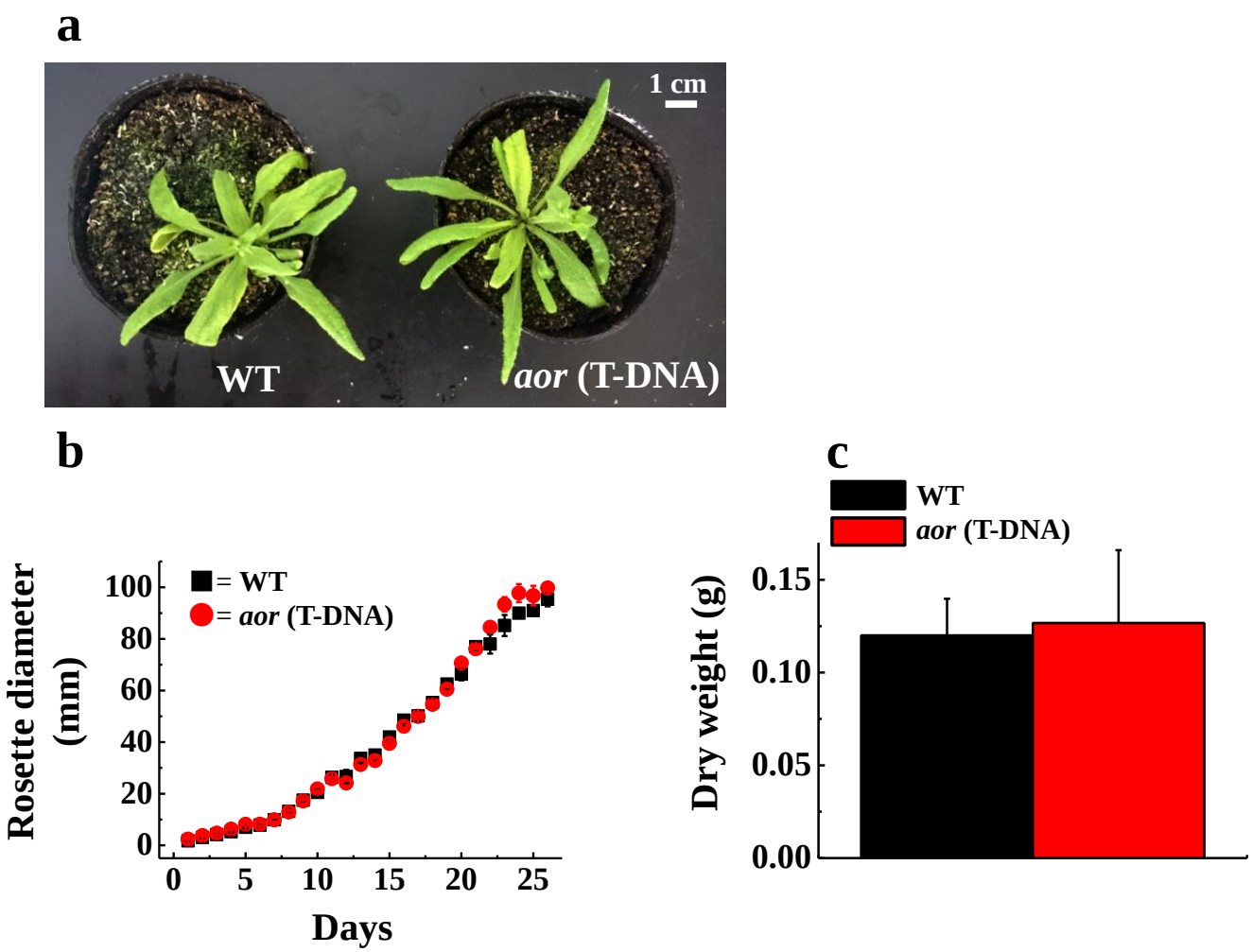

Figure VI-10

Characterization of *aor* (T-DNA) grown under constant light growth conditions. (a) The plant phenotype of WT and *aor* (T-DNA). These plants are 3-weeks old after germination. Representable plants were shown. (b) The plant growth evaluated as the increase in maximum rosette diameter was shown. Data are expressed as means ± SEM of three to six independent plants. (c) Dry weight of plants was compared between WT and *aor* (T-DNA). Data are expressed as mean ± SEM of three independent experiments.

Table VI-8
Chlorophyll and nitrogen content in WT and *aor* (T-DNA) grown under continuous light condition

Line	Chl (mg m^{-2})	N (mmol m^{-2})
WT	**224.3 ± 8.9**	**51.3 ± 4.9**
***aor* (T-DNA)**	**221.7 ± 5.2**	**56.1 ± 1.3**

Chlorophyll and nitrogen content in WT and *aor* (T-DNA) mutant leaves. WT and *aor* (T-DNA) mutants were grown under constant light conditions. Chlorophyll and nitrogen contents were determined on leaves in 3- to 4-weeks old plants. Data are expressed as mean ± SEM of three independent experiments.

Table VI-9

Dark respiration rate and photosynthetic parameters in WT and *aor* (T-DNA) grown under constant light conditions

	Fv/Fm	Respiration (μmol CO_2 m^{-2} s^{-1})	CO_2 assimilation (μmol CO_2 m^{-2} s^{-1})	Y(II)	g_s (μmol CO_2 m^{-2} s^{-1})	Ci (μmol mol^{-1})
WT	**0.809±0.006**	**0.96±0.18**	**5.24±0.22**	**0.704±0.011**	**0.164±0.002**	**374.9±4.2**
***aor* (T-DNA)**	**0.822±0.001**	**0.45±0.13†**	**5.06±0.20**	**0.685±0.004**	**0.162±0.015**	**379.4±6.4**

Photosynthesis activity was determined under growth light conditions (light intensity = 150 µE m^{-2} s^{-1}), and respiration was determined in the dark. Data are expressed as mean ± SEM of three independent experiments. Dagger indicates a significant difference between WT and *aor* (T-DNA) (Student's t-test: † $p < 0.1$).

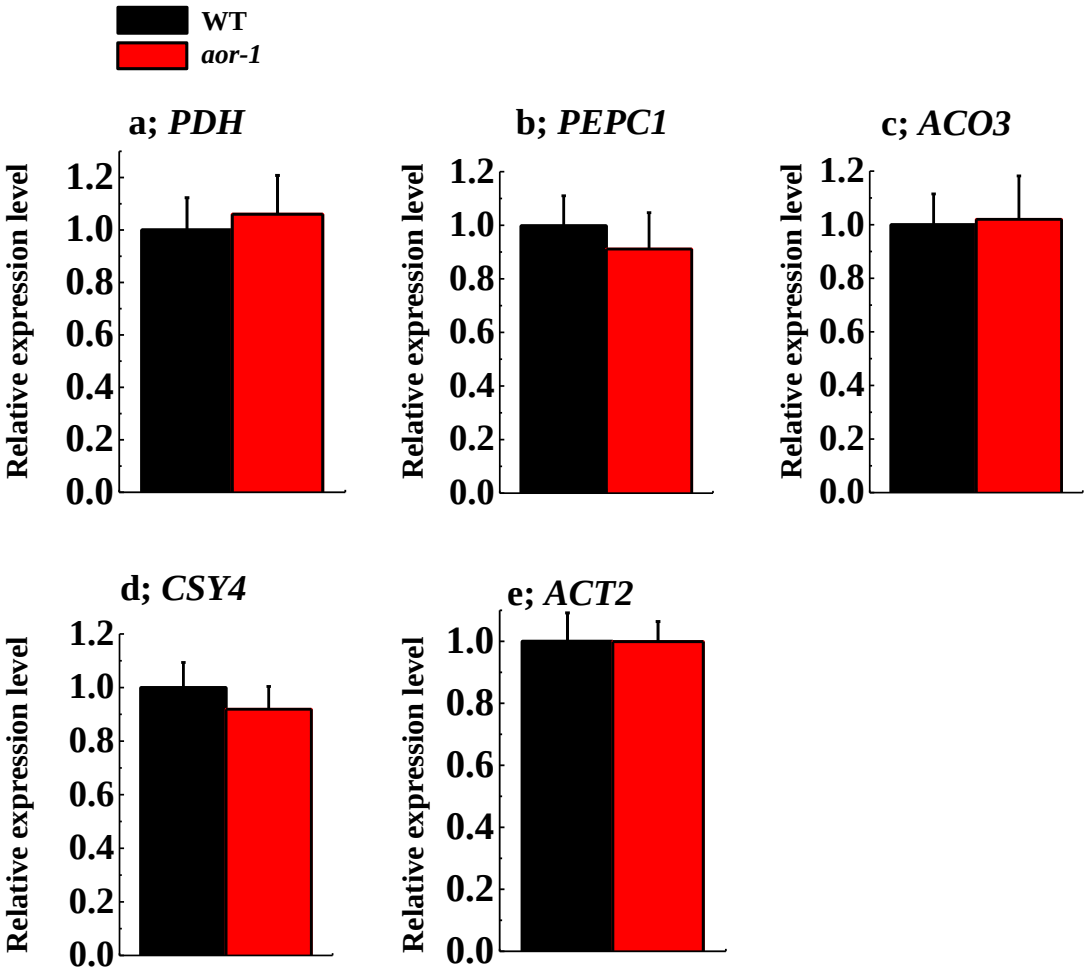

Figure VI-11

mRNA expression analysis related to respiration and *ACT2* in leaves. Leaves were harvested from WT and *aor-1* grown under constant light conditions. mRNA expression level of (a) *PDH*, (b) *PEPC1*, (c) *ACO3*, (d) *CSY4*, and (e) *ACT2* were shown. In each gene, mRNA expression level in WT was set to 1, and relative expression change was shown. Black bar indicates WT, and red bar indicates *aor-1*. Data are expressed as mean ± SEM of three to six independent experiments.

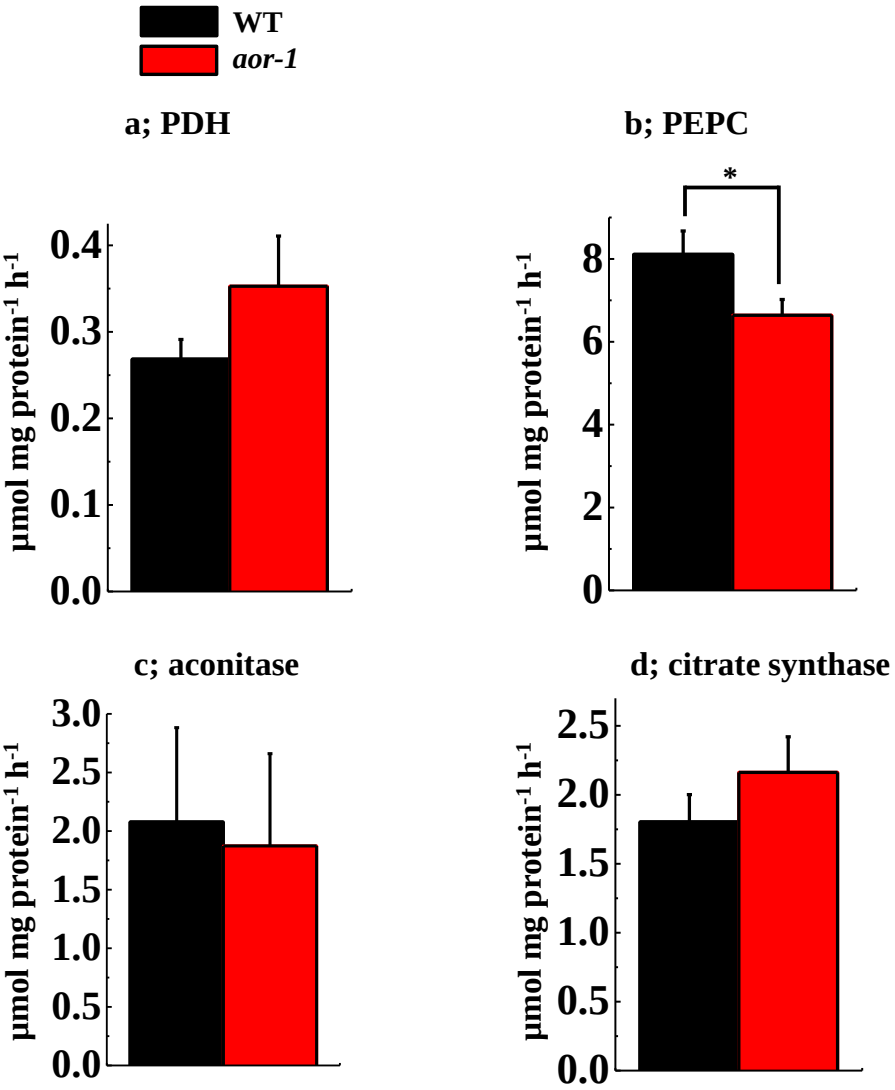

Figure VI-12

Evaluation of enzyme activity of pyruvate dehydrogenase (a), phosphoenolpyruvate carboxylase (b), aconitase (c), and citrate synthase (d) in WT and *aor-1* leaves. Leaves were harvested from WT and *aor-1* grown under constant light conditions. Black bar indicates WT, red bar indicates *aor-1*. Data are expressed as mean ± SEM of four independent experiments. Asterisks indicate a significant difference between WT and *aor-1* (Student's t-test: *, $p < 0.05$).

DISCUSSION

In this study, I analyzed the physiological importance of the detoxification of lipid-derived RCS in chloroplasts by using *Arabidopsis thaliana* mutants, which have a lower amount of AtAOR [aor (RNAi); *aor-1* and *aor-4*] or do not express a functional AtAOR [*aor* (T-DNA)]. I revealed that the suppression of AtAOR function inhibited carbon metabolism initiated by starch degradation during the night, leading to a lowering of dark respiration activity, and suppressed plant growth (Figs. VI-4, VI-8). These results conflict with a previous report, where the *aor* (T-DNA) was analyzed (Yamauchi et al., 2012). However, I found that the same *aor* (T-DNA) also showed smaller growth size than WT, when they were grown under day/night cycle conditions (Fig. VI-1). These results corresponded to those of *aor* (RNAi). Therefore, these different results for the growth of *aor* (T-DNA) in the present paper would be due to the difference in the growth conditions, including nutrition, growing medium, light intensity or growth stages. In fact, the plant sizes of *aor* (T-DNA) reported by Yamauchi et al. (2012) were smaller than those reported in the present study (Fig. VI-1).

I revealed that the growth retardation in *aor* mutants under day/night conditions was not caused by carbon acquisition capacity during the day. Under the growth light intensity, CO_2 assimilation and Y (II) in *aor* mutants were similar to WT (Tables VI-4, VI-5). Based on these results, the growth retardation in *aor* mutants was not accounted for by their photosynthetic ability. However, these results did not mean that the suppression of AtAOR hardly affects photosynthetic ability. In *aor-1*, the Calvin cycle enzymes, FBPase and PRK activity was significantly lowered as compared to WT (Fig. VI-13). FBPase and PRK have thioredoxin-regulated Cys in their structures, and the reduction of the disulfide-bridge between two Cys residues activates their activities (Martin et al., 2000). These enzymes are susceptible to oxidation by ROS, furthermore these enzymes are modified by lipid-derived RCS, which inhibit their functions (Asada and Takahashi, 1987; Tamoi et al., 1996a; Mano et al., 2009, 2014b). Based on these previous reports, the decrease in FBPase and PRK activities in *aor-1* could be due to oxidative stress induced by the suppression of AtAOR in chloroplasts. In fact, I observed that oxidative stress evaluated by the DAB-staining method was

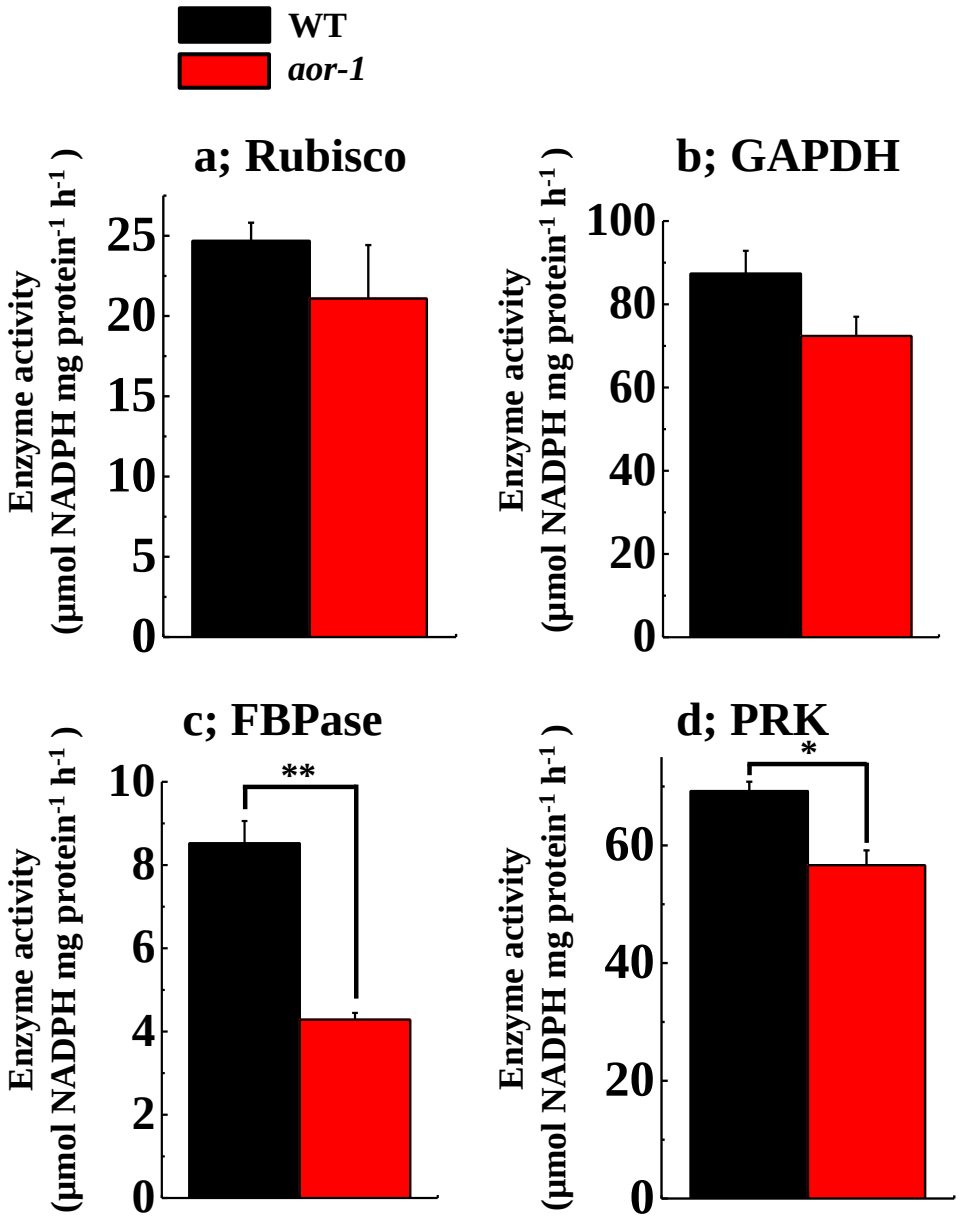

Figure VI-13

Evaluation of enzyme activity of Rubisco (a), GAPDH (b), FBPase (c), and PRK (d) in WT and *aor-1* leaves. Leaves were harvested from WT and *aor-1* grown under day/night cycle conditions. Black bar indicates WT, red bar indicates *aor-1*. Data are expressed as mean ± SEM of four independent experiments. Asterisks indicate a significant difference between WT and *aor-1* (Student's t-test: *, $p < 0.05$; **, $p < 0.01$).

stimulated in *aor-1*, compared to WT, under their growth conditions (Fig. VI-14). FBPase and PRK activities decreased in *aor-1*, nevertheless CO_2 assimilation rate and Y (II) were similar between WT and *aor-1* under their growth light conditions (Table VI-4). These results showed that the lack of AtAOR in chloroplasts induces oxidative stress, which affects the Calvin cycle enzymes. However, it did not cause the suppression of photosynthesis under the present growth conditions, because photosynthesis was not limited by the regeneration of RuBP under the present growth conditions (Farquhar et al., 1980). Under the present growth conditions, the light intensity did not saturate against photosynthesis, that is, photosynthesis was limited by the supply of photon energy to the photosystems in the thylakoid membranes. WT and *aor-1* showed the same values in Fv/Fm, therefore there was no difference in photosynthetic activity between WT and *aor-1* grown under the growth light conditions (Table VI-4). On the other hand, under high light and high CO_2 conditions, where photosynthesis is limited by the regeneration of RuBP, I observed that *aor-1* showed lower CO_2 assimilation rate and lower Y(II) compared to WT; otherwise Ci was similar between WT and *aor-1* (Fig. VI-15). In contrast, under high light and ambient CO_2 conditions, ranging from 20 to 30 Pa Ci, where photosynthesis is limited by the carboxylation reaction of RuBP by Rubisco, WT and *aor-1* showed the same CO_2 assimilation rate and Y(II) (Fig. VI-15). Therefore, *aor* mutants may show more severe phenotype under high CO_2 and high light conditions.

Carbon utilization during the night period is suppressed in *aor* mutants. Although *aor* mutants grown under day/night cycle showed growth retardation, the growth retardation was alleviated under constant light conditions (Figs. VI-1, VI-4, VI-9, VI-10). These results indicated that the growth retardation observed in *aor* mutants grown under day/night cycle might be due to the dark respiration during night. In fact, *aor* mutants showed a decreased rate of dark respiration, compared to WT (Tables VI-4, VI-5; Fig. VI-5). Photosynthesis assimilates CO_2 to accumulate carbon as a starch in chloroplasts during the day period; in contrast, respiration degrades starch to acquire energy for supplying carbon to the catabolic metabolism. Under the day/night growth conditions, relative growth rate shows a linear correlation with starch degradation rate during the night period, rather

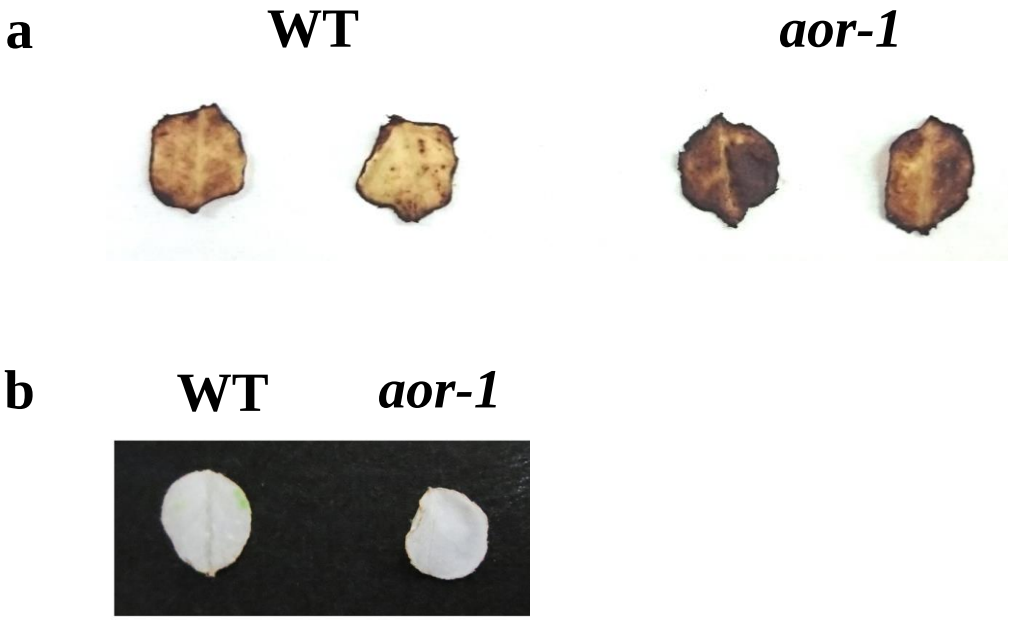

Figure VI-14

The Detection of H_2O_2 Accumulation in WT and *aor-1* leaves grown under day/night cycle growth conditions. The detached leaves were infiltrated DAB solution. After infiltration, the leaves placed under growth light conditions (150 μE m^{-2} s^{-1}) for 3 h (a) or under darkness for 3h (b). After this treatment, each leaves were boiled in 96% ethanol until green color become invisible.

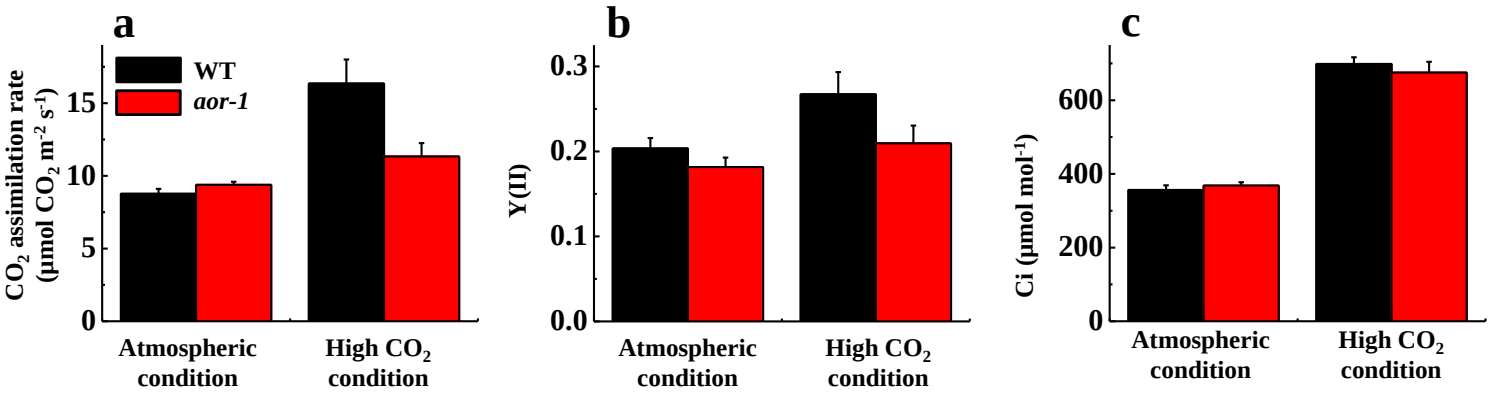

Figure VI-15

Photosynthetic activities in WT and *aor-1* grown under day/night condition. (a) CO_2 assimilation rate, (b) Y(II) and (c) Ci were evaluated under strong light condition (1,000μE m^{-2} s^{-1}). In this experiment, atmospheric condition (40 Pa CO_2, 21 kPa O_2) and high CO_2 condition (80 Pa CO_2, 21 kPa O_2) were set. Data are expressed as mean ± SEM of four independent experiments

than starch synthesis rate during the day (Gibon et al., 2009). Furthermore, starch degradation rate during the night period also shows a linear correlation with the utilization efficiency of organic acid metabolism (Gibon et al., 2009). This means that carbon flow from starch in chloroplasts to glycolysis in the cytosol and TCA-cycle in mitochondria is important for plant growth. Indeed, mutant analysis showed that the suppression of starch degradation caused lower respiration rate and severe growth retardation (Zeeman and Rees, 1999; Yu et al., 2001; Chia et al., 2004; Nittylä et al., 2004; Kötting et al., 2005; Fulton et al., 2008).

In this study, I found that *aor* mutants showed a lower dark respiration rate (Table VI-4; Fig. VI-5), where PEPC expression level during the night period and its enzyme activity significantly decreased, compared to WT (Fig. VI-6, VI-7). PEPC converts phosphoenolpyruvate (PEP) and HCO_3^- to oxaloacetic acid (OAA) and Pi by β-carboxylation of PEP in the presence of Mg^{2+}, and this reaction contributes to the supply of carbon skeletons to TCA-cycle and amino acid synthesis by the production of OAA (Lepiniec et al., 1994; Izui et al., 2004). PEPC activity greatly affects carbon and nitrogen metabolism. For example, an *Arabidopsis* knock-out mutant of PEPC showed growth retardation (Shi et al., 2015). Furthermore, the decrease of PEPC activity in plants caused a decrease in starch degradation during the night period (Häusler et al., 1999; Shi et al., 2015). In addition, N assimilation was also suppressed and amino acid content produced from OAA (Asp, Asn) was lowered, compared to WT (Häusler et al., 1999; Shi et al., 2015). In contrast, plants overexpressing PEPC showed higher nitrogen content compared to WT, and stimulation of starch degradation (Häusler et al., 1999; Agarie et al., 2002; Rademacher et al., 2002; Chen et al., 2004). Furthermore, the change in PEPC activity is related to that in the dark respiration rate in leaves. PEPC suppression mutant showed a lower dark respiration rate and plants overexpressing PEPC showed a higher respiration rate, compared to WT (Häusler et al., 1999; Agarie et al., 2002; Rademacher et al., 2002). These changes accompanied the change of carbon supply from starch to respiratory metabolism. The phenotype of PEPC suppression mutant reported in these previous studies is similar to the phenotype of *aor-1* observed in this study (Figs. VI-4, VI-8; Table VI-4). Based on these observations, one of

the reasons why *aor* mutants showed a suppression of the dark respiration rate, a lower nitrogen content, and growth retardation would be due to the lower activity of PEPC (Tables VI-3, VI-4) (Reich et al., 1998; Agarie et al., 2002; Foyer et al., 2011).

PEPC is one of the targeted molecules that are oxidatively modified by lipid-derived RCS *in vivo*. Mano et al. (2014b) reported that the production of lipid-derived RCS is stimulated in plants under severe salt stress conditions, and they showed that several candidate proteins are carbonylated by lipid-derived RCS and oxidative stress (Mano et al., 2014b). Amongst the candidate proteins, PEPC was detected as a target for protein carbonylation (Mano et al., 2014b). PEPC has nucleophilic amino acids located at the prerequisite for its activity in its structure. For example, a His residue is located in the hydrophobic pocket of PEPC; this His residue stabilizes an intermediate of carboxylation products, and extracts H^+ from the carboxyl group in PEP (Lepiniec et al, 1994; Izui et al., 2004). Furthermore, PEPC has a Lys residue in its active site for the carboxylation reaction (Podesta et al., 1986; Jiao et al., 1990). Interestingly, this Lys residue reacts with an aldehyde group in pyridoxal 5'-phosphate, whereby PEPC activity is reduced by the formation of a Schiff base between Lys and aldehyde group (Podesta et al., 1986; Jiao et al., 1990). In addition, plant PEPC isozymes conserve seven Cys residues in their amino acid alignments, and their oxidation of thiol groups suppresses PEPC activity (Chardot et al., 1992). Based on these reports, PEPC is structurally highly susceptible to oxidative modification by reactive aldehyde groups. Therefore, I suggest that oxidative modification of these nucleophilic amino acid residues in PEPC might have occurred, and this might be one of the reasons of a decrease in PEPC activity in *aor-1* because the detoxification activity of lipid-derived RCS is suppressed, and oxidative stress is stimulated, in *aor* mutants (Fig. VI-14).

Under constant light conditions, the change of carbon supply activity from starch degradation to glycolysis and TCA-cycle does not affect plant growth (Izumi et al., 2013). Furthermore, the dark respiration rate is largely suppressed (about ~80 %) under illumination, compared to under darkness because TCA-cycle activity and the supply of hexose molecules like glucose and sucrose to

glycolysis are inhibited under illumination (Brooks and Farquhar, 1985; Villar et al., 1995; Shapiro et al., 2004; Tcherkez et al., 2005, 2008; Yin et al., 2011). These reports indicate that the carbon flow started from photosynthesis to glycolysis and TCA-cycle is severely restricted under illumination, compared to that occurring under darkness. Therefore, I suggest that the decrease of PEPC activity in the *aor* mutant would be masked by lowering the carbon flow in glycolysis under constant light conditions, and the growth retardation in *aor* mutant would be alleviated (Figs. VI-9, VI-10).

In natural conditions, not in Arctic and Antarctica, the sun rises and sets, and plants experience night life. Furthermore, global warming is predicted to accompany the increases in both earth temperature and the partial pressure of CO_2 in the atmosphere (Stocker et al., 2013). The elevated temperature increases the dark respiration rate in plants (Atkin and Tjoelker, 2003; Noguchi et al., 2015). The increased partial pressure of CO_2 in the atmosphere shifts the rate-limiting step of photosynthetic CO_2 assimilation rate from Rubisco-limiting to RuBP-regeneration (Farquhar et al., 1980). The lack of AtAOR suppressed dark respiration and the regeneration efficiency of RuBP in the Calvin cycle. Based on our findings, I predict that the requirement of AOR function would increase in plants in order to adapt to the changing climate, and the enhanced activity of AOR would support plant growth, even under severe stress conditions.

GENERAL DISCUSSION AND FUTURE PROSPECTS

In photosynthetic electron transport reaction, PSI is a major ROS producing site in thylakoid membranes. ROS-detoxification systems consisted with Cu/Zn-SOD and APX, and Asc regeneration system for continuous ROS-detoxification present around PSI (Miyake and Asada, 1992; Miyake et al., 1998; Asada, 1999). Many reports believed that these ROS-detoxification systems have assumed to protect PSI from oxidative photoinhibition. However, in this study, I showed that ROS-detoxification systems which are exited in aqueous phase in chloroplast cannot protect PSI from ROS. This would be because that ROS are produced within the thylakoid membrane, and ROS inactivate the electron carriers in PSI (Takahashi and Asada, 1988; Kozuleva and Ivanov, 2010; Kozuleva et al., 2014). Therefore, I suggest that conventional strategy to improve ROS-detoxification system in chloroplasts might not be successful for protecting PSI photoinhibition induced by ROS under environmental stress conditions. In contrast, I found that high light acclimation improve the tolerance against PSI photoinhibition depending on wheat cultivars. This result clearly demonstrates that wheat plants possess useful genetic resources related to the protection of PSI from its photoinhibition. Because I found the cultivar difference about the tolerance in PSI photoinhibition, the genetic locus which regulates the tolerance of PSI photoinhibition in wheat plants might be discovered by quantitative trait locus (QTL) analysis. In this study, I failed to the exact component to improve the tolerance of PSI photoinhibition, however, it is expected that plant fitness under the environmental conditions is improved by the increase in PSI tolerance against ROS through the discovering the genetic locus related to the tolerance against PSI photoinhibition in the future studies.

For preventing PSI photoinhibition in photosynthetic electron transport reaction, the formation of ΔpH across the thylakoid membrane is also considerably important. I found that H^+-efflux regulation by chloroplastic ATPase, instead of H^+-influx by WWC and CEF, plays an important role in the regulation of ΔpH. These results suggest that photosynthetic electron transport

reaction on the thylakoid membrane recognizes the ATP consumption rate in the Calvin-cycle through chloroplastic ATP/ADP ratio, and modulates the energy supply by photosynthetic electron transport reaction (Avenson et al., 2004, 2005; Kanazwa and Kramer, 2002; Kohzuma et al, 2009; Takizawa et al., 2007, 2008).

Photorespiration has been recognized wasteful reaction because additional ATP is required for RuBP regeneration, compared to the Calvin-cycle. However, in this study, I found that higher plants operate photorespiration under the conditions where the supply of CO_2 into the leaf is limited, and stimulate the formation of ΔpH to oxidize electron carriers in PSI. Therefore, ATP consumption rate would be slower than that in the Calvin-cycle although photorespiration functions as electron sink consuming ATP. This slower ATP consumption rate in photorespiration achieved to decrease H^+-efflux in ATPase, and contribute to form large ΔpH. In addition to ATP, photorespiration consumes NADPH. That is, I suggest that higher plants operate photorespiration by using O_2 to form ΔpH and consume reducing equivalents, and photorespiration prevents over-reducing state in the electron carriers in PSI and the production of ROS. Based on this suggestion, the strategy which reduces the photorespiration activity in C3 plant for increasing crop yield might cause the stimulation of oxidative stress and PSI photoinhibition.

H^+-efflux regulation by chloroplastic ATPase was directly related to the PSI photoinhibition. Based on these result, I proposed that chloroplastic ATPase is a regulatory valve of ROS production in photosynthetic electron transport reaction. Therefore, I suggest that chloroplastic ATPase is one of the molecular targets to regulate the ROS production in photosynthesis under environmental stress conditions. If plants achieve to regulate H^+-efflux through ATPase, and modulate the photosynthetic electron transport reaction under transient environmental stress conditions, the risk of ROS production in photosynthetic electron transport reaction would be reduced. In this study, it remains unclear why chloroplastic ATPase in *hope2* does not respond to light intensity or the partial pressure of intercellular CO_2. However, the analysis of protein interaction or structure of ATPase in *hope2* might contribute to elucidate the H^+-efflux regulation in ATPase. It would be expected that hope2

serves as an important allele for understanding the physiological functions of chloroplastic ATPase, and leads academic and agricultural development.

Cultivation environment for crop plants on earth is gradually changing, and atomospheric CO_2 concentration continues to increase after the Industrial Revolution (Wheeler and Braum, 2013). The increase in CO_2 means the increase in the substrate for CO_2-assimilation in plant, therefore, apparently this environmental change makes expect to stimulating photosynthesis in higher plants. Indeed, the increase in CO_2 from today's ambient CO_2 concentration (about 400 ppm) simply stimulates photosynthesis in C3 crop plants (Ainsworth and Rogers, 2007). However, in this study, I found that the stimulating photosynthesis also accelerates the production of sugar-derived RCS in chloroplasts. Among sugar-derived RCS, MG acts as a Hill oxidant in photosynthesis, and MG stimulates ROS production by obtaining electron at PSI in thylakoid membranes (Saito et al., 2011). In addition, MG has been reported to suppress photosynthesis in isolated chloroplasts, or the activity of cytosolic ascorbate peroxidase (Hoque et al., 2012a; Mano et al., 2009). Furthermore, MG induces stomatal closure in leaves trough the ROS production (Hoque et al., 2012b). Based on these reports, the stimulation of photosynthesis would lead the accumulation of MG, and the accumulation of MG could accelerate oxidative stress by direct ROS production or by ROS production in photosynthetic electron transport reaction through the imbalance between electron source activity and electron sink activity (Kramer and Evans, 2011; Schöttler et al., 2015). In addition to CO_2 concentration in atmosphere, temperature is also increasing (Stocker et al., 2013). I also found that increasing temperature from 25^{o}C to 35^{o}C further stimulates MG production in photosynthesis. Therefore, even under future environment where CO_2-assimilation rate is expected to increase in higher plants, the chance to cause damage by sugar-derived RCS could increase in higher plants.

I found that not only the activity of the Calvin cycle enzymes, but also the activity of cytosolic PEPC decreased in *Arabidopsis aor* mutant. In addition, the growth in *aor* was retarded by suppressing starch utilization during night. From these results, I propose two important points as follows. First, for the plant growth regulation, carbon utilization during the night is very important,

as well as carbon acquisition during the day. That is, it is necessary for improving plant productivity to develop carbon utilization pathway like glycolysis and TCA-cycle, and strengthen the stress tolerance of them. Second, the detoxification of lipid-derived RCS in chloroplasts is required for supporting plant growth even under laboratory optimal growth conditions. Simultaneously, this result indicates that chloroplasts are the sauce of lipid-derived RCS. As mentioned in general introduction section, PUFAs which constitute the chloroplasts would be an origin of lipid-derived RCS (Mano et al., 2014a). Based on these observations, I suggest the physiological significance of chloroplast localized-AOR is to prevent the diffusion of lipid-derived RCS from chloroplasts to cytosol, and protect cellular components from the toxicity of lipid-derived RCS. It has been reported that the production of lipid-derived RCS also stimulated by high temperature (Yamauchi et al., 2008). On the other hand, I found that *aor* showed lower CO_2-assimilation rate under high CO_2 conditions, compared to WT. This would be because of the suppression of the Calvin cycle enzymes like FBPase and PRK. Therefore, future environment increasing CO_2 and temperature could accelerate the production of lipid-derive RCS, and could cause damage to both carbon-acquisition and carbon-utilization in higher plants. From these studies, chloroplasts in higher plants have potential to stimulate oxidative stress by producing sugar-derived and lipid-derived RCS, in addition to ROS production in photosynthetic electron transport reaction. Furthermore, future environment on earth would be accelerated the sugar-derived- and lipid-derived RCS-dependent oxidative stress in plant cells. In fact, the carbonylation of leaf protein is stimulated under high CO_2 conditions (Qiu et al., 2008). Based on these considerations, I suggest that the detoxification systems for RCS in higher plants are important molecular target for maintaining and improving plant fitness in the future environment on earth. For elucidating the importance of the detoxification of RCS in higher plant under future environment, the effect of high CO_2 or temperature on higher plants which are modified RCS detoxification activities is worth studying.

ACKNOWLEDGEMENT

I would like to express my greatest gratitude to Associate Professor Dr. Chikahiro Miyake for his great directions and encouragements in my studies during my doctoral course.

I also express my gratitude to Associate Professor Dr. Shigeo Takumi for his support, and giving me a chance to analyze the interesting wheat cultivars.

I would like to offer special thanks to Professor Dr. Yukio Tosa, and Professor Dr. Toshio Sugimoto for encouragements in my studies and giving fruitful discussion.

I express my heartfelt appreciation to Professor Dr. Hidehiro Fukaki, and Dr. Tatsuaki Goh in Kobe University for their technical supports to isolate EMS mutant in *A. thaliana*, and generate transgenic plant.

I also express my heartfelt appreciation to Assistant Professor Dr. Kentaro Ifuku in Kyoto University for the collaboration with my experiments, and having a great discussion.

I also express my great appreciation to Associate Professor Dr. Katsumi Amako in Jin-ai Universoty for lending me the two-dementional chlorophyll fluorescence analyzer to screen EMS mutant in *A.thaliana.*

I also express my heartfelt appreciation to Associate Professor Dr. Kimitune Ishizaki in Kobe University, Professor Dr. Shinichiro Sawa in Kumamoto University, Professor Dr. Taku Demura and Dr. Ryosuke Sano in Nara Institute of Science and Technology, and Assistant Professor Dr. Tetsuya Kurata in Tohoku University for giving me an opportunity to use next-generation sequencer.

I also express my heartfelt appreciation to Professor Dr. Park Pyoyun, Associate Professor Dr. Ken-ichi Ikeda, and Dr. Kanako Inoue for giving me an opportunity to use Transmission Electron Microscopy, and teaching a valuable quantification method.

I express my graditude to Associate Professor Dr. Masahiro Tamoi in Kindai University, Associate Professor Dr. Yo-ichiro Fukao in Ritsumeikan University, and Associate Professor Dr. Katsuhiko Sakamoto in Kobe University for their experimental supports.

I am very grateful to Professor Dr. Toru Hisabori and Assistant Professor Dr. Keisuke Yoshida in

Tokyo Institute of Technology for giving great advices and antiserum of ATPsynthase.

I am also very grateful to Professor Dr. Kintake Sonoike in Waseda University, and Professor Dr. Isao Enami in Tokyo University of Science for giving me the antiserum for PSI.

I am also very grateful to Proressor Dr. Toshiharu Shikanai, Dr. Hiroshi Yamamoto, and Mr. Taishi Nisimura in Kyoto University, and Assistat Professor Dr. Yasuo Yamauchi in Kobe University for giving experimental materials and their technical advices.

I would like to offer special thanks to Professor Dr. Ichiro Terashima, and Dr. Masaru Kono in Unversity of Tokyo, Professor Dr. Ko Noguchi in Tokyo University of Pharmacy and Life Science, and Professor Dr. Amane Makino in Tohoku University for giving great advice for my experiments.

I also would like to offer special thanks to Professor Dr. Ulich Schreiber in Universität Würzburg, and Professor Dr. David M. Kramer in Michigan State University for having fruitful discussion to develop my experiments.

I would like to thank to Dr. Ryota Saito, and the members in Plant Nutrition laboratory in Kobe University for helping my studies.

Finally, I wish to thank to my family for giving me the opportunity to study in Kobe University, and supporting me.

LITERATURE CITED

Agarie S, Miura A, Sumikura R, Tsukamoto S, Nose A, Arima S, Matsuoka M, Miyao-Tokutomi M (2002) Overexpression of C4 PEPC caused O_2-insensitive photosynthesis in transgenic rice plants. Plant Sci 162: 257-265

Ainsworth EA, Rogers A (2007) The response of photosynthesis and stomatal conductance to rising [CO_2]: mechanisms and environmental interactions. Plant Cell & Environ 30: 258-270

Aldini G, Dalle‐Donne I, Facino RM, Milzani A, Carini M (2007) Intervention strategies to inhibit protein carbonylation by lipoxidation‐derived reactive carbonyls. Med Res Rev 27: 817-868

Aldini G, Vistoli G, Stefk M, Chondrogianni N, Grune T, Sereikaite J, Sadowska-Bartosz I, Bartosz G (2013) Molecular strategies to prevent, inhibit, and degrade advanced glycation and advanced lipoxidation end products. Free Rad Res 47: 93-137

Allahverdiyeva Y, Mamedov F, Mäenpää P, Vass I, Aro EM (2005) Modulation of photosynthetic electron transport in the absence of terminal electron acceptors: Characterization of the *rbcL* deletion mutant of tobacco. Biochim Biophys Acta Bioenerg 1709: 69–83

Allen JF (2002) Photosynthesis of ATP-electrons, proton pumps, rotors, and poise. Cell 110: 273-276

Allen JF (2003) Cyclic, pseudocyclic and noncyclic photophosphorylation: new links in the chain. Trends Plant Sci 8: 15-19

Andrews JR, Fryer MJ, Baker NR (1995) Consequences of LHC II deficiency for photosynthetic regulation in chlorina mutants of barley. Photosynthesis Res 44: 81-91

Apel K, Hirt H (2004) Reactive oxygen species: metabolism, oxidative stress, and signal transduction. Annu Rev Plant Biol 55: 373-399

Armbruster U, Carrillo LR, Venema K, Pavlovic L, Schmidtmann E, Kornfeld A, Jahns P, Berry JA, Kramer DM, Jonikas MC (2014) Ion antiport accelerates photosynthetic acclimation in fluctuating light environments. Nat commun 5: doi:10.1038/ncomms6439

Arnon DI (1949) Copper enzymes in isolated chloroplasts. Polyphenoloxidase in *Beta vulgaris.* Plant Physiol 24: 1–15

Arnon DI (1959) Conversion of light into chemical energy in photosynthesis. Nature 184:10-21

Aro EM, Virgin I, Andersson B (1993) Photoinhibition of photosystem II. Inactivation, protein damage and turnover. Biochim Biophys Acta Bioenerg 1143: 113-134

Asada K (1999) The water-water cycle in chloroplasts: scavenging of active oxygens and dissipation of excess photons. Annu Rev Plant Biol 50: 601-639

Asada K (2000) The water–water cycle as alternative photon and electron sinks. Philosophical Transactions of the Royal Society of London. Series B: Biological Sciences 355: 1419–1431

Asada K, Badger MR (1984) Photoreduction of $^{18}O_2$ and $H_2{}^{18}O_2$ with concomitant evolution of $^{16}O_2$ in intact spinach chloroplasts: evidence for scavenging of hydrogen peroxide by peroxidase. Plant Cell Physiol 25: 1169-1179

Asada K, Kiso K, Yoshikawa K (1974) Univalent reduction of molecular oxygen by spinach chloroplasts on illumination. J Biol Chem 249: 2175-2181

Asada K, Takahashi M (1987) Production and scavenging of active oxygen in photosynthesis. In: Kyle DJ, Osmond CB and Arntzen CJ (eds.) Photoinhibition, pp 227–287. Elsevier, Amsterdam

Atkin OK, Tjoelker MG (2003) Thermal acclimation and the dynamic response of plant respiration to temperature. Trends Plant Sci. 8: 343-351.

Avenson TJ, Cruz JA, Kramer DM (2004) Modulation of energy-dependent quenching of excitons in antennae of higher plants. Proc Natl Acad Sci USA 101: 5530-5535

Avenson TJ, Cruz JA, Kanazawa A, Kramer DM (2005) Regulating the proton budget of higher plant photosynthesis. Proc Natl Acad Sci USA 102: 9709-9713

Babbs CF, Pham JA, Coolbaugh RC (1989) Lethal hydroxyl radical production in paraquat-treated plants. Plant Physiol 90: 1267–1270

Badger MR, von Caemmerer S, Ruuska S, Nakano H (2000) Electron flow to oxygen in higher plants and algae: rates and control of direct photoreduction (Mehler reaction) and rubisco oxygenase. Philos Trans R Soc B 355: 1433-1446

Bailey S, Walters RG, Jansson S, Horton P (2001) Acclimation of *Arabidopsis thaliana* to the light environment: the existence of separate low light and high light responses. Planta 213: 794–801

Baker NR (2008) Chlorophyll fluorescence: a probe of photosynthesis *in vivo*. Annu Rev Plant Biol 59: 89–113

Baker NR, Harbinson J, Kramer DM (2007) Determining the limitations and regulation of photosynthetic energy transduction in leaves. Plant Cell & Environ 30: 1107-1125

Bechtold U, Rabbani N, Mullineaux PM, Thornalley PJ (2009) Quantitative measurement of specific biomarkers for protein oxidation, nitration and glycation in *Arabidopsis* leaves. Plant J 59: 661-671

Block MA, Douce R, Joyard J, Rolland N (2007) Chloroplast envelope membranes: a dynamic interface between plastids and the cytosol. Photosynth Res 92: 225-244

Bondarava N, Gross CM, Mubarakshina M, Golecki JR, Johnson GN, Krieger‐Liszkay A (2010) Putative function of cytochrome *b559* as a plastoquinol oxidase. Physiol Plant 138: 463–473

Brestic M, Cornic G, Freyer MJ, Baker NR (1995) Does photorespiration protect the photosynthetic apparatus in French bean leaves from photoinhibition during drought stress? Planta 196: 450-457

Brestic M, Zivcak M, Kunderlikova K, Sytar O, Shao H, Kalaji HM, Allakhverdiev SI (2015) Low PSI content limits the photoprotection of PSI and PSII in early growth stages of chlorophyll b-deficient wheat mutant lines. Photosynthesis Res 125: 151-166

Breyton C, Nandha B, Johnson GN, Joliot P, Finazzi G (2006) Redox modulation of cyclic electron flow around photosystem I in C3 plants. Biochemistry 45: 13465-13475

Brooks A, Farquhar GD (1985) Effect of temperature on the CO_2/O_2 specificity of ribulose-1, 5-bisphosphate carboxylase/oxygenase and the rate of respiration in the light. Planta 165: 397-406

Bunney TD, van Walraven HS, de Boer AH (2001) 14-3-3 protein is a regulator of the mitochondrial and chloroplast ATP synthase. Proc Nat Aca Sci USA 98: 4249-4254

Butler WL, Kitajima M (1975) Fluorescence quenching in photosystem II of chloroplasts. Biochim Biophys Acta Bioenerg 376: 116-125

Carraretto L, Formentin E, Teardo E, Checchetto V, Tomizioli M, Morosinotto T, Giacometti GM, Finazzi G, Szabó I (2013) A thylakoid-located two-pore K^+ channel controls photosynthetic light utilization in plants. Science 342: 114-118

Catalá A (2010) A synopsis of the process of lipid peroxidation since the discovery of the essential fatty acids. Biochem Biophys Res Commun 399: 318-323

Cazzaniga S, Li Z, Niyogi KK, Bassi R, Dall'Osto L (2012) The Arabidopsis *szl1* mutant reveals a critical role of β-carotene in photosystem I photoprotection. Plant Physiol 159: 1745–1758

Chardot TP, Wedding RT (1992) Role of cysteine in activation and allosteric regulation of maize phosphoenolpyruvate carboxylase. Plant Physiol 98: 780-783

Chen LM, Li KZ, Miwa T, Izui K (2004) Overexpression of a cyanobacterial phosphoenolpyruvate carboxylase with diminished sensitivity to feedback inhibition in *Arabidopsis* changes amino

acid metabolism. Planta 219: 440-449

Chia T, Thorneycroft D, Chapple A, Messerli G, Chen J, Zeeman SC, Smith SM, Smith AM (2004) A cytosolic glucosyltransferase is required for conversion of starch to sucrose in Arabidopsis leaves at night. Plant J 37: 853-863

Chiu W, Niwa Y, Zeng W, Hirano T, Kobayashi H, Sheen J (1996) Engineered GFP as a vital reporter in plants. Curr Biol 6: 325–330

Clarke JE, Johnson GN (2001) *In vivo* temperature dependence of cyclic and pseudocyclic electron transport in barley. Planta 212: 808-816

Clough SJ, Bent AF (1998) Floral dip: a simplified method forAgrobacterium‐mediated transformation of *Arabidopsis thaliana*. Plant J., 16: 735-743.

Cornic G, Bukhov NG, Wiese C, Bligny R, Heber U (2000) Flexible coupling between light-dependent electron and vectorial proton transport in illuminated leaves of C3 plants. Role of photosystem I-dependent proton pumping. Planta 210: 468-477

Cramer WA, Zhang H, Yan J, Kurisu G, Smith JL (2006) Transmembrane traffic in the cytochrome b_6f complex. Annu Rev Biochem 75: 769-790

Cruz JA, Sacksteder CA, Kanazawa A, Kramer DM (2001) Contribution of electric field ($\Delta\psi$) to steady-state transthylakoid *proton motive force* (*pmf*) *in vitro* and *in vivo*. Control of pmf parsing into $\Delta\psi$ and ΔpH by ionic strength. Biochemistry 40: 1226-1237

Dahal K, Kane K, Gadapati W, Webb E, Savitch LV, Singh J, Sharma P, Sarhan F, Longstaffe FJ, Grodzinski B, Hüner N (2012) The effects of phenotypic plasticity on photosynthetic performance in winter rye, winter wheat and *Brassica napus*. Physiol Plant 144: 169-188

Dai Z, Ku MS, Edwards GE (1993) C4 photosynthesis (the CO_2-concentrating mechanism and photorespiration). Plant Physiol 103: 83-90

Dal Bosco C, Lezhneva L, Biehl A, Leister D, Strotmann H, Wanner G, Meurer J (2003) Inactivation of the chloroplast ATP synthase γ subunit results in high non-photochemical fluorescence quenching and altered nuclear gene expression in *Arabidopsis thaliana*. J Biol Chem 279: 1060-1069

DalCorso G, Pesaresi P, Masiero S, Aseeva E, Schünemann D, Finazzi G, Joliot P, Barbato R, Leister D (2008) A complex containing PGRL1 and PGR5 is involved in the switch between linear and cyclic electron flow in *Arabidopsis*. Cell 132: 273–285

del Riego G, Casano LM, Martín M, Sabater B (2006) Multiple phosphorylation sites in the β subunit of thylakoid ATP synthase. Photosynth Res 89: 11-18

De Veau EJ, Burris JE (1989) Photorespiratory rates in wheat and maize as determined by ^{18}O-labeling. Plant Physiol 90: 500-511

Deliu T, Walker DA (1981) Polarographic measurement of photosynthetic O_2 evolution by leaf discs. New Phytol 9: 165-175

Demmig-Adams B, Adams WW (1996) The role of xanthophyll cycle carotenoids in the protection

of photosynthesis. Trends Plant Sci 1: 21-26

Dietz KJ, Heber U (1984) Rate-limiting factors in leaf photosynthesis. I. Carbon fluxes in the Calvin cycle. Biochim Biophys Acta Bioenerg 767: 432-443

Douce R, Holtz RB, Benson AA (1973) Isolation and properties of the envelope of spinach chloroplasts. J Biol Chem 248: 7215-7222

Driever SM, Baker NR (2011) The water–water cycle in leaves is not a major alternative electron sink for dissipation of excess excitation energy when CO_2 assimilation is restricted. Plant Cell & Environ 34: 837-846

Esterbauer H, Schaur RJ, Zollner H (1991) Chemistry and biochemistry of 4-hydroxynonenal, malonaldehyde and related aldehydes. Free Radical Biol Med 11: 81-128

Farquhar GD, von Caemmerer SV, Berry JA (1980) A biochemical model of photosynthetic CO_2 assimilation in leaves of C3 species. Planta 149: 78-90.

Fisher N, Kramer DM (2014) Non-photochemical reduction of thylakoid photosynthetic redox carriers *in vitro*: Relevance to cyclic electron flow around photosystem I? Biochim Biophys Acta Bioenerg 1837: 1944-1954

Flügge U, Heldt HW (1984) The phosphate-triose phosphatephosphoglycerate translocator of the chloroplasts. Trend Biol Sci 9: 530-534

Forti G, Elli G (1995) The function of ascorbic acid in photosynthetic phosphorylation. Plant Physiol

109: 1207-1211

Forti G, Elli G (1996) Stimulation of photophosphorylation by ascorbate as a function of light intensity. Plant Physiol 112: 1509-1511

Foyer CH, Noctor G, Hodges M (2011) Respiration and nitrogen assimilation: targeting mitochondria-associated metabolism as a means to enhance nitrogen use efficiency. J Exp Bot 62: 1467-1482

Fristedt R, Martins NF, Strenkert D, Clarke CA, Suchoszek M, Thiele W, Shöttler MA, Merchant SS (2015) The Thylakoid Membrane Protein CGL160 Supports CF_1CF_0 ATP Synthase Accumulation in *Arabidopsis thaliana*. PloS one 10: doi: 10.1371/journal.pone.0121658

Fryer MJ (1992) The antioxidant effects of thylakoid Vitamin E (α‐tocopherol). Plant Cell & Environ 15: 381-392

Fucci L, Oliver CN, Coon MJ, Stadtman ER (1983) Inactivation of key metabolic enzymes by mixed-function oxidation reactions: possible implication in protein turnover and aging. Proc Natl Acad Sci USA 80: 1521-1525

Fujita M, Hossain MZ (2003) Modulation of pumpkin glutathione S-transferases by aldehydes and related compounds. Plant Cell Physiol 44: 481-490

Fujita T, Noguchi K, Terashima I (2013) Apoplastic mesophyll signals induce rapid stomatal responses to CO_2 in *Commelina communis*. New Phytol 199: 395-406

Fukayama H, Hatch MD, Tamai T, Tsuchida H, Sudoh S, Furbank RT, Miyao M (2003) Activity regulation and physiological impacts of maize C4-specific phosphoenolpyruvate carboxylase overproduced in transgenic rice plants. Photosynth Res 77: 227-239

Fulton DC, Stettler M, Mettler T, Vaughan CK, Li J, Francisco P, Gil M, Reinhold H, Eicke S, Messerli G, Dorken G, Halliday K, Smith AM, Smith SM, Zeeman SC (2008) β-AMYLASE4, a non-catalytic protein required for starch breakdown, acts upstream of three active β-amylases in *Arabidopsis* chloroplasts. Plant Cell 20: 1040-1058

Furbank RT, Badger MR (1983) Oxygen exchange associated with electron transport and photophosphorylation in spinach thylakoids. Biochim Biophys Acta Bioenerg 723: 400-409

Genty B, Briantais JM, Baker NR (1989) The relationship between the quantum yield of photosynthetic electron transport and quenching of chlorophyll fluorescence. Biochim Biophys Acta Gen Subj 990: 87-92

Gibon Y, Pyl ET, Sulpice R, Lunn JE, Höhne M, Günther M, Stitt M (2009) Adjustment of growth, starch turnover, protein content and central metabolism to a decrease of the carbon supply when Arabidopsis is grown in very short photoperiods. Plant Cell & Environ 32: 859-874

Gibon Y, Pyl ET, Sulpice R, Lunn JE, Höhne M, Günther M, Stitt M (2009) Adjustment of growth, starch turnover, protein content and central metabolism to a decrease of the carbon supply when *Arabidopsis* is grown in very short photoperiods. Plant Cell & Environ 32: 859-874

Gill SS, Tuteja N (2010) Reactive oxygen species and antioxidant machinery in abiotic stress tolerance in crop plants. Plant Physiol Biochem 48: 909–930

Golding AJ, Johnson GN (2003) Down-regulation of linear and activation of cyclic electron transport during drought. Planta 218: 107-114

Gotoh E, Matsumoto M, Ogawa KI, Kobayashi Y, Tsuyama M (2010) A qualitative analysis of the regulation of cyclic electron flow around photosystem I from the post-illumination chlorophyll fluorescence transient in *Arabidopsis*: a new platform for the *in vivo* investigation of the chloroplast redox state. Photosynth Res 103: 111-123

Grams G, Inglett GE (1972) Sensitized photooxidation of α-tocopherol and of 2, 2, 5, 7, 8-pentamethyl-6-chromanol in ethyl acetate. Lipids 7: 442-444

Gray GR, Savitch LV, Ivanov AG, Huner NP (1996) Photosystem II excitation pressure and development of resistance to photoinhibition (II. Adjustment of photosynthetic capacity in winter wheat and winter rye). Plant Physiol 110: 61–71.

Grieco M, Tikkanen M, Paakkarinen V, Kangasjärvi S, Aro EM (2012) Steady-state phosphorylation of light-harvesting complex II proteins preserves photosystem I under fluctuating white light. Plant Physiol 160: 1896–1910.

Groth G, Strotmann H (1999) New results about structure, function and regulation of the chloroplast ATP synthase (CF_0CF_1). Physiol Plant 106: 142-148

Heber U, Egneus H, Hanck U, Jensen M, Köster S (1978) Regulation of photosynthetic electron transport and photophosphorylation in intact chloroplasts and leaves of *Spinacia oleracea* L. Planta 143: 41-49

Heber U, Santarius K (1970) Direct and indirect transfer of ATP and ADP across the chloroplast envelope. Z Naturforsch B Chem Sci 25: 718-728

Heber U, Walker D (1992) Concerning a dual function of coupled cyclic electron transport in leaves. Plant Physiol 100: 1621-1626

Helliwell C, Waterhouse P (2003) Constructs and methods for high-throughput gene silencing in plants. Methods 30: 289-295

Hideg É, Kós PB, Vass I (2007) Photosystem II damage induced by chemically generated singlet oxygen in tobacco leaves. Physiol Plant 131: 33–40

Hisabori T, Konno H, Ichimura H, Strotmann H, Bald D (2002) Molecular devices of chloroplast F_1-ATP synthase for the regulation. Biochim Biophys Acta Bioenerg 1555: 140-146

Hisabori T, Kothen G, Strotmann H (1993) Effect of Covalent Binding of a Derivative of 2', 3'-O-(2, 4, 6-Trinitrophenyl). ADP to the Tight Binding Site of CF_1 on the Enzyme Activity. J Biochem 114: 324-328

Holzwarth AR, Miloslavina Y, Nilkens M, Jahns P (2009) Identification of two quenching sites active in the regulation of photosynthetic light-harvesting studied by time-resolved fluorescence. Chem Phys Lett 483: 262-267

Hoque M, Uraji M, Torii A, Banu M, Akhter N, Mori IC, Nakamura Y, Murata Y (2012a) Methylglyoxal inhibition of cytosolic ascorbate peroxidase from *Nicotiana tabacum*. J Biochem Mol Toxicol 26: 315-321

Hoque TS, Uraji M, Ye W, Hossain MA, Nakamura Y, Murata Y (2012b) Methylglyoxal-induced stomatal closure accompanied by peroxidase-mediated ROS production in *Arabidopsis*. J Plant Pysiol 169: 979-986

Hormann H, Neubauer C, Schreiber U (1994) An active Mehler-peroxidase reaction sequence can prevent cyclic PS I electron transport in the presence of dioxygen in intact spinach chloroplasts. Photosynth Res 41: 429-437

Hurry VM, Strand A, Tobiaeson M, Gardestrom P, Oquist G (1995) Cold hardening of spring and winter wheat and rape results in differential effects on growth, carbon metabolism, and carbohydrate content. Plant Physiol 109: 697–706

Häusler RE, Kleines M, Uhrig H, Hirsch HJ, Smets H (1999) Overexpression of phosphoenolpyruvate carboxylase from Corynebacterium glutamicum lowers the CO_2 compensation point (Γ*) and enhances dark and light respiration in transgenic potato. J Exp Bot 50: 1231-1242

Iba K, Gibson S, Nishiuchi T, Fuse T, Nishimura M, Arondel V, Hugly S, Somerville C (1993) A gene encoding a chloroplast ω-3 fatty acid desaturase complements alterations in fatty acid desaturation and chloroplast copy number of the *fad7* mutant of *Arabidopsis thaliana*. J Biol Chem 268: 24099-24105

Inoue K, Sakurai H, Hiyama T (1986) Photoinactivation sites of photosystem I in isolated chloroplasts. Plant Cell Physiol 27: 961-968

Ishida H, Nishimori Y, Sugisawa M, Makino A, Mae T (1997) The large subunit of ribulose-1,

5-bisphosphate carboxylase/oxygenase is fragmented into 37-kDa and 16-kDa polypeptides by active oxygen in the lysates of chloroplasts from primary leaves of wheat. Plant Cell Physiol 38: 471-479

Ishida H, Shimizu S, Makino A, Mae T (1998) Light-dependent fragmentation of the large subunit of ribulose-1, 5-bisphosphate carboxylase/oxygenase in chloroplasts isolated from wheat leaves. Planta 204: 305-309

Izui K, Matsumura H, Furumoto T, Kai Y (2004) Phosphoenolpyruvate carboxylase: a new era of structural biology. Annu Rev Plant Biol 55: 69-84

Izumi M, Hidema J, Makino A, Ishida H (2013) Autophagy contributes to nighttime energy availability for growth in *Arabidopsis*. Plant Physiol 161: 1682-1693

Jaganjac M, Tirosh O, Cohen G, Sasson S, Zarkovic N (2013) Reactive aldehydes–second messengers of free radicals in diabetes mellitus. Free Rad Res 47: 39-48

Jenner HL, Winning BM, Millar AH, Tomlinson KL, Leaver CJ, Hill SA (2001) NAD malic enzyme and the control of carbohydrate metabolism in potato tubers. Plant Physiol 126: 1139-1149

Jiao JA, Podestá FE, Chollet R, O'Leary MH, Andreo CS (1990) Isolation and sequence of an active-site peptide from maize leaf phosphoenolpyruvate carboxylase inactivated by pyridoxal 5′-phosphate. Biochim Biophys Acta Protein Struct Mol Enzymol 1041: 291-295

Johnson GN (2005) Cyclic electron transport in C3 plants: fact or artefact? J Exp Bot 56: 407-416

Joliot P, Béal D, Joliot A (2004) Cyclic electron flow under saturating excitation of dark-adapted *Arabidopsis* leaves. Biochim Biophys Acta Bioenerg 1656: 166-176

Joliot P, Joliot A (2002) Cyclic electron transfer in plant leaf. Proc Natl Acad Sci USA 99: 10209-10214

Joliot P, Joliot A (2005) Quantification of cyclic and linear flows in plants. Proc Natl Acad Sci USA 102: 4913-4918

Kaiser W (1976) The effect of hydrogen peroxide on CO_2 fixation of isolated intact chloroplasts. Biochim Biophys Acta Bioenerg 440: 476-482

Kaiser WM (1979) Reversible inhibition of the Calvin cycle and activation of oxidative pentose phosphate cycle in isolated intact chloroplasts by hydrogen peroxide. Planta 145: 377-382

Kalapos MP (2008) The tandem of free radicals and methylglyoxal. Chem Biol Interact 171: 251-271

Kalituho L, Beran KC, Jahns P (2007) The transiently generated nonphotochemical quenching of excitation energy in *Arabidopsis* leaves is modulated by zeaxanthin. Plant Physiol 143: 1861-1870

Kanazawa A, Kramer DM (2002) *In vivo* modulation of nonphotochemical exciton quenching (NPQ) by regulation of the chloroplast ATP synthase. Proc Natl Acad Sci USA 99: 12789-12794

Kanekatsu M, Saito H, Motohashi K, Hisabori T (1998) The β subunit of chloroplast ATP synthase (CF_0CF_1 - ATPase) is phosphorylated by casein kinase II. IUBMB Life 46: 99-105

Kelly AA, Froehlich JE, Dörmann P (2003) Disruption of the two digalactosyldiacylglycerol synthase genes DGD1 and DGD2 in *Arabidopsis* reveals the existence of an additional enzyme of galactolipid synthesis. Plant Cell 15: 2694-2706

Kirch HH, Bartels D, Wei Y, Schnable PS, Wood AJ (2004) The ALDH gene superfamily of *Arabidopsis*. Trends Plant Sci 9: 371-377

Klughammer C, Kolbowski J, Schreiber U (1990) LED array spectrophotometer for measurement of time resolved difference spectra in the 530–600 nm wavelength region. Photosynth Res 25: 317-327

Klughammer C, Schreiber U (1994) An improved method, using saturating light pulses, for the determination of photosystem I quantum yield via P700+-absorbance changes at 830 nm. Planta 192: 261–268

Klughammer C, Siebke K, Schreiber U (2013) Continuous ECS-indicated recording of the proton-motive charge flux in leaves. Photosynth Res 117: 471-487

Kobayashi D, Tamoi M, Iwaki T, Shigeoka S, Wadano A (2003) Molecular characterization and redox regulation of phosphoribulokinase from the cyanobacterium *Synechococcus* sp. PCC 7942. Plant Cell Physiol 44: 269-276

Kobayashi F, Takumi S, Nakata M, Ohno R, Nakamura T, Nakamura C (2004) Comparative study of the expression profiles of the *Cor*/*Lea* gene family in two wheat cultivars with contrasting levels of freezing tolerance. Physiol Plant 120: 585–594

Kohzuma K, Cruz JA, Akashi K, Hoshiyasu S, Munekage YN, Yokota A, Kramer DM (2009) The long‐term responses of the photosynthetic proton circuit to drought. Plant Cell & Environ 32: 209-219

Kohzuma K, Dal Bosco C, Meurer J, Kramer DM (2013) Light-and metabolism-related regulation of the chloroplast ATP synthase has distinct mechanisms and functions. J Biol Chem 288: 13156-13163

Kojima K, Oshita M, Nanjo Y, Kasai K, Tozawa Y, Hayashi H, Nishiyama Y (2007) Oxidation of elongation factor G inhibits the synthesis of the D1 protein of photosystem II. Mol Microbiol 65: 936-947

Kono M, Noguchi K, Terashima I (2014) Roles of the cyclic electron flow around PSI (CEF-PSI) and O_2-dependent alternative pathways in regulation of the photosynthetic electron flow in short-term fluctuating light in *Arabidopsis thaliana*. Plant Cell Physiol 55: 990–1004

Kotchoni SO, Kuhns C, Ditzer A, Kirch HH, Bartels D (2006) Over-expression of different aldehyde dehydrogenase genes in Arabidopsis thaliana confers tolerance to abiotic stress and protects plants against lipid peroxidation and oxidative stress. Plant Cell & Environ 29: 1033-1048

Kotchoni SO, Kuhns C, Ditzer A, Kirch HH, Bartels D (2006) Over-expression of different aldehyde dehydrogenase genes in *Arabidopsis thaliana* confers tolerance to abiotic stress and protects plants against lipid peroxidation and oxidative stress. Plant Cell & Environ. 29: 1033-1048

Kozaki A, Takeba G (1996) Photorespiration protects C3 plants from photooxidation. Nature 384:

557-560

Kozuleva MA, Ivanov BN (2010) Evaluation of the participation of ferredoxin in oxygen reduction in the photosynthetic electron transport chain of isolated pea thylakoids. Photosynth Res 105: 51–61

Kozuleva MA, Petrova AA, Mamedov MD, Semenov AY, and Ivanov BN (2014) O_2 reduction by photosystem I involves phylloquinone under steady-state illumination. FEBS Lett 588: 4364–4368

Kramer DM, Avenson TJ, Edwards GE (2004a) Dynamic flexibility in the light reactions of photosynthesis governed by both electron and proton transfer reactions. Trends in Plant Sci 9: 349-357

Kramer DM, Crofts AR (1989) Activation of the chloroplast ATPase measured by the electrochromic change in leaves of intact plants. Biochim Biophys Acta Bioenerg 976: 28-41

Kramer DM, Cruz JA, Kanazawa A (2003) Balancing the central roles of the thylakoid proton gradient. Trends in Plant Sci 8: 27-32

Kramer DM, Evans JR (2011) The importance of energy balance in improving photosynthetic productivity. Plant Physiol 155: 70-78

Kramer DM, Johnson G, Kiirats O, Edwards GE (2004b) New fluorescence parameters for the determination of Q_A redox state and excitation energy fluxes. Photosynth Res 79: 209-218

Kramer DM, Sacksteder CA, Cruz JA (1999) How acidic is the lumen? Photosynth Res 60: 151-163

Kramer PJ, Boyer JS (1995) Water relations of plants and soils. Academic press. Elsevier Science

Krieger A, Weis E (1993) The role of calcium in the pH-dependent control of photosystem II. Photosynth Res 37: 117-130

Krieger-Liszkay A (2005) Singlet oxygen production in photosynthesis. J Exp Bot 56: 337–346

Kurisu G, Zhang H, Smith JL, Cramer WA (2003) Structure of the cytochrome b_6f complex of oxygenic photosynthesis: tuning the cavity. Science 302: 1009-1014

Kötting O, Pusch K, Tiessen A, Geigenberger P, Steup M, Ritte G (2005) Identification of a novel enzyme required for starch metabolism in *Arabidopsis* leaves. The phosphoglucan, water dikinase. Plant Physiol 137: 242-252

Külheim C, Ågren J, Jansson S (2002) Rapid regulation of light harvesting and plant fitness in the field. Science 297: 91–93

Laemmli UK (1970) Cleavage of structural proteins during the assembly of the head of bacteriophage T4. Nature 227: 680-685

Laisk A, Eichelmann H, Oja V, Peterson RB (2005) Control of cytochrome b_6f at low and high light intensity and cyclic electron transport in leaves. Biochim Biophys Acta Bioenerg 1708: 79-90

Laisk A, Eichelmann H, Oja V, Talts E, Scheibe R (2007) Rates and roles of cyclic and alternative

electron flow in potato leaves. Plant Cell Physiol 48: 1575-1588

Laisk A, Talts E, Oja V, Eichelmann H, Peterson RB (2010) Fast cyclic electron transport around photosystem I in leaves under far-red light: a proton-uncoupled pathway? Photosynth Res 103: 79-95

Lepiniec L, Vidal J, Chollet R, Gadal P, Crétin C (1994) Phosphoenolpyruvate carboxylase: structure, regulation and evolution. Plant Sci 99: 111-124

Li XP, BjoÈrkman O, Shih C, Grossman AR, Rosenquist M, Jansson S, Niyogi KK (2000) A pigment-binding protein essential for regulation of photosynthetic light harvesting. Nature 403: 391-395

Makino A, Mae T, Ohira K (1988) Differences between wheat and rice in the enzymic properties of ribulose-1, 5-bisphosphate carboxylase/oxygenase and the relationship to photosynthetic gas exchange. Planta 174: 30-38

Makino A, Osmond B (1991) Effects of nitrogen nutrition on nitrogen partitioning between chloroplasts and mitochondria in pea and wheat. Plant Physiol 96: 55-362

Mano J, Belles-Boix E, Babiychuk E, Inzé D, Torii Y, Hiraoka E, Takimoto K, Slooten L, Asada K, Kushnir S (2005) Protection against photooxidative injury of tobacco leaves by 2-alkenal reductase. Detoxication of lipid peroxide-derived reactive carbonyls. Plant Physiol 139: 1773-1783

Mano J, Khorobrykh S, Matsui K, Iijima Y, Sakurai N, Suzuki H, Shibata D (2014a) Acrolein is

formed from trienoic fatty acids in chloroplast: A targeted metabolomics approach. Plant Biotechnol doi: 10.5511/plantbiotechnology.14.1112a

Mano J, Miyatake F, Hiraoka E, Tamoi M (2009) Evaluation of the toxicity of stress-related aldehydes to photosynthesis in chloroplasts. Planta 230: 639-648

Mano J, Nagata M, Okamura S, Shiraya T, Mitsui T (2014b) Identification of oxidatively modified proteins in salt-stressed *Arabidopsis*: a carbonyl-targeted proteomics approach. Plant Cell Physiol 55: 1233-1244

Mano J, Torii Y, Hayashi SI, Takimoto K, Matsui K, Nakamura K, Inzé D, Babiychuk E, Kushnir S, Asada K (2002) The NADPH: quinone oxidoreductase P1-ζ-crystallin in Arabidopsis catalyzes the α, β-hydrogenation of 2-alkenals: detoxication of the lipid peroxide-derived reactive aldehydes. Plant Cell Physiol 43: 1445-1455

Martin W, Scheibe R, Schnarrenberger C (2000) The Calvin cycle and its regulation. In Leegood RC, Sharkey TD and Von Caemmerer S (Eds.) Photosynthesis. Springer Netherlands. (pp. 9-51).

Mavric, E., Wittman, S., Barth, G. and Henle, T. (2008) Identification and quantification of methylglyoxal as the dominant antibacterial constituent of Manuk (Leptospermum scoparium) honeys from New Zealand. Mol Nutr Food Res 52: 483-489

McConn M, Hugly S, Somerville C (1994) A mutation at the *fad8* locus of Arabidopsis identifies a second chloroplast ω-3 desaturase. Plant Physiol 106: 1609-1614

McCord JM, Fridovich I (1969) Superoxide dismutase an enzymic function for erythrocuprein

(hemocuprein). J Biol Chem 244: 6049–6055

Medina-Navarro, R., Duran-Reys, G., Diaz-Flores, M. and Diaz-Rodriguez, M. (2003) Glucose autooxidation produce acrolein from lipid peroxidation *in vitro*. Clin Chim Acta 337: 183-185

Melis A (1999) Photosystem-II damage and repair cycle in chloroplasts: what modulates the rate of photodamage *in vivo* ? Trends Plant Sci 4: 130–135

Millar AH, Leaver CJ, Hill SA (1999) Characterization of the dihydrolipoamide acetyltransferase of the mitochondrial pyruvate dehydrogenase complex from potato and comparisons with similar enzymes in diverse plant species. Eur J Biochem 264: 973-981

Misra HP, Fridovich I (1971) The generation of superoxide radical during the autoxidation of ferredoxins. J Biol Chem 246: 6886–6890

Mittler R (2006) Abiotic stress, the field environment and stress combination. Trends Plan Sci 11: 15-19

Miyake C (2010) Alternative electron flows (water–water cycle and cyclic electron flow around PSI) in photosynthesis: molecular mechanisms and physiological functions. Plant Cell Physiol 51: 1951-1963

Miyake C, Asada K (1992) Thylakoid-bound ascorbate peroxidase in spinach chloroplasts and photoreduction of its primary oxidation product monodehydroascorbate radicals in thylakoids. Plant Cell Physiol 33: 541–553

Miyake C, Horiguchi S, Makino A, Shinzaki Y, Yamamoto H, Tomizawa KI (2005a) Effects of light intensity on cyclic electron flow around PSI and its relationship to non-photochemical quenching of Chl fluorescence in tobacco leaves. Plant Cell Physiol 46: 1819-1830

Miyake C, Miyata M, Shinzaki Y, Tomizawa KI (2005b) CO_2 response of cyclic electron flow around PSI (CEF-PSI) in tobacco leaves—relative electron fluxes through PSI and PSII determine the magnitude of non-photochemical quenching (NPQ) of Chl fluorescence. Plant Cell Physiol 46: 629-637

Miyake C, Okamura M (2003) Cyclic electron flow within PSII protects PSII from its photoinhibition in thylakoid membranes from spinach chloroplasts. Plant Cell Physiol 44: 457–462

Miyake C, Schreiber U, Hormann H, Sano S, Asada K (1998) The FAD-enzyme monodehydroascorbate radical reductase mediates photoproduction of superoxide radicals in spinach thylakoid membranes. Plant Cell Physiol 39: 821–829

Miyake C, Shinzaki Y, Miyata M, Tomizawa KI (2004) Enhancement of cyclic electron flow around PSI at high light and its contribution to the induction of non-photochemical quenching of Chl fluorescence in intact leaves of tobacco plants. Plant Cell Physiol 45: 1426-1433

Miyashita K, Tanakamaru S, Maitani T, Kimura K (2005) Recovery responses of photosynthesis, transpiration, and stomatal conductance in kidney bean following drought stress. Environ Exp Bot 53: 205-214

Miyata T, Kurokawa K, De Strikou CVY (2000) Advanced glycation and lipoxidation end products

role of reactive carbonyl compounds generated during carbohydrate and lipid metabolism. J Am Soc Nephrol 11: 1744-1752

Mizokami Y, Noguchi K, Kojima M, Sakakibara H, Terashima I (2015) Mesophyll conductance decreases in the wild type but not in an ABA‐deficient mutant (*aba1*) of *Nicotiana plumbaginifolia* under drought conditions. Plant Cell & Environ 38: 388-398

Mundree SG, Whittaker A, Thomson JA, Farrant JM (2000) An aldose reductase homolog from the resurrection plant *Xerophyta viscosa* Baker. Planta 211: 693-700

Munekage Y, Hojo M, Meurer J, Endo T, Tasaka M, Shikanai T (2002) PGR5 is involved in cyclic electron flow around photosystem I and is essential for photoprotection in *Arabidopsis*. Cell 110: 361-371

Munekage YN, Genty B, Peltier G (2008) Effect of PGR5 impairment on photosynthesis and growth in *Arabidopsis thaliana*. Plant Cell Physiol 49: 1688–1698

Munns R, Tester M (2008) Mechanisms of salinity tolerance. Annu Rev Plant Biol 59: 651-681

Munné-Bosch S (2005) The role of α-tocopherol in plant stress tolerance. J Plant Physiol 162: 743-748

Møller IM, Jensen PE, Hansson A (2007) Oxidative modifications to cellular components in plants. Annu Rev Plant Biol 58: 459-481

Müller P, Li XP, Niyogi KK (2001) Non-photochemical quenching. A response to excess light energy.

Plant Physiol 125: 1558-1566

Naito Y, Yamada T, Matsumiya T, Ui-Tei K, Saigo K, Morishita S (2005) ds Check: highly sensitive off-target search software for double-stranded RNA-mediated RNA interference. Nucleic Acids Res 33: W589-W591

Nakagawa T, Suzuki T, Murata S, Nakamura S, Hino T, Maeo K, Tabata R, Kawai T, Tanaka K, Niwa Y, Watanabe Y, Nakamura K, Kimura T, Ishiguro S (2007) Improved Gateway binary vectors: high-performance vectors for creation of fusion constructs in transgenic analysis of plants. Biosci Biotechnol Biochem 71: 2095-2100.

Nandha B, Finazzi G, Joliot P, Hald S, Johnson GN (2007) The role of PGR5 in the redox poising of photosynthetic electron transport. Biochim Biophys Acta Bioenerg 1767: 1252-1259

Nelson N, Yocum CF (2006) Structure and function of photosystem I and II. Annu Rev Plant Biol 57: 521-565

Niittylä T, Messerli G, Trevisan M, Chen J, Smith AM, Zeeman SC (2004) A previously unknown maltose transporter essential for starch degradation in leaves. Science 303: 87-89

Nilkens M, Kress E, Lambrev P, Miloslavina Y, Müller M, Holzwarth AR, Jahns P (2010) Identification of a slowly inducible zeaxanthin-dependent component of non-photochemical quenching of chlorophyll fluorescence generated under steady-state conditions in *Arabidopsis*. Biochim Biophys Acta Bioenerg 1797: 466-475

Nishikawa Y, Yamamoto H, Okegawa Y, Wada S, Sato N, Taira Y, Sugimoto K, Makino A, Shikanai

T (2012) PGR5-dependent cyclic electron transport around PSI contributes to the redox homeostasis in chloroplasts rather than CO_2 fixation and biomass production in rice. Plant Cell Physiol 53: 2117-2126

Nishiyama Y, Allakhverdiev SI, Murata N (2011) Protein synthesis is the primary target of reactive oxygen species in the photoinhibition of photosystem II. Physiol Plant 142: 35–46

Nishiyama Y, Allakhverdiev SI, Yamamoto H, Hayashi H, Murata N (2004) Singlet oxygen inhibits the repair of photosystem II by suppressing the translation elongation of the D1 protein in *Synechocystis* sp. PCC 6803. Biochemistry 43: 11321-11330

Niyogi KK, Grossman AR, Björkman O (1998) *Arabidopsis* mutants define a central role for the xanthophyll cycle in the regulation of photosynthetic energy conversion. Plant Cell 10: 1121-1134

Niyogi KK, Li XP, Rosenberg V, Jung HS (2005) Is PsbS the site of non-photochemical quenching in photosynthesis? J Exp Bot 56: 375-382

Noguchi K, Yamori W, Hikosaka K, Terashima I (2015) Homeostasis of the temperature sensitivity of respiration over a range of growth temperatures indicated by a modified Arrhenius model. New Phytol 207: 34-42

Oberschall A, Deák M, Török K, Sass L, Vass I, Kovács I, Fehrér A, Dudits D, Horváth GV (2000) A novel aldose/aldehyde reductase protects transgenic plants against lipid peroxidation under chemical and drought stresses. Plant J 24: 437-446

Oelze ML, Vogel MO, Alsharafa K, Kahmann U, Viehhauser A, Maurino VG, Dietz KJ (2011) Efficient acclimation of the chloroplast antioxidant defence of Arabidopsis thaliana leaves in response to a 10-or 100-fold light increment and the possible involvement of retrograde signals. J Exp Bot 63: 1297–1313

Okegawa Y, Kagawa Y, Kobayashi Y, Shikanai T (2008) Characterization of factors affecting the activity of photosystem I cyclic electron transport in chloroplasts. Plant Cell Physiol 49: 825-834

Okumura KI, Goh T, Toyokura K, Kasahara H, Takebayashi Y, Mimura T, Kamiya Y, Fukaki H (2013) GNOM/FEWER ROOTS is required for the establishment of an auxin response maximum for arabidopsis lateral root initiation. Plant Cell Physiol 54: 406-417

Osmond CB, Grace SC (1995) Perspectives on photoinhibition and photorespiration in the field: quintessential inefficiencies of the light and dark reactions of photosynthesis? J Exp Bot 46: 1351-1362

Palatnik JF, Carrillo N, Valle EM (1999) The role of photosynthetic electron transport in the oxidative degradation of chloroplastic glutamine synthetase. Plant Physiol 121: 471-478

Pamplona R (2011) Advanced lipoxidation end-products. Chem-Biol Interact 192: 14-20

Papdi C, Ábrahám E, Joseph MP, Popescu C, Koncz C, Szabados L (2008) Functional identification of *Arabidopsis* stress regulatory genes using the controlled cDNA overexpression system. Plant Physiol 147: 528-542

Paulus C, Köllner B, Jacobsen H-J (1993) Physiological and biochemical characterization of glyoxalase I, a general marker for cell proliferation, from a soybean cell suspension. Planta 189: 561-566

Pfündel E, Klughammer C, Schreiber U (2008) Monitoring the effects of reduced PS II antenna size on quantum yields of photosystems I and II using the Dual-PAM-100 measuring system. PAM Appl Notes 1: 21-24

Phillips SA, Thornalley PJ (1993) The formation of methylglyoxal from triose phosphates investigation using a specific assay for methylglyoxal. Eur J Biochem 212: 101-105

Pocock TH, Hurry V, Savitch LV, Huner N (2001) Susceptibility to low‐temperature photoinhibition and the acquisition of freezing tolerance in winter and spring wheat: The role of growth temperature and irradiance. Physiol Plant 113: 499–506

Podesta FE, Iglesias AA, Andreo CS (1986) Modification of an essential amino group of phosphoenolpyruvate carboxylase from maize leaves by pyridoxal phosphate and by pyridoxal phosphate-sensitized photooxidation. Arch Biochem Biophys 246: 546-553

Poon HF (2009) Redox proteomics and bioinformatics. Identification of oxidized proteins and their pharmacological modulation: Insights into oxidative stress in age-related cognitive impairment. (LAP LAMBERT Academic Publishing), pp. 54-83

Porra RJ, Thompson WA, Kriedemann PE (1989) Determination of accurate extinction coefficients and simultaneous equations for assaying chlorophylls a and b extracted with four different solvents: verification of the concentration of chlorophyll standards by atomic absorption

spectroscopy. Biochim Biophys Acta Bioenerg 975: 384-394

Porra RJ, Thompson WA, Kriedemann PE (1989) Determination of accurate extinction coefficients and simultaneous equations for assaying chlorophylls *a* and *b* extracted with four different solvents: verification of the concentration of chlorophyll standards by atomic absorption spectroscopy. Biochim Biophys Acta Bioenerg 975: 384-394

Qiu Q-S, Huber JL, Booker FL, Jain V, Leakey ADB, Fiscus EL, Yau PM, Ort DR, Huber SC (2008) Increasing protein carbonylation in leaves of *Arabidopsis* and soybean in response to elevated [CO_2]. Photosynth Res 97: 155-166

Rademacher T, Häusler RE, Hirsch HJ, Zhang L, Lipka V, Weier D, Kreuzaler F, Peterhänsel C (2002) An engineered phosphoenolpyruvate carboxylase redirects carbon and nitrogen flow in transgenic potato plants. Plant J 32: 25-39

Reich PB, Walters MB, Tjoelker MG, Vanderklein D, Buschena C (1998) Photosynthesis and respiration rates depend on leaf and root morphology and nitrogen concentration in nine boreal tree species differing in relative growth rate. Funct Ecol 12: 395-405

Ren D, Yang H, Zhang S (2002) Cell death mediated by MAPK is associated with hydrogen peroxide production in *Arabidopsis*. J Biol Chem 277: 559-565

Richard JP (1991) Kinetic parameters for the elimination reaction catalyzed by triosephosphate isomerase and an estimation of the reaction's physiological significance. Biochemistry 30: 4581-4585

Rodrigues SM, Andrade MO, Gomes APS, DaMatta FM, Baracat-Pereira MC, Fontes EP (2006) *Arabidopsis* and tobacco plants ectopically expressing the soybean antiquitin-like *ALDH7* gene display enhanced tolerance to drought, salinity, and oxidative stress. J Exp Bot 57: 1909-1918

Rott M, Martins NF, Thiele W, Lein W, Bock R, Kramer DM, Schöttler MA (2011) ATP synthase repression in tobacco restricts photosynthetic electron transport, CO_2 assimilation, and plant growth by overacidification of the thylakoid lumen. Plant Cell 23: 304-321

Rutherford AW, Osyczka A, Rappaport F (2012) Back-reactions, short-circuits, leaks and other energy wasteful reactions in biological electron transfer: redox tuning to survive life in O_2. FEBS Lett 586: 603–616

Ruuska SA, Badger MR, Andrews TJ, von Caemmerer S (2000) Photosynthetic electron sinks in transgenic tobacco with reduced amounts of Rubisco: little evidence for significant Mehler reaction. J Exp Bot 51: 357-368

Sacksteder CA, Kramer DM (2000) Dark-interval relaxation kinetics (DIRK) of absorbance changes as a quantitative probe of steady-state electron transfer. Photosynth Res 66: 145-158

Saito R, Shimakawa G, Nishi A, Iwamoto T, Sakamoto K, Yamamoto H, Amako K, Makino A, Miyake C (2013) Functional Analysis of the AKR4C Subfamily of *Arabidopsis thaliana*: model structures, substrate specificity, acrolein toxicity, and responses to light and [CO_2]. Biosci Biotechnol Biochem 77: 2038-2045

Saito R, Yamamoto H, Makino A, Sugimoto T, Miyake C (2011) Methylglyoxal functions as hill oxidant and stimulates the photoreduction of O_2 at photosystem I: a symptom of plant diabetes.

Plant Cell & Environ 34: 1454-1464

Santelia D, Kötting O, Seung D, Schubert M, Thalmann M, Bischof S, Meekins DA, Lutz A, Patron N, Gentry MS, Allain FHT, Zeeman SC (2011) The phosphoglucan phosphatase like sex Four2 dephosphorylates starch at the C3-position in *Arabidopsis*. Plant Cell 23: 4096-4111

Sato T (1968) A modified method for lead staining of thin sections. J Electron Microsc 17: 158–159

Satoh K (1970) Mechanism of photoinactivation in photosynthetic systems II. The occurrence and properties of two different types of photoinactivation. Plant Cell Physiol 11: 29–38

Savitch LV, Harney T, Huner N (2000) Sucrose metabolism in spring and winter wheat in response to high irradiance, cold stress and cold acclimation. Physiol Plant 108: 270–278

Sawada S, Usuda H, Hasegawa Y, Tsukui T (1990) Regulation of ribulose-l, 5-bisphosphate carboxylase activity in response to changes in the source/sink balance in single-rooted soybean leaves: The role of inorganic orthophosphate in activation of the enzyme. Plant Cell Physiol 31: 697-704

Scheller HV, Haldrup A (2005) Photoinhibition of photosystem I. Planta 221: 5-8

Schreiber U, Neubauer C (1990) O_2-dependent electron flow, membrane energization and the mechanism of non-photochemical quenching of chlorophyll fluorescence. Photosynth Res 25: 279-293

Schreiber U, Reising H, Neubauer C (1991) Contrasting pH-optima of light-driven O_2-and

H_2O_2-reduction in spinach chloroplasts as measured via chlorophyll fluorescence quenching. Z Naturforsch C Bio Sci 46: 635-643

Schöttler MA, Tóth SZ, Boulouis A, Kahlau S (2015) Photosynthetic complex stoichiometry dynamics in higher plants: biogenesis, function, and turnover of ATP synthase and the cytochrome b_6f complex. J Exp Bot 66: 2373-2400

Sejima T, Hanawa H, Shimakawa G, Takagi D, Suzuki Y, Fukayama H, Makino A, Miyake C (2015) Post‐illumination transient O_2‐uptake is driven by photorespiration in tobacco leaves. Physiol Plant doi: 10.1111/ppl.12388

Sejima T, Takagi D, Fukayama H, Makino A, Miyake C (2014) Repetitive Short-Pulse Light Mainly Inactivates Photosystem I in Sunflower Leaves. Plant Cell Physiol 55: 1184–1193

Shapiro JB, Griffin KL, Lewis JD, Tissue DT (2004) Response of *Xanthium strumarium* leaf respiration in the light to elevated CO_2 concentration, nitrogen availability and temperature. New Phytol 162: 377-386

Shi J, Yi K, Liu Y, Xie L, Zhou Z, Chen Y, Hu Z, Zheng T, Liu R, Chen Y, Chen J (2015) Phosphoenolpyruvate carboxylase in *Arabidopsis* leaves plays a crucial role in carbon and nitrogen metabolism. Plant Physiol 167: 671-681

Shikanai T (2007) Cyclic electron transport around photosystem I: genetic approaches. Annu Rev Plant Biol 58: 199-217

Shin JH, Kim SR, An G (2009) Rice aldehyde dehydrogenase7 is needed for seed maturation and

viability. Plant Physiol 149: 905-915

Shirao M, Kuroki S, Kaneko K, Kinjo Y, Tsuyama M, Förster B, Takahashi S, Badger MR (2013) Gymnosperms have increased capacity for electron leakage to oxygen (Mehler and PTOX reactions) in photosynthesis compared with angiosperms. Plant Cell Physiol 54: 1152-1163

Shuvalov VA, Nuijs AM, Van Gorkom HJ, Smit HWJ, Duysens LNM (1986) Picosecond absorbance changes upon selective excitation of the primary electron donor P-700 in photosystem I. Biochim Biophys Acta Bioenerg 850: 319-323

Simpson PJ, Tanitadapitak C, Reed AM, Mather OC, Bunce CM, White SA, Ride JP (2009) Characterization of two novel aldo–keto reductases from *Arabidopsis*: expression patterns, broad substrate specificity, and an open active-site structure suggest a role in toxicant metabolism following stress. J Mol Biol 392: 465-480

Singla-Pareek SL, Reddy MK, Sopory SK (2003) Genetic engineering of the glyoxalase pathway in tobacco leads to enhanced salinity tolerance. Proc Natl Acad Sci USA 100: 14672-14677

Smith SM, Fulton DC, Chia T, Thorneycroft D, Chapple A, Dunstan H, Hylton C, Zeeman SC, Smith AM (2004) Diurnal changes in the transcriptome encoding enzymes of starch metabolism provide evidence for both transcriptional and post-transcriptional regulation of starch metabolism in *Arabidopsis* leaves. Plant Physiol 136: 2687-2699

Sonoike K (1995) Selective photoinhibition of photosystem I in isolated thylakoid membranes from cucumber and spinach. Plant Cell Physiol 36: 825–830

Sonoike K (1996a) Degradation of *psaB* gene product, the reaction center subunit of photosystem I, is caused during photoinhibition of photosystem I: possible involvement of active oxygen species. Plant Sci 115: 157–164

Sonoike K (1996b) Photoinhibition of photosystem I: its physiological significance in the chilling sensitivity of plants. Plant Cell Physiol 37: 239-247

Sonoike K (2011) Photoinhibition of photosystem I. Physiol Plant 142: 56-64

Sonoike K, Kamo M, Hihara Y, Hiyama T, Enami I (1997) The mechanism of the degradation of psaB gene product, one of the photosynthetic reaction center subunits of photosystem I, upon photoinhibition. Photosynth Res 53: 55-63

Sonoike K, Terashima I (1994) Mechanism of photosystem-I photoinhibition in leaves of *Cucumis sativus* L. Planta 194: 287–293

Sonoike K, Terashima I, Iwaki M, Itoh S (1995) Destruction of photosystem I iron-sulfur centers in leaves of *Cucumis sativus* L. by weak illumination at chilling temperatures. FEBS Lett 362: 235–238

Spurr AR (1969) A low-viscosity epoxy resin embedding medium for electron microscopy. J Ultrastruct Res 26: 31–43

Stadtman ER, Levine RL (2003) Free radical-mediated oxidation of free amino acids and amino acid residues in proteins. Amino Acids 25: 207-218

Stiti N, Missihoun TD, Kotchoni S, Kirch HH, Bartels D (2011) Aldehyde dehydrogenases in *Arabidopsis thaliana*: biochemical requirements, metabolic pathways, and functional analysis. Front. Plant Sci 2: 1-11

Stocker TF, Qin D, Plattner GK, Tignor M, Allen SK, Boschung J, Nauels A, Xia Y, Bex V, Midgley PM, eds. IPCC, 2013: Summary for Policymakers. In: Climate Change 2013: The Physical Science Basis. Contribution of Working Group I to the Fifth Assessment Report of the Intergovernmental Panel on Climate Change. Cambridge University Press, Cambridge, United Kingdom and New York, NY, USA.

Stroebel D, Choquet Y, Popot JL, Picot D (2003) An atypical haem in the cytochrome b_6f complex. Nature 426: 413-418

Sunkar R, Bartels D, Kirch H-H (2003) Overexpression of a stress-inducible aldehyde dehydrogenase gene from *Arabidopsis thaliana* in transgenic plants improves stress tolerance. Plant J 35: 452-464

Suorsa M, Järvi S, Grieco M, Nurmi M, Pietrzykowska M, Rantala M, Kangasjärvi S, Paakkarinen V, Tikkanen M, Jansson S, Aro EM (2012) PROTON GRADIENT REGULATION5 is essential for proper acclimation of *Arabidopsis* photosystem I to naturally and artificially fluctuating light conditions. Plant Cell 24: 2934–2948

Takagi D, Miyake C (2014) The evaluation of Alternative electron flow (AEF) activity based on the kinetic parameters, and the physiological role of O_2-dependent AEF in plants. 光合成研究 News letter 24: 97-110

Takagi D, Yamamoto H, Amako K, Makino A, Sugimoto T, Miyake C (2012) O_2 supports 3-phosphoglycerate-dependent O_2 evolution in chloroplasts from spinach leaves. Soil Sci Plant Nutr 58: 462-468

Takahashi M, Asada K (1982) Dependence of oxygen affinity for Mehler reaction on photochemical activity of chloroplast thylakoids. Plant Cell Physiol 23: 1457-1461

Takahashi M, Asada K (1988) Superoxide production in aprotic interior of chloroplast thylakoids. Arch Biochem Biophys 267: 714-722

Takahashi S, Badger MR (2011) Photoprotection in plants: a new light on photosystem II damage. Trends in Plant Sci 16: 53-60

Takizawa K, Cruz JA, Kanazawa A, Kramer DM (2007) The thylakoid proton motive force in vivo. Quantitative, non-invasive probes, energetics, and regulatory consequences of light-induced *pmf*. Biochim Biophys Acta Bioenerg 1767: 1233-1244

Takizawa K, Kanazawa A, Kramer DM (2008) Depletion of stromal Pi induces high ‘energy‐dependent’ antenna exciton quenching (qE) by decreasing proton conductivity at CF_0‐CF_1 ATP synthase. Plant Cell & Environ 31: 235-243

Tamoi M, Ishikawa T, Takeda T, Shigeoka S (1996a) Molecular characterization and resistance to hydrogen peroxide of two fructose-1, 6-bisphosphatases from *Synechococcus* PCC 7942. Arch Biochem Biophys 334: 27-36

Tamoi M, Ishikawa T, Takeda T, Shigeoka S (1996b) Enzymic and molecular characterization of

NADP-dependent glyceraldehyde-3-phosphate dehydrogenase from *Synechococcus* PCC 7942: resistance of the enzyme to hydrogen peroxide. Biochem J 316: 685-690

Tcherkez G, Bligny R, Gout E, Mahé A, Hodges M, Cornic G (2008) Respiratory metabolism of illuminated leaves depends on CO_2 and O_2 conditions. Proc Natl Acad Sci USA 105: 797-802

Tcherkez G, Cornic G, Bligny R, Gout E, Ghashghaie J (2005) *In vivo* respiratory metabolism of illuminated leaves. Plant Physiol 138: 1596-1606

Telfer A (2014) Singlet oxygen production by PSII under light stress: mechanism, detection and the protective role of β-carotene. Plant Cell Physiol 55: 1216-1223

Terashima I, Funayama S, Sonoike K (1994) The site of photoinhibition in leaves of *Cucumis sativus* L. at low temperatures is photosystem I, not photosystem II. Planta 193: 300–306

Terashima I, Kashino Y, Katoh S (1991a) Exposure of leaves of *Cucumis sativus* L. to low temperatures in the light causes uncoupling of thylakoids I. Studies with isolated thylakoids. Plant Cell Physiol 32: 1267-1274

Terashima I, Sonoike K, Kawazu T, Katoh S (1991b) Exposure of leaves of Cucumis sativus L. to low temperatures in the light causes uncoupling of thylakoids II. Non-destructive measurements with intact leaves. Plant Cell Physiol 32: 1275-1283

Thornalley PJ (2006) Quantitative screening of protein glycation, oxidation, and nitration adducts by LC-MS/MS: protein damage in diabetes, uremia, cirrhosis, and alzheimer's disease. In Redox Proteomics: from Protein Modifications to Cellular Dysfunction and Diseases. (eds I.

Dalle-Donne, A. Scaloni & D.A. Butterfield), John Willey & Sons, New Jersey, pp. 681-727

Thornalley PJ, Langborg A, Minhas HS (1999) Formation of glyoxal, methylglyoxal and 3-deoxyglucosone in the glycation of proteins by glucose. Biochem J 344: 109-116

Tikhonov AN (2013) pH-Dependent regulation of electron transport and ATP synthesis in chloroplasts. Photosynth Res 116: 511–534

Tikkanen M, Aro EM (2014) Integrative regulatory network of plant thylakoid energy transduction. Trends in Plant Sci 19: 10-17

Tikkanen M, Suorsa M, Gollan PJ, Aro EM (2012) Post-genomic insight into thylakoid membrane lateral heterogeneity and redox balance. FEBS Lett 586: 2911-2916

Tjus SE, Møller BL, Scheller HV (1998) Photosystem I is an early target of photoinhibition in barley illuminated at chilling temperatures. Plant Physiol 116: 755-764

Tjus SE, Scheller HV, Anderson B, Møller BL (2001) Active oxygen produced during selective excitation of photosystem I is damaging not only to photosystem I, but also to photosystem II. Plant Physiol 125: 2007-2015

Trouillard M, Shahbazi M, Moyet L, Rappaport F, Joliot P, Kuntz M, Finazzi G (2012) Kinetic properties and physiological role of the plastoquinone terminal oxidase (PTOX) in a vascular plant. Biochim Biophys Acta Bioenerg 1817: 2140-2148

Turóczy Z, Kis P, Török K, Cserháti M, Lendvai Á, Dudits D, Horváth GV (2011) Over-production

of a rice aldo–keto reductase increases oxidative and heat stress tolerance by malondialdehyde and methylglyoxal detoxification. Plant Mol Biol 75: 399-412

Vass I (2011) Role of charge recombination processes in photodamage and photoprotection of the photosystem II complex. Physiol Plant 142: 6–16

Villar R, Held AA, Merino J (1995) Dark leaf respiration in light and darkness of an evergreen and a deciduous plant species. Plant Physiol 107: 421-427

Vistoli G, De Maddis D, Cipak A, Zarkovic N, Carini M, Aldini G (2013) Advanced glycoxidation and lipoxidation end products (AGEs and ALEs): an overview of their mechanisms of formation. Free Radical Res 47: 3-27

von Caemmerer S (2000) Biochemical models of leaf photosynthesis. CSIRO publishing, Collingwood, pp 1-165

von Caemmerer SV, Farquhar GD (1981) Some relationships between the biochemistry of photosynthesis and the gas exchange of leaves. Planta 153: 376-387

Voss I, Goss T, Murozuka E, Altmann B, McLean KJ, Rigby SE, Munro AW, Scheibe R, Hase T, Hanke GT (2011) FdC1, a novel ferredoxin protein capable of alternative electron partitioning, increases in conditions of acceptor limitation at photosystem I. J Biol Chem 286: 50–59

Walters RG, Shephard F, Rogers JJ, Rolfe SA, Horton P (2003) Identification of mutants of *Arabidopsis* defective in acclimation of photosynthesis to the light environment. Plant Physiol 131: 472–481

Wang C, Yamamoto H, Shikanai T (2014) Role of cyclic electron transport around photosystem I in regulating proton motive force. Biochim Biophys Acta Bioenerg doi:10.1016/j.bbabio.2014.11.013

Watanabe CK, Sato S, Yanagisawa S, Uesono Y, Terashima I, Noguchi K (2013) Effects of elevated CO_2 on levels of primary metabolites and transcripts of genes encoding respiratory enzymes and their diurnal patterns in Arabidopsis thaliana: possible relationships with respiratory rates. Plant Cell Physiol 55: 341-357

Weibel ER (1979) Stereological Methods: Vol.: 1: Practical Methods for Biological Morphometry. Academic press, chapter4. pp101-161

Wellburn AR (1994) The spectral determination of chlorophyll *a* and *b*, as well as total carotenoids, using various solvents with spectrophotometers of different resolution. J Plant Physiol 144: 307–313

Wheeler T, von Braun J (2013) Climate change impacts on global food security. Science 341: 508-513

Wu G, Ortiz-Flores G, Ortiz-Lopez A, Ort DR (2007) A point mutation in *atpC1* raises the redox potential of the Arabidopsis chloroplast ATP synthase γ-subunit regulatory disulfide above the range of thioredoxin modulation. J Biol Chem 282: 36782-36789

Wu J, Neimanis S, Heber U (1991) Photorespiration is more effective than the Mehler reaction in protecting the photosynthetic apparatus against photoinhibition. Bot Acta 104: 283-291

Yamamoto H, Peng L, Fukao Y, Shikanai T (2011) An Src homology 3 domain-like fold protein forms a ferredoxin binding site for the chloroplast NADH dehydrogenase-like complex in *Arabidopsis*. Plant Cell 23: 1480-1493

Yamamoto H, Shikanai T (2013) In planta mutagenesis of Src homology 3 domain-like fold of NdhS, a ferredoxin-binding subunit of the chloroplast NADH dehydrogenase-like complex in *Arabidopsis* A conserved arg-193 plays a critical role in ferredoxin binding. J Biol Chem 288: 36328-36337

Yamauchi Y, Furutera A, Seki K, Toyoda Y, Tanaka K, Sugimoto Y (2008) Malondialdehyde generated from peroxidized linolenic acid causes protein modification in heat-stressed plants. Plant Physiol Biochem 46: 786-793

Yamauchi Y, Hasegawa A, Mizutani M, Sugimoto Y (2012) Chloroplastic NADPH-dependent alkenal/one oxidoreductase contributes to the detoxification of reactive carbonyls produced under oxidative stress. FEBS Lett 586: 1208-1213

Yamauchi Y, Hasegawa A, Taninaka A, Mizutani M, Sugimoto Y (2011) NADPH-dependent reductases involved in the detoxification of reactive carbonyls in plants. J Biol Chem 286: 6999-7009

Yamauchi Y, Sugimoto Y (2010) Effect of protein modification by malondialdehyde on the interaction between the oxygen-evolving complex 33 kDa protein and photosystem II core proteins. Planta 231: 1077-1088.

Yamori W, Masumoto C, Fukayama H, Makino A (2012) Rubisco activase is a key regulator of non‐steady‐state photosynthesis at any leaf temperature and, to a lesser extent, of steady‐state photosynthesis at high temperature. Plant J 71: 871-880

Yim, H-S., Kang, S-O., Hah, Y-C., Chock, P.B. and Yim, M.B. (1995) Free radicals generated during the glycation reaction of amino acids by methylglyoxal. A model study of protein-cross-linked free radicals. J Biol Chem 270: 28228-28233

Yin X, Sun Z, Struik PC, Gu J (2011) Evaluating a new method to estimate the rate of leaf respiration in the light by analysis of combined gas exchange and chlorophyll fluorescence measurements. J Exp Bot 62: 3489-3499

Ylä‐Anttila P, Vihinen H, Jokitalo E, Eskelinen EL (2009) Monitoring autophagy by electron microscopy in mammalian cells. Methods Enzymol 452: 143-164

Yoo SD, Cho YH, Sheen J (2007) *Arabidopsis* mesophyll protoplasts: a versatile cell system for transient gene expression analysis. Nat Protoc 2: 1565–1572

Yoshida K, Matsuoka Y, Hara S, Konno H, Hisabori T (2014) Distinct redox behaviors of chloroplast thiol enzymes and their relationships with photosynthetic electron transport in *Arabidopsis thaliana*. Plant Cell Physiol 55: 1415-1425

Yu TS, Kofler H, Häusler RE, Hille D, Flügge UI, Zeeman SC, Smith AM, Kossmann J, Lloyd J, Ritte G, Steup M, Lue WL, Chen J, Weber A (2001) The *Arabidopsis sex1* mutant is defective in the R1 protein, a general regulator of starch degradation in plants, and not in the chloroplast hexose transporter. Plant Cell 13: 1907-1918.

Zaks J, Amarnath K, Kramer DM, Niyogi KK, Fleming GR (2012) A kinetic model of rapidly reversible nonphotochemical quenching. Proc Natl Acad Sci USA 109: 15757-15762

Zeeman SC, Kossmann J, Smith AM (2010) Starch: its metabolism, evolution, and biotechnological modification in plants. Annu Rev Plant Biol 61: 209-234

Zeeman SC, Rees TA (1999) Changes in carbohydrate metabolism and assimilate export in starch‐excess mutants of *Arabidopsis*. Plant Cell & Environ 22: 1445-1453

Zhang S, Scheller HV (2004) Photoinhibition of photosystem I at chilling temperature and subsequent recovery in *Arabidopsis thaliana*. Plant Cell Physiol 45: 1595-1602

Zivcak M, Brestic M, Kunderlikova K, Olsovska K, Allakhverdiev SI (2015b) Effect of photosystem I inactivation on chlorophyll a fluorescence induction in wheat leaves: Does activity of photosystem I play any role in OJIP rise? J Photochem Photobiol B doi: 10.1016/j.jphotobiol.2015.08.024

Zivcak M, Brestic M, Kunderlikova K, Sytar O, Allakhverdiev SI (2015a) Repetitive light pulse-induced photoinhibition of photosystem I severely affects CO_2 assimilation and photoprotection in wheat leaves. Photosynth Res doi; 10.1007/s11120-015-0121-1.

Zulfugarov IS, Tovuu A, Eu YJ, Dogsom B, Poudyal RS, Nath K, Hall M, Banerjee M, Yoon UC, Moon YH, An G, Jansson S, Lee CH (2014) Production of superoxide from Photosystem II in a rice (*Oryza sativa* L.) mutant lacking PsbS. BMC Plant Biol 14: 242 doi:10.1186/s12870-014-0242-2